1-1-2012

Polymeric nanocarriers for the regional and systemic delivery of therapeutics to and through the lungs

Balaji Bharatwaj
Wayne State University,

POLYMERIC NANOCARRIERS FOR THE REGIONAL AND SYSTEMIC DELIVERY OF THERAPEUTICS TO AND THROUGH THE LUNGS

by

BALAJI BHARATWAJ

DISSERTATION

Submitted to the Graduate School

of Wayne State University,

Detroit, Michigan

in partial fulfillment of the requirements

for the degree of

DOCTOR OF PHILOSOPHY

2012

MAJOR: CHEMICAL ENGINEERING

Approved by:

_____

Advisor Date

_____

_____

_____

_____

ACKNOWLEDGEMENT

During my tenure as a graduate student I have been fortunate enough to be acquainted with several individuals who have been instrumental in leading me to the current stage. At the outset, I would like to extend a heartfelt gratitude to my parents and my younger brother whose undying love, affection, support and patience has maneuvered me effectively through the vicissitudes of my doctorate studies. My parents have been a constant source of encouragement, lifting my spirits in the face of adversity, and have stood by me through joy and agony molding me into the character that I am today. I would like to extend my warmest regards to my fiancée Yogita for her love, care and motivation over the past few months that have helped me to a great extent in leading me to the destination that I have been seeking. I would like to acknowledge a close friend Purnaa Prabhakar, who, despite her untimely demise, taught me that all it takes is a warm smile and cheerfulness to tackle the most excruciating of predicaments – a value that I will strive to inculcate and follow judiciously.

This river could not have been crossed without the unequivocal support of my advisor Prof. Sandro da Rocha and his invaluable guidance over the course of my studentship. During this time, not only did he don the role of a mentor to chisel my academic and research acumen, but also has been a father-figure, a friend, a brother and a role model helping me overcome every obstacle that I had encountered as a graduate student. A special thanks to my co-advisor Dr. Judith Whittum-Hudson and collaborating Professors Dr. David Bassett and Dr. Joshua Reineke, whose supervision, expertise and suggestions aided greatly in the successful completion of

this dissertation. I would also like to thank Dr. R M Kannan and Dr. Howard Matthew for agreeing to be on my dissertation committee and providing constructive advice pertinent to my research. With gratitude, I acknowledge Abdul Khadar, Mirabela Hali and Xiufeng Gao for all their assistance with various aspects of my research.

I would like to express my deepest regards to my aunt Dr. Vijayalakshmi for her guidance during my formitive years as a fledgling undergraduate student and laying the foundation for my graduate education. I am greatly indebted to my cousins and relatives in the USA who ensured that I never missed home and family during my extended period of stay in North America. I would like to thank my current lab members Denise Conti, Lin Yang, Qian Zhong, Sumanth Avasarala, Radovan Dimovski, Williyan Giufrida, Daniel Brewer, Julianna Carneiro and Jordan Grashik whose wonderful company ensured that my presence in the lab was not confined to just research. I would like to acknowledge my former labmates and colleagues Parthiban Selvam, Nandhini Sokkalingam, Robson Peguin, Libo Wu, Sowmya Saiprasad, Fernando Cassio, Mariam Al-Haydari and Udyan Chokshi for their valuable assistance during my stay at the da Rocha Group and for their precious friendship which I will cherish for eons to come. Words can do no justice to the help that was afforded by my former roommates Ganesh, Harish and Amit whose company was instrumental in helping me settle in and adapt to the American way of life during my initial days in the USA.

I would also like to thank the Department of Chemical Engineering and The Graduate School at Wayne State University for their financial support during my tenure as a graduate student. Last, but certainly not the least, I would like to thank all my

family members and friends whose valuable support at every opportune moment has helped me scale this peak, finally.

TABLE OF CONTENTS

LIST OF TABLES

LIST OF FIGURES

ACRONYMS AND NOTATIONS

ACI	Anderson Cascade Impactor
AIC	Air-interface Culture
ATC	American Thoracic Society
ATCC	American Type Culture Collection
AUC	Area under the Curve
BAL	Bronchoalveolar lavage
BALF	Bronchoalveolar lavage fluid
BSA	Bovine Serum Albumin
COPD	Chronic Obstructive Pulmonary Disorder
CS	Chitosan
Cl	Clearance
C_{ss}	Steady state plasma concentration
DAPI	4´,6-diamidino-2-phenylindole, dilactate
DCC	N,N'-dicyclohexylcarbodiimide
DCM	Dichloromethane
DCU	Dicyclohexylisourea
DI	Deionized Water
DLS	Dynamic Light Scattering
DMF	Dimethyformamide
DMEM	Dulbecco's Modified Eagle Medium
DMSO	Dimethyl sulfoxide
DNCs	Dendrimer Nanocarriers
DPIs	Dry Powder Inhalers

EB	Elementary Body
EDC	1-ethyl-3-(3-dimethylaminopropyl) carbodiimide
EDTA	Ethylenediamine tetraacetic acid
FA	Fluoresceinamine
FACS	Fluorescence activated cell sorting
FBS	Fetal Bovine Serum
FITC	Fluorescein isothiocyanate
FPF	Fine Particle Fraction
GSD	Geometric Standard Deviation
HBSS	Hank's Balanced Salt Solution
HEPA	High Efficiency Particulate Filtered Air
HEPES	4-(2-hydroxyethyl)-1-piperazineethanesulfonic acid
HFA	Hydrofluoroalkanes
HPLC	High Performance Liquid Chromatography
IC_{50}	(minimum inhibitory concentration required to kill 50% of viable cells)
i.v.	Intravenous
LA-g-CS	oligo(lactide)-grafted Chitosan
MFI	Mean Fluorescence Intensity
MMAD	Mass Median Aersol Diameter
MTT	3-(4,5-Dimethylthiazol-2-yl)-2,5-diphenyltetrazolium bromide
NCs	Nanocarriers
NPs	Nanoparticles
NHS	N-hydroxysuccinimide
OI	Oral Inhalation
(OLA-g-CS)	oligolactide grafted chitosan

OVA	Ovalbumin
P_{app}	Apparent Permeability Co-efficient
PAMAM	Polyamidoamine
PBS	Phosphate Buffered Saline
PEG	Polyethyleneglycol
PK	Pharmacokinetic
PLGA	Poly(d.l-lactide-co-glycolide)
pMDIs	Pressurized Metered Dose Inhalers
PNCs	Polymeric Nanocarriers
PNPs	Polymeric Nanoparticles
PVA	Poly-vinyl alcohol
RB	Reticulate Body
RES	Reticulo-Endothelial System
RF	Respirable Fraction
RPMI	Roswell Park Memorial Institute Medium
SEM	Scanning Electron Microscopy
TEER	Transepithelial Epithelial Resistance

LIST OF ORIGINAL PUBLICATIONS

This dissertation is based on the following publications.

1. Bharatwaj, B.; and da Rocha, S.R.P. "Interfacial phenomena at the compressed CO2-water interface", *Brazilian Journal of Chemical Engineering*, 2006, 23(2). 183-190.

2. Bharatwaj, B.; Wu, L; and da Rocha, S.R.P**.** "Biocompatible, Lactide-based surfactants for the CO2-water interface: High-Pressure Contact Angle Goniometer, Tensiometry and Emulsion Formation", *Langmuir*, 2007, 23(24), 12071-12078

3. Wu, L; Bharatwaj, B.; Panyam, J; and da Rocha, S.R.P. "Core-shell Particles for the Dispersions of Small Polar Drugs and Biomolecules in Hydrofluoroalkane Propellants".*Pharmaceutical Research*, 25 (2),289-301, 2008.

4. Bharatwaj, B.; Wu, L; Whittum-Hudson, J and da Rocha, S.R.P, "The potential for the noninvasive delivery of polymeric nanocarriers using propellant-based inhalers in the treatment of Chlamydial respiratory infections", *Biomaterials*, 31(28), 7376-7385, 2010.

5. Conti, D.; Bharatwaj, B; Brewer, D and da Rocha, S.R.P, "Propellant-based Inhalers for the Non-invasive Delivery of genes to the Lungs". *Journal of Controlled Release*. 157(3), 406-417, 2011.

6. Selvam, P.; Bharatwaj, B.; Porcal, L.; da Rocha, S.R.P. "Reverse Aqueous Microemulsions in Hydrofluoroalkane Propellants and their Aerosol Characteristics". *International Journal of Pharmaceutics*. 2011 doi:10.1016/j.ijpharm.10.038.2011

7. Bharatwaj, B., Dimovski, R., Conti, D.S., and da Rocha, S.R.P., “Polymeric Nanocarriers for Transport Modulation Across the Pulmonary Epithelium: Dendrimers, Polymeric Nanoparticles, and their Nanoblends”. *J Control Release*, 2012. Submitted

8. Bharatwaj, B., Mohammad, A. K., Dimovski, R., Cassio, F., Conti, D. S., Bazito, R., Reineke, J., and da Rocha, S. R. P., “PEGylated Dendrimer Nanocarriers for Transport Modulation Across the Pulmonary Epithelium.” *Biomaterials*, 2012. To be submitted

9. Bharatwaj, B., Gao, X., Conti, D.S., Wu,L., Bassett, D. J. P., and da Rocha, S. R. P, “Pulmonary Inflammatory Response of a Versatile Chitosan-based Co-oligmeric Excipient for Pressurized-Metered Dose Inhalers”. *Biomaterials,* 2012. To be Submitted.

10. Bharatwaj, B., Wu, L and da Rocha, S.R.P., “Quantification of Interaction energy between Compressed CO_2 and CO_2-philes.” *Langmuir*, 2012. To be Submitted.

Chapter 1

Introduction

1.1 Overview and objectives

Oral inhalation (OI) is not only the most attractive therapy for the regional delivery of drugs *to the lungs*, but also a promising candidate route for the systemic administration of therapeutics *through the lungs*.[1, 4] There are many advantages in using the pulmonary route for targeting the systemic circulation, including the fact that it is non-invasive (both in terms of compliance and reducing the risk of transmission of infectious diseases), the alveolar region has a large surface area for drug absorption (~ 140 m^2), and the lung tissue has limited biochemical activity compared to the liver, thus typically resulting in improved drug bioavailability.[5-7] Despite these advantages, the potential of OI therapies remains relatively unexploited; a fact underscored by the absence of commercially available OI formulations for systemic drug delivery, or for the treatment of medically relevant, debilitating pulmonary diseases such as lung cancer and tuberculosis, which are currently being targeted with oral/intravenous (i.v.) formulations.[8-9] The advancement of OI formulations has been hindered to a large extent by our limited knowledge of the interaction of drugs with the lung tissue, extra and intra-cellular barriers to drug delivery, and the lack of efficient OI drug delivery carriers and systems.[10]

Pressurized metered dose inhalers (pMDIs) and dry powder inhalers (DPIs) are two of the most widely used pulmonary drug delivery devices in the market today. With an estimated market share in excess of $2 billion, and a patient base of over 70

million, pMDIs are the most commonly prescribed aerosol delivery devices in the world.[11-12] Following the pMDIs in terms of usage are the DPIs.[13] Owing to their high compliance, extensive usage, and portability, pMDIs and DPIs are potential candidates for the delivery of medically relevant therapeutics including proteins, peptides, and nucleotides to (regionally) and through (systemically) the lungs.[11] The impact of OI formulations is expected to be even broader if such technologies can be successfully combined with the desirable characteristics of polymeric nanocarriers (NCs), including targeted and controlled release of therapeutics, the ability to carry/encapsulate various types of solutes, and the ability to protect sensitive cargo.[14-18] Other advantages of NCs include the fact that due to their sub-micron size, they can be trafficked with relative ease into the cell cytosol, are capable of reaching intracellular organelles, can penetrate deep into tissues, and most importantly, may be tailored to overcome relevant barriers, including the epithelial cell layer (required for systemic delivery), the mucus layer (present in the upper airways), and alveolar macrophages and lung surfactant (present in the alveolar region), as well as intracellular barriers.[16, 19]

The formulation aspects of NCs in pMDIs and DPIs also pose significant challenges. One major hurdle that needs to be overcome is related to the aerosol size of the NCs.[20] Aerosol delivery with maximal particulate deposition in the deep lung occurs for those within the size between 0.5-5 μm.[1] Aerosols larger than approximately 5μm are deposited in mouth and throat, and those with sizes smaller than the lower limit (which is the range of interest for polymeric NCs), may be efficiently exhaled and have severely reduced deposition. The ability to target

different regions of the pulmonary epithelia is also relevant as different diseases are targeted (regional delivery). Another challenge that needs to be addressed while incorporating polymeric NCs into OI devices is their interaction (particles) with media and carriers. In the case of pMDIs, in order to obtain good dispersions in the compressed solvents used as dispersing and propellant media, and thus to achieve enhanced aerosol properties, the particle chemistry must be chosen such that it will be well solvated by the propellants.[21] For DPIs, the physicochemical characteristics of NCs should be tailored to ensure that adhesive/cohesive balance between NCs and/or NC/excipient are balanced so that they reach the lungs as un-aggregated particles, and release from the large carrier particles to get access to the deep lungs.[3] Finally, the interaction of NCs and other excipients used in the formulations with the lung milieu in *vivo* needs to be evaluated in order to understand the retention of these moieities in the airspace and potential inflammatory response they might stimulate, as addition of extraneous agents to the lung has been shown to foment inflammation.[16 , 20]

While the capabilities of polymeric NCs and delivery vehicles have been extensively investigated with respect to conventional delivery routes (e.g. oral and intravenous; i.v.), reports of the incorporation of NCs into inexpensive and portable OI devices, and their interaction with the lung epithelia has been fairly limited.[17, 22-23] Our long term goal is to develop novel inhalation formulations for the targeted and controlled delivery of therapeutics to (regional) and through (systemically) the lungs. The objective of this dissertation is to design polymeric NCs capable of modulating drug transport across the lung epithelium, and to develop efficient OI formulations of

such carriers. The rationale that underlies this investigation is that issues typically associated with the poor performance of free drugs delivered via OI, including the lack of control of the transport across / localization in the respiratory epithelium, and lack of controlled release and of tissue specificity may all be circumvented by employing polymeric NCs as delivery vehicles.

The primary objectives of this work were achieved by pursuing the following two aims:

Aim #01. Develop strategies for the formulation of polymeric NCs in portable inhalers. The size of the aerosol particles greatly affects lung deposition. The optimum aerosol size range varies between 0.4 to 5.0 μm, which falls outside the desirable size range for polymeric NCs (< 200 nm). This issue is relevant for both DPIs and pMDIs. In the case of propellant-based inhalers, the stability of colloidal particles in the low dielectric hydrofluoroalkanes (HFAs) also needs to be addressed. Particle aggregation leads to change in overall particle size, which may in turn affect both aerosol characteristics and dosage. In DPIs the concern is to optimize the forces between NC and inert carrier particles (or NC-NC if no inert carrier is used). In order to address these issues, we propose a new particle engineering strategy. Micron-sized core-shell particles will be produced via emulsification diffusion. The particle core will consist of polymeric NCs (polymeric nanoparticles- PNPs, dendrimer nanocarriers, DNCs, and their composites), while the shell that provides integrity to the micron particles will consist of a biodegradable co-oligomer. This co-oligomer shell will have an appropriate chemistry so as to enhance the stability of the colloids in propellant HFAs for propellant-based inhalers, and to modulate particle-particle

interaction for DPIs. We will discuss the feasibility of the proposed particle engineering strategy for the formation of micron-sized core shell particles, and the physical characterization of such constructs. The synthesis of candidate co-oligomers and their characterization will also be discussed. Finally, we will study the aerosol characteristics of the core-shell particles formulated in pMDIs. These studies will serve to guide the design of the co-oligomer shell in order to optimize the characteristics of the aerosol.

Aim #02: Investigate the interaction between polymeric NCs with varying chemistry and architecture with the lung epithelium *in vitro* and *in vivo*. The ability to modulate the interactions between the polymeric NCs and the lung epithelium offers many opportunities in terms of drug delivery via oral inhalation. One major challenge in targeting lung diseases via OI is that certain drugs permeate too rapidly across the epithelium, and are thus rendered ineffective for regional delivery. There are also issues related to tissue toxicity that might arise once these drugs reach the systemic circulation. On the other hand, the permeability of certain poorly water soluble drugs and large molecular weight (MW) therapeutics (e.g. biomacromolecules) through the lungs may be slow and/or too small. Targeting the alveolar and upper respiratory regions, and overcoming extracellular and intracellular barriers, especially in diseased lungs, are also major challenges. In this study we seek to design polymeric NCs capable of modulating the transport of therapeutics across the lung epithelium. The structure, size, chemistry, and surface characteristics of the NCs will be explored in an attempt to modulate transport. Polymeric nanoparticles (PNPs), dendrimer nanocarriers (DNCs), and composites of

DNCs and PNPs with and without functionalization will be investigated. Studies in healthy and diseased *in vitro* models of the lung epithelium, as well as the interaction of selected NCs with lung tissue *in vivo* will also be studied. The *in vivo* inflammatory potential of PNCs and the co-oliogomer utilized in formulating the core-shell structures and their rate of elimination from the lung will also be evaluated in an effort to understand the interaction of the co-oligomer and PNCs with the lung epithelium *in vivo.*

Results demonstrating the progress made towards these aims are discussed below. Some of the work shown next has been compiled in the form of a manuscript: **Bharatwaj. B.,** Wu, L., Whittum-Hudson, J. A., and da Rocha S. R. P. **"***The potential for the noninvasive delivery of polymeric nanocarriers using propellant-based inhalers in the treatment of Chlamydial respiratory infections*." Biomaterials 31 (2010) 7376-7385.

Studies detailing the interaction and the modulation of DNCs, NPs and their blends with pulmonary epithelium have been compiled into two other manuscripts entitled

(a) Bharatwaj, B., Dimovski,R., Conti, D.S., and da Rocha, S.R.P., *Polymer Nanocarriers for Transport Modulation Across the Pulmonary Epithelium: Dendrimers, Polymeric Nanoparticles, and their Nanoblends*. **J Control Rel, 2012. To be submitted.**

(b) **Bharatwaj, B., Mohammad, A.K., Dimovski, R., Cassio, F., Conti, D.S., Bazio, R., Reineke, J., and da Rocha, S. R. P.,** *PEGylated Dendrimer Nanocarriers for Transport Modulation Across the Pulmonary Epithelium.* **Biomaterials, 2012. To be submitted**

In chapter 2, we discuss the formulation of polymeric nanoparticles (PNPs) in pMDIs and their subsequent interaction with a disease model of pulmonary epithelium *in vitro.* A major hurdle impeding the development of NP laden pMDI formulations, in addition to their chemistry, is their size which is not conducive for deep lung deposition. Here, we discuss the formulation of NPs as micron-sized core-shell constructs and their evaluation of their stability and aerosol properties. Furthermore, we also discuss the ability of these NPs to internalize into infected epithelial cell models. This chapter is based on the following publication- **Bharatwaj. B.,** Wu, L., Whittum-Hudson, J. A., and da Rocha S. R. P. **"***The potential for the noninvasive delivery of polymeric nanocarriers using propellant-based inhalers in the treatment of Chlamydial respiratory infections*." **Biomaterials 31 (2010)** 7376-7385.

In Chapter 3, we discuss the interaction of DNCs with model airway epithelium, Calu-3. The objective of this study was to evaluate the permeability and uptake of generation-3 (G3) poly (amido amine) (PAMAM) dendrimers across an *in vitro* model of the airway epithelium – Calu-3. Additionally, we also discuss the ability of arresting (thereby modulating) the transport and enhancing the uptake of DNCs across and into Calu-3 monolayers by encapsulating the conjugates into biodegradable NPs. The ability to formulate DNCs as micron-sized structures in pMDIs and evaluating the pertinent aerodynamic properties of the resulting aerosol is also discussed here. This chapter is based on the following publication- **Bharatwaj, B.,** Dimovski,R., Conti, D.S., and da Rocha, S.R.P., *Polymer Nanocarriers for Transport Modulation Across the Pulmonary Epithelium: Dendrimers, Polymeric Nanoparticles, and their Nanoblends*. **J Control Rel, 2012. To be submitted.**

Modifying amine terminated DNCs with PEG imparts several advantageous properties to the dendrimers. Some of them include, lower cytotoxic potential, enhancement of mucosal transport and increased circulation time.[R] Chapter 4 deals with the synthesis of PEG tethered DNCs, their preparation, characterization and their ability to modulate transport and uptake across and into polarized Calu-3 monolayers. Furthermore, the pharmacokinetic (PK) behavior of select PEGylated DNCs was evaluated in BALB/C mice upon pulmonary administration and their bioavailability contrasted against conjugates administered intravenously (*i.v)* to mice. The chapter is based on the following publication- **Bharatwaj, B.,** Mohammad, A.K., Dimovski, R., Cassio, F., Conti, D.S., Bazito, R., Reineke, J., and da Rocha, S. R. P., *PEGylated Dendrimer Nanocarriers for Transport Modulation Across the Pulmonary Epithelium.* **Biomaterials, 2012. To be submitted.**

Chapter 5, deals with evaluating the inflammatory potential of the co-oligomer, oligolactide grafted chitosan (OLA-g-CS) in mice. OLA-g-CS, is the excipient widely used in our formulations to form dispersions in HFA. *In vitro* cytotoxic evaluation of the compound deemed it to be non-toxic up to concentrations as high as ca.13 $mg \cdot mL^{-1}$. Here, the co-oligomer was administered to mice lung intranasally and the inflammatory response was elicited by counting cell population in the bronchoalveolar lavage fluid (BALF) and lung tissue. Epithelial integrity to estimate the serum protein infiltration into the airspace was also determined to reaffirm the results obtained from the BALF cell count. Furthermore, the study also evaluated the inflammatory potential of the NP laden core-shell formulation discussed in chapter 2. The residence times of the co-oligomer and the NP laden core-shell formulation is also

discussed here. This chapter is based on the following publication - Bharatwaj, B., Gao, X., Conti, D. S., Wu,L., Bassett, D. J. P., and da Rocha, S. R. P, "Pulmonary Inflammatory Response of a Versatile Chitosan-based Co-oligmeric Excipient for Pressurized-Metered Dose Inhalers". **Biomaterials, 2012. To be Submitted.**

Conclusions and future directions are detailed in the final chapter.

1.2 Background.

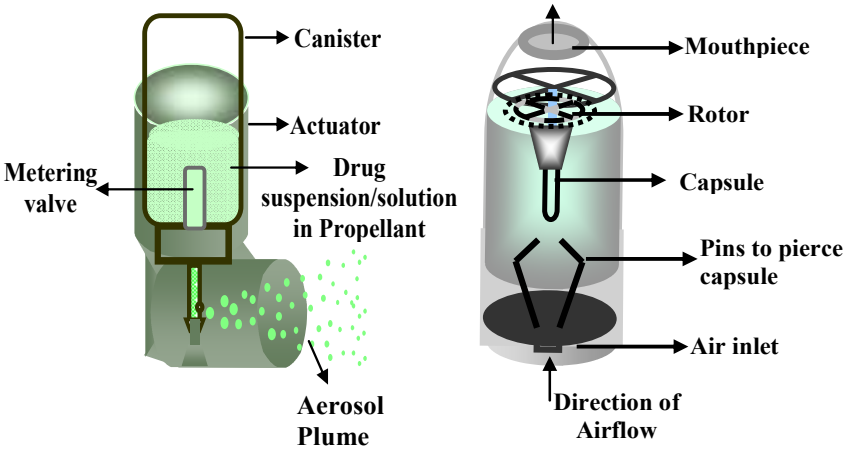

Figure 1.1 (a). A representative schematic of a pMDI housing a typical formulation (b) Schematic illustration of a Spinhaler® DPI. Adapted from [2].

1.2.1 Portable devices for oral inhalation (OI) delivery of drugs.

pMDIs are the least expensive and most widely used portable inhalers.[4, 11] They are reliable, have high compliance, and are easy to use.[24] A schematic diagram of a typical pMDI system is shown in Figure 1.1a. The ensemble consists of

three major components: (i) a canister that houses the propellant containing the drug formulation; (ii) a metering valve, which serves to dispense a specific quantity of the aerosol (~ 50-100 μl); (iii) and an actuator, which serves to lodge the canister upside down, and to direct the aerosol into the patients' respiratory tract. Commercially available pMDI formulations contain the liquid HFA propellant in equilibrium with its vapor (98% of the formulation), a drug (typically in suspension as most drugs of interest are insoluble in propellant HFAs which are simultaneously hydrophobic and oleophobic), and excipients.[25] Upon actuation, the propellant containing the drug and excipients flash vaporizes into an aerosol plume that is inhaled by the patient.

In DPIs, the active therapeutic is brought to an appropriate size, and (typically) mixed with a carrier, which is usually lactose. The function of the carrier particles is primarily to prevent aggregation, enhance flow and assist in the improvement of handling and metering of the drug.[3] A schematic diagram of a DPI is shown in Figure 1.1b. Different from pMDIs, the delivery of medicaments from typical DPIs to the lungs is achieved by way of the patient's inspiratory flow, thus not requiring coordinated actuation and inhalation.[3] The shear and turbulence created by the patients' inspiration causes fluidization and separation of the drug-carrier (when part of the formulation) blend. Owing to their larger size (tens of microns), the carrier particles remain in the oropharyngeal region and are cleared, and the smaller drug particles (appropriate size for deep lung deposition) are subsequently transported into the airways. [3, 13]

The delivery of polymeric NCs from pMDIs and DPIs may be challenging given that the size of the carriers fall outside the range desired in order to ensure maximal

lung deposition. One potential approach to overcome this challenge is the formulation of NCs as micron-sized agglomerates.[15] However, there are potential drawbacks when using this approach. Upon administration, these agglomerates may persist as micron-sized entities upon reaching the lung tissue, thereby presenting themselves to the cellular milieu in a clustered form, which could hamper cellular uptake and/or allow for more efficient uptake by macrophages.[16, 26] Additionally, the NCs need to possess appropriate chemistry in order to form stable dispersions in HFA. For instance, PLGA NCs are not dispersible in HFAs.[23] Ideally, having a common versatile formulation platform for NCs that would serve the needs of both DPIs and pMDIs in augmenting the delivery efficiency of NCs to and through the lungs would be greatly beneficial in expanding the drug delivery capabilities of both the devices, as there are several parameters that govern the patient choice/selection of one over the other.[3, 9, 15].

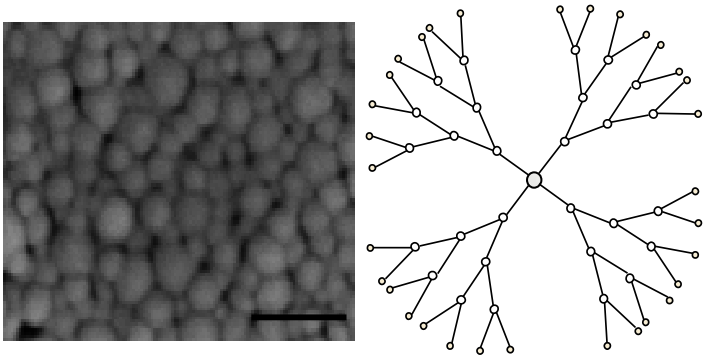

Figure 1.2. (a) NCs of PLGA prepared using emulsification solvent evaporation. Size bar denotes 0.5 μm; (b) A Pictographic rendition of G3 PAMAM dendrimer with 32 surface groups (-NH_2).

1.3 Polymeric NC candidates for OI delivery of drugs.

Two examples of polymeric NCs that may be employed for the delivery of drugs via OI are shown in Figure 1.2. In Figure 2a, an SEM micrograph of polymeric (PLGA) NPs (particle nanocarriers or PNPs) prepared by emulsification solvent evaporation is shown. PNPs have been extensively employed as drug and gene delivery vehicles.[19, 27] PNPs protect the payload from premature degradation, enhance drug penetration into cells and tissues, and may be designed in order to target and controllably release therapeutics.[17, 27] Additionally, it has been shown that certain PNPs can evade the mucociliary clearance, which is a particularly relevant barrier present in the respiratory system.[5, 22, 28] While PNPs have several notable advantages that would make them very amenable to local and sub-cellular delivery of therapeutics, their ability to target the pulmonary epithelia, and to translocate into systemic circulation via pulmonary route is just beginning to be investigated.[16]. One may expect that the translocation across the highly regulated and small tight junctional spaces, and transcellular transport may both be hindered to some extent by the large size of PNPs.[29-30] Additionally, prolonged accumulation of PNPs in the nether regions of the lung can lead to unwanted inflammatory effects.[31]

Other promising candidates for the regional and systemic delivery to and through the lungs are dendrimers nanocarriers (DNCs).[32-34] DNCs are well-defined, highly branched, nanostructured polymers, with a unique tree-like architecture comprising of distinct dendritic arms branching out from a common core. The monodispersity in their mass or size confers them with a controlled geometry,

with numerous surface groups that can be utilized for chemical modifications for a variety of purposes.[35-37] Figure 1.2b is a pictographic representation of a typical dendrimer. Each branching series is coined a 'generation'. Those with terminal amine groups are termed full generation (G1,2,3..) dendrimers, and those that are carboxylate ended are referred to as 'half-generation' (G1.5, 2.5….).[38] Their size is a function of dendrimer generation, with G3 dendrimers having a size of approximately 3 nm.[36, 38] This controlled geometry and size range is expected to be of great relevance when designing NCs that can overcome the mucus and epithelial barriers that the lung epithelium poses to drug delivery. For example, macromolecular therapeutics with sizes < 40KDa (5-6 nm in solution) are known to be quickly translocated through the lung epithelial cells, with peak circulation in blood in a matter of minutes,[39-40] while larger solutes may take days to translocate. It may be expected, therefore, that the transport of DNCs (and thus of therapeutics) across the epithelial monolayer may be modulated by controlling their size and functionality. Another example of the potential utility of DNCs is the fact that the permeability of PNPs across the mucus layer may be enhanced by the introduction of polyethylene glycol (PEG) moieties onto the surface of the PNPs.[41-42] A similar strategy may be easily implemented by functionalization of the many surface groups of dendrimers with PEG, in a very well controlled manner (density including).

1.4 Physiology of pulmonary epithelium and extracellular barriers to the delivery of drugs to the lungs.

The respiratory system consists of two functional parts, the airways (trachea, bronchi and bronchioles), and the alveoli (the region of gas exchange), as schematically shown in Figure 1.3. The surface area of the adult human lungs is estimated to be between 75 and 140 m^2, of which the bulk of the surface area is taken up by the alveolar region, which is nearly 100 m^2. The airways are pseudo-stratified, comprising of a leakier, gradually thinning columnar epithelium populated mainly by mucus and ciliatory cells collectively called the mucociliary escalator.[43-44] There are at least six major types of airway epithelial cells, including the basal, ciliated, the goblet, serous, granular and Clara cells. The thickness of the mucus layer in lungs under non-pathological circumstances is approximately between 10 and 30 μm in the airways and between 2 and 5 μm in the bronchial region. Respiratory mucus is composed primarily of a three-dimensional network of cross-linked mucin chains that bestow upon the mucus its viscoelastic properties.[45] The mucus layer offers a barrier to the transport of NCs. Both the chemistry and size of the NCs are known to influence their transport across the

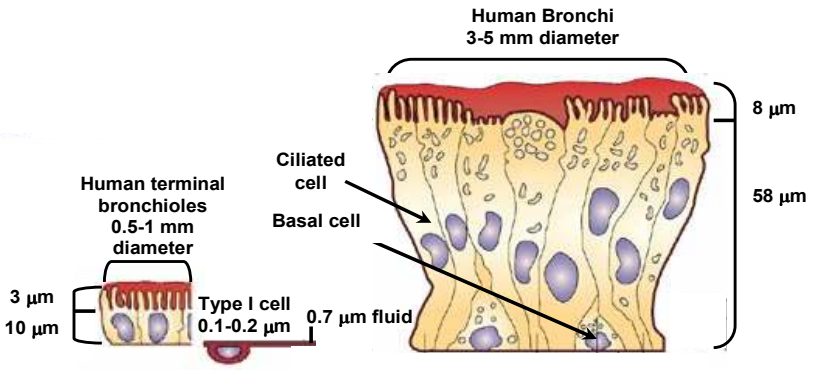

Figure 1.3. Diagrammatic illustration of the pulmonary epithelium showing various cell types lining its vasculature. Image sourced from [1].

mucus layer.[42] The alveolar epithelium consists of only two major cell types, viz. type I and type II. Type II cells serve as the progenitor for type I cells and produce the lung surfactant.[43] The alveolar epithelium is covered with an extremely thin layer of fluid (tens of nanometers) containing a water-insoluble surfactant layer, and alveolar macrophages. This surfactant layer may also work as a barrier to the transport of NCs, and the macrophages work in removing foreign particles - with preference to micron-sized. The pulmonary surfactant layer is a thin continuous coating of phospholipids and surfactant-associated proteins secreted by type II alveolar cells. The average thickness of this layer ranges between 0.18 μm to 0.89 μm and their primary function is to reduce tension at the air-water interface thereby minimizing the urge of alveoli to collapse.[45]

1.5 *In-vitro* models of the pulmonary epithelia.

In order to design novel carrier systems for drug delivery to and through the lungs, it is essential to understand the interaction of therapeutics and carriers with the complex pulmonary physiology.[10] Such fundamental information can be obtained by studying drug uptake, sub cellular localization, and their transport across model pulmonary epithelia.[10] The human bronchial adenocarcinoma cell line Calu-3 has been shown to best mimic the human airways *in vitro.*[6, 10, 46] When cultured under an air-interface (AIC), these cells form confluent monolayers, exhibit tight junctional proteins and possess all the relevant morphological features of the airway epithelium (mucus, cilia and apical microvilli).[10, 46] While, Calu-3 cells best mimic the airway epithelia, alveolar type-II cells sourced directly from the lungs (animal models typically used) through specific lavage techniques offer the best *in vitro* representation of the epithelial cells populating the alveolar region.[6, 10] Note here that A549 cells do not form tight junctions and thus cannot be utilized in transport experiments, but may be employed to understand cell uptake mechanisms. However, the studies with primary cells fall outside the scope of this work. Studies with primary alveolar epithelial cells are expected to be undertaken by our group in the future. Owing to their increased predictability and higher (and faster) throughput, these *in vitro* approaches are quite attractive, cost effective options when compared to *in vivo* studies.[10, 47-48]

1.6 Determining the mechanisms of transport and uptake of PNPs, DNCs, and their composites in *in-vitro* models of the pulmonary epithelium.

Although transport of polymeric NCs (PNPs and DNCs) across pulmonary epithelia has not been established yet, in pulmonary epithelia in general, it is believed that NCs may translocate through an assortment of mechanisms,[43, 49-51] some of the most common being illustrated in Figure 1.4. Previous studies have hypothesized that translocation of PNPs (~<200 nm) across model intestinal and pulmonary epithelia occurs via a non-specific, size and charge driven caveolae-mediated or in certain cases receptor mediated mechanism.[50, 52-53] DNCs, on the other hand

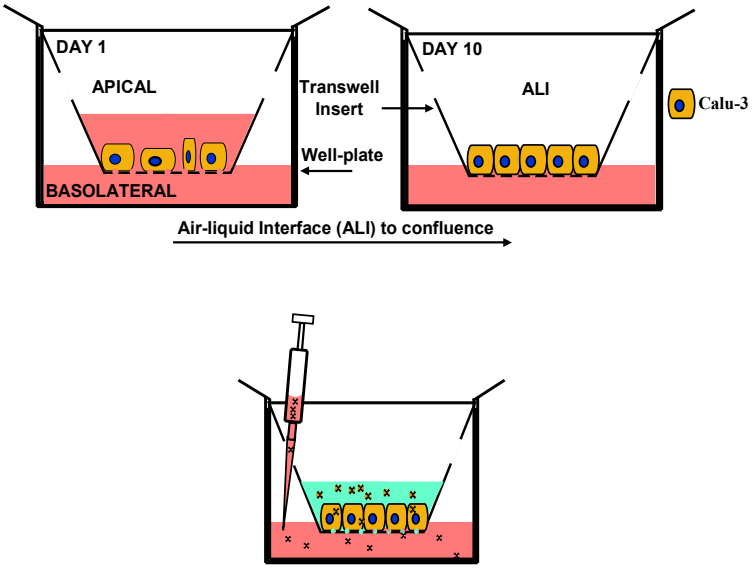

Figure 1.4. A schematic representation of *in vitro* transport studies undertaken in this work.

have been known to traverse through combinations of paracellular and transcellular mechanisms across intestinal epithelium.[40, 54] Their ability to exploit the paracellular pathways can be attributed to their small size (which is similar to the pores in the tight junctions), and their inherent nature in opening up these junctions as evidenced by electrophysiological measurements.[55] However, little is known about transport of DNCs or their composites with PNPs across Calu-3 cells, as earlier studies have been performed mostly on intestinal epithelial cells.[51] In the particular case of Calu-3 cells, previous literature has reported a strong correlation between permeability coefficients assessed *in vitro* to those obtained in *in vivo* lung absorption studies in rodents for certain low MW peptides,[56-57] which reinforce the idea that Calu-3 is one of the best *in vitro* cell models for the proposed work.

Figure 1.4 is a schematic representation of transport studies undertaken in this work. The transport of solutes, and, in our case, of DNCs, across the lung epithelium *in vitro* can be investigated by determining the apparent permeability coefficient (P_{app}) in an experiment as schematically represented in Figure 5. P_{app} is determined using the equation shown below (1)

$$P_{app} = F*(1/A*C_o) \qquad (1.1)$$

where F is the flux (rate of change in the cumulative mass transported – typically the value of slope obtained from a plot of mass transported against time), A is the area of the transwell insert, and C_o is the initial concentration in the donor chamber (apical side).

In a typical experiment, Calu-3 cells of a known cell density are seeded on the apical side of Transwell® inserts and grown to confluence. The monolayer confluence can be gauged by recording the increase in transepithelial electrical resistance (TEER), and also by staining the monolayers to detect presence of the tight junctional protein Zona Occludens-1 (ZO-1).[46] Alcian blue staining is done to assess the presence of mucosal glycoproteins on the monolayer surface.[46] SEM of cell monolayers fixed and stained with Osmium tetroxide (OsO_4) is also conducted to ascertain morphology of the cultured monolayer.[10, 46] Transport experiments are conducted after the qualitative and quantitative characterization of the monolayer confluence. A known concentration of DNCs (tethered with a fluorophore) and/or composites with PNPs dissolved or dispersed (in case of PNPs containing DNCs) in 1X Hank's balanced salt solution (HBSS) is pulsed on the apical side on the insert. At predetermined time points, samples are removed from the basolateral side and analyzed for the transported/translocated conjugates (and NPs) using fluorometry. The mass transported across is determined by comparing the fluorescence values to a previously prepared calibration curve. This data is then used in determining the flux (F), which is incorporated into equation (1) to calculate the apparent permeability, P_{app} which is a measure of the ease with which moieties traverse the epithelium.[46, 56]. After transport studies, the cell monolayers are lysed (using 2% Triton-X-100) and analyzed for internalized conjugates and NPs in order to quantitatively assess the extent of their uptake into Calu-3. In addition to cell lysis, flow cytometry studies is also employed as a means to evaluate the entry of DNCs as a function of time into polarized monolayers of Calu-3 in order to better understand

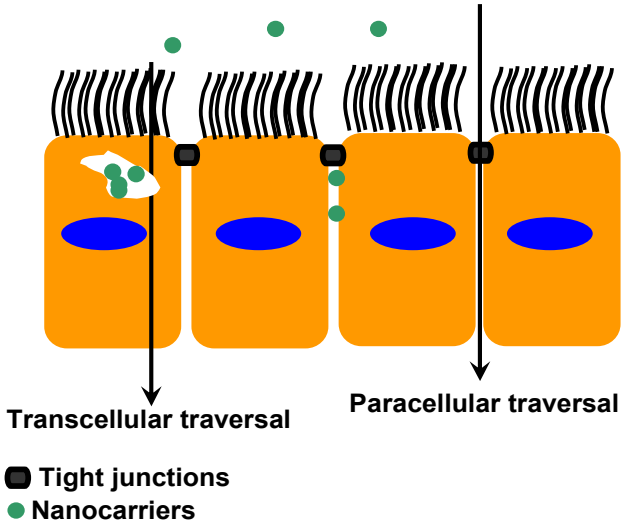

Figure 1.5. A diagrammatic illustration of transport mechanisms occurring across epithelial monolayers.

the kinetics of uptake. It is widely acknowledged that moieties traverse epithelial cell monolayers through either paracellular (via the tight junctions) or transcellular (through the cells) pathways, or a combination of those (Figure 1.5).

1.7 Relevance, innovation and broader impacts of research.

The research undertaken here is *innovative* in several aspects. For the first time, we report the formulation of PNPs in propellant based formulations. The evaluation of aerosol characteristics of such formulations is also reported here. The ability of PNPs to exclusively target an intracellular bacterium of the lung is also evaluated in this work. The transport and uptake of DNCs across and into model airway epithelium, Calu-3 is also undertaken here. The ability of surface tailored DNCs to modulate transport and their uptake across and into polarized monolayers of

Calu-3 and the formulation of DNCs as core-shell micron structures in pMDIs has also been evaluated. These results are highly *relevant* as utilizing nanocarriers to overcome cellular barriers and subsequently transport therapeutics across pulmonary epithelia can open up new possibilities of utilizing respiratory tract as a portal to target systemic circulation. The ability to modulate therapeutic transport across such epithelia could address the long standing issue of ensuring retention of the drug in the airspace for extended periods of time if the target is local milieu or rapidly percolate to systemic circulation if the therapeutic is intended for the bloodstream. Additionally, the synergy of such versatile nanoscopic vehicles like DNCs with compact, portable inhalation devices like pMDIs is expected to greatly enhance their applicability by expanding the realm of therapeutics that can be administered utilizing such inexpensive inhalers.

1.8 References

[1] Patton JS, Byron PR. Inhaling medicines: delivering drugs to the body through lungs. Nature Reviews. 2007;6:67-74.

[2] Concessio NM, Hickey AJ. Descriptors of irregular particle morphology and powder properties. Advanced Drug Delivery Reviews. 1997;26:29-40.

[3] Telko MJ, Hickey AJ. Dry powder inhaler formulation. Respir Care. 2005;50:1209-27.

[4] Laube B. The Expanding Role of Aerosols in Systemic Drug Delivery, Gene Therapy, and Vaccination. Respiratory Care. 2005;50:1161-76.

[5] Ryutting E, Nguyen J, Wang X, Kissel T. Biodegradable polymeric nanocarriers for pulmonary drug delivery. Expert Opinion in Drug Delivery. 2008;5:629-39.

[6] Sakagami M. In vivo, in vitro and ex vivo models to assess pulmonary absorption and disposition of inhaled therapeutics for systemic delivery. Advanced Drug Delivery Reviews. 2006;58:1030-60.

[7] Cryan SA. Carrier-based strategies for targeting protein and peptide drugs to the lungs. AAPS J. 2005;7:E20-41.

[8] Edwards DA, Dunbar C. Bioengineering of Therapeutic Aerosols. Annual Reviews in Biomedical Engineering. 2002;4:93-107.

[9] Courrier HM, Butz N, Vandamme FT. Pulmonary Drug Delivery Systems: Recent Developments and Prospects. Current Reviews in Therapeutic Drug Carrier Systems. 2002;19:425-98.

[10] Forbes B, Ehrhardt C. Human respiratory epithelial cell culture for drug delivery applications. European Journal of Pharmaceutics and Biopharmaceutics. 2005;60:193-205.

[11] Bell J, Newman S. The rejuvenated pressurized metered dose inhaler. Expert Opinion on Drug Delivery. 2007;4:215-34.

[12] Smyth HD. The influence of formulation variables on the performance of alternative propellant-driven metered dose inhalers. Advanced Drug Delivery Reviews. 2003;55:807-28.

[13] Islam N, Gladki E. Dry powder inhalers (DPIs)--a review of device reliability and innovation. International Journal of Pharmaceutics. 2008;360:1-11.

[14] Engstrom JD, Tam JM, Miller MA, Williams RO, 3rd, Johnston KP. Templated open flocs of nanorods for enhanced pulmonary delivery with pressurized metered dose inhalers. Pharmaceutical Research. 2009;26:101-17.

[15] Pilcer G, Amighi K. Formulation strategy and use of excipients in pulmonary drug delivery. International Journal of Pharmaceutics. 2010;392:1-19.

[16] Yang W, Peters JI, Williams RO, 3rd. Inhaled nanoparticles--a current review. International Journal of Pharmaceutics. 2008;356:239-47.

[17] Davis ME, Chen Z, Shin DM. Nanoparticle therapeutics: an emerging treatment modality for cancer. Nature Reviews. 2008;7:771-82.

[18] Soppimath KS, Aminabhavi TM, Kulkarni AR, Rudzinski WE. Biodegradable polymeric nanoparticles as drug delivery devices. Journal of Controlled Release. 2001;70:1-20.

[19] Panyam J, Labhasetwar V. Biodegradable nanoparticles for drug and gene delivery to cells and tissue Advanced Drug Delivery Reviews. 2003;55:329-47.

[20] Rogueda PG, Traini D. The nanoscale in pulmonary delivery. Part 1: deposition, fate, toxicology and effects. Expert Opin in Drug Delivery. 2007;4:595-606.

[21] Wu L, da Rocha SRP. Applications of Atomic Force Microscope in the Development of Propellant-based Inhalation Formulations. KONA Powder and Particle Journal. 2008;26:106-28.

[22] Azarmi S, Roa WH, Lobenberg R. Targeted delivery of nanoparticles for the treatment of lung diseases. Advanced Drug Delivery Reviews. 2008;60:863-75.

[23] Bharatwaj B, Wu L, Whittum-Hudson JA, da Rocha SR. The potential for the noninvasive delivery of polymeric nanocarriers using propellant-based inhalers in the treatment of Chlamydial respiratory infections. Biomaterials. 2010;31:7376-85.

[24] Rogueda P. Novel hydrofluoroalkane suspension formulations for respiratory drug delivery. Expert Opinion in Drug Delivery. 2005;2:625-38.

[25] McDonald KJ, Martin GP. Transition to CFC-free metered dose inhalers--into the new millennium. International Journal of Pharmaceutics. 2000;201:89-107.

[26] El-Sherbiny IM, McGill S, Smyth HD. Swellable microparticles as carriers for sustained pulmonary drug delivery. Journal of Pharmaceutical Sciences. 2010;99:2343-56.

[27] Petros RA, DeSimone JM. Strategies in the design of nanoparticles for therapeutic applications. Nature Reviews Drug Discovery. 2010;9:615-27.

[28] Smola M, Vandamme T, Sokolowski A. Nanocarriers as pulmonary drug delivery systems to treat and to diagnose respiratory and non respiratory diseases. International Journal of Nanomedicine. 2008;3:1-19.

[29] Lin YH, Chung CK, Chen CT, Liang HF, Chen SC, Sung HW. Preparation of nanoparticles composed of chitosan/poly-gamma-glutamic acid and evaluation of their permeability through Caco-2 cells. Biomacromolecules. 2005;6:1104-12.

[30] Ragnarsson EG, Schoultz I, Gullberg E, Carlsson AH, Tafazoli F, Lerm M, et al. Yersinia pseudotuberculosis induces transcytosis of nanoparticles across human intestinal villus epithelium via invasin-dependent macropinocytosis. Laboratory Investigation. 2008;88:1215-26.

[31] Dailey LA, Jekel N, Fink L, Gessler T, Schmehl T, Wittmar M, et al. Investigation of the proinflammatory potential of biodegradable nanoparticle drug delivery systems in the lung. Toxicology and Applied Pharmacology. 2006;215:100-8.

[32] Inapagolla R, Guru BR, Kurtoglu YE, Gao X, Lieh-Lai M, Bassett DJ, et al. In vivo efficacy of dendrimer-methylprednisolone conjugate formulation for the treatment of lung inflammation. International Journal of Pharmaceutics. 2010;399:140-7.

[33] Bai S, Ahsan F. Synthesis and evaluation of pegylated dendrimeric nanocarrier for pulmonary delivery of low molecular weight heparin. Pharmaceutical Research. 2009;26:539-48.

[34] Bai S, Thomas C, Ahsan F. Dendrimers as a carrier for pulmonary delivery of enoxaparin, a low-molecular weight heparin. Journal of Pharmaceutical Sciences. 2007;96:2090-106.

[35] Menjoge AR, Kannan RM, Tomalia DA. Dendrimer-based drug and imaging conjugates: design considerations for nanomedical applications. Drug Discovery Today. 2010;15:171-85.

[36] Esfand R, Tomalia DA. Poly(amidoamine) (PAMAM) dendrimers: from biomimicry to drug delivery and biomedical applications. Drug Discoeryv Today. 2001;6:427-36.

[37] Svenson S, Tomalia DA. Dendrimers in biomedical applications--reflections on the field. Advanced Drug Delivery Reviews. 2005;57:2106-29.

[38] Tomalia DA. Dendrons/dendrimers: quantized, nano-element like building blocks for soft-soft and soft-hard nano-compound synthesis. Soft Matter. 2010;6:456-74.

[39] Jevprasesphant R, Penny J, Attwood D, McKeown NB, D'Emanuele A. Engineering of dendrimer surfaces to enhance transepithelial transport and reduce cytotoxicity. Pharmaceutical Research. 2003;20:1543-50.

[40] Sweet DM, Kolhatkar RB, Ray A, Swaan P, Ghandehari H. Transepithelial transport of PEGylated anionic poly(amidoamine) dendrimers: implications for oral drug delivery. Journal of Controlled Release. 2009;138:78-85.

[41] Lai SK, O'Hanlon DE, Harrold S, Man ST, Wang YY, Cone R, et al. Rapid transport of large polymeric nanoparticles in fresh undiluted human mucus. Proceedings of the National Academy of Sciences (PNAS) U S A. 2007;104:1482-7.

[42] Lai SK, Wang YY, Hanes J. Mucus-penetrating nanoparticles for drug and gene delivery to mucosal tissues. Advanced Drug Delivery Reviews. 2009;61:158-71.

[43] Patton JS. Mechanisms of macromolecule absorption by the lungs. Advanced Drug Delivery Reviews. 1996;19:3-36.

[44] Gill S, Lobenberg R, Ku T, Azarmi S, Roa WH, Prenner EJ. Nanoparticles: Characteristics, Mechanisms of Action, and Toxicity in Pulmonary Drug Delivery- A review. Journal of Biomedical Nanotechnology. 2007;3:107-19.

[45] Sanders N, Rudolph C, Braeckmans K, De Smedt SC, Demeester J. Extracellular barriers in respiratory gene therapy. Advanced Drug Delivery Reviews. 2009;61:115-27.

[46] Grainger CI, Greenwell LL, Lockley DJ, Martin GP, Forbes B. Culture of Calu-3 cells at the air interface provides a representative model of the airway epithelial barrier. Pharmaceutical Research. 2006;23:1482-90.

[47] Foster KA, Yazdanian M, Audus KL. Microparticulate uptake mechanisms of in-vitro cell culture models of the respiratory epithelium. Journal of Pharmacy and Pharmacology. 2001;53:57-66.

[48] Foster KA, Avery ML, Yazdanian M, Audus KL. Characterization of the Calu-3 cell line as a tool to screen pulmonary drug delivery. International Journal of Pharmaceutics. 2000;208:1-11.

[49] Geys J, Coenegrachts L, Vercammen J, Engelborghs Y, Nemmar A, Nemery B, et al. In vitro study of the pulmonary translocation of nanoparticles: a preliminary study. Toxicology Letters. 2006;160:218-26.

[50] Madlova M, Jones SA, Zwerschke I, Ma Y, Hider RC, Forbes B. Poly(vinyl alcohol) nanoparticle stability in biological media and uptake in respiratory epithelial cell layers in vitro. European Journal of Pharmaceutics and Biopharmaceutics. 2009;72:437-43.

[51] Florence AT, Hussain N. Transcytosis of nanoparticle and dendrimer delivery systems: evolving vistas. Advanced Drug Delivery Reviews. 2001;50 Suppl 1:S69-89.

[52] Rejman J, Oberle V, Zuhorn IS, Hoekstra D. Size-dependent internalization of particles via the pathways of clathrin- and caveolae-mediated endocytosis. Biochemical Journal. 2004;377:159-69.

[53] Patton JS, Fishburn CS, Weers JG. The lungs as a portal of entry for systemic drug delivery. Proceedings of the American Thoracic Society. 2004;1:338-44.

[54] El-Sayed M, Ginski M, Rhodes C, Ghandehari H. Transepithelial transport of poly(amidoamine) dendrimers across Caco-2 cell monolayers. Journal of Controlled Release. 2002;81:355-65.

[55] El-Sayed M, Rhodes CA, Ginski M, Ghandehari H. Transport mechanism(s) of poly (amidoamine) dendrimers across Caco-2 cell monolayers. International Journal of Pharmaceutics. 2003;265:151-7.

[56] Mathias NR, Timoszyk J, Stetsko PI, Megill JR, Smith RL, Wall DA. Permeability Characteristics of Calu-3 Human Bronchial Epithelial Cells: In Vitro - In Vivo Correlation to Predict Lung Absorption in Rats. Journal of Drug Targeting. 2002;10:31-40.

Chapter 2

The potential for the noninvasive delivery of polymeric nanocarriers using propellant-based inhalers in the treatment of Chlamydial respiratory infections

2.1 Introduction

Besides its non-invasive nature, pulmonary drug delivery has many other advantages compared to alternative drug delivery strategies, including a large surface area for solute transport, fast drug uptake, and improved drug bioavailability.[1-2] It is, therefore, not surprising that oral inhalation therapy is considered not only the preferred mode of administration of drugs to the lungs (regional drug delivery), but also as a potential pathway to the blood stream.[1] However, the many challenges in formulation development,[3] and little understanding of the interactions between the therapeutic molecules and the respiratory surfaces has significantly constrained advances in pulmonary drug delivery strategies.[4-5] In this work we integrate aspects of both formulation development and therapeutic-tissue interaction. We propose a strategy to deliver polymeric nanocarriers (NCs) to the lungs using propellant-based formulations, and to investigate the ability of such carriers to gain access to inclusions of an intracellular pathogen (*Chlamydia pneumoniae*), which is associated with a host of chronic and acute lung diseases.[6-7]

One natural (but as will be discussed, non-trivial) step towards the development of the next generation of formulations that may help achieve the full potential of oral inhalation formulations is to take advantage of the high functionality that may be embedded into polymeric nanocarriers (NCs).[8-9] However, there are several issues associated with the delivery of polymeric NCs to the lungs. Biocompatibility and clearance are two very important considerations.[8, 10] A stringent aerosol particle size requirement represents another important challenge.[11-12] The delivery efficiency of many traditional aerosol formulations is low due to the fact that a large fraction of the particles have aerosol sizes that are too large (> ~ 5μm), and are thus retained in the mouth and throat to reach in the digestive tract rather than lungs. In contrast, aerosol particles that are too small (< 0.4 μm, which is within the range of typical polymeric NCs described in the literature) are also expected to have very low deposition efficiency.[11]

Several approaches have been suggested in order to address the issues related to the aerosol size of polymeric NCs for oral inhalation formulations. However, most studies have focused on dry powder inhalers (DPIs) and nebulizers.[10, 13-14] While the formulation of nanoscale active pharmaceutical ingredients in pressurized metered-dose inhalers (pMDIs) has been documented in the literature,[15-16] to the best of our knowledge, there has been no previous study on the formulation of polymeric NCs in propellant-based inhalation devices.[17-18] pMDIs are of great technological relevance as they are the least expensive oral inhalation devices.[2] Moreover, they are portable, easy to use and have high compliance, making pMDIs the most widely used devices for administration of

therapeutics to the pulmonary tract.[2] Compared to DPIs and nebulizers, however, there is yet an additional challenge in the development of polymeric NC-based pMDIs: it has been shown to be difficult to stabilize particle dispersions in the low dielectric hydrofluoroalkane (HFA) propellants.[3, 19] The particles for pMDIs thus need not only to be within the desired size range, but must also have an appropriate surface chemistry – one that is well solvated by the propellant so as to prevent particle aggregation, which may otherwise negatively impact the aerosol characteristics of the formulation.[19-21]

Based on this rationale, we propose in this work to develop a core-shell formulation which facilitates the delivery of polymeric NCs using pMDIs. Our approach consists of entrapping NCs within micron-sized particles whose shell is designed to be well-solvated by the propellant, and thus to provide adequate physical stability to the formulation, and consequently good aerosol characteristics.[19, 22] A suitable particle engineering technology that allows for easy control of the particle size was devised to prepare the core-shell particles containing the polymeric NCs. The shell is also designed with two key features: (1) to maintain the integrity of the construct while dispersed in the propellant (shell is insoluble in the propellant), and (2) to break down when in contact with an aqueous fluid (shell is soluble in water).[19] The aqueous solubility is an important design consideration. The micron-sized particles containing the NCs need to disintegrate into its separate constituents (shell and NCs) in order to efficiently evade the immune system. Macrophages in the alveolar region are known to quickly engulf micron-sized particles.[23] If the target region is the upper airways instead of the alveolar region, it is also desirable to

quickly release the NCs as particles in the sub-micron-nano range are expected to have better penetration in the mucus layer, and will thus be more likely to reach the underlying epithelial layer.[24] The aqueous solubility, biodegradability and low molecular weight of the shell are also important design considerations when selecting the appropriate chemistry of the polymer shell as the residence time of the polymer in the lungs needs to be minimized, and its biodegradation accelerated.[14]

Chlamydia pneumoniae (C. pneumoniae) is an obligate intracellular bacterium that is associated with a broad spectrum of acute and chronic diseases.[25] *C. pneumoniae* is a common cause of upper and lower respiratory tract infections in humans (all age groups), and is one of the leading causes of community–acquired pneumonia. It has been also recently linked to neutrophilic allergic airway disease, a rare form of asthma characterized by neutrophilic inflammation.[7] *C. pneumoniae*-related infections have been associated with asthma exacerbations, and are considered an important cofactor in chronic airway inflammation.[6]

All Chlamydiae, including *C. pneumoniae,* undergo an unusual biphasic developmental cycle, which is of great relevance when considering the design of novel drug delivery strategies.[26] After the attachment of the infectious form of the organism (elementary body, EB) onto the host cells, EBs reside within a vacuole termed an inclusion, and subsequently develop into the non-infectious, metabolically active form called the reticulate body (RB). Reinfection occurs after RBs dedifferentiate back to EBs and are released back into the tissue milieu by host cell lysis. Importantly, *C. pneumoniae,* along with other chlamydial strains, can enter a persistent state which can give rise to diseases like arthritis and asthma.[26-27]

Despite proven effectiveness of certain antibiotics (currently having oral or parenteral administration regimens[27]) to treat primary chlamydial infections, in certain cases, the infection may become persistent owing to a combination of factors ranging from metabolic refractivity to treatment, reinfection, and/or inaccessibility of the antibiotic to the region of infection.[27-28] The ability to target the inclusion membrane, where chlamydial development, replication and dedifferentiation take place, may offer new opportunities to overcome not only primary infections, but also persistent infections, which have been linked to other medically relevant diseases including atherosclerosis, neurological disease, and inflammatory arthritis.[29-33]

Polymeric NCs may offer an opportunity to target chlamydial organism within the inclusions, as NCs have been shown to be excellent intracellular carriers, and can be tailored to encapsulate a variety of therapeutics including biomacromolecules.[8] Compared to free drugs, polymeric NCs have several other advantages including improved drug bioavailability, high carrier capacity, the ability to release the payload in a controlled manner and to adapt to different routes of administration,[13] and to concentrate in inflammatory and infectious sites by virtue of their enhanced permeability and retention.[8] Conjugating NCs with specific moieties has also been shown to enhance their targeting to specific cells and tissues.[8, 34] The delivery of polymeric NCs to the respiratory tract is, therefore, a promising strategy in the treatment of pulmonary infections caused by *C. pneumoniae*,[35] as well as a range of other pulmonary disorders including cystic fibrosis and lung cancer.[8, 36]

Based on this rationale, the aim of this work is to develop a pMDI-based platform capable of efficiently delivering polymeric NCs to the lungs, and to demonstrate the potential of the formulation in the treatment of a medically relevant disease (*C. pneumoniae*-related infections). More specifically, we sought to test the ability of those NCs to target Chlamydial inclusions in airway epithelial cells *in vitro*. In what follows, we describe (i) the synthesis of the NCs with a fluorescent marker that allows us to follow the fate of the NCs *in vitro*; (ii) the engineering of micron-sized, core-shell particles that provides for a means of encapsulating the NCs onto particles with suitable sizes for oral inhalation delivery and with enhanced physical stability in HFA propellants; (iii) the aerosol characteristics of the corresponding NC-based pMDI formulations; and (iv) the ability of those formulations to target chlamydial inclusion membranes in airway epithelial cells.

2.2 Materials

Poly(d,l-lactide-co-glycolide) (PLGA, 50:50, MW 31.3 - 45.0 K) was purchased from Birmingham Polymers. Poly-vinyl alcohol (PVA), 6-Coumarin (98%) and Tin(II) 2-ethylhexanoate (95%) were purchased from Sigma. Chitosan (CS, medium molecular weight) was purchased from Aldrich Chemicals Ltd. D,L-lactide was obtained from Frinton Laboratories Inc., and was recrystallized twice from ethyl acetate. 2H,3H perfluoropentane (HPFP, Vertrel XF, > 99.5% purity) was kindly provided by TMC industries. 1,1,1,2,3,3,3-heptafluoropropane (HFA227, Dymel, pharmaceutical grade, purity > 99%) was a gift from Dupont Inc. Pressure proof glass vials (6800318) were purchased from West Pharmaceutical Services. The

metering valves (EPDM Spraymiser) were a gift from 3M. Actuators from Ventolin HFA® (Glaxo Smithkline) were used for cascade impaction studies. Deionized (DI) water (Nanopure Barnstead) with a resistivity of 18 $M\Omega \cdot cm^{-1}$ was used in all experiments. All other chemicals were obtained from Fisher and were of analytical grade.

2.3 Methods

2.3.1 Preparation and morphological characterization of the 6-Coumarin-loaded PLGA NCs.

Poly(d,l-lactide-co-glycolide) (PLGA) NCs were prepared by an emulsion solvent evaporation technique previously described in the literature.[37] Briefly, a 1 ml polymer solution (100 mg PLGA in 1 ml chloroform) containing a known concentration of 6-Coumarin (120 μg) was emulsified in a 2 % (w/v) poly(vinyl alcohol) (PVA) aqueous solution (5 ml) with the help of a sonicating probe (Omni Ruptor 250, Omni international Inc.) set to 55 W, for a period of 3 minutes. The resulting oil-in-water emulsion was stirred overnight. The organic phase evaporates, thus forming the dye-laden NC dispersion in water. The NCs were recovered by centrifugation (13000 rpm for 60 minutes at 4 °C, Thermo Fisher Sorvall Legend X1R), and then washed repeatedly with DI water to remove residual PVA. The NCs were subsequently lyophilized, and their morphology confirmed by scanning electron microscopy (SEM, Hitachi S-2400). Several drops of an aqueous dispersion of the NCs were transferred onto a cover glass slide (18 mm^2, Corning Inc.) and allowed to dry. The substrates were then sputter-coated with gold (Ernest Fullam) for 30s, and

SEM micrographs taken at 22 kV. The size of the PLGA NCs after lyophilization was determined by dynamic light scattering (DLS, ZetaPlus, Brookhaven Instruments, Holtsville, NY).

2.3.2 Preparation and morphological characterization of the core-shell particles containing the PLGA NCs.

Core-shell particles with a shell composed of oligo(lactide)-grafted-chitosan (*LA-g-CS*) co-oligomer and a core comprising of dye loaded PLGA NCs were prepared by a modified emulsification diffusion technique.[19] Medium molecular weight CS was degraded in presence of hydrogen peroxide to 1,400 Da as determined by size exclusion chromatography (Shimadzu LC-10ADVP), with a static light scattering detector and differential refractometer (BIMWA, BIDNDC, from Brookhaven). Known amounts of degraded CS and DL-lactide were charged into a dry vessel containing toluene. The contents were dispersed, and then made to react over an oil bath at a temperature of 110 °C in presence of tin (II) 2-ethylhexanoate for over 48 hours. The final product obtained was repeatedly washed with acetone, centrifuged, dried using a light stream of air, and stored in a desiccator. The copolymer obtained was characterized by NMR. The *LA* grafting ratio onto the CS was calculated to be 108% based on the weight difference before and after grafting as reported previously.[19] The procedure for encapsulating the NCs consisted of dissolving 25 mg of *LA-g-CS* in 0.9 ml DI water. Subsequently, 35 mg of dye-loaded PLGA NCs were added to the same solution, and the contents were dispersed gently using a sonicating probe. Once dispersed, the aqueous phase was emulsified into

19 ml ethyl acetate in a sonicating bath (VWR P250D, set to 180 W for 15 min). The water-in-oil emulsion thus formed was transferred into a round bottom flask containing a larger volume of ethyl acetate (200 ml). Due to the high solubility of water in ethyl acetate, the water that makes the dispersed emulsion phase diffuses out (similar to the solvent evaporation method) into the bulk phase, resulting in the formation of core-shell particles, as the interfacially active co-oligomer remains at the interface. The core-shell particles were collected by centrifugation and their morphology confirmed by SEM, TEM, and fluorescence microscopy. A small amount of the core-shell particles was dispersed in the model propellant (HPFP). Some drops of the dispersion were then transferred onto glass slides and dried. For SEM studies, the substrate was sputter coated as described earlier. For the fluorescence microscopy studies, the glass slides were directly observed under a fluorescence microscope (Nikon Diaphot 300, USA). For TEM analysis, the particle dispersion in HPFP was deposited onto a 200-mesh copper grid and observed at 200 kV. For DLS measurements, an appropriate mass (5 mg) of freshly prepared core-shell particles was dissolved in a known volume (3 mL) of serum-free culture media or DI water. The resulting NC dispersion was gently dispersed using a probe sonicator (OmniRuptor 250) and analyzed immediately using Zetasizer™ (Nano, Malvern Instruments) to determine the size of the NCs released from the oligomeric shell.

2.3.3 Loading of the NCs onto the *LA-g-CS* core-shell particles, and total 6-coumarin content.

In order to determine the loading of the PLGA NCs onto the core-shell particles, a simple gravimetric technique was employed. Briefly, a known mass of the core-shell particles was initially loaded in a known volume of DI water. As the *LA-g-CS* co-oligomer is soluble in water, the PLGA NCs were immediately released, and dispersed into the continuous phase. After the complete dissolution of the shell, a known volume of chloroform was added to the aqueous phase and the mixture was then transferred to a separating funnel and shaken vigorously to speed the dissolution of the polymer into the organic phase. While PLGA and 6-Coumarin are highly soluble in chloroform, the *LA-g-CS* shell is not. The organic phase was then carefully collected onto pre-weighed aluminum pans, evaporated, and weighed. The difference in the mass of the aluminum pans after evaporation of the solvent is the mass of the PLGA NCs. Based on the total mass added to the aqueous phase and the mass of the NCs, the loading of the NCs into the *LA-g-CS* particles was determined. Subsequently, the 6-Coumarin content in the NCs was determined by extracting the dye from the polymer by soaking in methanol which is a good solvent for only the dye, for 12 hours. The methanol extract was filtered (0.45 μm, VWR), and analyzed for levels of 6-Coumarin using high performance liquid chromatography (HPLC), with a reverse phase C_{18} column (100×3.5 μm, Waters). A fluorescence detector (Waters, Model 2475) set at an excitation wavelength of 450 nm and emission wavelength of 490 nm was used to quantify the levels of 6-Coumarin in the

extract by comparison to a standard curve. The experiments were performed in triplicate.

2.3.4 Calu-3 cell culture and infection with *C. pneumoniae*.

Calu-3 cells were purchased from ATCC (ATCC#: HTB-55; Manassas, VA). The cells (passage 20-24) were maintained in Dulbecco's Modified Eagle Medium (DMEM) supplemented with 10% Fetal Bovine Serum (FBS, Atlanta Biologicals, Lawrenceville, GA), 0.02% (100 μl) gentamycin (Sigma) and 200 mM of 10 mL (2%) 100X L-glutamine (Sigma). *C. pneumoniae* (strain AR-39) was cultured as described earlier.[38] Calu-3 cells were seeded onto two well chamber slides (NUNC, Rochester, NY) at a density of 1×10^6 cells per chamber, and allowed to attach for about 6 hours prior to infection. The growth medium was aspirated from the chambers and the cells in one of the chambers were infected with *C. pneumoniae* at a multiplicity of infection (MOI) of ~5 (5×10^6 inclusion forming units (IFU). The cells in other chamber were left uninfected as control. The cells were then incubated at 35 °C for one hour with gentle rocking of the chamber slides every 15 minutes in order to distribute the inoculum evenly on the cells, and to facilitate attachment and uptake of the IFUs. The inoculum was aspirated, and the cells were incubated at 35 °C in a freshly prepared growth medium supplemented with 1 $\mu g \cdot ml^{-1}$ cycloheximide (Sigma) for 72 hours. Infected and uninfected cells were fixed with absolute methanol and stained with Pathfinder FITC-labeled anti-chlamydial LPS antibody (Bio-Rad, Redmond, WA) and observed under a fluorescent microscope (Nikon E600) to

determine the level of infectivity. Images of the infected cells and cell clusters were captured using ImagePro Plus (Media Cybernetics, Bethesda, USA).

2.3.5 Pulsing of the infected cells with the core-shell particles and PLGA NCs.

Infected cells were pulsed with both the dye-loaded PLGA NCs, and the *LA-g-CS* core-shell particles containing the dye-loaded PLGA NCs. Pulsing was carried out at 72 hours post infection (hpi) when inclusions were approaching maximum size. Both infected and the uninfected (control) cells in the respective two chambers were pulsed. In a typical experiment, a known concentration (0.600 $mg \cdot ml^{-1}$ of core-shell particles containing the dye-loaded NCs, or 0.25 $mg \cdot ml^{-1}$ of PLGA NCs alone) of freshly prepared particles were dispersed in serum-free culture media with the help of a sonicating bath. In the case of the core-shell particles, this process results in the immediate release of the NC, as the co-oligomer is water-soluble. The medium containing the particles (0.5 ml) was then added to the chamber slides. The total volume of each chamber was maintained at 1 ml for the duration of all experiments. The cells were then incubated at 35 °C for up to 3 hours post pulsing (hpp).

2.3.6 Imaging of the Calu-3 cells post-infection and post–particle pulsing.

Imaging of the infected cells pulsed with the NCs were performed using fluorescence and confocal microscopy. The fluorescence microscopy procedure for the infected cells pulsed with NCs involved 4 sets of two chamber slides (a total of eight chambers). Out of the 8 chambers, 4 were infected with C. *pneumoniae*, and four of the chambers were uninfected. All of the chambers were prepared at the

same time to ensure consistency. Among the four infected chambers, two were pulsed with core-shell particles and two with dye loaded NCs in the absence of *LA-g-CS* shell. The remaining four chambers that were uninfected also received the same concentration of both types of particles and served as controls. Cells in the respective chambers were observed at 15 minutes (0.25 hours) and 3 hours post pulsing (hpp). Chamber slides intended for fluorescence microscopy were washed twice with PBS, fixed with 4% paraformaldehyde, and counterstained with Evans' Blue (Sigma) prior to imaging.

Confocal microscopy was also performed on another set of Calu-3 cells that were similarly infected with *C. pneumoniae* and pulsed with the particles as described above. Cells were fixed with 4% paraformaldehyde in PBS, and counter staining with Evan's Blue. The confocal imaging system consisted of a conventional fluorescent microscope with a Zeiss Axiophot Triple-Camera Photomicroscope and the Zeiss live cell imaging microscope with Apotome module capable of four dimensional imaging (and 3D in time). Stacks of 0.7 μm were analyzed axially for 6-Coumarin fluorescence. Confocal images were then quantified for their fluorescence intensity using the Metamorph Software (Molecular devices, CA).

2.3.7 Physical stability of PLGA NC-loaded core-shell particles in propellant HFAs.

A known mass of the core-shell particles containing the dye-loaded PLGA NCs was added to pressure proof vials and crimp-sealed using 50 μl metering valves. A known volume of the propellant HFA227 was then pressure-filled into the vials with

the aid of a manual syringe pump (HiP 50-6-15) and a home-made pressure filler, such that the concentration of the core-shell particles in the system was 2 $mg \cdot ml^{-1}$. The formulation was then subjected to gentle sonication in a low energy sonicating bath (VWR, P250D, set to 180 W) in order to break down any large aggregates. Digital images of the dispersed formulations as a function of the dispersion age (time after initial sonication had been stopped) were used as a qualitative measure of the physical stability of the dispersion. HFA227 formulations containing 2 $mg \cdot ml^{-1}$ and 0.2 $mg \cdot ml^{-1}$ PLGA NCs alone, without being formulated in the core-shell particles, were also prepared as described above in order to directly compare the quality of the dispersion to that with the *LA-g-CS* shell chemistry.

2.3.8 Aerodynamic characteristics of the formulations.

An Anderson Cascade Impactor (ACI, CroPharm Inc.) was used to quantitatively assess the aerosol characteristics of the core-shell formulations in the propellant HFA227. The ACI was fitted with an USP induction port and was operated at a standard flow rate of 28.3 $l \cdot min^{-1}$. Experiments were carried out at 298 K and 45% relative humidity. Prior to running the experiment, several shots of the formulations were fired to waste. A commercial actuator (Ventolin HFA®, Glaxo Smithkline) was used in all runs. Shots (a total of 20) with an interval of 10 seconds per actuation were fired into the ACI. The experiments were conducted in triplicate (with three independent formulations/canister), and the average of the three runs and their standard deviation are reported here. After each experiment, the apparatus was disassembled and each of the stages, along with the actuator and the induction port

of the ACI, were thoroughly washed with a known volume of methanol and collected separately. The 6-Coumarin content of the particles was assessed as described earlier. Based on the analysis of the total 6-Coumarin loading onto the core-shell particles, we can thus determine the mass of both the PLGA and the *LA-g-CS* shell particles on each stage. The results are calculated as mass and as percentages. The fine particle fraction (FPF), mass median aerosol diameter (MMAD) and geometric standard deviation (GSD) were determined from the aerosol studies. The FPF is defined as the percentage of particles on the respirable stages of the impactor (stages 3 to terminal filter) over the total particle content (IP to the filter). Respirable fraction (RF) is defined as the percentage of particles on stages 1 to filter, over the total particle content. MMAD is determined by plotting the aerosol particle size vs. cumulative percentage less than the size range on a log-probability scale, and interpolating for the value at 50 wt% of the aerosol size distribution. GSD is defined as the square root of the ratio of 84.13% over 15.87% particle size distribution from the same plot used to obtain MMAD, and it is a measure of the particle size distribution.[22] The single puff dose is obtained by dividing the total mass of the formulation fired from each canister to the total number of puffs fired during each run, which in this case was 20. Canisters of dye-loaded PLGA NCs, at a concentration of 0.2 $mg \cdot ml^{-1}$ in propellant, were also prepared. This concentration was used (instead of 2 $mg \cdot ml^{-1}$ as core-shell particles), as it corresponds to the concentration of NCs in 2 $mg \cdot ml^{-1}$ core-shell particles. The aerosol characteristics of these formulations were determined using the same procedure as described earlier for the core-shell particles.

2.4 Results and Discussion

2.4.1 Characterization of the dye-laden PLGA NCs.

PLGA was chosen as the model polymer to prepare the NCs in this work due to its biodegradability, aqueous dispersibility, and its ability to traffic into the cell cytosol with relative ease.[39] Another important property of PLGA-based NCs is their ability to sustain the release of therapeutic agents.[37, 39] This is particularly useful in delivering antibiotics and other drugs to tissues where persistent infections may exist (as is the case of chlamydial infections). It has also been shown that PLGA NCs delivered intratracheally to mice invoke least inflammation in the lung when compared to other chemistries, indicating the benign nature of the polymer *in vivo*.[40]

PLGA NCs were prepared by emulsification solvent-evaporation as described above. The NCs were loaded with a fluorescent dye, 6-Coumarin, thus providing for a means to follow the localization of the PLGA NCs in the lung airway epithelial Calu-3 cells.

The loading of the dye also demonstrates the ability to encapsulate hydrophobic solutes as a potential payload into the PLGA NCs. The NCs were characterized for their size and shape using DLS and SEM, and the results are as shown in Figure 2.1.

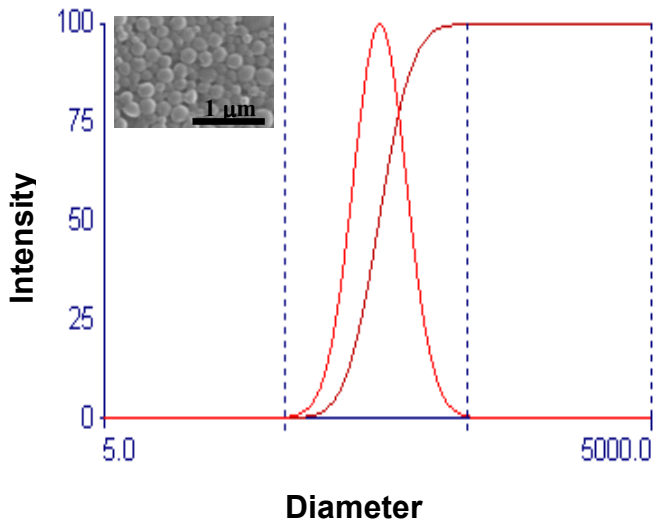

Figure 2.1. Size and morphology of the PLGA NCs as determined by dynamic light scattering (DLS) and (*inset*) scanning electron microscopy (SEM).

The results indicate the formation of spherical and slightly polydisperse particles as expected,[37] with an average diameter of 241 ± 4.7 nm, and a polydispersity of 0.13.

2.4.2 Characterization of core-shell particles containing dye-laden PLGA NCs.

2.4.2a Particle size and morphology.

Core-shell particles containing the NCs and an interfacially active co-oligomer as the shell were prepared by a modified emulsification-diffusion methodology, as previously described by our group.[19] The central idea of the methodology is that an aqueous phase containing the co-oligomer and the solute of interest is first emulsified into an organic phase in which water has a considerable solubility. As the

emulsion thus formed is diluted into a larger volume of the organic solvent, the water is forced to diffuse out from within the emulsion droplet core and into the continuous (organic) phase, causing super saturation of the solute, which leads to nucleation and growth of the core, templated by the spherical emulsion droplet. As the co-oligomer is interfacially active, it remains at the water-organic interface (of the emulsion droplet) during the process. The co-oligomer, therefore, becomes the particle shell. The outer most portion of the shell (*LA*) has been designed to be well-solvated by HFA, and thus to enhance the dispersibility of the particles in the propellant.[19, 41] In the present study, we extend this methodology for the encapsulation of water-dispersible particles. The dye laden PLGA NCs were loaded within the core of the *LA-g-CS* co-oligomer using the same methodology as described above, except that the NCs were dispersed in water instead of the drug (aqueous solution), as described in the Materials and Methods section. SEM micrographs shown in Figure 2.2 were obtained to confirm the morphology of the particles.

The particles are spherical and polydisperse in nature, with sizes ranging from approximately 0.5 μm to 4 μm. This size range is expected to be appropriate for the delivery of particles to the lungs, as they tend to have improved pulmonary penetration – the actual average aerodynamic size will be determined as discussed later. The aerosol size can be optimized to target particular region of the lungs, as the size and the polydispersity of the particles obtained using such methodology can be tuned by varying processing parameters of the emulsification-diffusion technique.[19]

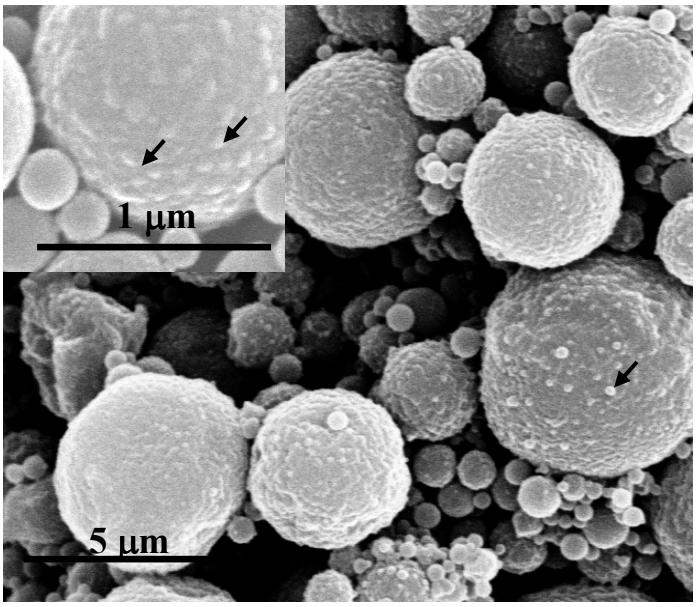

Figure 2.2. SEM micrographs of the LA-*g*-CS core-shell particles containing the PLGA NCs. The particles were prepared by the emulsification diffusion, at 298 K. *Inset:* a high magnification image of the core-shell particles showing the corrugated morphology of the particle surface. The arrows in the inset show NCs trapped at the particle surface. The arrow in main micrograph shows a NC that was not encapsulated.

A closer examination of the SEM micrographs also indicates the presence of some free NCs that were not encapsulated, and some nestled on the surface of the polymeric shell. Some of the PLGA NCs are expected to become trapped at the oil-water interface during the emulsification diffusion process. While they are not necessarily interfacially active, once adsorbed, the adsorption energy of the particles is very high, and they remain attached at the interface. The adsorption of particles at

the oil-water interface is a well-established emulsion stabilization process, giving rise to the so-called Pickering emulsions.[42]

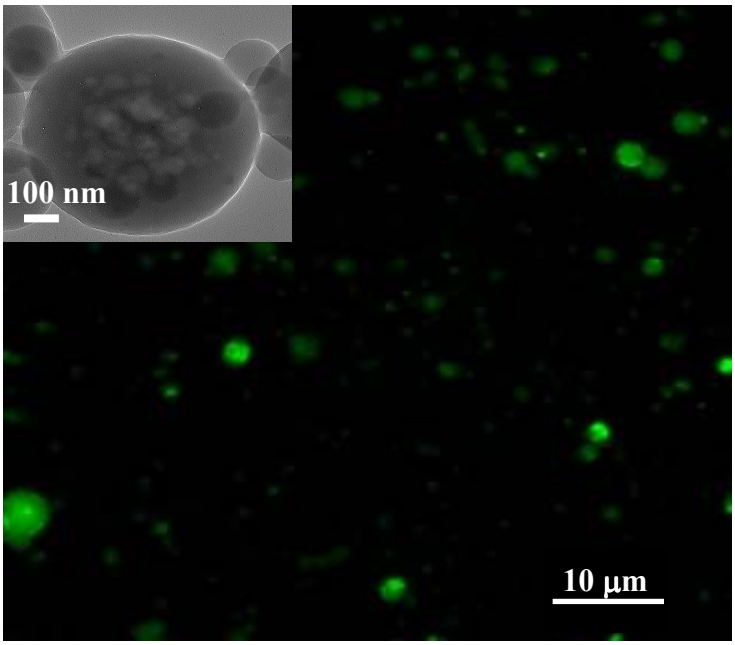

Figure 2.3. Fluorescent field microscope image of the core-shell particles containing the fluorescent green dye-laden NCs. (Inset) TEM image of a core-shell particle.

The fluorescent image and TEM micrograph shown in Figure 2.3 and inset, respectively, further confirm the encapsulation of the NCs in the core-shell morphology as suggested by the fluorescent green micron particles (from the dye encapsulated within the NCs), and further by the observation of nanoparticles within the micron particles as revealed by the regions with different contrast inside the micron particle detailed in the TEM image.

The integrity of the NCs after encapsulation within the core-shell particles was also evaluated, by determining the size of the NCs before and after the formation of

the core-shell particles via DLS. The experiment consisted in adding the core-shell particles to either DI water or DMEM (serum-free), and measuring the size of the particles in those media so to compare to the results before encapsulation. DLS results show that the size of the NCs remained the same before and after the encapsulation within the core-shell particles, indicating that there is no aggregation of the NCs, and that the shell breaks down immediately in both water and DMEM, as no micron-sized particles could be observed.

2.4.2b Loading of the PLGA NCs within the core of the *LA-g-CS* microparticles.

The loading of the PLGA NCs within the core-shell particles was determined gravimetrically, using the solvent extraction technique as described above. A known mass of freshly prepared core-shell particles was dissolved completely in water, thus releasing the NCs entrapped within the core, as the oligomer is water soluble. A specific volume of chloroform was added to this aqueous phase and the system mixed for several minutes and then allowed to equilibrate. Since PLGA and 6-Coumarin are both soluble in chloroform (the co-oligomer is not), this step will ensure the complete dissolution of those components into the organic phase. This experiment was repeated in triplicate. The loading of NCs entrapped within the core-shell particles was determined to be 10.5 ± 2.1%. The contents were then resolubilized in chloroform and then subjected to HPLC analysis to determine the 6-Coumarin content. The results revealed a loading of 0.08 ± 0.02% in weight (to that of PLGA).

2.4.3 Infection of Calu-3, a Model of the Airway Epithelial Cells, with *C. pneumoniae*.

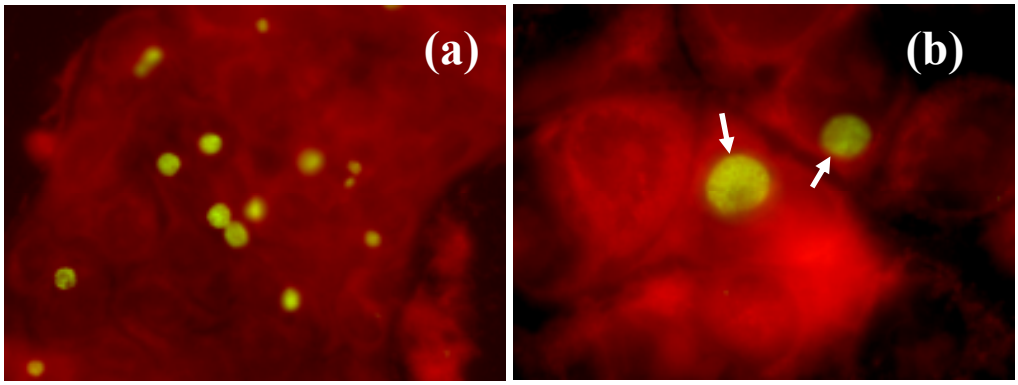

Figure 2.4. Fluorescence microscopy images of Calu-3 cells infected with *Chlamydia pneumoniae* captured 72 hours post infection (hpi) at a MOI of 5. The inclusions are seen in green and some have been selected (denoted by the white arrows). The cells were fixed with methanol and stained with *Chlamydia* Pathfinder antibody (green). The original images were obtained at 40x (left) and 100x (right) magnification

Calu-3 cells were infected with *C. pneumoniae* as detailed above. Figure 2.4 is a set of fluorescent microscope images at different magnifications which indicate the successful infection of the Calu-3 cells. The infection was confirmed by staining the cells with FITC-labeled anti-chlamydial lipopolysaccharide antibody, which detects the presence of *Chlamydiae in inclusions.* The images shown in Figure 2.4 were obtained at 72 hpi, and they clearly illustrate high levels of infectivity.

2.4.4 Pulsing and imaging of *C. pneumoniae* infected Calu-3 cells.

After infection with *C. pneumoniae*, the Calu-3 cells were then pulsed (at 72 hpi) with either the core-shell particles containing the dye-loaded NCs, or the dye-loaded PLGA NCs alone. Core-shell particles containing the NCs and bare dye-laden NCs were pulsed onto Calu-3 monolayers at concentrations of 0.6 $mg \cdot ml^{-1}$ and 0.25 $mg \cdot ml^{-1}$, respectively. Core-shell particles were pulsed at the aforementioned concentration as it was found to be non-cytotoxic. Cellular ATP levels (MTS assay) reveal that core-shell particles within the concentration range of from 0.1 to 6 $mg \cdot ml^{-1}$ are non-cytotoxic to Calu-3 cells. The concentration of NCs was chosen based on concentration ranges previously studied to interpret cellular internalization.[37, 43]

As a negative control, additional wells of uninfected Calu-3 cells were also pulsed with both types of particles. *C. pneumoniae* inclusions are slow to develop and take about 72-96 hours to completely differentiate to new EBs.[44] Hence the experiments performed on *C. pneumoniae*-infected cells were performed at 72 hours after infection. Calu-3 cells were chosen for this purpose as they best represent the airway epithelium.[5] Moreover, Calu-3 cells were shown to internalize particles of various chemistries supporting the applicability of this particular cell line for our study.[45]

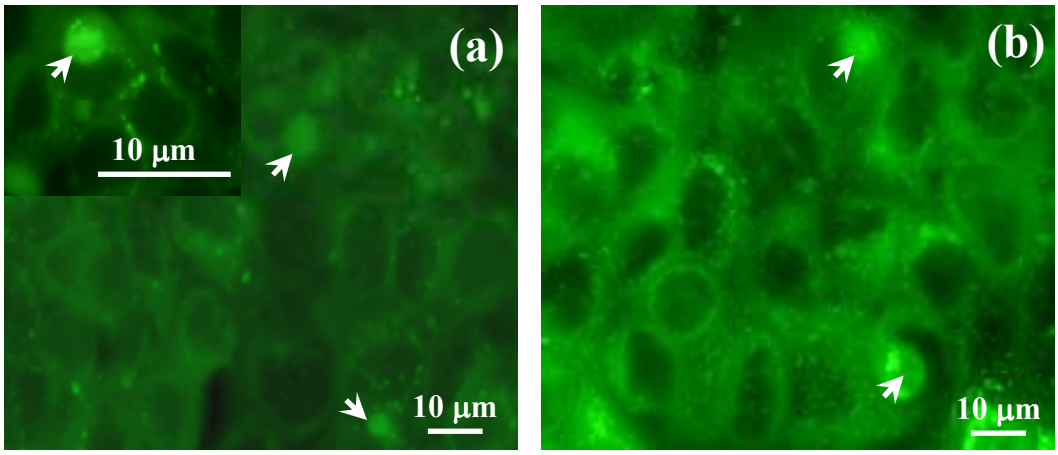

Figure 2.5. Fluorescent microscopy images of Calu-3 cells infected with *C.pneumoniae* and pulsed with (a) NC-laden core-shell particles, and (b) bare NCs. The images were captured using a 40X magnification 72 hours post infection (hpi) and 3 hours post pulsing (hpp). White arrows in the images indicate the location of inclusions within the cytosol. The increased fluorescence intensity in (b) is indicative of the higher concentration of NCs when cells were pulsed alone (250 μg) compared to the concentration of NCs in cells that were pulsed with NCs encapsulated in the core-shell particles (600 μg). (*inset)* 100X fluorescent field image evidencing the presence of NC (released from the core-shell particles) within an inclusion.

The intracellular localization of the NCs pulsed onto the infected cells was monitored under a fluorescent microscope after pulsed cells were fixed with 4% paraformaldehyde and counterstained with Evans Blue. The results at 3 hpp are summarized in Figure 2.5 for the NC pulsed as core-shell particle system (Figure 2.5a) and for the bare NCs (Figure 2.5b). NCs are observed to be not only within the

cell cytosol, but also concentrated in the inclusion. Selected inclusions containing NCs are indicated by white arrows.

Figure 2.5 indicates that NCs in the core-shell particles and the bare NCs were readily internalized by the cells, presumably by fluid phase endocytosis. The images also suggest that the NCs are capable of not only entering the cell cytosol, but also readily gain access to the chlamydial inclusions. The internalization of the NCs in non-infected cells was also fast, and observed for both NC alone and NC within core-shell particle formulations. Similar results were observed for repeat experiements with other batches of NCs with similar sizes, and with Calu-3 cells infected with another chlamydial strain (*Chlamydia trachomatis*).

The strong and localized intracellular fluorescence can be attributed to the presence of the (dye loaded) NCs which entered the cells and concentrated in the inclusions. The concentration of free dye is expected to be very small at such short times (3hs), as less than 1% leaches out of the NCs after a 24 hour incubation period in physiological buffer (PBS, pH 7.4) at 37°C.[37] This is an important finding and suggests the ability of the NCs to gain entry into the chlamydial inclusion can be exploited for delivering drugs and therapeutics to sites of this bacterial infection in the lungs.

Cells traffic NCs through a multitude of mechanisms that vary with cell types. [13, 43, 46] Some of the salient ones include phagocytosis and endocytosis (either fluid phase or receptor mediated).[39, 43] Most epithelial cell lines have been shown to internalize NCs through an endocytic pathway.[43] This was observed in the case of two prominent airway epithelial cell lines.[43, 47] Although the rate and the extent

of uptake can vary, a similar endocytic route can be suggested as a possible route of uptake for Calu-3 as well. While we report the results obtained at 3 hpp, it is worth mentioning that the NCs (both bare and from the core-shell ensemble) gained access to the cell cytosol within minutes after pulsing (images not shown) both infected and uninfected cells. These results corroborate previous studies that suggest that such rapid NP uptake occurs through an endocytic pathway.[37, 43]

To unambiguously confirm the uptake of the NCs into chlamydial inclusions, sections of confocal micrographs of Calu-3 cells infected with *C. pneumoniae* and pulsed with NCs and core-shell particle containing NCs were analyzed. The results are summarized in Figures 2.6(a) and (b). Inclusions within the cells were selected, and the fluorescence intensity of the planes across the inclusion was recorded. The bar graphs insets represent fluorescence intensities normalized by the area being observed (area increases towards the equatorial region of the inclusion). Images of selected planes are shown below the plots. Figure 2.6a represents cells pulsed with the core-shell particles containing the NCs and Figure 2.6b depicts the results for bare NCs.

The quantitative results from the confocal images (fluorescence intensity) corroborate the qualitative information obtained from the fluorescence micrographs (Figure 2.5).

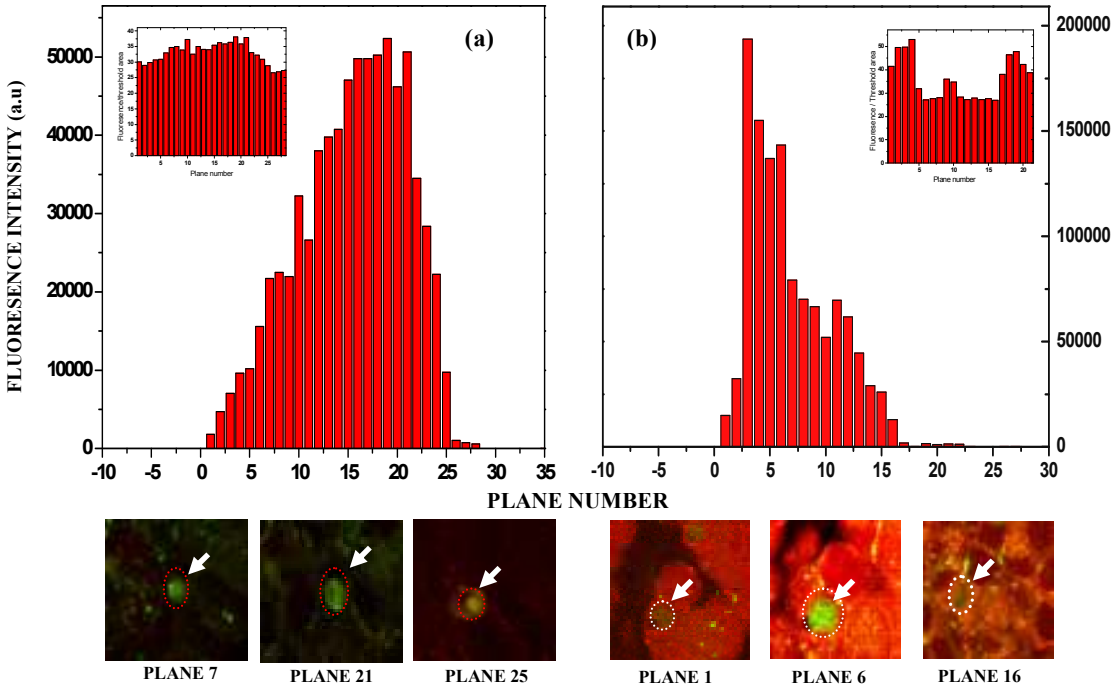

Figure 2.6. Fluorescence intensity (a.u.) from selected chlamydial inclusions vs. plane number across the inclusion obtained from confocal micrographs of Calu-3 cells infected with *C. pneumoniae* (72 hpi) and 3 hours post pulsing (3 hpp) captured at 40X magnification with (a) PLGA NCs formulated within core-shell particles, and (b) bare PLGA NCs. The sets of images shown below the plots represent different planes across the selected inclusion. The inset plots are the fluorescence intensities normalized with respect to the threshold area.

They show that the NCs are located not only within the cytoplasm, but clearly gain access and concentrate within the inclusion as well – the inset with normalized intensity as the planes cross the inclusion show strong intensity at all planes inside the inclusion. The difference in the fluorescence intensities between the two

systems (bare NCs vs. NCs within core-shell particles) can be attributed to lower concentration of the NCs pulsed along the core-shell particles compared to the NCs alone.

One can speculate on the mechanism of access of the NCs onto the inclusions based on how such negatively charged particles gain access into the cell cytoplasm. As mentioned earlier, the internalization of PLGA NCs into the cell cytosol occurs through an endocytic pathway where the primary endosomes traffic the NCs and direct them to a sorting compartment (sorting endosomes) from where most NCs are transferred to secondary endosomes. Under normal circumstances, these secondary endosomes will merge with lysosomes to form endo-lysosomes.[37, 39] However, chlamydiae inhibit phagosome/lysosome fusion and this may account for the observed concentration of NCs in the inclusions, as they do not proceed further in the endocytic pathway.[48-49] It is also important to note that the NCs did not gain access to the cell nuclei in neither infected nor uninfected cells, as desired, since the target here are the inclusions. While the details of the internalization mechanism, and the fate of the internalized NCs fall outside the scope of this work, such studies could help shine light into the effect of several important parameter such as NC chemistry and size.[37, 43, 50]

This unique characteristic of the NCs can be exploited as a tool for delivering therapeutics through the respiratory tract to treat local and systemic disorders including chlamydial infections. However, this can only be accomplished if such NCs can be formulated in oral inhalation delivery devices, and efficiently delivered to the

lungs. In the next sections we discuss how this can be achieved using the inexpensive and widely used pMDIs.

2.4.5. Dispersion stability of NC-laden core-shell formulations in HFA 227.

Dispersion stability of the PLGA NCs alone and those formulated as core-shell particles was determined in the propellant HFA227. The physical stability of the dispersion was qualitatively assessed through sedimentation rate experiments at 298 K and saturation pressure of the propellant. Particles were weighed, fed into pressure proof vials, crimp sealed and then dispersed using a sonicating bath. The formulation stability was monitored as a function of the time after sonication was stopped (age of the dispersion). Digital images of the prepared aerosols at the starting point (0 time - insets) and a certain time after the system was dispersed are shown in Figure 2.7 –NCs alone are shown as insets.

The results show that PLGA NCs alone are poorly stable in HFA227 propellant. The NC formulation started flocculating copiously soon after (< 1 min) removal from the sonicating bath (Figure 7a). Similar results were observed at 2 and 0.2 mg NC per ml propellant. On the other hand, the *LA-g-CS* shell is clearly capable of imparting much superior stability to the core-shell particles containing the NCs, and can thus be used as a strategy for dispersing the NC in propellant-based pMDIs. A small creamed layer of flocculated core-shell particles can be seen after 3h (Figure 7b). This creamed layer was easily redispersible by simple mechanical shaking, indicating that the particles are loosely flocculated and not irreversibly aggregated – the same is not true for the NC particles when dispersed alone. In low

dielectric solvents such as HFAs, suspension stability may be achieved via steric stabilization, which is largely dictated by the ability of the solvent to solvate the stabilizing moieties – in this case the HFA-LA interaction.[19, 51]

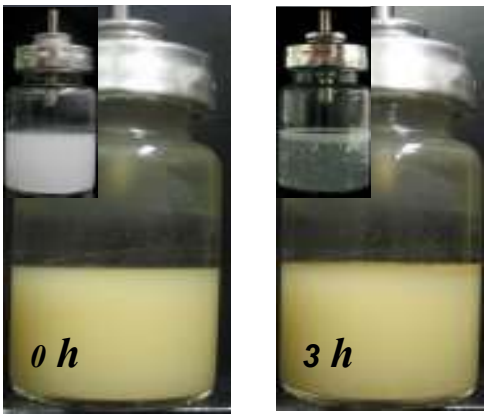

Figure 2.7. Dispersion stability of PLGA-laden LA-*g*-CS core-shell particles in HFA 227 at 2 mg.ml^{-1}, 298 K, and saturation pressure of the propellant mixture. The images were captured immediately after sonication (0 h) and 3 h after mechanical energy input ceased. *(inset)* Images of formulations prepared using PLGA NCs alone (no shell). Images were captured at the same time points mentioned above, and the formulation was prepared at the same particle concentration and also in HFA227 propellant.

2.4.6. Aerosol characteristics of the NP laden core-shell formulation.

An eight stage Anderson Cascade Impactor (ACI) was used to determine the aerosol characteristics of the core-shell pMDI formulations containing the NCs.[3] Freshly prepared canisters at 2 mg.ml^{-1} core-shell particles were actuated into the ACI, which was held at a constant flow rate. The particles are deposited on each of

the eight stages of the ACI, depending on the aerosol particle size, with larger particles (higher inertial impaction) being retained on the earlier stages of the impactor (from the induction port to stage 2), while the smaller particles find their way to the lower stages of the impactor (stages 3-7).[19] The aerosol characteristics (ACI) of the formulation at 0.2 $mg.ml^{-1}$ NC in HFA227 propellant, in the absence of a shell, were also determined. This concentration range is the nominal NC concentration in the ACI study of the core shell formulation, based on the estimated 10% loading of NCs. The amount of particles deposited onto the stages was determined using prescribed analytical techniques. The absolute (mass) deposition results for both bare NCs and core-shell NCs are given in Table 2.1. The results from Table 2.1 are expressed as percentages and shown in Figure 2.8.

Respirable and fine particle fractions (RF and FPF) are two parameters used to gauge the efficiency of lung deposition using pMDIs.[52] A higher FPF denotes greater deposition of the formulation in the deep lung.[19, 52] In addition to these parameters, other measures such as MMAD and GSD are relevant in the quantification of the aerosol characteristics of pMDIs, and were also determined from the ACI studies.[19, 52]

Table 2.1. Aerosol characteristics of the core-shell formulation containing biodegradable NCs (loaded with 6-Coumarin) in HFA227 at 298 K, saturation pressure of the propellant and 2 $mg \cdot ml^{-1}$ particle concentration. The results represent the average and deviation of three independent runs (*n*=*3*). RF denotes the respirable fraction, FPF, the fine particle fraction, AC = actuator, SP = spacer, and IP = induction port. MMAD and GSD are the mass mean aerodynamic diameter and geometric standard deviation, respectively

Stages	Total Particle concentration (μg) (Shell+NCs)	Concentration of NCs (μg)
AC	72.3 ± 11.2	7.6 ± 9.4
SP	123.8 ± 10.1	13.0 ± 11.2
IP	76.8 ± 1.2	8.1 ± 2.6
Stage 0 (9.0-10.0μm)	43.6 ± 1.9	4.6 ± 1.5
Stage 1 (5.8-9.0 μm)	78.1 ± 2.6	8.2 ± 1.9
Stage 2 (4.7-5.8 μm)	48.4 ± 0.2	5.1 ± 1.2
Stage 3 (3.3-4.7 μm)	84.3 ± 3.8	8.9 ± 0.5
Stage 4 (2.1-3.3 μm)	180.7 ± 2.0	19.0 ± 0.4
Stage 5 (1.1-2.1 μm)	114.5 ± 1.0	12.1 ± 1.5
Stage 6 (0.7-1.1 μm)	74.0 ± 2.6	7.8 ± 1.9
Stage 7 (0.4-0.7 μm)	19.2 ± 2.4	2.0 ± 1.6
Filter (0-0.4 μm)	72.3 ± 2.6	0.6 ± 2.7
Single Puff Dose (μg)	49.4 ± 4.7	4.9 ± 1.4
RF (%)	72.4 ± 2.2	
FPF (%)	55.2 ± 1.8	
MMAD (μm)	2.1 ± 0.8	
GSD	3.0 ± 1.2	

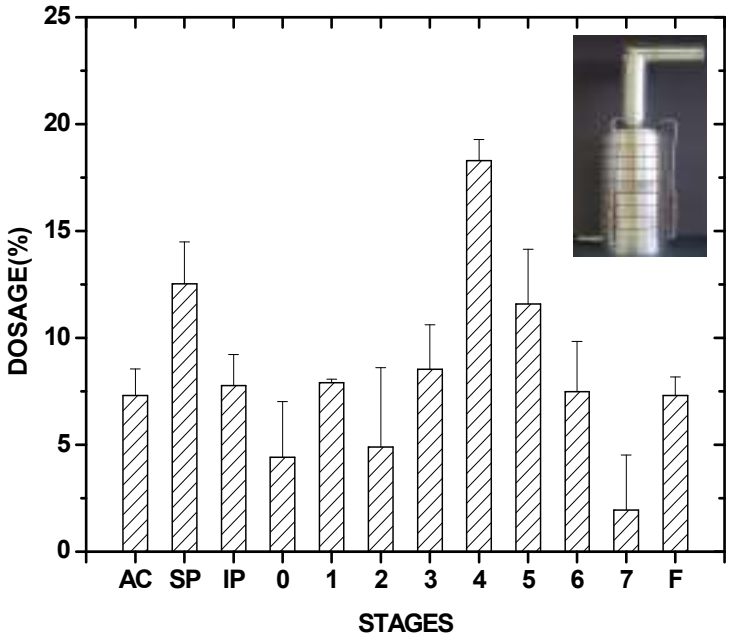

Figure 2.8. Aerodynamic characteristics of the core-shell microparticle formulation containing the PLGA NCs in HFA 227, at 298 K and saturation pressure of the propellant. Particle concentration was 2 $mg \cdot ml^{-1}$ (same as in Figure 7) AC, IP, SP, and F refer to actuator, induction port, spacer and filter, respectively. (*Inset)* A digital image of the impactor (Andersen Cascade Impactor, ACI) used to determine the aerosol fractions.

The impaction tests reveal a RF of 72 % and an FPF of 55% for the NC-based core-shell formulation. The RF and FPF for the bare NC based formulation were considerably lower, as expected, at 20.1% and 10.5%, respectively. A large fraction of the NC formulation was found to be entrapped in the actuator when compared to the stages of the ACI (vs. the amount found in the core-shell formulation), presumably due to the aggregation of the particles in the propellant in the absence of the stabilizing shell. It is also interesting to note that a significant portion of the

actuated dose in the formulation containing NCs alone was detected in the filter, in agreement to the much smaller MMAD - 0.5 μm for NC formulation compared to 2.1 μm for core-shell formulation.

We have shown in the past that particle stability in the propellant correlates with the aerosol characteristics of the corresponding formulation; i.e., formulations that have good dispersion stability also have good aerosol characteristics, and those with poor stability, have poor aerosol characteristics.[21-22] We have also demonstrated that this trend also holds at the particle-particle level (force of interaction), as determined by colloidal probe microscopy;[19] i.e., the ability of reducing particle-particle interactions as achieved here by the core-shell strategy, results in an improved dispersion stability and aerosol characteristics of the corresponding formulation. The experiments above are in agreement with those expectations and previous studies, in that the formulations containing NCs alone (not within core-shell particles) showed undesirable aerosol characteristics when compared to the NC formulation within the core-shell particles, as NCs alone are not dispersible in the propellant.

While no other NC-based pMDI formulation has been discussed in the literature yet, it is instructive to compare and contrast these results with other pMDI formulations. The FPF of 55% obtained here for the core-shell particles compares very favorably with Ventolin HFA®, a commercial formulation for asthma and chronic obstructive pulmonary disease (COPD) that has a reported FPF of 46%. An FPF of over 74% has been reported by our group from a core-shell formulation encapsulating free therapeutics (instead of NCs) – even higher values were achieved

with a spacer.[19] It is worth mentioning that the high FPF observed here may be further optimized by controlling the particle preparation parameters and the hardware as it is done in the industry. The proposed core shell formulation had an MMAD of 2.1 μm and a GSD of 3.0 μm, which was well within the desirable range for pMDIs.[19]

The aerosol results discussed above, which demonstrate the ability to efficiently formulate polymeric NCs in HFA-based pMDIs, suggest this approach to be a general strategy for the delivery of therapeutics to and through the lungs using pMDI formulations. Allied with the ability of such polymeric NCs (i) to target chlamydial inclusions within airway epithelial cells, as demonstrated in this work, (ii) to encapsulate effective carriers for a number of relevant chlamydial therapeutics including antibiotics and vaccine candidates,[35, 53] and (iii) recent developments in mucosal delivery with polymeric NCs[46, 54] point to the proposed strategy as a methodology for treating Chlamydia-related infections in the lung.

2.5 Conclusions

In this work we demonstrated polymeric NCs can be successfully formulated in propellant-based metered-dose inhalers. Biodegradable polymeric NCs were encapsulated within HFA-philic, biodegradable and water-soluble copolymer shells by emulsification diffusion. The core-shell particles thus formed provide for an opportunity to efficiently deliver NCs to the lungs, by enhancing their dispersibility in the propellant, and by providing the appropriate geometry (aerodynamic size) so as to enhance the aerosol characteristics of the corresponding pMDIs (RF of 72%, with

an MMAD of 2.3 μm). *In vitro* results reveal that NCs from such core-shell formulations can be readily internalized by Calu-3 (airway epithelial) cells infected with *C. pneumoniae*, and more importantly, they can gain access to chlamydial inclusions. These results are of great relevance not only for the potential treatment of chlamydial infections, but also in the treatment of a host of diseases where the regional (to the lungs) or systemic (through the lungs) delivery of drugs can be enhanced through the use of tailored polymeric NCs

Note – *This work was done with the assistance of Dr. Judith Whittum-Hudson, Professor of Immunology and Microbiology, Ms. Mirabela Hali, Ms. Arulselvi Anbalagan and Dr.Susan Wykes.*

2.6 References

[1] Patton JS, Byron PR. Inhaling medicines: delivering drugs to the body through lungs. Nature Reviews Drug Discovery. 2007;6:67-74.

[2] Laube BL. The expanding role of aerosols in systemic drug delivery, gene delivery and vaccination. Respiratory Care. 2005;50:1161-76.

[3] Rogueda P. Novel hydrofluoroalkane suspension formulations for respiratory drug delivery. Expert Opinion in Drug Delivery. 2005;2:625-38.

[4] Sakagami M. In vivo, in vitro and ex vivo models to assess pulmonary absorption and disposition of inhaled therapeutics for systemic delivery. Advanced Drug Delivery Reviews. 2006;58:1030-60.

[5] Forbes B, Ehrhardt C. Human respiratory epithelial cell culture for drug delivery applications. European Journal of Pharmaceutics and Biopharmaceutics. 2005;60:193-205.

[6] Hahn DL. Treatment of Chlamydia pneumoniae infection in adult asthma: a before-after trial. Journal of Family Practice. 1995;41:345-51.

[7] Horvat JC, Starkey MR, Kim RY, Beagely KW, Preston JA, Gibson PG, et al. Chlamydial respiratory infection during allergen sensitization drives neutrophilic allergic airways disease. Journal of Immunology. 2010;doi:10.4049.

[8] Davis ME, Chen Z, Shin DM. Nanoparticle therapeutics: an emerging treatment modality for cancer. Nature Reviews Drug Discovery. 2008;7:771-82.

[9] Lai SK, Wang YY, Hanes J. Mucus-penetrating nanoparticles for drug and gene delivery to mucosal tissues. Advanced Drug Delivery Reviews. 2009;61:158-71.

[10] Ryutting E, Nguyen J, Wang X, Kissel T. Biodegradable polymeric nanocarriers for pulmonary drug delivery. Expert Opinion in Drug Delivery. 2008;5:629-39.

[11] Rogueda PG, Traini D. The nanoscale in pulmonary delivery. Part 1: deposition, fate, toxicology and effects. Expert Opinion in Drug Delivery. 2007;4:595-606.

[12] Engstrom J, Tam J, Miller MA, Williams III RO, Johnston KP. Templated open flocs of nanorods for enhanced pulmonary delivery with pressurized metered dose inhalers. Pharmaceutical Research. 2009;26:101-17.

[13] Azarmi S, Roa WH, Lobenberg R. Targeted delivery of nanoparticles for the treatment of lung diseases. Advanced Drug Deliver Reviews. 2008;60:863-75.

[14] Sung JC, Pulliam BL, Edwards DA. Nanoparticles for drug delivery to the lungs. Trends in Biotechnology. 2007;25:564-70.

[15] Tam J, Engstrom J, Ferrer D, Williams III RO, Johnston KP. Templated open flocs of anisotropic particles for pulmonary delivery with pressurized metered dose inhalers. Journal of Pharmaceutical Sciences. 2010;10.1002/jps.22091.

[16] Rytting E, Nguyen J, Wang X, Kissel T. Biodegradable polymeric nanocarriers for pulmonary drug delivery. Expert Opinion in Drug Delivery. 2008;5:629-39.

[17] Rogueda PG, Traini D. The nanoscale in pulmonary delivery. part 2: formulation platforms. Expert Opinion in Drug Delivery. 2007;4:607-20.

[18] Yang W, Peters JI, Williams III RO. Inhaled nanoparticles - a current review. Int Journal of Pharmaceutical Sciences. 2008;356:239-47.

[19] Wu L, Bharatwaj B, Panyam J, da Rocha S. Core–shell particles for the dispersion of small polar drugs and biomolecules in hydrofluoroalkane propellants. Pharmaceutical Research. 2008;25:289-301.

[20] Peguin RPS, da Rocha SRP. Solvent-solute interactions in ydrofluoroalkane propellants. The Journal of Physical Chemistry B. 2008;112:8084-94.

[21] Wu L, Peguin RP, da Rocha SR. Understanding solvation in hydrofluoroalkanes: ab initio calculations and chemical force microscopy. The Journal of Physical Chemistry B. 2007;111:8096-104.

[22] Wu L, Al-Haydari M, da Rocha SR. Novel propellant-driven inhalation formulations: engineering polar drug particles with surface-trapped hydrofluoroalkane-philes. European Journal of Pharmaceutical Sciences. 2008;33:146-58.

[23] Kleinstreuer C, Zhang Z, Donohue JF. Targeted drug-aerosol delivery in the human respiratory system. Annual Review of Biomedical Engineering. 2008;10:195-220.

[24] Lai SK, O'Hanlon DE, Harrold S, Man ST, Wang YY, Cone R, et al. Rapid transport of large polymeric nanoparticles in fresh undiluted human mucus. Proceedings of the National Academy of Sciences (PANS) U S A. 2007;104:1482-7.

[25] Kern JM, Maass V, Maass M. Molecular pathogenesis of chronic chlamydia pneumoniae infection: a brief overview. Clinical Microbiology and Infection. 2009;15:36-41.

[26] Whittum-Hudson JA, Hudson AP. Human chlamydial infections: persistence, prevalence and outlook for the future. Natures Science SOC. 2005;13:371-82.

[27] Hammerschlag MR, Chirgwin RK, Roblin PM, Gelling M, Dumornay W, Mandel L, et al. Persistent Infection with *chlamydia pneumoniae* following acute respiratory illness. Clinical Infectious Diseases. 1992;14:178-82.

[28] Siewert K, Rupp J, Klinger M, Solbach W, Gieffers J. Growth cycle-dependent pharmacodynamics of antichlamydial drugs. Antimicrob Agents and Chemotherapy. 2005;49:1852-6.

[29] Balin BJ, Gerard HC, Arking JE, Appelt DM, Branigan PJ, Abrams TJ, et al. Identification and localization of chlamydia pneumoniae in the alzheimer's brain. Medical Microbiology and Immunology. 1998;187:23-42.

[30] Beatty WL, Byrne GI, Morrison RP. Repeated and persistent infection with chlamydia and the development of chronic inflammation and disease. Trends in Microbiology. 1994;2:94-8.

[31] Campbell LA, Kuo CC. Chlamydia pneumoniae - an infectious risk factor for atherosclerosis? Nature Reviews Microbiology. 2004;2:23-32.

[32] Inman RD, Whittum-Hudson JA, Schumacher RH, Hudson AP. Chlamydia and associated arthritis. Current Opinion in Rheumatology. 2000;12:254-62.

[33] Watson C, App NJ. Role of *chlamydia pneumoniae* in atherosclerosis. Clinical Science. 2008;114:509-31.

[34] Patil Y, Toti U, Khdair A, Ma L, Panyam J. Facile single-step multifunctionalization of nanoparticles for targeted drug delivery. Biomaterials. 2009;30:859-66.

[35] Hickey A, Lu D, Ashley ED, Stout J. Inhaled Azithromycin Therapy. Journal of Aerosol Medicine and Pulmonary Drug Delivery. 2006;19:54-60.

[36] Griesenbach U, Ferrari S, Geddes DM, Alton EW. Gene therapy progress and prospects: cystic fibrosis. Gene Therapy. 2002;9:1344-50.

[37] Panyam J, Labhasetwar V. Dynamics of endocytosis and exocytosis of poly(D,L-lactide-co-glycolide) nanoparticles in vascular smooth muscle cells. Pharmaceutical Research. 2003;20:212-20.

[38] Byrne GI, Ouellette SP, Wang Z, Rao JP, Lu L, Beatty WL, et al. Chlamydia pneumoniae expresses genes required for DNA replication but not cytokinesis during persistent infection of HEp-2 cells. Infection and Immunity. 2001;69:5423-9.

[39] Panyam J, Labhasetwar V. Biodegradable nanoparticles for drug and gene delivery to cells and tissues. Advanced Drug Delivery Reviews. 2003;55:329-47.

[40] Dailey LA, Jekel N, Fink L, Gessler T, Schmehl T, Wittmar M, et al. Investigation of the proinflammatory potential of biodegradable nanoparticle drug delivery systems in the lung. Toxicology and Applied Pharmacology. 2006;215:100-8.

[41] Peguin RPS, Wu L, da Rocha SRP. The ester group: how hydrofluoroalkane-philic is it? Langmuir. 2007;23:8291-4.

[42] Galindo-Rodriguez S, Allemann E, Fessi H, Doelker E. Physicochemical parameters associated with nanoparticle formation in the salting-out, emulsification–diffusion, and nanoprecipitation methods. Pharmaceutical Research. 2004;21:1428-39.

[43] Cartiera MS, Johnson KM, Rajendran V, Caplan MJ, Saltzman WM. The uptake and intracellular fate of PLGA nanoparticles in epithelial cells. Biomaterials. 2009;30:2790-8.

[44] Werringloer U-D, Gerard HC, Whittum-Hudson JA, Hudson AP. Chlamydophila (chlamydia) pneumoniae infection of human astrocytes and microglia in culture

displays an active, rather than a persistent, phenotype. The American Journal of Medical Sciences. 2006;332:168-74.

[45] Foster KA, Yazdanian M, Audus KL. Microparticulate uptake mechanisms of in-vitro cell culture models of the respiratory epithelium. Journal of Pharmacy and Pharmacology. 2001;53:57-66.

[46] Hillaireau H, Couvreur P. Nanocarriers' entry into the cell: relevance to drug delivery. Cell and Molecular Life Sciences. 2009;66:2873-96.

[47] Brzoska M, Langer K, Coester C, Loitsch S, Wagner TO, Mallinckrodt C. Incorporation of biodegradable nanoparticles into human airway epithelium cells-in vitro study of the suitability as a vehicle for drug or gene delivery in pulmonary diseases. Biochemical and Biophysical Research Communications. 2004;318:562-70.

[48] Fields KA, Hackstadt T. The chlamydial inclusion: escape from the endocytic pathway. Annual Review of Cell and Developmental Biology. 2003;18:221-45w.

[49] Scidmore MA, Fischer ER, Hackstadt T. Restricted fusion of chlamydia trachomatis vesicles with endocytic compartments during the initial stages of infection. Infection and Immunity. 2003;71:973-84.

[50] Grenha A, Grainger CI, Dailey LA, Seijo B, Martin GP, Remunan-Lopez C, et al. Chitosan nanoparticles are compatible with respiratory epithelial cells in vitro. European Journal of Pharmaceutical Sciences. 2007;31:73-84.

[51] Traini D, Young PM, Rogueda P, Price R. In vitro investigation of drug particulates interactions and aerosol performance of metered dose inhalers. Pharmaceutical Research. 2007;24:125-35.

[52] Smyth HD. The influence of formulation variables on the performance of alternative propellant-driven metered dose inhalers. Advanced Drug Delivery Reviews. 2003;55:807-28.

[53] Keegan ME, Whittum-Hudson JA, Saltzman MW. Biomimetic design in microparticulate vaccines. Biomaterials. 2003;24:4435-43.

[54] Roy I, Vij N. Nanodelivery in airway diseases: challenges and therapeutic applications. Nanomedicine 2010.

Chapter 3

Polymer Nanocarriers for Transport Modulation Across the Pulmonary Epithelium: Dendrimers, Polymeric Nanoparticles, and their Nanoblends

3.1 Introduction

Oral inhalation (OI) is not only the most sensible route for the regional administration of drugs to the lungs, but it has also been more recently recognized as a potential alternative platform for the systemic delivery of a host of therapeutic molecules.[1, 2] Some of the potential advantages of using the lungs as a portal to the systemic circulation include the lower enzymatic activity in the lung tissue,[2, 3] which may improve drug bioavailability,[1, 4, 5] and the large absorptive area and high vascularization of the alveolar region, which is expected to facilitate the transport of therapeutics.[2, 3, 6] As a matter of fact, literature reports indicate that the peak in the systemic circulation of many if not most small molecule therapeutics delivered to the lungs via OI is in the order of minutes, or even shorter.[7] Such fast transport rates may actually represent a challenge, as most commercial OI formulations in the market today target the lungs, and short residence times may require more frequent[8, 9] and higher dosages,[10] which may lead to more pronounced side effects.[9, 10] The reverse problem is also observed in cases when the lung epithelium works as an effective (and dominant) barrier to the transport of therapeutics that are intended for systemic delivery.[3, 7, 11]

Novel OI formulations that take full advantage of controlled delivery systems may help modulate the transport of therapeutics across the lung epithelium, and thus improve the effectiveness of existing OI therapies. Controlled drug delivery may also help augment the market share of such a simple and non-invasive route, by facilitating systemic administration of therapeutics through the lungs. Polymeric nanocarriers (PNCs) are especially suited within this context. PNCs may help overcome many of the drug delivery challenges facing OI therapies, as cellular uptake and transport across the epithelium, the main barriers to the systemic circulation,[6, 12-14] may be potentially modulated by carefully designing the carriers, as has been demonstrated for other epithelia.[15-18] Important design characteristics of PNCs that may be used to improve the control over the transport of therapeutics across epithelial barriers include their architecture (e.g. dendrimer nanocarriers (DNCs) vs. polymeric nanoparticles (NPs)),[19-22] size,[23, 24] surface charge, and surface chemistry (e.g. presence of targeting or non-fouling moieties).[19, 20, 23, 25] However, while significant attention has been given to the transport of PNCs across traditional epithelial barriers,[6, 15, 17, 26] little is known on how PNCs interact with the lung epithelium.[27] Similarly, the ability to deliver PNCs to the lungs using portable inhalers has been only recently demonstrated,[28-30] while a substantial body of work is available in the literature regarding the formulation of PNCs for other delivery routes.[15, 21, 31]

Based on the challenges and opportunities described above, the goal of this work was to investigate the uptake and transport of DNCs across polarized Calu-3 monolayers, an *in vitro* model of the lung airway epithelium, and the ability to further

modulate the cellular uptake and transport of the DNCs by forming polymeric blends between DNCs and polymeric NPs. Generation 3 (G3), amine terminated, poly(amido amine) (PAMAM) dendrimers (G3-NH_2) and poly (d,l-lactide-co-glycolide) (PLGA) NPs were selected as models in this study due to the extensive literature available for these systems as drug delivery carriers. Transport studies were performed across polarized monolayers grown onto porous inserts at the air-interface culture condition (AIC). Cellular internalization of the DNCs, polymeric NPs, and their blends were determined by flow cytometry, and cell lysis, also on polarized cell monolayers. Another goal of this study was to demonstrate the ability to formulate DNCs in portable OI formulations that show aerosol characteristics conducive to enhanced deep lung deposition. Core-shell structures containing the DNCs were prepared, and the aerosol characteristics of corresponding formulations in pressurized metered-dose inhalers (pMDIs) quantitatively determined.

3.2 Materials

Carboxyl-terminated PLGA **(**COOH-PLGA, 50:50, MW 31.3 - 45.0 KDa) was purchased from Birmingham Polymers (Birmingham, AL). G3 PAMAM dendrimer (G3-NH_2), containing 32 surface groups (MW 6,909 Da), fluorescein isothiocyanate (FITC), glutaraldehyde (25%), Triton-X-100 (reagent grade), Bovine Serum Albumin (BSA), Osmium tetroxide (OsO_4, 4% in water), penicillin-streptomycin (100 U/mL, AB), poly(vinyl alcohol) (PVA, 87-90% hydrolyzed), Alcian Blue, Trypan Blue, DPX® mounting media, N-Hydroxysuccinimide (NHS), N,N'-dicyclohexylcarbodiimide (DCC), and dialysis membranes (SpectraPor, MWCO 1 kDa) were all procured from

Sigma. Ethylenediamine was purchased from Fluka. Deionized (DI) water with a resistivity of 18.0 MΩ·cm (NanoPURE Diamond, Barnstead) was used in all experiments. BCA® protein assay was purchased from Pierce. Phosphate Buffered Saline (PBS, 10X) was purchased from Fisher Scientific and was diluted to 1X using DI water. Hank's Balanced Salt Solution (HBSS 1X, pH 7.3) supplemented with 0.01M HEPES was prepared. Rabbit Anti ZO-1 (Mid) primary antibody (product # A11010), Alexa Fluor® 546 labeled goat anti-rabbit IgG (product # 402200), 4', 6-diamino-2-phenylidole diacetate (DAPI) and the cell viability assay, MTT (Vybrant® cell proliferation assay kit), were purchased from Molecular Probes. Transwell® inserts (Corning, 0.4 μm pore size, polyester, 0.33 cm^2), cell culture flasks (75 cm^2), 24 well culture plates, coverglass slides (18 mm^2), and 96-well flat bottomed culture plates (Cellstar), and trypsin supplemented with 0.25% ethylene diamine tetraacetic acid (EDTA) were purchased from VWR. Dulbecco's Modified Eagle's Medium (DMEM, product # 10569) was procured from Invitrogen. Fetal Bovine Serum (FBS, non-heat inactivated) was purchased from Atlanta Biologicals. Metering valves were kindly provided by Valois (DF30) and 3M (EPDM Spraymiser). Pressure proof vials (5 mL, 6800318) were purchased from West Pharmaceutical Services. Pharma Grade (>99.99% purity) hydrofluoroalkane, 1,1,1,2,3,3,3-heptafluoropropane (HFA227) was a gift from Solvay Fluor und Derivate GmbH & Co. 2H,3H-perfluoropentane (Vertrel XF, HPFP) was purchased from TMC Industries. Glutaraldehyde was diluted from 25% to 2.5%, and osmium tetroxide diluted to 1% using DI water prior to their utilization. G3-NH_2 dendrimers were dried in vacuum overnight to remove methanol prior to usage. Anhydrous dimethylsulfoxide (anh.

DMSO) and anhydrous dichloromethane (anh. DCM) were obtained from EMD chemicals. All other chemicals used in this work were procured from EMD, were of analytical grade, and were used as received, unless otherwise noted.

3.3 Methods.

3.3.1 Conjugation of FITC to G3-NH_2.

Conjugation of FITC to G3-NH_2 was performed according to a procedure described earlier.[32] Briefly, a known mass of dendrimer was dissolved in PBS (5 mL). A known mass of FITC (concentration < 5 $mg \cdot mL^{-1}$) was solubilized in acetone and reacted with the aforementioned solution of G3-NH_2 under darkness for 24 hours, resulting in the FITC-conjugated G3-NH_2 (G3-NH_2-FITC). The organic phase was evaporated by gently sparging nitrogen, and the remaining contents from the flask were transferred to a dialysis bag and dialyzed extensively against DI water for 48 hours, with periodic changing in DI water every 6h, to remove any unreacted FITC. The contents of the dialysis bag were then transferred to a centrifuge tube, flash frozen using liquid N_2 and lyophilized (Labconco Freezone) for 48 hours to obtain the final product. The presence and the extent of FITC conjugation onto the dendrimer was ascertained by ^{1}H-NMR (DMSO-d_6 Varian 400 MHz).

3.3.2 Preparation of G3-NH_2-FITC-loaded PLGA nanoparticles (NPs).

Loading of the G3-NH_2-FITC into the NPs to form the nanoblends was accomplished using a modified version of the double emulsion solvent evaporation technique.[33] Briefly, 0.9 mg of the FITC-labeled dendrimer was dissolved in 50 μL

of DI water. The aqueous solution was emulsified over an ice bath with 80 mg of PLGA dissolved in 6 mL of an organic mixture containing ethyl acetate and acetone (4:1 ratio) using a sonicating probe (OmniRUPTOR 250, Omni Inc.) set at 50W power for 2 minutes. The primary emulsion formed was added dropwise to 5 mL of an ice-cold, 5% PVA solution under heavy vortexing (3000 RPM). The secondary emulsion formed was emulsified over an ice bath using the probe set to the same power, for another 1min. The emulsified mixture was diluted in about 150 mL of chilled 1% PVA solution and stirred overnight to evaporate the organic solvent. The NPs were recovered by centrifugation (26000×*g* for 60 minutes at 4°C, Sorvall Legend X1R) and washed thrice with DI water to remove residual PVA. The washed NPs were redispersed in DI water, flash frozen in liquid N_2 and lyophilized for 36h to obtain the final product. The recovered G3-NH_2-FITC loaded NPs (the nanoblend) were characterized for size, surface charge and morphology using the Zetasizer Nano (Malvern) (dynamic light scattering (DLS), and zeta potential), and scanning electron microscopy (SEM). For DLS, 2 mg of NPs were gently dispersed in 1.5 mL of 1X HBSS using a probe sonicator over an ice bath. For SEM, a few drops of the aforementioned dispersion were deposited on the surface of a cover glass and subsequently evaporated overnight. The cover glass was then sputter coated with gold for 25 seconds (Ernst Fullam) and imaged using SEM (Hitachi S-2400) at a voltage of 25 kV.

3.3.3 Loading efficiency of the G3-NH_2-FITC into PLGA NPs.

Loading efficiency of the FITC conjugated PAMAM dendrimers from the NPs was determined using fluorescence spectroscopy. 5 mg of the G3-NH_2-FITC loaded PLGA NPs was dissolved in 2 mL methylene chloride. The organic phase was then contacted with an equal volume of 1X HBSS and the mixture was subject to vortexing for 1 minute at 3000 rpm followed by extraction (LabQuake, Thermo Fisher) overnight under gentle mixing. The aqueous phase was isolated after extraction and subjected to fluorescence spectroscopy (Synergy Mx, Biotek Instuments, λ_{ex} 490 nm and λ_{em} 520 nm). The readings obtained were compared against a previously prepared calibration curve of the G3-NH_2-FITC to quantify the extent of the conjugate in the NPs. This procedure was done in triplicate, and the value reported here is an average of the three independent preparations of dendrimers loaded NPs.

3.3.4 Controlled release studies of the G3-NH_2-FITC from the NPs.

The sustained release of the G3-NH_2-FITC from the PLGA NPs was performed in 1X HBSS maintained at 37°C. 5 mg of the G3-NH_2-FITC-loaded PLGA NPs (ca. 50 μg G3-NH_2-FITC) were incubated in 5 mL of buffer maintained at constant temperature (37°C) in a water bath. At predetermined times, the suspension was centrifuged (26000× g, for 30 min at 4°C) and 200 μl of the HBSS was sampled from the supernatant. The amount of the G3-NH_2-FITC released was estimated by fluorometry, as described in the previous section. An equal volume of fresh HBSS was added back to the release media in order to compensate for the

buffer removed. The system was then redispersed and replaced back into the water bath for further sampling. The release profile is presented as a cumulative estimate of the G3-NH_2-FITC conjugate released over a period of 24h. The release of G3-NH_2-FITC from the NPs in presence of mucus laden HBSS was also evaluated. Synthetic regular mucus was prepared according to a methodology in literature and was diluted in the ratio 1:1000 in HBSS.[34] The ratio 1:1000 (Mucus:HBSS) was estimated by determining the volume of mucus on confluent Calu-3 monolayers seeded in the insert, which was calculated based on the thickness of the mucosal layer in the airways estimated to be 8 μm and the surface area of the insert to be 0.33 mm^2.[35] The release studies were conducted as described for the release in HBSS. The measurements were conducted in triplicate, and the values reported here are averages of three independent runs.

3.3.5 Preparation of FITC-conjugated PLGA NPs.

FITC was conjugated to PLGA according to a procedure detailed in the literature.[36] Briefly, COOH-PLGA (200 mg, 5 μM) was solubilized in anh. dichloromethane (DCM, 5 mL) and allowed to react with DCC (1.5 mg, 7 μM) and NHS (1 mg, 7 μM) overnight in order to activate the terminal carboxyl group on PLGA. The dicyclohexylisourea (DCU) formed as a precipitate was filtered, and the resulting product was allowed to react with ethylenediamine (1 mg, 16 μM) in DCM in order to convert the succinimidyl ester group on PLGA to primary amine.[36] The product obtained was purified by precipitating in diethyl ether, and the resulting solid was dried under vacuum. This amine terminated PLGA was allowed to react with

FITC (2.2 mg, 6 μM) overnight in anhydrous DMSO (5 mL). The resulting product was purified by dialysis against water, and lyophilized to recover the final product. The polymer thus prepared was characterized using ^{1}H-NMR to ascertain the conjugation of FITC to the polymer backbone – carboxyl group. NPs of the resulting polymer (FITC-conjugated PLGA) were prepared using emulsification solvent evaporation technique as detailed earlier. The NPs recovered were characterized for size and surface charge as described in previous sections.

3.3.6 Cell culture.

The human airway epithelial cell line, Calu-3, was purchased from the American Type Culture Collection (ATCC). Cells from passages 35-45 were used in the transport experiments. Calu-3 cells were plated in 75 cm^2 culture flasks, in DMEM supplemented with 10% FBS and 1% AB, and allowed to grow to confluence. Once the confluence of the monolayer in the culture flasks was ascertained visually they were subcultured and reseeded in Transwell® inserts at a density of 0.5×10^6 cells per well, and allowed to proliferate in a humidified atmosphere maintained at 37°C and 5% CO_2. The cells were grown initially under liquid culture conditions (LCC) for 48h, after which the medium on the apical side was removed and the cells were allowed to grow under an air interface culture (AIC). The culture medium on the basolateral side was replaced every two days, and the integrity of the Calu-3 monolayer was ascertained by determining its transepithelial electrical resistance (TEER). The measurements were conducted using an electrovoltohmmeter (EVOM, WPI Inc.,) equipped with chopstick electrodes. TEER of the monolayer was

monitored every day until the values peaked to a high value and leveled, indicating that the monolayer had reached confluence. Additional techniques, including electron microscopy and immunocytochemical analysis were employed to ascertain the presence of tight junctions and to confirm monolayer integrity.

3.3.7 Electron microscopy and immunocytochemistry.

Confluent Calu-3 monolayers were subjected to SEM to visually ascertain the morphology of the cell monolayers. Fixing and staining of the cells was done according to a procedure enlisted in the literature.[37] Once the confluence of cell monolayers was confirmed by TEER, select inserts were isolated and incubated in a 1:1 mixture of 2.5% glutaraldehyde (in DI water) and cell culture medium for 5 minutes at room temperature. The inserts were gently rotated in this medium during incubation. The mixture was replaced with the fixative, 2.5% glutaraldehyde, and was incubated for 30 minutes at room temperature. The cells were then stained with a 1% solution of OsO_4 for a period of 90 minutes after which they were washed in increasing gradients of ethanol (20%, 40%, 60%, 80% and 100% all v/v), each for a period of 10 minutes. The dehydrated monolayers were lyophilized for a period of 48h, sputter coated with gold (Ernst Fullam) and imaged using SEM (JEOL, JSM-6510LV-LGS) at 25 kV.

Alcian Blue stain was used in confirming the secretion of glycoproteins on the surface of Calu-3 cells. Confluent Calu-3 monolayers were isolated and were washed with HBSS after which they were incubated for a period of 20-30 minutes in 1% Alcian Blue (in 3% Acetic acid) at room temperature. After incubation, the

staining reagent was removed from the apical side, and the monolayers were washed with excess HBSS until the rinsate ran clear. The membrane from the inserts were carefully removed and mounted on microscope slides using DPX mountant, and imaged using an optical microscope (Diaphot 300, Nikon).

Immunocytochemical staining was conducted on confluent Calu-3 monolayers to detect and confirm the presence of the Zona Occludens (ZO-1) protein that populates the tight junctions of confluent Calu-3 monolayers.[37, 38] The procedure was performed according to the protocol prescribed by the manufacturer. Briefly, select monolayers, whose TEER values had peaked and leveled were washed with 1X PBS twice and were fixed in a 4% solution of paraformaldehyde for 20 minutes at room temperature. The fixed monolayers were washed with PBS and permeabilized with 0.5% Triton-X-100 solution containing 1% BSA (blocking agent), in HBSS for a duration of 30 minutes. The permeabilizer was removed and cells were washed well with PBS, and subsequently incubated for 60 minutes in a 6% BSA solution in HBSS to block non-specific interactions. The cells were then incubated in Rabbit Anti ZO-1 (Mid) primary antibody (5 $\mu g \cdot mL^{-1}$) dissolved in the blocking agent for 45 minutes followed by another 45 minute incubation in an Alexa Fluor® 546 labeled goat anti-rabbit IgG in blocking solution. The cells were washed with PBS and counterstained with DAPI (0.1 $\mu g \cdot mL^{-1}$in DI water), mounted on glass slides using DPX mounting media and stored at 4ºC overnight. The stained monolayers were observed using a fluorescent microscope (Zeiss Axiocam mRM, Carl Zeiss) to visually ascertain the presence of ZO-1. The images were captured using the software, Axiovision (Zeiss).

3.3.8 Cytotoxicity Studies.

The viability of Calu-3 cells in presence of G3-NH_2-FITC and G3-NH_2-FITC loaded NPs was estimated using the MTT assay, according to a protocol outlined by the manufacturer. Briefly, Calu-3 cells were seeded at a density of 10,000 cells per well in 96-well culture plates, and allowed to grow for a period of 24h. Cells were then washed twice with HBSS and the medium was replaced with 100 μL of HBSS containing varying concentrations of either G3-NH_2-FITC or the NPs containing the conjugates. The cells were allowed to incubate in the test solutions for a period of 7h. This duration was selected as it was 2 hours longer than the time utilized for the transport experiment. After the duration of the test period, cells were washed thrice with 1X HBSS and incubated at 37ºC in 100μL of HBSS containing 20 μL of MTT solution for a period of 4h. The incubation was followed by replacing 75 μL of the solutions in the wells with 50 μL of DMSO and allowing the cells to stand for 10 minutes in order to dissolve the formazan crystals. The well plates were read at an absorbance of 540 nm using a plate reader (Synergy Mx, BioTek Instruments). Cell monolayers exposed to only 1X HBSS were used as controls. Cell viability was determined by comparing the absorbance values of cells exposed to G3-NH_2-FITC and G3-NH_2-FITC loaded into NPs to that of the control.

3.3.9 *In-vitro* transport, cellular uptake, and mass balance studies

3.3.9a Transport.

Transport of bare G3-NH_2-FITC and G3-NH_2-FITC from blends with the polymeric NPs was determined across confluent Calu-3 monolayers using a strategy

similar to that reported in the literature for therapeutics and other probe molecules.[39, 40] Once an acceptable in vitro epithelial barrier was established as described above, the permeability experiments commenced. Prior to starting the transport studies, the medium on the apical and basolateral sides were replaced with warm 1X HBSS and the monolayers were allowed to equilibrate at 37ºC for a period of 45 minutes. The TEER of the monolayer was recorded, after which the PNCs were pulsed onto the cell monolayers in 0.2 mL HBSS solution. For the case of bare G3-NH_2-FITC, the 0.2 mL HBSS solution contained 25 μg of dendrimers. For the case of the dendrimer-NP blends, the 0.2 mL HBSS solution contained 3 mg of NPs. The NP concentration was selected based on the loading of the G3-NH_2-FITC – so as to correspond to a total mass of dendrimer of 25 μg. These experiments guarantee the same mass/molar concentration of dendrimer in both systems. The basolateral side (receptor compartment) was fed with 0.6 mL fresh 1X HBSS. The transport across the cell monolayer to the basolateral side was monitored over a 5h period. At predetermined times, inserts were transferred to wells containing fresh 1X HBSS in the receptor compartment and the transport study was continued. This was done in order to maintain sink conditions during the duration of the experiment. The amount of G3-NH_2-FITC that traversed onto the basolateral side was quantified by fluorescence spectroscopy (λ_{ex} 485 nm λ_{em} 520 nm). The apparent permeability (P_{app}) was determined according to equation (3.1).

$$P_{app} = \frac{F}{AC_O} \quad (3.1)$$

Where *F* is the flux (rate of cumulative mass of G3-NH_2-FITC transported), *A* is the area of the insert (0.33 cm^2) and C_o is the initial concentration of G3-NH_2-FITC on the apical side of the insert. *F* was calculated by plotting the cumulative mass of G3-NH_2-FITC transported as a function of time, and corresponds to the slope from the resultant curve.[37]

3.3.9b Cellular uptake and mass balance.

Cellular uptake was determined using two approaches. Here we report the procedure for the uptake determined from the cell lysate. This is an absolute determination (total concentration of the species of interest), and was used to perform an overall mass balance with respect to the amount of the dendrimer. In the next section we discuss cellular uptake determined by flow cytometry. The concentration of G3-NH_2-FITC and G3-NH_2-FITC encapsulated in the NPs into Calu-3 cells was quantified at the end of the transport experiments – at the 5h time point. After completion of the transport studies, the apical media was removed and stored under darkness at 4ºC. The cell monolayers were washed with ice-cold HBSS to arrest uptake and remove non-bound NPs and conjugates. The particles washed during this rinse were also collected and accounted for as non-internalized. The amount of G3-NH_2FITC in the fluids collected was measured by fluorescence spectrometry as described in earlier sections. For bare G3-NH_2-FITC, the apical fluid collected was centrifuged (1500 rpm, 6 minutes) and directly read using a fluorometer, whereas for the dendrimer-NP blends, the apical fluid laden with NPs was contacted with organic solvent (methylene chloride) to break down the polymeric

matrix and release the dendrimer. The mixture was allowed to stand until the organic and the aqueous phases separated. The aqueous phase was subsequently analyzed for the conjugate released as detailed above. The monolayers were subsequently lysed by allowing them to stand in 2% triton-X-100 in HBSS for 24 h under darkness.[41] In case of bare G3-NH_2-FITC, lysed cell monolayers were centrifuged (800 rpm, 5 min) and the supernatant was analyzed for the G3-NH_2-FITC using fluorometry (λ_{ex} 485 nm and λ_{em} 520 nm, Synergy Mx, Biotek Instruments). In case of the G3-NH_2-FITC loaded into NPs, the lysate was centrifuged (800 rpm, 5 minutes), the supernatant separated and contacted with methylene chloride to dissolve the internalized NPs and extract the G3-NH_2-FITC into the aqueous phase. After a 24h extraction, the aqueous phase was analyzed for G3-NH_2-FITC using fluorometry. The results were normalized with respect to the total protein content using BCA protein assay, according to the protocol given by the manufacturer. By determining the concentration of the G3-NH_2-FITC in the apical side of the monolayer, the concentration that was internalized within the cell, and the amount transported onto the basoleteral side, a mass balance of the G3-NH_2-FITC could thus be performed.

3.3.9c Flow Cytometry.

Flow cytometry analysis was conducted on polarized Calu-3 cells according to methodology detailed in the literature, with some modifications.[42, 43] Calu-3 cells (passages 35-45) were seeded at a density of 1 x 10^6 cells per well in 24-well plates, and allowed to grow to confluence. The monolayer confluence was confirmed by

staining select wells for ZO-1 and subjecting them to fluorescence spectrometry as detailed earlier, a day before commencing the uptake studies. The presence of ZO-1 protein suggested that the cells were confluent. Prior to pulsing G3-NH_2-FITC or NPs loaded with G3-NH_2-FITC, the cell monolayers were incubated with 1X HBSS (at 37ºC) for a period of 30 minutes. The cells were then incubated with: (i) G3-NH_2-FITC; or (ii) NPs loaded with G3-NH_2-FITC; or (iii) FITC-PLGA NPs in HBSS for varying time periods (5h, 4h, 3h, 2h, 1h, 30 minutes and 15 minutes). Care was taken to ensure that the concentration of G3-NH_2-FITC was same for both systems. The concentration FITC-PLGA was the same as that of NPs loaded with G3-NH_2-FITC. After incubation for a specified duration, the test solutions were removed and the cell monolayers were washed thrice with ice-cold HBSS. The extracellular fluorescence was quenched with trypan blue (0.25% w/v in HBSS), and the monolayers were washed again, before being subjected to trypsinzation (trypsin supplemented with 0.25% EDTA). The detached cells were centrifuged (1200 rpm, 6 minutes) to obtain the cell pellet which was subsequently resuspended in 1 mL of fresh HBSS and analyzed using a flow cytometer (BD LSR II (BD Biosciences, San Jose, CA), with the samples excited with a Coherent Sapphire laser (488 nm) and detected through a 530/30 bandpass filter (FITC). Only viable cells were gated for fluorescence analysis. As controls for G3-NH_2-FITC, 1X HBSS was utilized, whereas for NP system, blank PLGA NPs were used. At least, 6000 events were counted for each condition. All experiments were repeated / performed independently by two different investigators in our laboratories, with three wells each time, 4 weeks apart from each other. The results shown here are thus averages of 6 wells. The cellular

entry was expressed in percentages as a function of time by plotting the mean fluorescence intensity (MFI) values of cells gated for FITC from histograms sourced from the FACS data. In addition, the rate of cellular entry was also plotted as a function of time, by normalizing the MFI data with respect to the 5h MFI values, which were set at 100%.

3.3.10 Preparation and characterization of G3-NH_2-FITC loaded core-shell particles.

Synthesis and characterization of a biodegradable co-oligomer, oligo(lactide) grafted chitosan (OLA-*g*-CS) that forms the shell encapsulating the G3-NH_2-FITC has been documented in detail elsewhere.[44] The CS was depolymerized from 310 kDa to a MW of about 1 kDa according to procedure described in the literature, with a degree of deacetylation of 77% as estimated by ^{1}H-NMR.[44] Ring opening polymerization was used in grafting lactide chains onto the degraded CS backbone. The resulting co-oligomer had a MW of 1.7 kDa, with at least 3 OLA chains (8 LA units, 21% graft percentage) onto each CS backbone as determined using ^{1}H-NMR.[30] Preparation of G3-NH_2-FITC loaded core-shell particles was accomplished via emulsification diffusion. Briefly, 30 mg of the co-oligomer was dissolved in 0.9 mL DI water and to this solution 1.2 mg of the dendrimer was added. This aqueous solution was emulsified with 19 mL of ethyl acetate in a bath sonicator (VWR P250D, 180 W) for 8 minutes at 17°C. The resulting water in oil emulsion was quickly added to a large volume of ethyl acetate (200 mL). The high solubility of water in ethyl acetate causes it to migrate from the dispersed droplet phase into the

bulk phase. Being interfacially active,[44] the co-oligomer resides at the interface, templating the G3-NH_2-FITC as spherical particles with a core-shell morphology, where the co-oligomer becomes the shell and dendrimers the core. Core-shell particles thus formed were collected by centrifugation (Sorvall Legend X1R, 5000 rpm, 20 mins), air dried and stored in a desiccator prior to usage. The particles were characterized for shape and size using DLS and SEM. A known amount (2 mg) of particles was dispersed in 1.5 mL of HPFP at 18ºC in a bath sonicator and subject to DLS analysis. A small quantity of the dispersion was deposited onto cover glass slides, dried in a light stream of air, and sputter coated with gold for 40s prior to imaging them under SEM (Hitachi S-2400) at 25 kV.

The loading of the dendrimer conjugates in the core of the particles was determined using fluorescent spectroscopy. A known mass of the particles (3 mg) containing the G3-NH_2-FITC and the water-soluble shell was dissolved in a known volume (3 mL) of HBSS. The resulting solution was analyzed using fluorescence plate reader at excitation and emission wavelengths of 495 and 520 nm respectively (those corresponding to FITC) and compared against a previously prepared calibration curve of the G3-NH_2-FITC to quantify their loading.

3.3.11 Physical stability of G3-NH_2-FITC loaded core-shell particles in HFA propellant.

A known mass of the core-shell particles containing the G3-NH_2-FITC was loaded into pressure proof glass vials (West Pharma, 6800318), and crimp sealed using metering valves (DF30, Valois). The propellant was fed into the pressure proof

vials using a manual high pressure pump (HiP 50-6-15) and a home-made aerosol filler. The volume of HFA added was such that the final concentration in the vial was 2 $mg \cdot mL^{-1}$. The formulation was gently agitated in a low intensity sonicating bath (VWR P250D set to 180W) between 16 and 18°C for a few min to break up larger aggregates. Digital images of the dispersion were captured immediately after ceasing the mechanical energy input, and later at predetermined times. The physical stability of the dispersion was qualitatively estimated as a function of the dispersion age. As a comparison, bare G3-NH_2-FITC was also formulated in pMDIs (0.15 $mg \cdot mL^{-1}$) as described above for core-shell particles, and its dispersion stability also evaluated as a function of time.

3.3.12 Aerodynamic properties of G3-NH_2-FITC core-shell formulations.

An eight stage Andersen Cascade Impactor (ACI, Copley Scientific) operating at a flow rate of 28.3 $L \cdot min^{-1}$ was used to evaluate the aerosol characteristics of the G3-NH_2-FITC loaded core-shell formulations. Formulations of G3-NH_2-FITC alone were also tested for comparison. The studies were carried out at room temperature and 52% relative humidity. Freshly prepared canisters of the formulations were dispersed with the help of a sonicating bath maintained at 18°C for 30 minutes. Several shots of the formulation were fired to waste prior to subjecting them to the impaction experiments. 20 shots were then fired into the ACI at an interval of 10s between each actuation. After the study, the amount of dendrimer deposited on the actuator (Ac), the induction port (IP) and each of the stages of the ACI was estimated by rinsing the stage plates in 20 mL of 1X HBSS overnight, and subjecting the

resulting solution to fluorometry. Three independent runs (different canisters) were conducted, and the results reported here are averages of those runs. In addition to the fine particle fraction (FPF), other relevant aerosol properties including the mass median aerodynamic diameter (MMAD), and geometric standard deviation (GSD) were also determined from the ACI results.

3.4 Results and Discussion

3.4.1 Synthesis and characterization of G3-NH_2-FITC, and FITC conjugated PLGA.

FITC was tagged onto dendrimers in order to allow their detection during transport and uptake studies. FITC conjugation to G3-NH_2 was accomplished by linking the isothiocyanate group of FITC to the amine group of G3-NH_2.[45] Characterization of the prepared G3-NH_2-FITC was done using ^{1}H-NMR. The NMR spectrum of the prepared conjugates, along with the reaction scheme is shown in Figure 3.1.

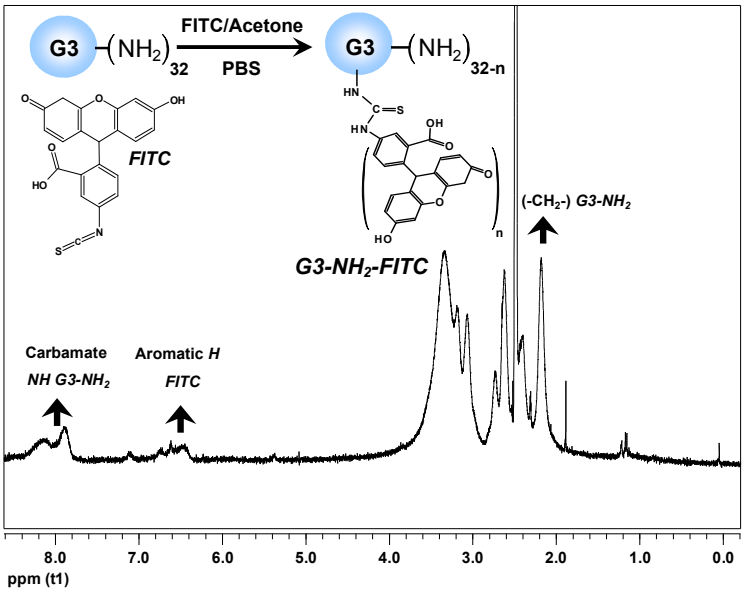

Figure 3.1. ^{1}H-NMR (400 MHz, d_6 DMSO) spectra of the G3-NH_2-FITC. The singlet at 2.19 ppm can be attributed to the methylene peak of G3-NH_2. This peak was used as the internal standard, and was set to 120 protons. The multiplets between 6.82-6.51 ppm denote the aromatic protons on the FITC molecule. Multiplets between 8.22-7.82 ppm denote the carbamate –NH protons. (*Inset)* Scheme depicting the synthesis of the G3-NH_2-FITC.

A singlet observed at 2.19 ppm can be attributed to the methylene (–CH_2-) protons of G3-NH_2. This peak was used as an internal standard to estimate the extent of FITC conjugation, and was set at 120(H) protons.[46] Multiplets between 7.82-8.22 ppm can be attributed to the carbamate (-NH-) peaks of the G3-NH_2. The presence of FITC can be confirmed by the appearance the multiplet at 6.42-6.61 ppm, attributed to the aromatic protons (4H) on FITC.[47] The ratio of the integral area of the signals between 6.42-6.61 to the integral area of the methylene protons of the G3-NH_2, weighted by the respective number of protons gives the number of FITC molecules per G3-NH_2, in this case determined to be 1.7. FITC conjugated

PLGA was synthesized so as to evaluate the rate of cellular uptake of PLGA NPs and to compare with the uptake results of the dendrimer-NP blends as discussed below. The conjugation was also characterized by ^{1}H-NMR. The presence of multiplet peaks between 6.5 and 6.7 ppm can be attributed to the presence of FITC (spectrum not shown), which was conjugated to the carboxyl group (converted to a primary amine) on the PLGA terminus.

3.4.2 Loading of G3-NH_2-FITC onto PLGA NPs, characterization of the NPs and release of the dendrimers from the polymeric nanoblends.

Loading moieties into biodegradable polymeric matrices can lead to sustained release of the encapsulate over extended periods of time.[48] Sustained and controlled release of therapeutics from the NPs is an effective methodology to ensure retention and prolonged therapeutic effect at the target site, and has further relevance in the delivery of high potency, and/or more costly drugs such as chemotherapeutics.[48, 49] Such strategies have also been demonstrated for large therapeutics such as biomacromolecules, with molecular weight and hydrophilicity similar to that of DNCs investigated in this work.[50, 51] Incorporating dendrimer conjugates within polymeric NPs (blends) can potentially augment the capabilities of the dendrimers and polymeric nanocarriers as potent drug delivery vehicles, by providing an avenue for further control of the release and transport of the DNCs across biological barriers, and consequently that of the therapeutic cargo conjugated to the dendrimer. Additionally, these NPs can act as protective depots for fragile molecules that may be conjugated to the dendrimers, thereby ensuring greater

retention of their activity.[52] The encapsulation of dendrimers in polymeric NPs can also be used to mediate the interaction of the dendrimers with both extra and intracellular barriers present in the lung epithelia. As drugs and other moieties are grafted onto DNCs, the surface chemistry of the carriers is affected, which may also impact their interaction with both intra and extracellular barriers.[49, 53] The encapsulation of the dendrimers into NPs may thus serve as a strategy for the transport of different dendrimer nanocarriers.

The double emulsion solvent evaporation technique was employed to load the G3-NH_2-FITC onto the NPs.[33, 48] The particles formed were lyophilized and characterized using SEM and DLS. A representative SEM micrograph (10000X) of the NPs and the size distribution as determined by DLS *(as inset)* is shown in Figure 3.2(a). DLS experiments were conducted in 1X HBSS as the medium, which is the same solvent medium used in the uptake and transport experiments.

.

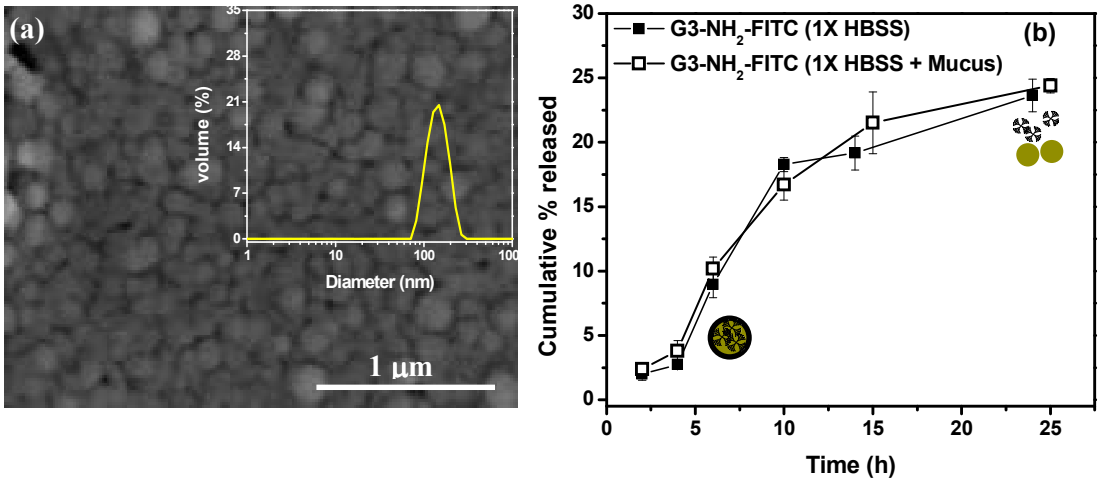

Figure 3.2. (a) SEM micrograph of the G3-NH_2-FITC-loaded PLGA NPs prepared using double emulsion solvent evaporation technique. *(inset)* Size distribution of the G3-NH_2-FITC-loaded PLGA NPs as determined by dynamic light scattering (DLS); (b) Sustained release profile of G3-NH_2-FITC from PLGA NPs in 1X HBSS (pH 7.3) and mucus containing 1X HBSS (pH 7.4) measured at 37ºC. *(Inset)* Illustration indicating release of the G3-NH_2-FITC from PLGA NPs. Error bars that do not show are smaller than symbol sizes. Results reported here are the average of three independent runs.

The particle size as determined by DLS was 175±28 nm, with a polydispersity of 0.08. SEM images indicated that the particles formed were smooth spheres with an average size of 221±35 nm, as determined with the ImageJ software (v1.4, NIH). The zeta potential of the particles was found to be -10.1±2.4 mV. The loading of the G3-NH_2-FITC into the NPs was estimated using fluorometry. A known mass of the NPs recovered after lyophilization was dissolved in a known volume of methylene chloride to break down the polymeric matrix and release the G3-NH_2-FITC. The organic phase was then mixed with an equal volume of 1X HBSS to extract the G3-

NH_2-FITC released from the NPs into the aqueous phase, which was subsequently estimated using fluorometry as described earlier. The amount of G3-NH_2-FITC was then estimated by comparing the fluorescence of the extract to a previously constructed calibration curve of the conjugate. The amount of G3-NH_2-FITC loaded into the NPs was determined to be 7.8±1.2 μg per mg NPs. This average is an estimate of three independent runs (different batches of NPs). The overall encapsulation efficiency of the G3-NH_2-FITC into the NPs was found to be 10±1.8%. The relatively low loading of the G3-NH_2-FITC into the NPs can be attributed to the hydrophilicity of the dendrimer, which enhances the rapid partition of the G3-NH_2-FITC to the external aqueous phase during the dilution procedure, as observed for other drugs and biomacromolecules such as proteins and peptides.[49, 54, 55] The NPs of FITC conjugated PLGA had a size of 245 ± 40 nm as determined by DLS, and a zeta potential of -12±3.1 mV.

There have been a few studies in the literature that have reported the formulation of dendrimers into particulate carriers.[56, 57] Most of those studies have focused on the encapsulation of G3-NH_2-plasmid DNA complex (dendriplexes) into PLGA microparticles.[57] One of the important findings from those studies was the ability to sustain the release of these dendriplexes from the polymeric core over extended periods of time, suggesting that formulating dendrimer conjugates into polymeric matrices can be a potential strategy to further enhance their efficacy as drug delivery agents.[56] To the best of our knowledge, there have been no previous articles reporting the encapsulation of dendrimers into polymeric NPs.

Release studies of the G3-NH_2-FITC from the polymeric matrix were conducted in 1X HBSS, the medium in which the transport experiments were to be conducted, as described in the earlier sections. Additionally release studies were conducted in mucus laden HBSS, in order to simulate an environment that the NPs will encounter in the vicinity of the cell milieu and understand the impact of the surroundings on the G3-NH_2-FITC release. These experiments were conducted in triplicate. The release studies were conducted for a period of 24h, with supernatant removed and tested at periodic time points for the released conjugates. A plot of cumulative release G3-NH_2-FITC from PLGA NPs as a function of time is shown in Figure 3.2(b). It is observed that a sustained release of G3-NH_2-FITC can be achieved from the NPs within the time span investigated, with about 24% of the conjugate being released into the buffer by 24h. A similar release profile was also exhibited by the NPs when the studies were conducted in the mucus dissolved buffer. In order to put these release studies in perspective, it would be instructive to compare the results to compounds of similar size as the DNCs that have been encapsulated into PLGA NPs, with PLGA of similar molecular weight. Interestingly, insulin (MW 5808 Da) loaded into PLGA (MW 50 kDa) NPs exhibited a similar release profile as the G3-NH_2-FITC reported in this work.[58] However, in our work, we observed a more subtle, sustained release of the conjugates during the initial times as opposed to a sudden burst release, which has been reported for the aforementioned and several other systems.[59, 60] This can be attributed to the relatively low loading efficiency of the conjugates within the NPs, and the MW of the polymer.[54] The effect of lower loading of encapsulates into NPs on the release characteristics has

been extensively reported in literature.[61] For instance, PLA NPs containing varying payloads of savoxepine, a potent antipsychotic compound, displayed dual release profiles. An initial burst and faster release characteristics were observed for NPs with higher encapsulated payloads, while those with lower drug contents displayed little or no burst release, and considerably slower release profiles.[62] This behavior was also observed for a protein, Bovine Serum Albumin (BSA) loaded into PLGA microspheres.[63] Another factor that could possibly influence the release characteristics of G3-NH_2-FITC from the polymeric matrix is the presence of surface-associated PVA, which is usually present on the smaller NP surface, and which has been shown to hinder the diffusion of encapsulated compounds from within the NPs.[63] This is an important observation, as sustained-release profiles of moieties from polymeric matrices is expected to be primarily governed by diffusion processes during the early stages of release.[63]

3.4.3 Cytotoxicity of G3-NH_2-FITC and G3-NH_2-FITC loaded NPs on Calu-3 cells.

The cytotoxicity of the conjugates and the dendrimer-NP blends were tested on Calu-3 cells. Cell viability was determined using the MTT assay as described in *Methods*. The cell viability results are plotted as a function of the concentration of G3-NH_2-FITC and of the dendrimer-NP blend, and are shown in Figure 3.3. The results reported here are those for a period of 7 h, as transport studies conducted in this work lasted 5h – see transport result below.

The results show that neither the bare conjugate dendrimer nor the conjugate formulated as NPs induced any appreciable cytotoxicity on Calu-3 cells within the concentration ranges and the duration investigated. It has been well established that cytotoxicity of dendrimers are concentration, charge and generation dependent, with cationic dendrimers of higher generations exhibiting greater cell kill than their anionic and lower generation counterparts.[15, 64] As there have been no previous

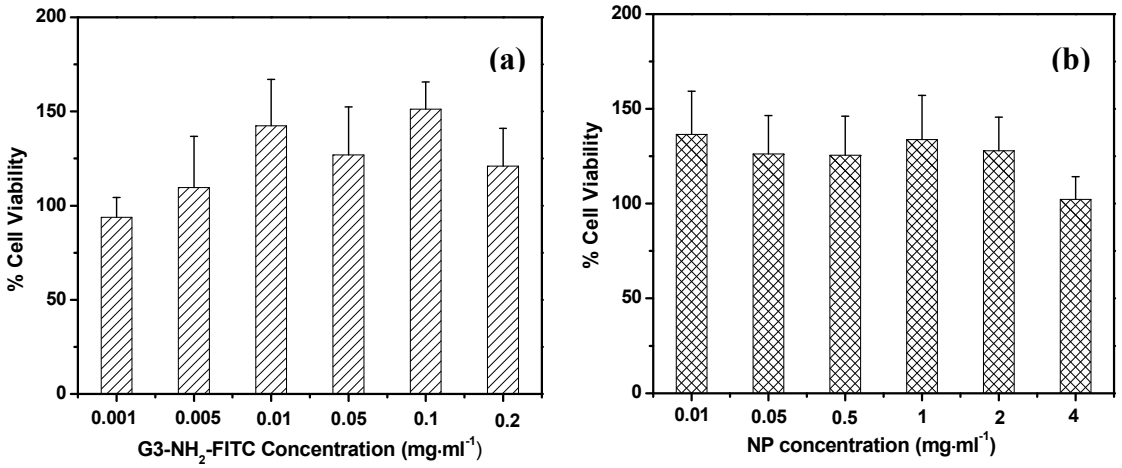

Figure 3.3 Viability of Calu-3 cells upon exposure to varying concentrations of (a) G3-NH_2-FITC; and (b) G3-NH_2-FITC-loaded PLGA NPs. Viability determined by MTT assay (n=4), after 7h of exposure.

cytotoxicity studies of G3-NH_2-FITC onto Calu-3 cells, it would be appropriate to compare our results to studies performed on Caco-2 cells, which is a colon cancer cell line that exhibits certain characteristics somewhat similar to Calu-3 (possess microvilli on the apical surface and form tight epithelial junctions).[20, 65] Experiments conducted on Caco-2 cells show that G3–NH_2-FITC are non-toxic up to

a concentration of 10 μmol (~69 mg) per mL, which is much higher than the concentration range investigated in this work.[66] The combination of G3-NH_2-FITC and PLGA NPs did not exert any toxic effect on the cell monolayers within the concentration tested either, as shown in Figure 3.3b. This is not surprising, as previous cell viability studies on Calu-3 cells have reported that PLGA NPs did not induce any pronounced cytotoxic effects even at 48h after exposure for concentrations of up to 5 mg of NPs per mL.[67, 68] The non-toxic nature of the G3-NH_2-FITC loaded NPs suggests that the encapsulation of dendrimer conjugates within NPs may possibly also be seen as a viable strategy to alleviate the potential toxicity associated with higher concentrations and / or high dendrimer generation, and their corresponding conjugates. The encapsulation of dendrimers in NPs may also alleviate issues regarding to the solubility of dendrimer nanocarriers in physiological environment in cases when their surface is modified with hydrophobic therapeutics.

3.4.4 Characterization of the Calu-3 monolayers for transport studies.

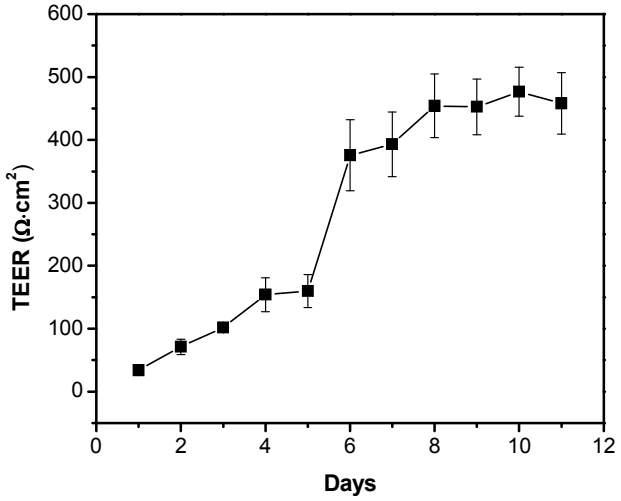

Figure 3.4. Variation in transepithelial electrical resistance (TEER) across Calu-3 monolayers (n=12) grown in Transwell® inserts (0.4 μm pore size and 0.33 cm^2 area) under an air-interface culture (AIC) as a function of time. The TEER values were obtained after equilibrating the apical chamber with the culture medium for 30 minutes. The TEER reported here was corrected for the resistance of the blank

The human airway epithelial cell line Calu-3 was used to assess the permeability and uptake of the G3-NH_2-FITC and G3-NH_2-FITC encapsulated into PLGA NPs. Calu-3 is a well-differentiated and characterized cell line derived from human bronchial sub mucosal glands.[27] Besides producing tight junctions, Calu-3 is one of the few respiratory cell lines capable of expressing many important characteristics of the bronchial epithelium *in vitro*, viz. production of airway surface liquid, mucin excretion, cilia, and other immunologically active substances that make

Calu-3 an appropriate candidate for elucidating tracheobronchial permeability *in vitro*.[27, 37]

Calu-3 cells were plated at a density of 0.5×10^6 cells per insert, in DMEM supplemented with 15% FBS and 1% antibiotics as described earlier. The cells were grown under a liquid-covered culture for 48 hours, after which the medium in the apical compartment was removed and the cells were allowed to grow under AIC. It has been shown that when grown at AIC, Calu-3 cells exhibit a greater resemblance to the native epithelium (microvilli/cilia, mucins and other relevant glycoproteins), and hence that particular method of culture was employed in this study.[37]

The TEER of the Calu-3 monolayers was measured to ascertain their confluence.[37]. A plot of the TEER afforded by the cell monolayer as a function of time (days in culture) is shown in Figure 3.4. The TEER of the Calu-3 monolayers is seen to increase steadily above baseline by day 5, and to reach confluence by day 8. The values leveled by day 11, indicating that the monolayer had reached the level of confluence required to conduct the transport studies.[37, 38] These results compare favorably with the results reported in the literature for Calu-3 cells cultured under AIC, which are deemed confluent for TEER values peaking beyond ca. 300 $\Omega\cdot cm^2$,[37, 69] values which are dependent to some extent to the culture conditions and cell passage.[70]

In addition to determining the TEER of the monolayers, immunocytochemical (IC) analysis and electron microscopy studies were conducted to visually ascertain the presence of tight junctions and morphology of the confluent Calu-3 monolayers. In this work, IC analysis and electron microscopy experiments were performed a day

prior to commencement of the transport studies. The cell monolayers were prepared for both studies as detailed in the methods section. Figure 3.5 (a) is a representative electron micrograph of a Calu-3 monolayer fixed and stained with osmium tetroxide, and reveals that the confluent Calu-3 monolayers displayed some of the requisite morphology possessed by confluent Calu-3 viz. microvilli (filled white arrows).

IC analysis was performed on the cell monolayers to detect the presence of Zona Occludens Protein - 1 (ZO-1), which is a major protein expressed in the tight junctions of confluent Calu-3 cells.[70] The presence of the protein was detected by staining the fixed cells with an anti-ZO-1 antibody labeled with Alexa Fluor® 546.[37] The nuclear stain, DAPI, was utilized as a counterstain. A representative fluorescent microscope image of the fixed and stained Calu-3 monolayer is shown in Figure 3.5(b). The presence of orange boundaries (denoted by the yellow arrows) around the cells can be attributed to the expression of ZO-1 protein. Calu-3 cells when cultured under AIC have been shown to secrete a greater amount of glycoproteins (mucins) on their surface,[37] which can be detected by staining the cell surface with Alcian Blue.[37, 70] Figure 3.5(c) is an optical microscope image captured after the cells were stained with Alcian Blue and fixed. The heavy blue staining on the monolayer surface (open black arrows) is an indicator of the presence of mucosal glycoproteins on Calu-3 cultures grown under AIC. The observations reported here are in agreement with those reported in earlier studies characterizing confluent Calu-3 monolayers.[38, 70] Once the monolayers were characterized and their morphology ascertained, they were subject to transport experiments, which are discussed next.

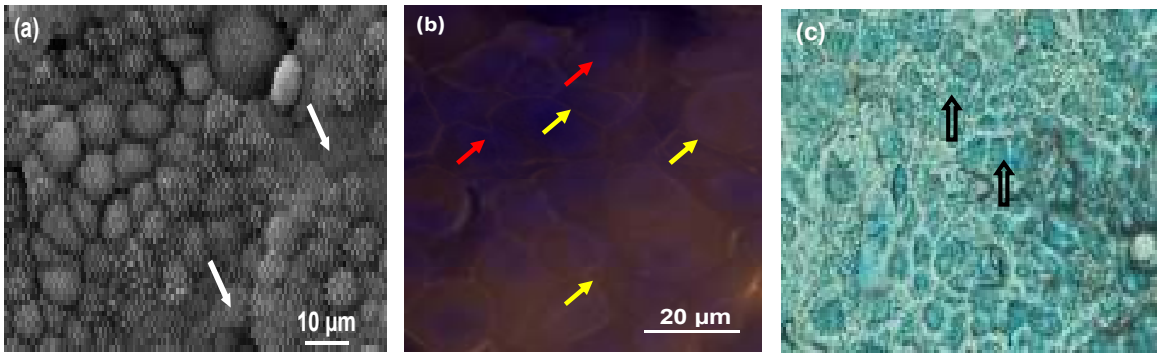

Figure 3.5. (a) Representative SEM micrograph of Calu-3 monolayers grown under an air-interface culture (AIC). Monolayers were isolated once the TEER values peaked and leveled. Cell monolayers were fixed and stained with osmium tetroxide, and dehydrated in increasing gradients of ethanol after which they were lyophilized. White arrows indicate the presence of microvilli on the monolayer surface. (b) Fluorescent microscope image of Calu-3 monolayers showing the presence of tight junctions (yellow arrows) populating the cell periphery. Red arrows indicate the location of the nuclei (stained with DAPI - blue). Cells were seeded at a density of 0.5×10^6 per well and were grown under AIC. The cells were stained for the tight junctional protein, Zona Occludens-1 (ZO-1) labeled with Alexa Fluor® 546 dye (orange) and counterstained with DAPI for nuclei. (c) Optical microscope image of a Calu-3 monolayer stained with Alcian blue, indicating the presence of glycoproteins (mucins, unfilled black).

3.4.5 *In-vitro* transport and uptake.

In-vitro transport of bare G3-NH_2-FITC and those loaded into NPs were conducted on confluent Calu-3 cell monolayers for a period of 5h. A summary of the P_{app} (y_1 axis) results as a function of time for bare G3-NH_2-FITC, and those

formulated as blends within PLGA NPs across Calu-3 is shown in Figure 3.6. The y_2 axis in the plot denotes the cumulative mass of G3-NH_2-FITC transported (in percentage) across the cell monolayer as a function of time after pulsing.

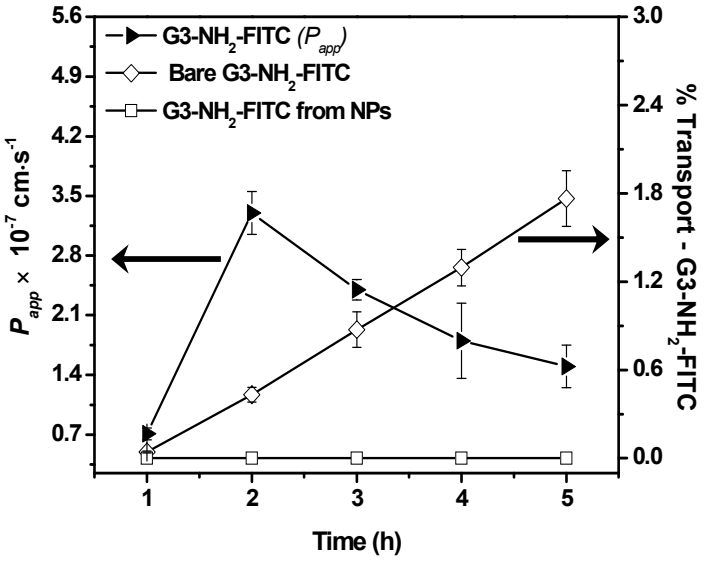

Figure 3.6. Apparent permeability (y_1 ; P_{app}) and % transported (y_2) of G3-NH_2-FITC and G3-NH_2-FITC–loaded into NPs, plotted as a function of time. (n=4) Error bars that do not show are smaller than symbol sizes.

At the end of the 5h time point, the P_{app} of the G3-NH_2-FITC across Calu-3 was found to be 1.4 × 10^{-7} cm·s^{-1}. About 1.7% of the conjugates had traversed across the monolayer within 5h. An increase in the P_{app} value from 0.7 to (a peak of) 2.8 × 10^{-7} cm·s^{-1} was observed at 2h, followed by a subsequent decrease to 1.4 × 10^{-7} cm·s^{-1} by at the end of the experiment, indicating the presence of an 'activation' time for transport. This coincides with a minimum in the TEER, which may indicate a

preference with regards to transport route. On the other hand, for the system comprised of G3-NH_2-FITC formulated as blends with the PLGA-NPs, no transport was observed within the duration of the experiment. Slow release of the conjugates (low concentration of the G3-NH_2-FITC in the donor chamber) from the NPs is expected to help mediate the transport of the DNCs across the monolayer. From the sustained release studies discussed above, it is estimated that only ca. 5% of the encapsulated conjugate is released from the polymeric matrix within 5h. Because the concentration of the DNCs is expected to impact their permeability,[20] the encapsulation of the dendrimer within the NPs is expected to impact (reduce) the rate of transport. Moreover, the NPs themselves are not expected to be transport across the Calu-3 monolayer, further reducing the potential for transport of the DNCs.[40]

Cell monolayers incubated with bare G3-NH_2-FITC and G3-NH_2-FITC loaded PLGA NPs were lysed after the transport experiments so as to quantify cellular uptake. The results indicated that 16±1.7% of the bare G3-NH_2-FITC (0.08 nmol) and 19±2.1% (0.1 nmol) of the G3-NH_2-FITC from the NPs were internalized into the cells during the study. It is quite interesting to observe that the dendrimer internalization seems to be greater with NPs compared to free dendrimers. A mass balance of the dendrimers was accomplished by quantifying the contents of the apical chamber for G3-NH_2-FITC after the completion of the transport studies, and combining those values with those obtained from analyzing the contents internalized into cells and the contents transported across to the basolateral side. The total amount recovered from these analyses (for both systems) was 85% - out of the total

pulsed onto the cells. In comparison, earlier translocation studies conducted on Calu-3 cells utilizing polymeric NPs of similar size as those discussed here reported an internalization of 11%, with a recovery of up to 93%.[40] The lower recovery could be attributed to losses associated with the fraction of carriers that may be bound to the cell surface despite washing – that fraction will settle down along with the cell debris during the centrifugation. Losses may also arise due to adsorption of particles to other surfaces, and also quenching of the fluorophore.

While no previous results for internalization or transport of dendrimers across Calu-3 cells have been reported yet, it is interesting to put the results of this work in perspective by comparing with other cell types. The transport of G3-NH_2-FITC across Calu-3 cells is observed to be qualitatively different than that reported for Caco-2 cells, where no apparent maximum in permeability has been reported.[20, 71] However, the magnitude of the P_{app} of the G3-NH_2-FITC across the Calu-3 monolayer was observed to be similar to that reported across Caco-2 monolayers, which was ca. 0.8×10^{-7} cm·s^{-1} at 150 min.[71] While these numbers seem to be in agreement, caution should be exercised when drawing such comparisons, as factors including cell type, donor chamber concentration, and duration of the study can greatly influence the overall rate of transport.[15, 72] For instance, in the aforementioned studies, typical donor concentrations employed were at least 0.1 mM, which is considerably larger compared to this study (3.2 nmol). The similarities in these numbers at such dramatically different concentrations of the nanocarriers highlight the potential impact of the cell type. For instance, at concentrations of 0.1 mg·mL^{-1} G3-NH_2-FITC dendrimers had P_{app} values of 5.5×10^{-7} cm·s^{-1} across Madin-

Darby canine kidney cells (MDCK).[73] These values were markedly different when compared to what was observed for both Caco-2 and Calu-3 cells. Another factor that can also influence the permeability of G3-NH_2-FITC is the donor chamber concentration and incubation time.[15, 17, 71] For Caco-2 cells, at two different donor concentrations of 10 mM and 1 mM, the P_{app} values were determined to be 2.7× 10^{-7} cm·s^{-1} and 0.6× 10^{-7} cm·s^{-1}, respectively.[71] In another study, transport of G2-NH_2 (generation 2 dendrimers) studied on MDCK cells at increasing donor chamber concentrations from 50 μg to 300 μg resulted in ca. 4-fold increase of the P_{app} values.[73] These studies highlight the dependence of P_{app} on the initial donor chamber concentration. To put things in perspective, a comparison of the P_{app} values can be also made against some of the most common paracellular and transcellular markers. FITC-dextran, a common paracellular marker, of similar MW (10 KDa) was reported to have an P_{app} value of ca. 2 ×10^{-7} cm·s^{-1} across Calu-3 monolayers cultured under AIC – similar to what was observed in this case, while small lipophilic compounds that primarily traverse across Calu-3 monolayers via transcellular route, have much higher permeabilities, with P_{app} in the range of 10^{-5} to 10^{-6} cm·s^{-1} [37, 74]

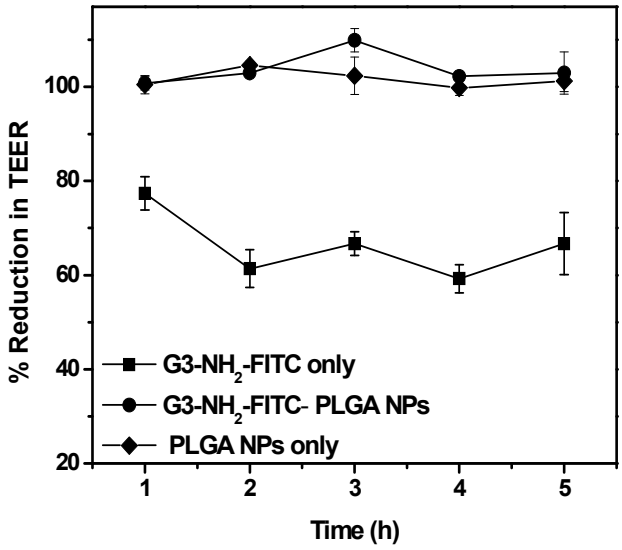

Figure 3.7. Variation in TEER of Calu-3 monolayers as a function of time, upon incubation with bare G3-NH_2-FITC, bare PLGA NPs, and NPs loaded with G3-NH_2-FITC. Results are reported as % reduction in TEER compared to control (cells incubated in blank HBSS). (n=4)

TEER measurements were used to understand the impact of the nanocarriers onto the monolayer integrity. The results for G3-NH_2-FITC, NP containing G3-NH_2-FITC, and NPs alone are shown in Figure 3.7. From the plot, a marked reduction (~60% of control) in the TEER of the Calu-3 cell monolayers incubated with G3-NH_2-FITC was observed. Similar results have been reported when studying the transport of dendrimer conjugates across Caco-2 cell lines,[75] where a strong association between paracellular transport (through the cellular tight junctions) and TEER reduction was proposed. The integrity of the tight junctions populating the cell monolayers has been shown to be altered in the presence of positive charges such

as the amine surface groups of G3-PAMAM dendrimers.[76] Our experiments revealed that replacing the G3-NH_2-FITC laden media with culture medium after 5h resulted in the revival of TEER to 80% of the control after 3 days – we stopped the experiments at that time, but it is possible that further TEER recovery could be observed after that time period. This is an important finding as these results, coupled with the lack of cytotoxicity on Calu-3 cells within the concentration ranges tested, reaffirm the potential of G3-NH_2 dendrimers as drug carriers for lung delivery.

The TEER reduction was also evaluated for the cell monolayers incubated with G3-NH_2-FITC loaded NPs. The studies revealed that there was no significant reduction in the TEER values of the cells incubated with the G3-NH_2-FITC loaded NPs compared to that of the control. The same observation was recorded for blank PLGA NPs pulsed onto Calu-3 cells. These results agree with earlier studies where it has been shown that PLGA NPs incubated on Calu-3 and on other epithelial cells did not alter the TEER, suggesting that the NPs do not interfere with the tight junctional integrity.[41, 77] An impact on the TEER seems to correlate well with the ability of the nanocarrier to transport across the monolayer. This is also clearly a concentration dependent effect, as when the dendrimers are released in small concentrations from the NPs, they do not to significantly affect the TEER, and are also not transported across the monolayer either.

3.4.6 Uptake studies with FACS.

Flow cytometry was employed in order to quantitatively determine the extent of internalization of bare G3-NH_2-FITC, G3-NH_2-FITC loaded NPs and PLGA-FITC NPs

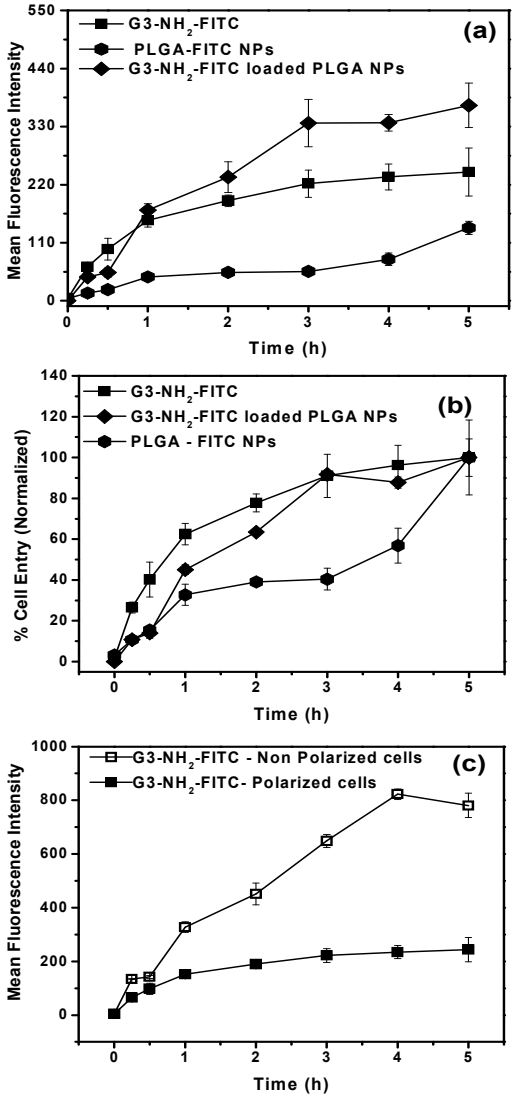

Figure 3.8 (a) Cellular entry of G3-NH_2-FITC, G3-NH_2-FITC loaded PLGA NPs, and PLGA-FITC NPs into Calu-3 as a function of time, as determined by FACS - mean fluorescence intensity values (MFI). The results shown here are averages of 6 replicates for each system, with at least 6000 events counted per system; (b) Rate of cell entry vs. time obtained by recasting MFI values relative to their cellular uptake at 5h; (c) Effect of cell polarization on the cellular entry of G3-NH_2-FITC. The error bars represent standard deviation (n=6 wells per time point; 6000 events for each well).

into polarized Calu-3 cells as a function of time. These results are highly complementary to the quantification of dendrimer concentration in the cell lysate discussed above. The results above provide an internalized amount based on an absolute scale - % out of total pulsed into the apical side of the insert, which is obtained at a single time point – at the end (5h) of the experiment. The FACS results on the other hand provide a relative scale of the extent of the internalization, where the kinetics of cellular uptake is emphasized. In the FACS work we also include a study with the PLGA-FITC NPs, which was run at the same concentration as the NP blend with dendrimer. This extra system was added in order to decouple the effect of NP internalization to that of the internalization of the FITC-dendrimer released from the NPs into the medium during the experiment, as discussed in more detail below.

For each system, at least 6000 events were counted. The results of the mean fluorescent intensity (MFI) values obtained from FACS for each system (G3-NH_2-FITC, G3-NH_2-FITC loaded NPs and PLGA-FITC NPs) are summarized in Figure 3.8 as a function of time. The results from Figure 3.8a are recast in Figure 3.8b as a percentage relative to the total internalization at 5h (which was set as 100%) in order to better understand the rate of cellular entry.[42] Note that this is done in spite of the fact that not all curves seem to have leveled off at that time, but nonetheless it will prove useful in this discussion. The results in Figure 3.8c serve to highlight the effect of monolayer polarization on cellular uptake - the uptake results for a selected system (G3-NH_2-FITC) are summarized in Figure 8c for polarized vs. non-polarized Calu-3 monolayers.

A sustained increase in cellular uptake, followed by a subsequent leveling off was observed in the case of G3-NH_2-FITC nanocarriers – Figure 3.8a. The leveling off in the cellular uptake was consistent with previous studies, where a similar trend with respect to the uptake of FITC-conjugated cationic dendrimers was observed on A549 cells.[42] This phenomenon was attributed to the fact that cationic dendrimers are typically internalized via adsorptive endocytosis, mediated by the presence of negatively charged proteoglycans on the cell membrane.[42] The uptake kinetics for this mode of internalization follows a curvilinear pattern likely due to saturation of membrane binding sites. A similar observation was also reported in B16f10 melanoma cells.[78] Interestingly, the internalization for cationic dendrimers in A549 cells leveled off within an hour after pulsing.[42] However, in this work, we observed a more gradual leveling off in the rate of internalization, with ca. only 60% being internalized after 1h – Figure 3.8b. This could possibly be attributed to differences in dendrimer generation and cell type, as both can influence cellular uptake.[15, 79] Another factor that could have potentially affected the rate of internalization is that, different from A549 cells, Calu-3 cells express mucins, which are negatively charged proteins that may interact with the dendrimers via electrostatic interactions, effectively hindering their transport to the cell surface.[80]

When compared to the G3-NH_2-FITC nanocarriers, the NPs (FITC-PLGA NPs) are seen to be internalized at a much lower rate – Figure 3.8b. It has been previously reported that particles in the size range of 30 nm diffuse unhindered across mucosal layers, while larger particles diffused at a much slower pace.[80] It seems, therefore, that despite their positive charge, G3-NH_2-FITC, being much

smaller than NPs, traverse the mucus layer at a much faster rate compared to what has been observed for NPs. It is also interesting to observe that there seems to be an induction period in terms of the internalization of the NPs, which was not observed for the free dendrimers. After an initial internalization, very little in terms of NPs seems to be taken up between 1 and 3h, when the rate of internalization starts increasing again. Even after 5h, the trend in the uptake curve appears to suggest that NPs continue to be internalized. This could be potentially related to the difficulty in diffusing through the mucosal layer at early times, as discussed above, but the ability of those particles to eventually traverse the mucus layer and to start being subsequently internalized.

The G3-NH_2-FITC-NP blends internalized at a rate similar to that of the FITC-PLGA NPs in the first 30 min of experiments, after which the rate of internalization more closely resembled that of the free G3-NH_2-FITC – Figure 3.8b. These results suggest that initial dendrimer internalization happened mostly as a blend (within the NPs). Different from the G3-NH_2-FITC, the uptake of PLGA NPs into the cell milieu is mostly expected to occur via internalization mechanisms distinct to those of positively charged dendrimers (at least how it is mediated at the cell surface), such as pinocytosis or clathrin-mediated endocytosis, owing to the negative charge and size of NPs.[81] This may help explain the variation in the rate of uptake when compared to that of bare G3-NH_2-FITC. However, after 1h, even when the release of the dendrimer from the NPs is relatively small at ca. 1.5%, the internalization of (free) dendrimers released from the NPs, and not as blends, seem to take over the internalization process. It is interesting to see that even after 5h, the internalization

process does not seem to have leveled off, different from the case of free dendrimers. This may be due to the fact that the internalization of the NPs increase at later times – after an induction period as discussed for the FITC-PLGA NPs. The increasing presence of free dendrimer released from the NPs is also likely to contribute to the fact that the curve seems to not level off at 5h.

Given that the same mass/molar concentration of dendrimer is added to the system for both free dendrimer and dendrimer encapsulated within the NPs (dendrimer in the blends), the MFI for the respective curves shown in Figure 8a can be directly compared. The dual mode of uptake of the dendrimer when formulated as blends (within the NPs as a blend, and as free dendrimer) seems to facilitate the internalization of a greater amount of dendrimer into the cell, thus effectively preventing the saturation seen in the case of free dendrimer. This is especially attractive as a drug delivery strategy as one can control not only the rate of delivery, but also the total cellular uptake. The ability to enhance uptake may be achieved by eliciting different endocytic pathways as can be done by varying the surface characteristics of nanocarriers,[64, 81] and this is currently under investigation.

Another important aspect of the FACS study was to elucidate the effect of Calu-3 polarization on cellular uptake. Polarized Calu-3 cells are expected to form tight junctional monolayers and exhibit all requisite morphological features inherent to them,[82] which also includes a different composition of the apical and basolateral membrane.[83] Because cellular uptake is surface-mediated, the composition of the apical side of the membrane is expected to impact uptake. Calu-3 was cultured to form polarized monolayers as described in the earlier sections. In case of the non-

polarized cells, the cells were seeded at the same density in 24-well plates and allowed to proliferate for a period of (only) 4 days prior to pulsing them with the G3-NH_2-FITC, when the cells were determined to be non-confluent. A plot of the MFI as a function of time for both non-polarized and polarized cells is shown in Figure 3.7c. From the figure, a marked increase in cellular uptake was observed for the non-polarized Calu-3 cells, with no signs of saturation in internalization by 5h, in sharp contrast to the results observed for the polarized layer. The results thus emphasize the relevance in performing the internalization studies on polarized monolayers.

In summary, the transport and internalization results described above suggest that the G3-NH_2-FITC can not only be effectively transported across Calu-3 monolayers, but also efficiently internalized in the cell milieu. The results also show that further mediation in terms of both cellular uptake into Calu-3 cells, and transport across the respective monolayers may be achieved by blending the DNCs within polymeric NPs. In the sections that follow, we present a strategy to formulate dendrimer nanocarriers into propellant-based OI formulations (pressurized metered-dose inhalers, pMDIs), with aerosol characteristics conducive to the deep lung deposition. Together with a recent publication from our group that demonstrate the ability to formulate polymeric NPs in pMDIs,[28, 30] the results demonstrate the potential in using the nanocarriers discussed here as platforms for the delivery of therapeutics to the lungs for local or systemic delivery.

3.4.7 Preparation and characterization of G3-NH_2-FITC loaded core-shell particles.

Given the fact that the dendrimer nanocarriers are highly positively charged, we expected them not to be easily dispersible in the low dielectric HFAs.[84, 85] Another potential issue in formulating the nanocarriers in propellant-based inhalers that needed to be considered is the fact that the optimum size of the aerosol particles for deep lung deposition (a few microns in diameter)[3] falls far outside the size of the dendrimer nanocarriers (a few nanometers in diameter). These will be considered in more detail in the discussion that follows. In this section we present a particle engineering technology that was pursued to formulate the dendrimer nanocarriers as micron-sized particles with enhanced physical stability in the propellant HFA, as an attempt to address the concerns mentioned above.

Loading of G3-NH_2-FITC into core-shell particles was accomplished via a modified emulsification-diffusion methodology.[28, 44] OLA-*g*-CS is a water soluble co-oligomer that has been shown to aid in the formation of stable particle dispersions in propellant HFAs due to the presence of ester groups, which have been shown to be highly HFA-philic.[86] A representative SEM micrograph of the G3-NH_2-FITC loaded core-shell particles is shown in Figure 3.9. The size distribution of these particles as determined by DLS in a model HFA (HPFP, which is liquid at ambient conditions) is shown as an inset in the same figure 3.8.

The SEM micrograph indicates the formation of smooth, fairly polydisperse (but with a single peak) particles. The average size of the particles was determined to be 1.0 ± 0.2 μm, with a polydispersity of 0.3. The geometric size range of the

particles formed here is well within the range prescribed for efficient deep lung deposition of inhaled aerosols.[2] The encapsulation efficiency of the G3-NH_2-FITC was determined using fluorometry.

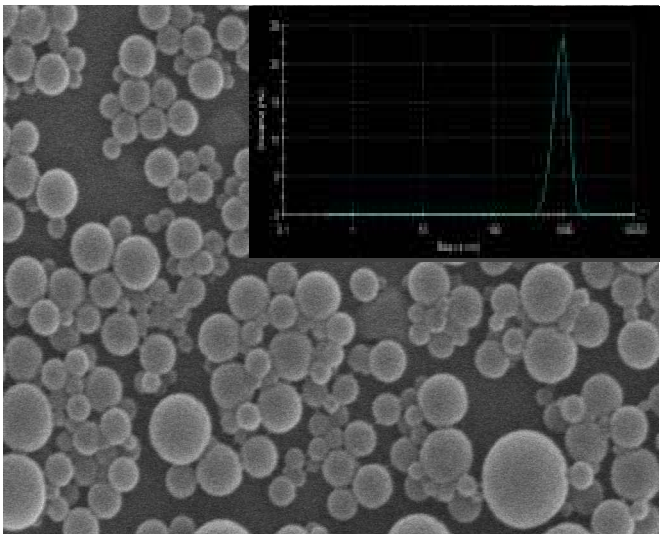

Figure 3.9. SEM micrograph of the G3-NH_2-FITC-loaded core-shell particles prepared via emulsification-diffusion. (*Inset)* Size distribution of G3-NH_2-FITC-loaded core-shell particles prepared using emulsification diffusion, as estimated by DLS, in HPFP, a model (liquid at ambient conditions) propellant HFA.

The loading of G3-NH_2-FITC in the core-shell particles was determined to be 0.06 ± 0.01 mg of dendrimer per mg co-oligomer, which corresponds to an encapsulation efficiency of 37±5%. While we have not attempted to encapsulate the G3-NH_2-FITC-loaded NPs in such core-shell particles, we have recently demonstrated the applicability of similar methodology in the encapsulation of polymeric NPs containing a fluorescent probe, which is of similar size and surface

characteristics, and thus expect that strategy to be also applicable to the to the G3-NH_2-FITC-loaded PLGA NPs.[28]

3.4.8 Physical stability of G3-NH_2-FITC loaded core-shell particles in HFA227.

The stability of freshly prepared G3-NH_2-FITC loaded core-shell particles and bare G3-NH_2-FITC dispersions in HFA227 was assessed by visually ascertaining the rate of sedimentation of the formulations as a function of time. Digital photographs were captured at predetermined times after the mechanical energy for dispersing the particles ceased, in order to assess the quality of the dispersions. Images captured at t=0h and t=2h are shown in Figure 3.10. The physical stability of formulations prepared using bare G3-NH_2-FITC are also shown as insets. The concentration of the core-shell particles was 2 $mg \cdot mL^{-1}$ (corresponding to 0.14 mg of the conjugate). A similar concentration of the G3-NH_2-FITC (0.15 $mg.mL^{-1}$) was utilized for the bare formulation.

From the images, as expected, the dispersions formulated using the core-shell particles are seen to possess superior physical stability when compared to the bare G3-NH_2-FITC formulation. The bare G3-NH_2-FITC formulated in the propellant creamed within a few seconds, and remained as aggregate, even after further mechanical energy input. For the core-shell formulation, creaming of the particles due to gravitational forces was observed - these are micron particles compared to the nanometer-sized dendrimers. These particles form loose aggregates that can be easily broken up and redispersed by simple manual agitation, indicating that the particles did not irreversibly flocculate.

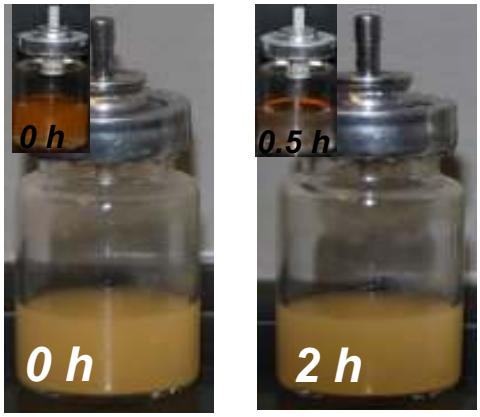

Figure 3.10. Dispersion stability of G3-NH_2-FITC formulated as core-shell particles in HFA 227 at 2 mg.mL^{-1}, 298 K, and saturation pressure of the propellant mixture. The digital images were obtained as soon as the mechanical energy input for dispersing the system was halted, and as a function of time after that. *(Inset)* Formulations prepared using bare G3-NH_2-FITC at 0.15 mg.mL^{-1} concentration.

3.4.9. Aerosol characteristics of G3-NH_2-FITC loaded core-shell particles.

Cascade impaction studies were conducted using an ACI in order to quantitatively assess the aerosol quality of the pMDI formulations, and the effect of the proposed particle engineering technology. ACI is an *in vitro* testing device comprised of 8-stages, with each stage representing a region of the lung, as benchmarked by *in vivo* and *in vitro* studies.[44, 87] Actuating the formulation

Table 3.1 Aerodynamic characteristics of the G3-NH_2-FITC-loaded core-shell and bare G3-NH_2-FITC formulations in HFA227 at 298 K and saturation pressure of the propellant. The particle concentration was 2 mg·mL^{-1} for the G3-NH_2-FITC-loaded core-shell formulation and 0.15 mg·mL^{-1} (corresponding to G3-NH_2-FITC mass loading in the core-shell particles) for bare G3-NH_2-FITC formulation. The mass reported is that of the G3-NH_2-FITC. The average and deviation were obtained from three independent runs (*n=3*). *FPF* = fine particle fraction, *AC* = actuator, and *IP* = induction port. MMAD and GSD are the mass mean aerodynamic diameter and geometric standard deviation, respectively.

Stages	**G3-NH_2-FITC concentration (Core-shell) (μg ± s.d) (n=3 runs)**	**G3-NH_2-FITC concentration (bare) (μg ± s.d) (n=3 runs)**
AC	2.4 ± 1.6	1.4 ± 0.5
IP	25.2 ± 7.8	2.1 ± 0.8
Stage 0 (9.0-10.0μm)	4.7 ± 1.9	0.4 ± 0.1
Stage 1 (5.8-9.0 μm)	9.2 ± 7.1	-
Stage 2 (4.7-5.8 μm)	3.5 ± 1.5	-
Stage 3 (3.3-4.7 μm)	16.7 ± 3.5	-
Stage 4 (2.1-3.3 μm)	15.3 ± 1.3	-
Stage 5 (1.1-2.1 μm)	11.6 ± 2.6	-
Stage 6 (0.7-1.1 μm)	3.3 ± 2.1	-
Stage 7 (0.4-0.7 μm)	2.0 ± 1.2	-
Filter (0-0.4 μm)	6.4 ± 4.7	3.2± 1.3
Single Puff Dose (μg)	4.7 ± 0.7	-
FPF (%)	55.1 ± 5.2	-
MMAD (μm)	3.0 ± 0.4	-
GSD	2.5 ± 0.1	

through the device under vacuum at a constant flow rate deposits the particles (free dendrimers or core-shell particles containing the G3-NH_2-FITC) on different stages depending on the aerosol size - larger aerosol particles are retained on the earlier stages of the impactor, while the smaller ones are retained in the later stages.[88] The amount of the G3-NH_2-FITC deposited on these stages was quantified by fluorometry, and relevant aerosol properties, including the FPF, MMAD and GSD were determined. FPF (fraction on stages 3-F of the ACI) is a measure of the efficiency of deposition in the deep lungs. MMAD is defined as the median of the airborne particle mass distribution with respect to the aerodynamic diameter. MMAD is always accompanied by GSD, which characterizes the variability of the particle size distribution.[88]

The ACI results for both the core-shell and the bare G3-NH_2-FITC formulation are summarized in Table 3.1, and recast as a % in Figure 3.11. The figure in % is easier for visualization and comparison of the different formulations, but does not contain the raw information required for the various calculations. Therefore, we include both figure and table. The values reported here are averages of three independent experiments obtained with three different canisters, with 20 actuations per canister.

The FPF for the formulation with the G3-NH_2-FITC loaded core-shell particles was 55±5%. We also achieved a high recovery efficiency for this formulation - mass collected relative to the estimated amount delivered based on the formulation concentration and reservoir volume - 80±8%. In comparison, the bare G3-NH_2-FITC formulation had a very poor recovery efficiency (ca. 5%), making a reliable estimation

of the FPF and other aerosol properties impractical. The low recovery for the formulation with free dendrimer can be attributed to the fact that the system is not well dispersed within the canister, and other losses due to perhaps the small sizes of the dendrimers.

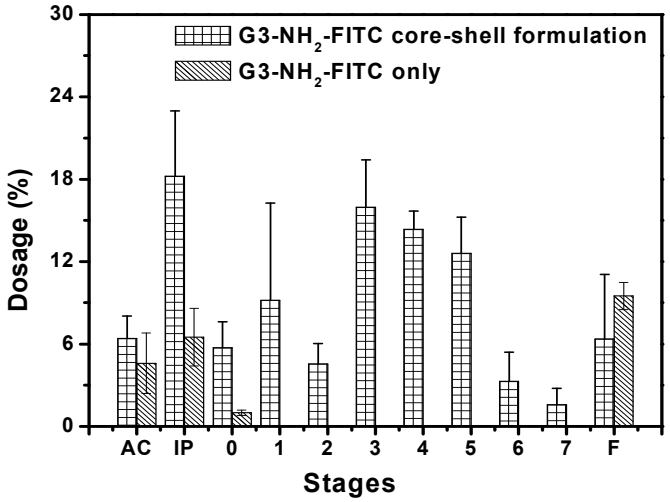

Figure 3.11. Anderson Cascade impaction results of the G3-NH_2-FITC formulated (a) as core-shell microparticles, and (b) as bare G3-NH_2-FITC in HFA 227, at 298 K and saturation pressure of the propellant. Particle concentration was 2 mg·mL^{-1} for the core-shell preparation while the concentration for the bare G3-NH_2-FITC formulation was 0.15 mg·mL^{-1}. *AC*, *IP* and *F* refer to actuator, induction port, and filter, respectively.

From what was collected, a large fraction was detected in the induction port and filter regions of the actuator, indicating the aggregation and erratic dispersion of these carriers within the propellant. These results further corroborate our earlier hypothesis, where, through a combination of sedimentation rate experiments and colloidal probe microscopy,[44, 84] we have shown that there is a direct correlation

between the physical stability of the formulations in the propellant, and the corresponding aerosol characteristics.[44] The aerosol properties of the G3-NH_2-FITC core-shell formulation compare favorably with those of commercial pMDI formulations containing dispersed crystals of small molecular weight therapeutics.[44, 89] For instance, Ventolin HFA®, a commercial formulation for asthma and chronic obstructive pulmonary disease (COPD) reported an FPF of 46% under the same conditions – note we have not attempted to optimize the FPF through changes in hardware nor particle size/distribution, when we would expect to achieve even larger FPFs.[44] The MMAD and GSD of the core-shell formulation, was calculated to be 3.0 μm and 2.5 μm, respectively, which is in good agreement with values required for enhanced deposition to the deep lungs.[3]

These results suggest that G3-NH_2-FITC formulations with good aerosol characteristics can be prepared using the proposed particle engineering strategy. Such platforms have thus the potential to be utilized to treat local ailments of the lungs, or in the treatment of systemic disorders through careful carrier design – transport modulation, as discussed above.

3.5 Conclusions.

In this work we demonstrate that the internalization and transport of G3-NH_2-FITC across a model of the pulmonary epithelium can be modulated by forming nanoblends of G3-NH_2-FITC with PLGA. The kinetics of internalization of the blends is very different from that of the free dendrimers. While saturation in cellular uptake is observed in the case of free G3-NH_2-FITC, the same is not seen for the solid NP blends containing the dendrimers, within the time frame of the experiments – 5h. Another interesting feature observed is that while there seems to be an induction period over which the uptake of the NPs is slow, as expected due to the larger size of the NPs, the presence of a mucus layer covering the Calu-3 cells, and the negative surface charge of the NPs, the total uptake of the dendrimers blended into the NPs increases at later times, and ends up being larger than the loading of free dendrimers at 5h - and it does not seem to have reached saturation at that time. These results thus indicate that the formation of nanoblends may help overcome saturation, and thus enhance cellular uptake, by exploring alternative internalization mechanisms. The formulation of dendrimers as nanoblends is also seen to be very efficient in preventing the transport across the monolayer, as seen by a decrease in the apparent permeability from 10^{-7} $cm.s^{-1}$ for the free dendrimers, to zero for dendrimers formulated as nanoblends. It is also relevant to mention that, within the concentration range investigated in this work, both the dendrimer and nanoblends were seen to be fairly non cytotoxic to Calu-3 cells. These results are particularly exciting as dendrimers have been suggested as effective drug delivery carriers for several chemotherapeutics, biomolecules, imaging agents and other relevant high potency

drugs. These results, combined with the ability to efficiently formulate free dendrimers or solid NPs (our previous work) in pMDIs, highlight the potential of these nanocarriers for the OI delivery of a range of therapeutics for the treatment of regional and systemic diseases.

3.6 References.

[1] Cipolla DC, Gonda I. Formulation technology to repurpose drugs for inhalation delivery. Drug Discovery today : Therapeutic Strategies. 2011.

[2] Patton JS, Byron PR. Inhaling medicines: delivering drugs to the body through lungs. Nature Reviews. 2007;6:67-74.

[3] Rogueda PG, Traini D. The nanoscale in pulmonary delivery. Part 1: deposition, fate, toxicology and effects. Expert Opinion in Drug Deliv. 2007;4:595-606.

[4] Sakagami M. In vivo, in vitro and ex vivo models to assess pulmonary absorption and disposition of inhaled therapeutics for systemic delivery. Advanced Drug Delivery Reviews. 2006;58:1030-60.

[5] Yang W, Peters JI, Williams RO, 3rd. Inhaled nanoparticles--a current review. International Journal of Pharmaceutics. 2008;356:239-47.

[6] Rytting E, Nguyen J, Wang X, Kissel T. Biodegradable polymeric nanocarriers for pulmonary drug delivery. Expert Opinion in Drug Delivery. 2008;5:629-39.

[7] Siekmeier R, Scheuch G. Systemic treatment by inhalation of macromolecules--principles, problems, and examples. Journal of physiology and pharmacology : an official journal of the Polish Physiological Society. 2008;59 Suppl 6:53-79.

[8] Laube BL, Janssens HM, de Jongh FH, Devadason SG, Dhand R, Diot P, et al. What the pulmonary specialist should know about the new inhalation therapies. European Respiratory Journal. 2011;37:1308-31.

[9] Sung JC, Pulliam BL, Edwards DA. Nanoparticles for drug delivery to the lungs. Trends in biotechnology. 2007;25:563-70.

[10] Rodrigo GJ, Castro-Rodríguez JA. Safety of long-acting β agonists for the treatment of asthma: clearing the air. Thorax. 2010.

[11] Fernandes CA, Vanbever R. Preclinical models for pulmonary drug delivery. Expert Opinion in Drug Delivery. 2009;6:1231-45.

[12] Azarmi S, Roa WH, Lobenberg R. Targeted delivery of nanoparticles for the treatment of lung diseases. Advanced Drug Delivery Reviews. 2008;60:863-75.

[13] Bai S, Thomas C, Ahsan F. Dendrimers as a carrier for pulmonary delivery of enoxaparin, a low-molecular weight heparin. Journal of Pharmaceutical Sciences. 2007;96:2090-106.

[14] Bai S, Ahsan F. Synthesis and evaluation of pegylated dendrimeric nanocarrier for pulmonary delivery of low molecular weight heparin. Pharmaecutical Research. 2009;26:539-48.

[15] Kitchens KM, Ghandehari H. PAMAM Dendrimers as Nanoscale Oral Drug Delivery Systems. In: de Villiers MM, AraMWit P, Kwon GS, editors.2009. p. 423-59.

[16] Yang Y, Bajaj N, Xu P, Ohn K, Tsifansky MD, Yeo Y. Development of highly porous large PLGA microparticles for pulmonary drug delivery. Biomaterials. 2009;30:1947-53.

[17] Lin YL, Khanafer K, El-Sayed ME. Quantitative evaluation of the effect of poly(amidoamine) dendrimers on the porosity of epithelial monolayers. Nanoscale. 2010;2:755-62.

[18] Jevprasesphant R, Penny J, Attwood D, D'Emanuele A. Transport of dendrimer nanocarriers through epithelial cells via the transcellular route. J Control Res. 2004;97:259-67.

[19] Yoo JW, Doshi N, Mitragotri S. Adaptive micro and nanoparticles: Temporal control over carrier properties to facilitate drug delivery. Advanced Drug Delivery Reviews. 2011.

[20] Kitchens KM, El-Sayed MH, Ghandehari H. Transepithelial and endothelial transport of poly (amido amine) dendrimers. Advanced Drug Deliver Reviews. 2005;57:2163-76.

[21] Petros RA, DeSimone JM. Strategies in the design of nanoparticles for therapeutic applications. Nature Review Drug Discovery. 2010;9:615-27.

[22] D'Emanuele A, Attwood D. Dendrimer–drug interactions. Advanced Drug Delivery Reviews. 2005;57:2147-62.

[23] Plapied L, Duhem N, des Rieux A, Preat V. Fate of polymeric nanocarriers for oral drug delivery. Current Opinion in Colloid and Interface Science. 2011;16:228-37.

[24] Saad M, Garbuzenko OB, Ber E, Chandna P, Khandare JJ, Pozharov VP, et al. Receptor targeted polymers, dendrimers, liposomes: which nanocarrier is the most efficient for tumor-specific treatment and imaging? Journal of Controlled Release. 2008;130:107-14.

[25] Bandhopadhyay A, Fine RL, Demento S, Bockenstedt LK, Fahmy TM. The impact of nanoparticle ligand density on dendritic-cell targeted vaccines. Biomaterials. 2011.

[26] Pisal DS, Yellepeddi VK, Kumar A, Palakurthi S. Transport of surface engineered polyamidoamine (PAMAM) dendrimers across IPEC-J2 cell monolayers. Drug Delivery. 2008;15:515-22.

[27] Forbes B, Ehrhardt C. Human respiratory epithelial cell culture for drug delivery applications. European journal of pharmaceutics and biopharmaceutics : official journal of Arbeitsgemeinschaft fur Pharmazeutische Verfahrenstechnik eV. 2005;60:193-205.

[28] Bharatwaj B, Wu L, Whittum-Hudson JA, da Rocha SRP. The potential for the noninvasive delivery of polymeric nanocarriers using propellant-based inhalers in the treatment of Chlamydial respiratory infections. Biomaterials. 2010;31:7376-85.

[29] Al-Hallak MH, Sarfraz MK, Azarmi S, Roa WH, Finlay WH, Lobenberg R. Pulmonary delivery of inhalable nanoparticles: dry powder inhalers. Therapeutic Delivery. 2011;2:1313-24.

[30] Conti DS, Bharatwaj B, Brewer D, da Rocha SRP. Propellant-based inhalers for the non-invasive delivery of genes via oral inhalation. Journal of Controlled Release. 2011.

[31] Cho H-J, Yoon HY, Koo H, Shim J-S, Lee J-H, Kim K, et al. Self-assembled nanoparticles based on hyaluronic acid-ceramide (HA-CE) and Pluronic® for tumor-targeted delivery of docetaxel. Biomaterials. 2011.

[32] Kolhe P, Misra E, Kannan RM, Kannan S, Lieh-Lai M. Drug complexation, in vitro release and cellular entry of dendrimers and hyperbranched polymers. International Journal of Pharmaceutics. 2003;259:143-60.

[33] Cartiera MS, Johnson KM, Rajendran V, Caplan MJ, Saltzman WM. The uptake and intracellular fate of PLGA nanoparticles in epithelial cells. Biomaterials. 2009;30:2790-8.

[34] Sanders NN, Van Rompaey E, De Smedt SC, Demeester J. Structural Alterations of Gene Complexes by Cystic Fibrosis Sputum. American Journal of Respiratory and Critical Care Medicine. 2001;164:486-93.

[35] Patton JS. Mechanisms of macromolecule absorption by the lungs. Advanced Drug Delivery Reviews. 1996;19:3-36.

[36] Kim SH, JEong JH, Chun KW, Park TG. Target-Specific Cellular Uptake of PLGA Nanoparticles Coated with Poly(l-lysine)−Poly(ethylene glycol)−Folate Conjugate. Langmuir. 2005;21:8852-7.

[37] Grainger CI, Greenwell LL, Lockley DJ, Martin GP, Forbes B. Culture of Calu-3 cells at the air interface provides a representative model of the airway epithelial barrier. Pharmaceutical Research. 2006;23:1482-90.

[38] Fiegel J, Ehrhardt C, Schaefer UF, Lehr CM, Hanes J. Large porous particle impingement on lung epithelial cell monolayers--toward improved particle characterization in the lung. Pharmaceutical Research. 2003;20:788-96.

[39] Grainger CI, Greenwell LL, Martin GP, Forbes B. The permeability of large molecular weight solutes following particle delivery to air-interfaced cells that model the respiratory mucosa. European Journal of Pharmaceutics and Biopharmaceutics. 2009;71:318-24.

[40] Madlova M, Jones SA, Zwerschke I, Ma Y, Hider RC, Forbes B. Poly(vinyl alcohol) nanoparticle stability in biological media and uptake in respiratory epithelial cell layers in vitro. European Journal of Pharmaceutics and Biopharmaceutics : official journal of Arbeitsgemeinschaft fur Pharmazeutische Verfahrenstechnik eV. 2009;72:437-43.

[41] Qaddoumi MG, Ueda H, Yang J, Davda J, Labhasetwar V, Lee VH. The characteristics and mechanisms of uptake of PLGA nanoparticles in rabbit conjunctival epithelial cell layers. Pharmaceutical Research. 2004;21:641-8.

[42] Perumal OP, Inapagolla R, Kannan S, Kannan RM. The effect of surface functionality on cellular trafficking of dendrimers. Biomaterials. 2008;29:3469-76.

[43] Win KY, Feng SS. Effects of particle size and surface coating on cellular uptake of polymeric nanoparticles for oral delivery of anticancer drugs. Biomaterials. 2005;26:2713-22.

[44] Wu L, Bharatwaj B, Panyam J, da Rocha SRP. Core–shell Particles for the Dispersion of Small Polar Drugs and Biomolecules in Hydrofluoroalkane Propellants. Pharmaceutical Research. 2008;25:289-301.

[45] Majoros IJ, Thomas TP, Mehta CB, Baker JR, Jr. Poly(amidoamine) dendrimer-based multifunctional engineered nanodevice for cancer therapy. Journal of Medicinal Chemistry. 2005;48:5892-9.

[46] Kim Y, Klutz AM, Jacobson KA. Systematic investigation of polyamidoamine dendrimers surface-modified with poly(ethylene glycol) for drug delivery applications: synthesis, characterization, and evaluation of cytotoxicity. Bioconjugate Chemistry. 2008;19:1660-72.

[47] Mishra MK, Kotta K, Hali M, Wykes S, Gerard HC, Hudson AP, et al. PAMAM dendrimer-azithromycin conjugate nanodevices for the treatment of Chlamydia trachomatis infections. Nanomedicine : nanotechnology, biology, and medicine. 2011.

[48] Panyam J, Labhasetwar V. Biodegradable nanoparticles for drug and gene delivery to cells and tissue Advanced Drug Delivery Reviews. 2003;55:329-47.

[49] Mundargi RC, Babu VR, Rangaswamy V, Patel P, Aminabhavi TM. Nano/micro technologies for delivering macromolecular therapeutics using poly(D,L-lactide-co-glycolide) and its derivatives. Journal of Controlled Release. 2008;125:193-209.

[50] Hamdy S, Haddadi A, Hung RW, Lavasanifar A. Targeting dendritic cells with nano-particulate PLGA cancer vaccine formulations. Advanced Drug Delivery Reviews. 2011.

[51] Babu VR, Patel P, Mundargi RC, Rangaswamy V, Aminabhavi TM. Developments in polymeric devices for oral insulin delivery. Expert opinion in drug delivery. 2008;5:403-15.

[52] Wang X, Inapagolla R, Kannan S, Lieh-Lai M, Kannan RM. Synthesis, characterization, and in vitro activity of dendrimer-streptokinase conjugates. Bioconjugate chemistry. 2007;18:791-9.

[53] de la Fuente M, Csaba N, Garcia-Fuentes M, Alonso MJ. Nanoparticles as protein and gene carriers to mucosal surfaces. Nanomedicine. 2008;3:845-57.

[54] Hans ML, Lowman AM. Biodegradable nanoparticles for drug delivery and targeting. Current Opinion in Solid State and Material Science. 2002;6:319-27.

[55] Li X, Xu Y, Chen G, Wei P, Ping Q. PLGA nanoparticles for the oral delivery of 5-Fluorouracil using high pressure homogenization-emulsification as the preparation method and in vitro/in vivo studies. Drug Development and Industrial Pharmacy. 2008;34:107-15.

[56] Intra J, Salem AK. Fabrication, characterization and in vitro evaluation of poly(D,L-lactide-co-glycolide) microparticles loaded with polyamidoamine-plasmid DNA dendriplexes for applications in nonviral gene delivery. Journal of Pharmaceutical Sciences. 2010;99:368-84.

[57] Zhang XQ, Intra J, Salem AK. Conjugation of polyamidoamine dendrimers on biodegradable microparticles for nonviral gene delivery. Bioconjugate chemistry. 2007;18:2068-76.

[58] Liu J, Zhang SM, Chen PP, Cheng L, Zhou W, Tang WX, et al. Controlled release of insulin from PLGA nanoparticles embedded within PVA hydrogels. Journal of Material Science, Materials in Medicine. 2007;18:2205-10.

[59] Mao S, Xu J, Cai C, Germershaus O, Schaper A, Kissel T. Effect of WOW process parameters on morphology and burst release of FITC-dextran loaded PLGA microspheres. International Journal of Pharmaceutics. 2007;334:137-48.

[60] Lee W-K, Park J-Y, Yang EH, Suh H, Kim SH, Chung DS, et al. Investigation of the factors influencing the release rates of cyclosporin A-loaded micro- and nanoparticles prepared by high-pressure homogenizer. Journal of Controlled Release. 2002;84:115-23.

[61] Cohen-Sela E, Chorny M, Koroukhov N, Danenberg HD, Golomb G. A new double emulsion solvent diffusion technique for encapsulating hydrophilic molecules in PLGA nanoparticles. Journal of Controlled Release. 2009;133:90-5.

[62] Allemann E, Leroux JC, Gurny R, Doelker E. In vitro extended-release properties of drug-loaded poly(DL-lactic acid) nanoparticles produced by a salting-out procedure. Pharmaceutical Research. 1993;10:1732-7.

[63] Panyam J, Dali MM, Sahoo SK, Ma W, Chakravarthi SS, Amidon GL, et al. Polymer degradation and in vitro release of a model protein from poly(D,L-lactide-co-glycolide) nano- and microparticles. Journal of Controlled Release. 2003;92:173-87.

[64] Menjoge AR, Kannan RM, Tomalia DA. Dendrimer-based drug and imaging conjugates: design considerations for nanomedical applications. Drug Discovery Today. 2010;15:171-85.

[65] Sambuy Y, De Angelis I, Ranaldi G, Scarino ML, Stammati A, Zucco F. The Caco-2 cell line as a model of the intestinal barrier: influence of cell and culture-related factors on Caco-2 cell functional characteristics. Cell biology and toxicology. 2005;21:1-26.

[66] Jevprasesphant R, Penny J, Jalal R, Attwood D, McKeown NB, D'Emanuele A. The influence of surface modification on the cytotoxicity of PAMAM dendrimers. International journal of pharmaceutics. 2003;252:263-6.

[67] Csaba N, Caamano P, Sanchez A, Dominguez F, Alonso MJ. PLGA:poloxamer and PLGA:poloxamine blend nanoparticles: new carriers for gene delivery. Biomacromolecules. 2005;6:271-8.

[68] Walter E, Merkle HP. Microparticle-mediated transfection of non-phagocytic cells in vitro. Journal of Drug Targeting. 2002;10:11-21.

Chapter 4

PEGylated Dendrimer Nanocarriers for Transport Modulation Across the Pulmonary Epithelium

4.1. Introduction.

Oral inhalation (OI) is not only the preferred mode of administration of therapeutics intended for the regional delivery *to the lungs*, but it has been also recognized as a promising route for the non-invasive targeting to the systemic circulation – *through the lungs*.[1, 2] Systemic delivery through the lungs is facilitated due to its large surface area, low proteolytic activity, and a thin cellular barrier, characteristics that may enhance the bioavailability of therapeutics, and provide fast access to those molecules to the bloodstream.[2, 3] Several recent clinical trials of OI formulations dealing with therapeutics intended to the systemic circulation attest to this potential.[4-6]

Polymeric nanocarriers (PNCs) may be successfully explored in combination with OI formulations for the controlled and targeted local delivery of therapeutics to the lung tissue, and to modulate the transport of drugs across the airway epithelia. Such advancements hold great promise in the delivery of both small molecules and biomacromolecules for the treatment of medically relevant diseases such as lung cancer, tuberculosis, COPD, and asthma, among others.[7-13]

The ease at which the size, morphology and surface chemistry of PNCs can be tailored is perhaps the most attractive feature of such drug carriers, as those

properties can be used to modulate the interaction of the nanocarriers with intra and extracellular barriers, and to selectively target desired cell populations, and even specific cellular organelles.[7, 14, 15] Given these potential advantages, there are tremendous opportunities in combining the development of innovative OI formulations for the regional and systemic delivery to an through the lungs using PNCs.

Dendrimer nanocarriers (DNCs) represent a particularly interesting class of polymeric nanocarriers (PNCs) as they are especially suited to tackle the many challenges that exist in the development of carriers for the delivery of drugs to and through the lungs. DNCs are hyperbranched synthetic molecules with high monodispersity, and multivalency at the surface that allows the facile attachment of a range of moieties, including therapeutic and imaging agents.[9, 16-18] This surface polyfunctionality can be exploited to tailor the DNCs with functional groups that can be used to modulate (i) the rate and mechanism of cellular uptake, and (ii) the extent of permeation across unyielding extra and intracellular barriers populating the lung epithelium,[16, 19, 20] and thus optimize the carrier for either local or systemic deliver. The tethering of poly (ethylene glycol) (PEG) to the surface of DNCs is a particularly relevant strategy in this case as PEGylation to PNCs has been shown to minimize the carrier toxicity,[18, 21] improve transport across extracellular barriers,[14, 22] decrease non-specific interactions, including with serum proteins (opsonization),[23] lung surfactant[24] and constituents of the mucosal tissues,[25] to improve systemic circulation,[23, 26] and to influence the mechanisms of cellular transport and uptake.[16, 21]

The goal of this study was to investigate the effect of PEGylation on the interaction of DNCs with *in vitro* and *in vivo* models of the pulmonary epithelium. Generation 3 (G3) poly(amido amine) (PAMAM) dendrimers with varying surface density of PEG (MW 1000 Da, $G3NH_2$-nPEG1000) were synthesized, characterized, and their toxicity evaluated on a model airway epithelial cell line, Calu-3. Transport studies of the synthesized conjugates were conducted across polarized Calu-3 monolayers cultured under an air-interface. Rate of cellular uptake was followed by flow cytometry, and the total cellular uptake quantified using cell lysis, also on polarized cell monolayers. The pharmacokinetic parameters of selected conjugates were investigated upon lung delivery (pharyngeal aspiration) to BALB-C mice so as to assess the potential of PEGylation to mediate the transport of the DNCs across the pulmonary epithelium.

4.2 Materials.

Amine-terminated, generation 3 (G3) poly(amido amine) (PAMAM) dendrimer ($G3NH_2$), with 32 surface groups, and 6882 Da as determined by MALDI (mass reported by the vendor is 6909 Da), poly(ethylene glycol) monomethyl ether (mPEG, M_n 1000 Da), 1-ethyl-3-(3-dimethylaminopropyl) carbodiimide (EDC), N-Hydroxysuccinimide (NHS), potassium *tert* butoxide, ethyl bromoacetate, fluorescein isothiocyanate (FITC), Bovine Serum Albumin (BSA), Trypan Blue (0.4%), Trypsin supplemented with 0.25% EDTA (for flow cytometry), osmium tetroxide (OsO_4), and Triton-X-100 were all purchased from Sigma (St.Louis, MO), and used as received unless otherwise specified. $G3NH_2$ dendrimers were dried in vacuum for 24 hours to

remove traces of methanol before the reaction. mPEG was purified by dissolving the raw compound in chloroform, and drying the resulting solution over anhydrous magnesium sulfate. The final product was obtained by filtering and then evaporating the sample in a rotavapor. Samples were stored in a desiccator prior to usage. Anhydrous dimethylsulfoxide (DMSO) was purchased from Acros. Deionized water (DI water) with a resistivity of 18.2 $M\Omega \cdot cm^2$ was used in all experiments. Hanks' balanced salt solution (HBSS, 1X) supplemented with 0.01 M (4-(2-hydroxyethyl)-1-piperazineethanesulfonic acid) (HEPES) was prepared according to a procedure detailed elsewhere.[27] Human bronchial epithelial cell line Calu-3 (HTB-55) was purchased from ATCC (Manassas, VA). Tissue culture flasks (Greiner BioOne, 75 cm^2), 24 (Corning Costar) and 96 well plates (Greiner BioOne), Transwell Inserts (#3470 - polyester membrane, Corning, 0.33 cm^2, 0.4 μm pore size) were all purchased from VWR. Dulbecco's Modified Eagle's Media (DMEM) and trypsin (TRYple™ express) were obtained from Invitrogen. Fetal Bovine Serum (non-heat inactivated) was procured from Atlanta Biologicals (Atlanta, GA). Rabbit anti ZO-1 (Mid) antibody, Alexa Fluor 546 goat anti-rabbit IgG (H+L), and 4´,6-diamidino-2-phenylindole, dilactate (DAPI, dilactate) were purchased from Molecular Probes. All antibodies were diluted a 100 times in phosphate buffered saline (5 □g, PBS, pH 7.4), supplemented with 6% (w/v) BSA (to prevent non-specific binding of the antibody) prior to usage. DPX mounting medium was obtained from Fluka. MTT (3-(4,5-Dimethylthiazol-2-yl)-2,5-Diphenyltetrazolium Bromide) assay was purchased from Life Technologies, and was utilized as per the protocol detailed by the manufacturer. BCA protein assay was purchased from Pierce (Evanston, IL).

Microscope slides and cover glass slides (18 mm^2) were obtained from Fisher. All glassware was washed thoroughly in water and dried under vacuum prior to usage. All other chemicals used were purchased from Fisher and EMD, were of HPLC grade, and used as received unless otherwise noted.

All animal experiments were conducted in accordance to the Institutional Animal Care and Use Committee at Wayne State University. Seven week old, male Balb/c mice weighing between 20-25 g were purchased from Charles River Inc. All animals were allowed to acclimatize for a week prior to experimentation and were housed in a pathogen free environment in HEPA filtered cages. Animals had access to food and water ad libitum. Isoflurane was purchased from VetOne. Heparin sodium salt was purchased from Sigma and dissolved in sterile saline to make a 10 U/ml final concentration.

4.3. Methods.

4.3.1. Synthesis and Characterization of Carboxylic acid-terminated mPEGs (cmPEG).

cmPEG was synthesized according to a procedure described in the literature.[28] Purified mPEG (0.018 mmol) and potassium *tert*-butoxide (0.089 mol) were dissolved in 150 mL of *tert*-butanol at 40°C. Ethyl bromoacetate (0.045 mol) was subsequently slowly added to this solution. The contents were reacted for a period of 2h, after which the *tert*-butanol was evaporated. The residue recovered was dissolved in 1M sodium hydroxide (to hydrolyze the ester), and the solution was allowed to stand at room temperature for 2h, after which the pH of the solution was

adjusted to 2 using 4N HCl. The cmPEG obtained was extracted into chloroform (200 mL), and the extract was washed with water, and dried over anhydrous $MgSO_4$. The resulting product was characterized using ^{1}H-NMR (Varian 400 mHz), and MALDI-TOF (Ultraflex, Bruker Daltonics). The sample for MALDI analysis was prepared by mixing 2 μl of 1 mg·ml^{-1} solution of the PEG compound in a 1:1 (v/v) acetonitrile-water mixture with an equal volume of 2,5-dihydrobenzoicacid (DHB) matrix (10 mg·ml^{-1} in the same solvent mixture, 1:1 AcN:water). 2 μl of this mixture was spotted and evaporated to dryness on a stainless steel MALDI target plate (MTP 384, Bruker Daltonics). A mass spectrum was generated in the linear mode using a nitrogen laser at 20 kV. The mass of the compound was determined by comparing the resulting spectra against a compendium of calibrated peptide standards using FlexAnalysis™ software (Bruker Daltonics).

4.3.2. Conjugation of PEG grafts and FITC to G3-NH_2.

Conjugation of PEG to G3-NH_2 was accomplished by reacting the carboxyl-terminated end of the cmPEG to the amine surface group of G3NH_2 via EDC-NHS coupling reaction, with minor modifications.[29] Labeling of FITC to the G3NH_2 surface and the PEGylation were done in a one pot synthesis, using a procedure similar to that detailed in the literature.[30-32] A series of G3NH_2 with varying graft densities of PEG 1000 Da (G3NH_2-nPEG1000, where *n* is the number of PEG 1000 grafts) was prepared and characterized. Appropriate molar ratios of EDC and NHS, which depended on the desired extent of PEG surface density, were added to a stirred solution of G3NH_2 (150 mg, 21 μM) in anhydrous DMSO (3 mL), and the

mixture was stirred for 4 hours. This was followed by the addition of appropriate molar ratios of cmPEG and FITC (dissolved in 1 mL DMSO) dropwise to the reaction under stirring. The reaction mixture was allowed to stir for a period of at least 4 days in case of low PEG graft density, and for up to two weeks for the higher PEG densities. The contents from the flask were then transferred to a dialysis tube (Fisher, MWCO 12000 Da), and were dialyzed against DI water for 48h to remove any unreacted FITC, EDC, NHS and cmPEG. The final product was recovered by snap freezing the contents from the dialysis bag, and freeze drying the resulting product for 48h. Product yields were ca. 60%. Dendrimer conjugates were characterized by light scattering for size and zeta potential (ζ) using a Malvern Zetasizer, and by ^{1}H-NMR, and MALDI-TOF. DLS was performed by dissolving 1.5 mg of the purified conjugate in HBSS and analyzing the resulting sample. The size reported here is an average of 4 runs with 10 counts for each run. For ^{1}H-NMR 8 mg of the freeze dried G3NH$_2$-nPEG1000 was dissolved in *d*-DMSO (Cambridge Isotopes). The sample for MALDI-TOF analysis was prepared as described in the earlier section. Synthesis of FITC labeled G3NH$_2$ with no PEG was accomplished by reacting appropriate molar amounts of FITC dissolved in DMSO with G3NH$_2$ overnight in DMSO (5 mL). The resulting product was purified dialyzed (MWCO 1000 Da) against DI water for 48h, and the product was recovered by freeze drying.

4.3.3. Culture of Calu-3 Cells.

Calu-3 cells, derived from human bronchial airway epithelium, between passages 36 and 50, were used as models to study the transport and internalization

of dendrimers conjugates. Cells were plated in 75 cm^2 culture flasks in medium comprising of Dulbecco's Modified Eagle's Medium (DMEM) supplemented with 10% FBS and 2% antibiotic (AB, penicillin-streptomycin) solution. The medium was exchanged once every two days. Cells were split at a ratio of 2:3 when they attained ca. 90% confluence.

4.3.4. Cytotoxicity of G3NH_2-nPEG1000 conjugates.

Cell viability of G3NH_2-nPEG1000 conjugates was determined using the MTT assay (Promega) as described in the literature.[33] The assay was prepared as per the protocol given by the manufacturer and stored at -20°C prior to use. Cells were plated at a density of 10,000 cells per well, in 96 well plates, in DMEM supplemented with 10% FBS and 2% AB. Cells were allowed to attach and grow for a period of 24h, after which they were washed thrice with 1X PBS, and replenished with serum-free medium containing the G3NH_2-nPEG1000 conjugates at varying concentrations. The cells were incubated in the conjugate laden media for a period of 24h, after which the medium was removed, the cells washed thrice with 1X PBS and incubated in MTT assay at 37°C for 4h, after which 75 μl of the media was removed and the wells were incubated in 50 μl of DMSO for 10 minutes in order to dissolve the insoluble formazan crystals. Cell monolayers were subjected to UV analysis at a wavelength of 540 nm using a plate reader (Molecular Devices, CA) to assess the extent of their cell kill. As a positive control, untreated cells were used and the total cell kill was determined by comparing the absorbance of the treated cells with their

untreated counterparts. The results expressed here are cell viability averages of 5 wells for each concentration.

4.3.5. Cell Culture for Transport Studies.

For transport experiments, cells were seeded on the apical compartment of Transwell® cell culture supports at a density of 0.5×10^6 cells·cm^{-2}. The inserts were then positioned onto 24 well plates containing 0.6 mL of medium on the basolateral side of the insert. To the apical side, 0.2 mL of culture medium was added. The cells were incubated at 37°C and 5% CO_2 atmosphere, and grown in a liquid-covered culture (LCC) for 2 days. The medium in the apical compartment was then removed, and the cells were allowed to grow in an air-interfaced culture (AIC). The medium in the basolateral compartment was replaced every two days, and the cells continued to grow under AIC. Transepithelial electrical resistance (TEER) measurements were conducted using Chopstick electrodes (STX-2) and an EVOM voltohmmeter (World Precision Instruments, Florida) in order to ascertain the monolayer confluence. The apical (where the monolayer is cultured) and the basolateral chambers were fed with appropriate volumes of fresh warmed culture media and the inserts were returned to the incubator for equilibration for 30 minutes. The monolayer resistance was measured after equilibration, and the true monolayer resistance was calculated by subtracting the EVOM reading of the cell-free culture insert from the reading obtained from cell-laden insert, and normalizing for the surface area of the support. The TEER values reported in this study represent the average resistance of monolayers cultured in 16 separate Transwell® inserts.

4.3.6. Electron Microscopy of Cell monolayers.

. Once the peak TEER values were attained, some of the cell monolayers were subject to scanning electron microscopy (SEM) in order to evaluate their morphological features. The monolayers for SEM were prepared according to a procedure described in the literature.[34] Briefly, the monolayers were fixed in a 1:1 ratio of culture medium and 2.5% glutaraldehyde (fixing solution) in DI water. The fixing medium was added to both the apical and basolateral sides of the insert, and the insert was gently rotated for 5 minutes. Subsequently, the medium-fixative mixture was aspirated and replaced with 100% fixing solution (2.5% glutaraldehyde) for 1 hour. The fixed cell monolayers were bathed in 1% (w/v) OsO_4 in water for 2 hours. The cells were then dehydrated by washing in a series of increasing gradients of ethanol (20, 40, 60, 80 and 100% ethanol for 8-10 minutes each) and lyophilized (LabConco FreeZone) for 36h. Cell monolayers thus prepared were carefully removed from the insert and mounted onto aluminum stubs using adhesive carbon tapes. They were sputter-coated (Ernst Fullam, NY) with gold for 30s, and imaged using an SEM (Hitachi S-2400) at 22kV.

4.3.7. Immunocytochemistry.

Immunocytochemistry was performed on confluent Calu-3 monolayers in order to visualize the presence of tight junctional protein, ZO-1 according to the protocol detailed by the manufacturer.[35] Select monolayers, with appropriate TEER values (values peaked and leveled) were sequestered and washed with PBS to remove traces of culture media. The washed cell monolayers were fixed in 4%

paraformaldehyde (in PBS) for a period of 20 minutes. The fixed cells were washed thrice with PBS (5 minutes each time), and permeabilized with 0.2% triton X-100 in PBS for 30 minutes. The permeabilized monolayer was further washed with PBS and blocked using 6% BSA for 30 minutes to prevent non-specific antibody binding.[36] This procedure was followed by incubation of the cells for 60 minutes in Rabbit anti ZO-1 antibody at 37°C. The cells exposed to the primary antibody were washed thrice with PBS, and were incubated for 60 min in Alexa Fluor 546 goat anti-rabbit IgG, the secondary antibody, at 37°C. The cell layer was washed thoroughly with PBS, and counterstained with DAPI (0.5 $\mu g \cdot ml^{-1}$ in DI water) for 30 minutes at room temperature. The cell culture support membranes from the Transwell® inserts were carefully removed and mounted onto glass slides using DPX mounting media, and sealed using cover slides. The slide was stored at 4°C overnight prior to observation under a fluorescence microscope (Zeiss Axiocam MR, Carl Zeiss) to visualize the presence of tight junctions.

4.3.8. Epithelial Permeability of the Dendrimer Conjugates Across Calu-3 Monolayers Seeded in Transwell® Inserts.

Transport experiments were conducted once the cell monolayers reached confluence and the TEER values peaked (around day 15). The TEER of the cell monolayers was measured prior to starting the experiments. The culture media in the inserts was replaced with warm 1X Hank's Balanced salt solution (HBSS) at both the apical and basolateral chambers, and the cells were allowed to equilibrate for 30 min. After that, the HBSS on the side was removed, and replaced with HBSS

containing a known molar concentration (25 nmol) of FITC-conjugated G3NH_2-nPEG1000 of varying PEG surface density (*n*). In order to maintain sink conditions, the inserts were moved to a well containing fresh HBSS (1X) at predetermined times, and a known volume of HBSS from the basolateral side of the spent insert was removed and analyzed for the FITC-conjugated dendrimer using a fluorescence spectrometer (Perkin Elmer LS50B) in order to determine the extent of transport of dendrimer from the apical onto the basolateral (A → B) side. The apparent permeability (P_{app}) from A→B, which indicates the ease of flow of the dendrimers nanocarriers across the monolayer, was calculated according to Equation 4.1:

$$P_{app} = F / (A \cdot C_o) \qquad (4.1)$$

where *F* is the flux, or rate of change of cumulative mass transported, *A* is the area of the insert and C_o is the initial concentration of G3NH_2-nPEG1000 in the donor (apical) compartment.

Dendrimer-free HBSS incubated on the apical side of the insert was used as control. Recording of TEER was accomplished (as described earlier) at every single time point of basolateral sampling to determine the effect of G3NH_2-nPEG1000 incubation on the tight junctions of Calu-3 monolayers. After completion of the experiments, samples from the apical side were removed and stored for further analysis. Select cell monolayers (from each condition) were washed twice with HBSS and were replenished with the growth medium on the apical side to estimate the revival of TEER after completion of the permeability experiments.

For mass balance studies, after each time point, selected inserts were chosen (n=3 for each conjugate), and the dendrimer-laden buffer in the apical chamber was removed and analyzed to estimate the extent of dendrimer remaining after internalization and transport. The extent of transport of the conjugate onto the basolateral compartment was estimated as mentioned in the earlier part of this section. For quantifying the internalized conjugates, cell monolayers were first washed with cold HBSS to arrest uptake. Subsequently the monolayers were lysed using 2% triton-X-100 overnight and the lysate was analyzed for the internalized conjugates using fluorometry. The resulting lysate was centrifuged to isolate the cell debris, and the supernatant was analyzed for the FITC-labeled PEGylated dendrimer using fluorometry. The dendrimer uptake was normalized to the cellular protein content using BCA assay, according to the protocol described by the manufacturer.[37] Summation of the mass internalized, mass transported and the mass remaining on the apical side was compared against the initial mass pulsed to obtain the overall mass balance.

4.3.9. Cellular Internalization via Flow Cytometry.

Cellular internalization experiments using flow cytometry were conducted on polarized Calu-3 monolayers according to procedure detailed in the literature, with slight modifications.[32] Calu-3 cells were plated at a density of 1×10^6 cells per well in a 24-well plate in DMEM as described in earlier sections, and allowed to proliferate to confluence for a period of 8-10 days, with the monolayer periodically checked for confluence by staining the cells for tight junctional protein, ZO-1 and ascertaining its

presence through fluorescence microscopy. Once the monolayer integrity was confirmed, the cells were subject to uptake studies. Prior to commencing internalization studies, the cells were incubated for a period of 30 min in warm 1X HBSS. This was followed by incubating the acclimatized monolayers of Calu-3 with 25 nmol of G3NH_2-nPEG1000 (in 0.5 mL HBSS) of varying surface densities of PEG, for varying durations (5h, 4h, 3h, 2h, 1h, 0.5h and 0.25h). After lapse of the incubation period, the conjugate laden media was carefully aspirated, and the cell monolayers were washed thrice with cold HBSS. The extracellular fluorescence was quenched using 0.2% Trypan Blue, washed again with HBSS, and the cells trypsinized (trypsin supplemented with 0.25% EDTA) and subjected to centrifugation (1200 rpm, 6 minutes) to recover the cell pellet. The cell pellet thus recovered was resuspended in 1 mL fresh 1X HBSS and subjected to flow cytometry (BD LSR II, BD Biosciences, San Jose, CA) with a coherent sapphire laser (488 nm) and detected through a 530/30 bandpass filter (FITC). For analysis, at least 5000 events were counted, and only viable cells were gated for fluorescence analysis. 1X HBSS was used as controls for the conjugates. The extent and rate of cellular entry was determined by plotting the mean fluorescence intensity (MFI) values as a function of time. The results reported here are averages of 6 wells for each conjugate.

4.3.10. Administration of Dendrimers to mice.

Pulmonary administration of the G3NH_2-nPEG1000 of varying surface densities of PEG 1000 Da was performed using the pharyngeal aspiration technique. Briefly, the mice were anaesthetized by inhalation of 2.5% v/v isoflurane, and placed

on a slant board with the back resting on the board, and partially suspended with a rubber band by their incisors. The tongue was held gently in extension and the $G3NH_2$-nPEG1000 solution was placed in the pharynx region by means of a micro syringe. The tongue was continuously held in extension until several breaths had elapsed. Once the entire dosage (100µl) had been administered, the mice were returned to their housing and monitored for rapid recovery. This method has been validated in comparison to intratracheal administration, and allows for greater lung deposition and higher dose-dose consistency.[38] For intravenous administration, 100µl the $G3NH_2$-nPEG1000 solution was injected into the tail vein. The solutions of $G3NH_2$-nPEG1000 were prepared in sterile normal saline, and a dose of 200 µg (in 100 µL) was given to all study groups.

4.3.11. Blood Sampling and Lung Harvesting.

After administration of the solution of $G3NH_2$-nPEG1000 to mice, blood samples were collected at pre-determined time points (0.5, 1, 3, 6, 12, 24, 48, and 96 hours, and then at 1, 2, 3, and 4 weeks) from each animal. At each time point, 60 µl of blood was extracted via the tail vein into tubes containing 20 µl of heparin. The blood sample was centrifuged at 5000 rpm for 30 s, and plasma was collected. Plasma sampled was analyzed for FITC fluorescence (Synergy, BioTek Instruments) and the $G3NH_2$-nPEG1000 was determined by comparing the fluorescence values to a previously constructed calibration curve. At the terminal time point, blood was collected by cardiac puncture, and the lungs were excised. Whole lung tissues were homogenized, followed by extraction with 3N sodium hydroxide for a period of 72h in

darkness and analyzed for FITC fluorescence to determine total residual mass of $G3NH_2$-nPEG1000 within the lungs.[8]

4.3.12. Pharmacokinetic Analysis.

The area under the curve (AUC) for $G3NH_2$-nPEG1000 after intravenous administration (*AUCiv*) and after pulmonary administration (AUC_p) was calculated using OriginPro software (OriginLabs). The clearance (*Cl*) was calculated using the following equation:

$$Cl = Dose_{iv} / AUC_{iv} \qquad (4.2)$$

where $Dose_{iv}$ is the dose administered intravenously.

The absolute bioavailability after pulmonary administration (*F*) of the $G3NH_2$-nPEG1000 was calculated using the equation:

$$F = (AUC_p / AUC_{iv}) \cdot (Dose_{iv} / Dose_p) \cdot 100 \qquad (4.3)$$

where AUC_p is the area under the curve after pulmonary administration, and $Dose_p$ is the dose administered to lungs.

The rate of absorption (R_o) of dendrimers after pulmonary administration was calculated using the total clearance after intravenous administration, and considering the plasma concentration-time profiles analogous to infusion at constant rate using the equation:

$$R_o = Css \cdot Cl \qquad (4.4)$$

where the steady state concentration (C_{ss}) for each experimental group was determined individually from peak concentrations following pulmonary administration.

4.3.13. Statistical Analysis.

Statistical analysis of the data was performed by one-way ANOVA and student's t-test using OriginPro (Origin Labs). Probability values of $p<0.05$ were deemed significant.

4.4. Results and Discussion.

4.4.1. Synthesis of FITC-labeled G3NH$_2$-nPEG1000.

There are many potential advantages in PEGylating dendrimer nanocarriers for drug delivery applications. The literature show that PEGylation reduces the cytoxicity of amine-terminated PAMAM.[16] PEGylation has also show to improve the aqueous solubility of dendrimers,[39] which is particularly relevant when conjugating hydrophobic therapeutics to the carriers, and has also been shown to enhance circulation times upon systemic administration.[40] PEGylation of nanocarriers in general, can also potentially favor their transport across extracellular barriers of the respiratory epithelium, as they may facilitate transport across the mucosal layer lining the airways, and reduce the interaction between the nanocarrier and the surface fluid of the alveolar region.[14]

FITC-labeled G3NH$_2$, with varying surface densities of PEG1000 (G3NH$_2$-nPEG1000), were synthesized as described above. The resulting products were characterized by MALDI, ^{1}H-NMR and FT-IR - spectra provided in *Supplementary Material*. The first step in the process was the conversion of monomethoxy PEG (mPEG) to the carboxyl terminated PEG (cmPEG). An increase in the MW, with a distinct change in the MW distribution pattern as evidenced by the MALDI spectrum

(Figure S1a) was observed. The conversion from mPEG to cmPEG was also confirmed by the absence of a peak at in the ^{1}H-NMR spectrum of cmPEG 4.6 ppm (*H* from –OH in mPEG), and the appearance of a peak in the FTIR spectra at 1735 cm^{-1}, from the stretching band of the carbonyl moiety unique to cmPEG – Figure S1b,c.[27]

FITC was conjugated to the $G3NH_2$ surface according to a strategy described in the literature, with a target of 2 FITC per $G3NH_2$. The conjugation was accomplished through the formation of thiourea bond between FITC and $G3NH_2$,[41] and was performed in a one pot synthesis along with the cmPEG conjugation. Conjugation of cmPEG at various surface densities to $G3NH_2$ was accomplished through EDC-NHS chemistry, by coupling the $–NH_2$ group of the $G3NH_2$ to the –COOH on the cmPEG. The resulting products ($G3NH_2$-nPEG1000) were purified by dialysis of the contents of the reaction vessel against DI water. The $G3NH_2$-nPEG1000 were characterized using ^{1}H-NMR (DMSO-d_6) and MALDI-TOF - Figures S2-S5. The grafting density of PEG1000 was varied by controlling the molar ratio of cmPEG to $G3NH_2$, and the reaction time.

The singlet signal originating at 2.17 ppm in the ^{1}H-NMR spectra of the $G3NH_2$-nPEG1000 (Figure S2(a)-S5(a)) can be attributed to the methylene protons next to the carbonyl groups of the dendrimer.[42] The presence of the PEG moiety can be ascertained by the presence of broad peaks occurring between 3.3 to 3.6 ppm, which is attributed to the protons of the CH_2CH_2O repeat unit, and the signal due to the terminal $-CH_3$ group of PEG at 3.23 ppm.[42, 43] The number of PEG moieties attached to the $G3NH_2$ surface was determined by comparing the integral

values of the $-CH_3$ peak at 3.23 ppm, to that of the methylene peaks of the dendrimer at 2.18 ppm (set at 120 protons – internal standard).[42] The multiplet peaks between 6.5-6.8 ppm can be attributed to the aromatic protons of FITC.[44] From those results, the number of PEG1000 surface groups on the dendrimers conjugates was calculated to be to be 5, 13 and 25, and those of FITC were on target, and determined to be between 1.5-2.0. A summary of the conjugates synthesized in this work, along with their characteristics, including the number of PEG1000 and FITC grafts, their MW, size, and surface charge is provided in Table 4.1.

Table 4.1. Compilation of MW, size distribution and zeta (ζ) potential estimation of FITC linked G3-NH_2-nPEG 1000 conjugates determined using ^{1}H- NMR and MALDI, and DLS analysis respectively. MW reported here was determined by processing the MALDI spectra obtained using flexAnalysis™ software (Bruker Daltonics). DLS measurements were conducted in HBSS (pH 7.4) and room temperature.

Compound	NMR		MALDI*		Size±s.d[#] (nm)	ζ ±s.d[#] (mV)	n_{FITC}[X]
	n_{PEG}[@]	MW	n_{PEG}	MW			
G3-NH2	**0**	**6909**[**]	**0**	**6882**	**2.9±1**	**+21±4.8**	**0**
G3-NH2-0PEG 1000	**0**	**8076**	**0**	**7660**	**3.6±0.5**	**15.5±5.3**	**2**
G3-NH2-5PEG 1000	**5**	**13805**	**4**	**11403**	**4.8±0.9**	**1.09±0.4**	**1.5**
G3-NH2-13PEG 1000	**13**	**23586**	**9**	**18160**	**5.5±1.4**	**-1.41±0.8**	**1.7**
G3-NH2-25PEG 1000	**25**	**38267**	**23**	**34015**	**7.9±1.0**	**-4.7±1.2**	**2**

[@] Average no of PEG units conjugated per PAMAM molecule estimated using ^{1}H-NMR spectra of the compound in DMSO-d_6

[*] Estimated from the MALDI MW distribution using DHB as matrix using FlexAnalysis™ software.

**Provided by the manufacturer

[#] n=4

[X] As determined by ^{1}H-NMR

The MW of the commercial PAMAM dendrimer obtained from Sigma was determined to be 6882 Da, which was in good agreement with the value 6909 Da provided by the manufacturer. The average MW of the compound was determined

from the major peak of the MALDI spectra. MW of G3NH_2-0PEG1000 was 7660 Da – an increase in MW of 778 Da when compared to pure G3-NH_2. This indicates the presence of 2 FITC molecules per dendrimer – each new FITC conjugate is 390 Da. The MW for the other G3NH_2-nPEG1000 was 11,403 Da, 18,160 Da and 34,015 Da, respectively. With the knowledge of the MW of cmPEG, also from MALDI, and that of the G3NH_2-nPEG1000, the number of PEG1000 surface groups was thus determined also determined from MALDI. Those results are also included in Table 1, and can be compared to the results from ^{1}H-NMR. While the numbers estimated by NMR and MALDI are similar, it is interesting to note that there is an underestimation of the MW (ca. 10-15%) in the case of MALDI, when compared to that of NMR. This behavior is similar to that observed in the literature.[43] We believe the NMR numbers better represent the actual number of grafts,[42, 45] and we will thus refer to those numbers from now on.

Light scattering was used to ascertain the size and surface charge of the conjugates. The results are also included in Table 1. The size of G3NH_2 and G3-NH_2-0PEG1000 (just FITC-conjugated PAMAM) was determined to be 2.9 and 3.6 nm, respectively. These values are in good agreement with those reported in the literature of 3.2 nm and 3.6 nm, respectively.[46] Furthermore, a similar increase in size of ca. 0.6 nm has been reported when FITC was conjugated onto G4-PAMAM dendrimers.[47] With the increase in PEG1000 surface density, a gradual increase in hydrodynamic diameter from 3.6 nm (0 PEG) to ca. 8 nm (25 PEG) was observed. While a direct comparison cannot be made owing to lack of literature pertaining the DLS analysis of G3NH_2-nPEG1000, several studies have been published reporting a

similar increase in size of dendrimers upon grafting their end groups with PEG of varying MWs.[21, 40, 48] The increase in size reported here is observed to be within the size range reported in the case of G3-polylysine dendrimers (diameter of unmodified dendrimers ca. 2.8 nm) that were grafted with 32 surface groups of PEG750, with a reported size of ca.6.7 nm.[40] In another study, PEG of MW 3400 Da was tethered to the surface of G3 NH_2 and DLS analysis reported a size increase of 3.4 nm for a PEG surface coverage of 3.4. The increase in the size reported in this that is relatively higher, perhaps due to the presence of longer PEG chains.[49] Our results are also in line with the results reported for G3NH_2–PEG2000, where a diameter of ca. 12 nm has been reported at 99% surface coverage.[43] This value is higher than what we observed, but this increase is to be expected given the higher density and MW of PEG grafted on the dendrimer surface in that case. In another study, G4NH_2 with 50% PEG density and PEG with MW of 5000 Da was reported to have a size of ca. 13 nm,[48] further reaffirming that the conjugates synthesized in this work seem to fall within the expected size range.

A gradual decrease in the surface charge of the conjugates from +15.5 mV (G3NH_2-0PEG1000) to -4.7 mV (G3NH_2-25PEG1000) was observed upon increase in PEG density. Shielding of the positive charges in the dendrimers was actually observed even at the lowest PEG density, as the addition of 5PEG1000 decreased the surface charge to +1.1 mV. This drastic decrease in surface charge has also been reported in previous studies. For instance, in the case G4.5 dendrimers, addition of 1 PEG (MW 750 Da) moiety onto the dendrimer surface resulted in a change in surface charge from -56 mV to -39 mV.[21] Similarly, a significant

reduction in surface charge was also reported in case of G-NH_2 conjugated with PEG 5000 Da. A 50% surface coverage of PEG resulted in a decrease of ca. 11 mV, from +16.6 to +6.2 mV. That study also reported a graduate change of surface charge upon PEGylation as reported here.[48] Upon tethering 76-128 –NH_2 surface groups of G6 polylysine dendrimers with PEG MW 5000, a drastic reduction in charge was observed from ca. +20 mV to as low as ca. -6.5 mV.[40] These results provide valuable insight into the impact of linking PEG onto the surface charge of cationic dendrimers and further validate our observations.

The fact that PEGylation has such a dramatic impact in the size and surface charge of the dendrimers are of great relevance, as those characteristics of the nanocarriers are expected to also impact the rate, extent and mechanism of cellular uptake,[19, 32, 46, 50, 51] and their transport across epithelial barriers.[21, 52] For instance, addition of PEG (MW 2000 Da) to G5NH_2 surface at varying densities did not alter the uptake of the conjugates into NIH 3T3 cells, while the uptake of G4.5 dendrimers with just one PEG (MW 750 Da) on its surface increased its uptake into Caco-2 cells compared to the bare dendrimers.[21, 53] Transport of macromolecules and nanocarriers with the size range discussed here (which are of the order of size comparable to biomacromolecules) across the nano-sized, negatively charged tight junctional complex domains that exist in epithelial barriers, have been shown to be affected by their size and charge density.[52, 54-56] PEGylation of G3NH_2 is thus also expected to provide opportunities to modulate transport across the pulmonary epithelium. It has been shown that PEGylated dendrimers can interact and subsequently open tight junctions of Caco-2 cells even at low PEG surface density

and relatively low concentrations.[21] In general, it has been reported that hydrophilic compounds are predominantly transported paracellularly across epithelial barriers,[21, 57, 58] and that this process is cell dependent[21, 51, 59, 60]. In the sections that follow we will demonstrate that the rate and extent of internalization into and transport of $G3NH_2$ nanocarriers across models of the pulmonary epithelium can be modulated upon PEGylation.

4.4.2. Cytotoxicity of $G3NH_2$-nPEG1000 on Calu-3 cells.

Cytotoxicity of $G3NH_2$-nPEG1000 was evaluated on Calu-3 cells as described above. A summary of the cell viability results as a function of molar concentration of $G3NH_2$-nPEG1000 is shown in Figure 4.1.

As a general trend, $G3NH_2$-nPEG1000 had no appreciable inhibitory potential at concentrations below 0.01 μmol, with cell viabilities largely maintained at above 80%. While a 30% cell kill was observed for G3-NH_2-0PEG1000 at a concentration of 1 μmol, over 90% of cells exposed to the PEGylated conjugates were viable at the same concentration. Further increase in concentration resulted in a reduction in cell

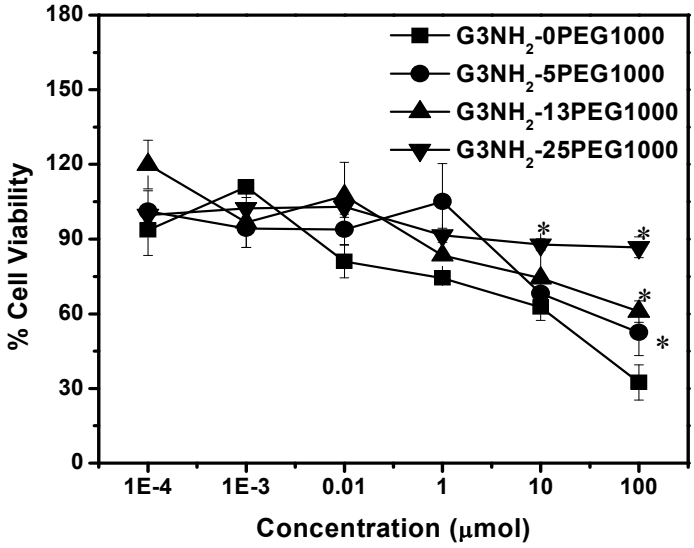

Figure 4.1. Viability of Calu-3 cells by MTT assay after incubation in $G3NH_2$-nPEG1000 conjugate laden media for a 24 h. Cells incubated in serum-free culture medium (DMEM) were used as control. Results denote mean ± s.d (n=5). * denotes statistically significant data ($p<0.05$) w.r.t control ($G3NH_2$-0PEG1000).

viability for all conjugates, except $G3NH_2$-25PEG1000. The IC_{50} (minimum inhibitory concentration required to kill 50% of viable cells) for $G3NH_2$-0PEG1000 was estimated to be ca. 55 μmol. On the other hand, within the concentrations investigated, none of the PEG terminated conjugates had exerted a 50% cell kill at 24h incubation. Based on the observed trend, the IC_{50} for $G3NH_2$-5PEG1000 and $G3NH_2$-13PEG1000 can be estimated to be greater than 100 μmol. Cells incubated in $G3NH_2$-25 PEG1000 had a viability of greater than 85% even at 100 μmol.

While no prior work on the effect of dendrimers on viability of Calu-3 cells has been reported in the past, it is worth comparing and contrasting the results from this work with literature on other relevant epithelial models. It has been observed that Caco-2 cells exposed to $G4NH_2$, dendrimers with no surface modification, had an IC_{50} of 0.12 mM. Upon adding 4 PEG moieties to its surface, the concentration at 50% cell kill dramatically increased to 0.8 mM. The increased cell viability in presence of PEGylated dendrimer is thought to be due to the shielding of the positive $–NH_2$ groups by PEG, as the cationic nature of $–NH_2$ groups is considered to be the primary cause for cytotoxicity.[14, 35, 53] Similarly, an increase in the concentration for 50% cell kill of over 60 μmol was reported in the case of NIH 3T3 cells exposed to $G5NH_2$ dendrimers, where 51 of the surface groups was modified with PEG 2000 Da, when compared to unmodified G5-NH_2.[19] Cytotoxic evaluation of PEGylated $G4NH_2$ PAMAM (16 and 32 surface amino groups PEGylated) dendrimers on B16 murine melanoma cells indicated that over 50% of the cells were alive even after 48h exposure to the highest concentration of conjugate - 100 □M, while their non-PEGylated counterpart had a very low IC_{50} of 1.95 □M, reaffirming the improved toxicity profile of PEGylated dendrimers.[42] The benign nature imparted by PEGylation of cationic dendrimers has also been documented on various other cell lines.[14, 54, 55]

4.4.3. Culture of Calu-3 cells, SEM and Immunocytochemical (IC) Analysis.

. The human airway epithelial cell line Calu-3 was used as an *in vitro* model to determine the effect of PEGylation on the permeability and uptake of $G3NH_2$-nPEG1000. Calu-3 is a well-differentiated and characterized cell line derived from human bronchial submucosal glands.[63] Besides forming tight junctions, Calu-3 cells have also been documented to possess many salient characteristics of the bronchial epithelium, viz. airway surface liquid, cilia, production of mucins and other immunologically active substances that make this cell line an appropriate candidate for elucidating tracheobronchial permeability and uptake *in vitro.*[63, 64] In order to ensure that the cell monolayers are of requisite morphology for the transport studies, they were characterized via electrophysiological measurements (TEER), SEM, and immunocytochemistry.

AIC culture was adopted as Calu-3 is known to exhibit all salient features of native epithelium when allowed to proliferate under AIC.[34, 65] The cultures became confluent 6 days after culture under AIC. Monolayer confluence was evaluated by periodically recording their TEER. A plot of the epithelial resistance afforded by the cell monolayer as a function of time (days in culture) is shown in Figure 4.2 (a). Under AIC, the TEER values of the cultured Calu-3 monolayer increased above the baseline values after about 5 days in culture, and peaked by day 11 at ca. 305 $\Omega \cdot cm^2$. TEER values between ca. 300 and 350 $\Omega \cdot cm^2$ are considered to be an indicator of attainment of monolayer confluence and formation of tight junctions.[34, 64, 65]

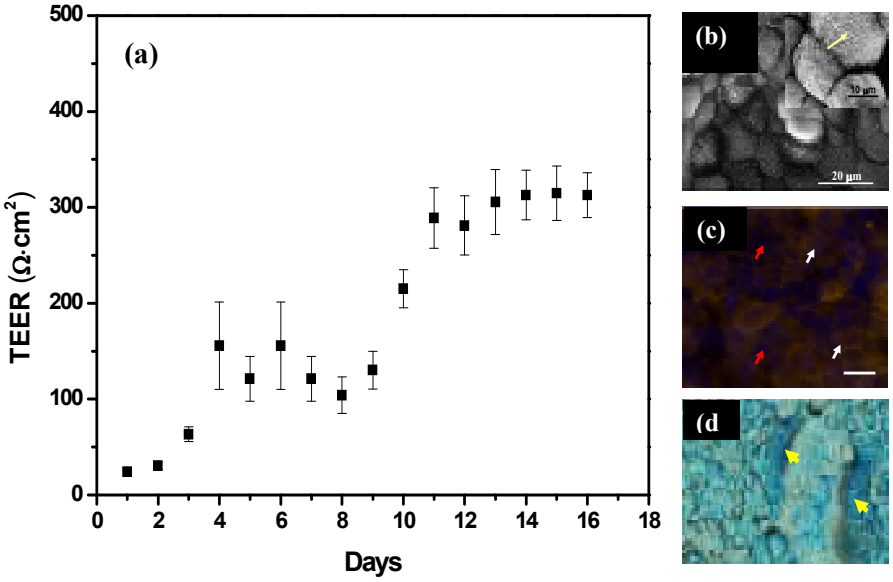

Figure 4.2. (a) Increase in transepithelial electrical resistance (TEER) of Calu-3 cells cultured under AIC on 0.33 cm^2 transwell inserts as a function of time. Data mean ± s.d (n=16). **(b)** SEM micrographs showing the morphology of AIC cultured Calu-3 cell monolayers, imaged once TEER values peaked and stabilized (day 15). Bar represents 20 μm. *(Inset)* A magnified SEM image of Calu-3 cell monolayer indicating the presence of microvilli (Open arrows). Bar represents 5 μm. **(c)** Representative XY-2D sections of confluent Calu-3 monolayers captured using a confocal microscope at 40X magnification. Monolayers were fixed with 2% paraformaldehyde and stained for ZO-1 (white arrows), a tight junctional protein. Cell monolayers were also counterstained with DAPI (blue; red arrows) to show the location of the nucleus. Size bar indicates 20 μm. **(d)** Optical micrograph of a Calu-3 monolayer stained with the mucosal stain, Alcian blue indicating the presence of glycoproteins on the cell surface (yellow arrows).

Prior to beginning the transport experiments, once the TEER values peaked, immunocytochemical (IC) analysis and electron microscopy studies were conducted to visually ascertain the presence of tight junctions and morphology of the confluent Calu-3 monolayers. The cell monolayers were prepared for both studies as detailed in the methods section. Figure 4.2(b) is a representative electron micrograph of a Calu-3 monolayer fixed and stained, and represents the nature of the monolayer at the time transport experiments commenced. In the same figure, as an inset, a higher magnification image of the monolayer is also shown. The presence of microvilli populating the surface of Calu-3 cells can be clearly observed from the electron micrograph. A closer inspection of the inset in Figure 2(b) reveals the presence of cilia (filled yellow arrow). Furthermore, we also observed the presence of mucus on the cell surface through electron microscopy (image not shown), another confirmation that the cell monolayer cultured under AIC possessed the requisite morphology mimicking the tracheobronchial epithelium.

IC analyses were also performed on confluent Calu-3 monolayers prior to commencing transport experiments. Studies were conducted to detect the presence of ZO-1 proteins, which are expressed in the tight junctions of confluent Calu-3 cells.[63, 64] The presence of the protein was detected by staining the fixed cells with an anti-ZO-1 antibody labeled with a fluorescent dye, Alexa Fluor® 546. The cells were counterstained with the nuclear stain, DAPI. Representative images (fluorescent microscope) of the fixed and stained Calu-3 cells monolayer is given in Figure 4.2(c). The clear orange patterns observed along the periphery of the individual cells of the monolayer can be attributed to the presence of ZO-1 - denoted

by the white arrows. The presence of dark blue (red arrows) within the cell milieu indicates the nuclei of the cells. Alcian Blue stain was utilized to detect the presence of glycoproteins on the surface of the Calu-3 monolayer. An optical image of a monolayer stained with Alcian Blue is shown in Figure 2(d). The distinct blue layer blanketing the cell surface (indicated by yellow arrows) can be attributed to the presence of mucosal glycoproteins. The results reported here with respect to monolayer characterization agree with observations reported in the literature.[64] Through a combination of TEER, IC and SEM it can be concluded that the monolayers are confluent and have appropriate morphology, and can thus be utilized for transport experiments, which are detailed in the section that follows.

4.4.4 *In vitro* Transport of $G3NH_2$-nPEG1000 across Polarized Calu-3 Monolayers.

In this section we discuss the effect of PEGylation on the transport of $G3NH_2$-nPEG1000 conjugates across confluent Calu-3 monolayers cultured under AIC. The results are summarized in Figures 4.3 and 4.4. Figure 4.3 depicts the effect of PEG density on the apparent permeability (P_{app}) of the nanocarriers. P_{app} is a parameter that represents the ease with which compounds are transported across epithelial barriers.[34]

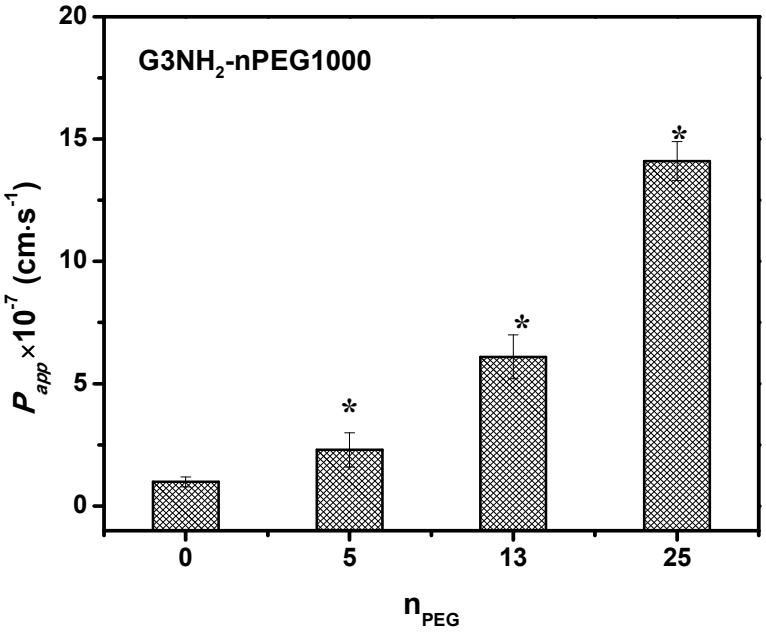

Figure 4.3. Effect of PEGylation density on the apparent permeability (P_{app}) of $G3NH_2$-nPEG1000 conjugates across confluent Calu-3 monolayers. P_{app} values reported here were determined at the 5 hour time point after incubation of the cell monolayers with the conjugates. Data represents mean ± s.d (n=4). 25 nmol of conjugates in 1X HBSS was pulsed on the apical side. * denotes statistically significant data ($p<0.05$) with respect to control ($n_{PEG}=0$).

Our results indicate that the P_{app} of the $G3NH_2$-nPEG1000 nanocarriers across Calu-3 monolayers increases with increasing PEG1000 density. The P_{app} for $G3NH_2$-0PEG1000 was determined to be 1.2×10^{-7} cm·s^{-1}, while that for $G3NH_2$-25PEG1000 was tenfold greater, at 14×10^{-7} cm·s^{-1}. The P_{app} values for the all conjugates containing PEG1000 moieties were determined to be statistically significantly ($p<0.05$) different compared to the P_{app} of the conjugate with no PEG ($G3NH_2$-0PEG1000).

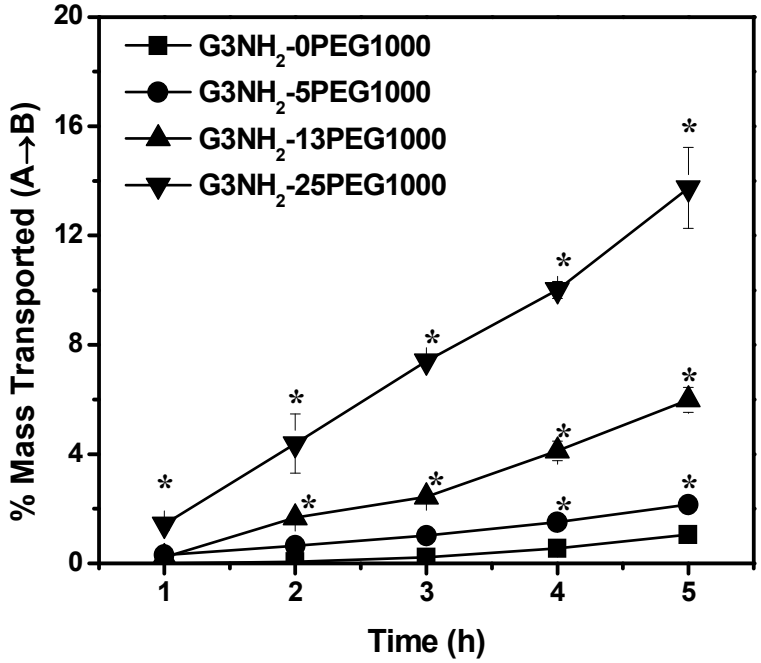

Figure 4.4. Effect of PEGylation on the cumulative mass of the $G3NH_2$-nPEG1000 conjugates transport across confluent Calu-3 monolayers (Apical → Basolateral) as a function of time. Error bars denote s.d (n=4). Error bars not showing are smaller than symbol size. 25 nmol of conjugates in 1X HBSS was pulsed on the apical side. * denotes statistically significant data ($p<0.05$) with respect to control ($n_{PEG}=0$).

In Figure 4.4, the cumulative mass of the conjugate transported from the apical to the basolateral side (A→B) of the insert is shown as a function of time. At 5h, only ca. 1% of the $G3NH_2$-0PEG1000 had been transported to the basolateral side. With conjugation of PEG1000 to the $G3NH_2$ surface, an increase in the rate of mass of conjugate transported was observed, with a maximum of ca. 12% for $G3NH_2$-25PEG1000. All the PEGylated conjugates viz., $G3NH_2$-5PEG1000, $G3NH_2$-

13PEG1000 and $G3NH_2$-25PEG1000 had statistically significant increases in the mass transported ($p<0.05$) compared to that seen for $G3NH_2$-0PEG1000, at all times, as shown in Figure 4.4.

In order to evaluate the effect of the PEGylation of the conjugates on the tight junctions, changes in electrophysiological behavior were monitored by recording the TEER during the course of the transport experiments. The results are summarized in Figure 4.5. From the plot, it is evident that $G3NH_2$-nPEG1000 had a pronounced effect on the tight junctional properties of the monolayer. A gradual reduction in the TEER of Calu-3 monolayers was observed during the course of the transport experiments, with all conjugates reducing the TEER of the monolayers to ca. 30% of the original value that of cells incubated in HBSS only. This phenomenon was somewhat reversible, as upon re-incubating the monolayers with culture media in the absence of the conjugates, the TEER values returned to ca. 80% of their original value within 3 days of incubation, as seen in Figure 4.5.

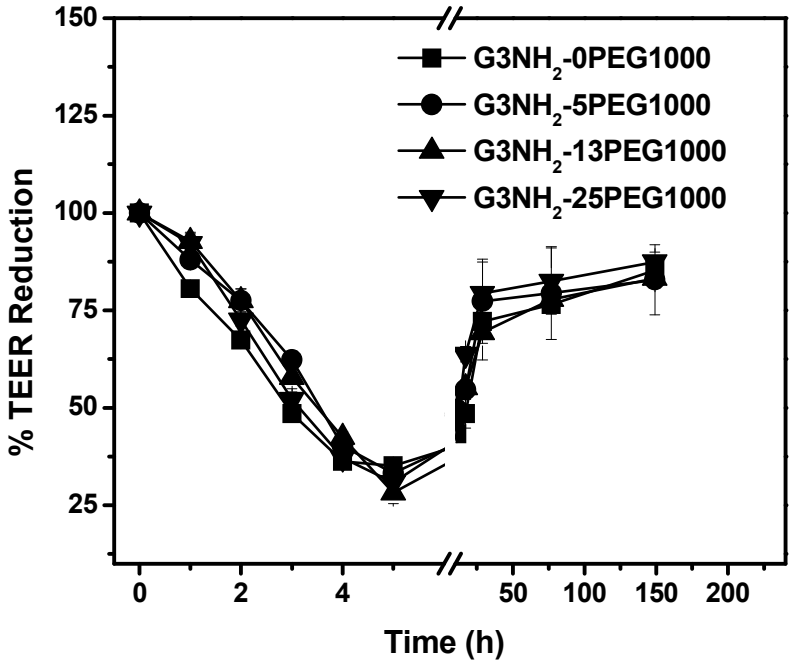

Figure 4.5. Effect of PEGylation density of the $G3NH_2$-nPEG1000 conjugates (in 1X HBSS (pH 7.4)) on the TEER values of AIC cultured Calu-3 cells as a function of time. Values shown in the plot are denoted as % of control, which is TEER of Calu-3 incubated in 1X HBSS before the start of transport experiments. The recovery of TEER after the transport experiments is also shown in the plot. The cell monolayers were washed after the transport studies and re-incubated in DMEM and the TEER was monitored with time.

A similar reduction in TEER has been also reported in the case of Caco-2 cells, upon incubation with PEG-surface modified $G3NH_2$ and $G4NH_2$.[55] The presence of conjugates resulted in a decrease in TEER down to 20% of the original value, but re-incubation in dendrimer-free medium also restored the TEER back to original levels by 24-48h.

Transport of surface-modified dendrimers across epithelial monolayers is highly dependent on the size, surface charge, the chemistry of functionalities attached to the surface, and the cell type.[18, 21, 56] Previous studies have suggested that dendrimers transport across monolayers via a combination of transcellular (through the cell milieu) or paracellular (through the tight junctions) routes.[18, 21] Most transport studies of PAMAM have focused on cell lines in the context of oral delivery, however, with Caco-2, IPEC-J2 and Madin-Darby Kidney cells being the primary *in vitro* models.[18, 59] To the best of our knowledge, the permeability characteristic of PEGylated G3NH2 conjugates (or any dendrimer) has not been evaluated on cell culture models relevant to the pulmonary epithelium.

Conjugation of a lipid, lauroyl chloride, to $G3NH_2$ surface increased P_{app} across Caco-2 monolayers by a factor of 2.5 from ca. 2×10^{-6} $cm\cdot s^{-1}$ to ca. 5×10^{-6} $cm\cdot s^{-1}$ within a 3h time period, possibly due to the permeation enhancing effects of the lipid chains.[46] Similarly, increasing the surface coverage of FITC to $G4NH_2$ also had a considerable impact on its transepithelial transport with enhanced permeability of the conjugates across Caco-2 monolayers reported after 2h. The increase in transport was attributed to a higher degree of tight junctional modulation.[55] In another study, addition of polyamines (ornithine and arginine) onto the $G4NH_2$ surface also improved the permeability of the conjugates across Caco-2 and IPEC-J2 cell monolayers after 3h, possibly due to a combination of polyamine transporter system aiding in the active uptake of the conjugates, and a passive transport through the tight junctions due to charge mediation.[56, 66]

In this work we observed that as the surface density of PEG increases, the transport of G3NH_2-nPEG1000 across the Calu-3 polarized monolayer also increased. Because all G3NH_2-nPEG1000 impact the tight junctions to the same extent, at least as probed by the ionic mobility across the epithelial barrier (TEER), we argue that this enhanced transport for G3NH_2-nPEG1000 with higher number of graft PEGs, compared to those with lower PEG density does not reflect a permeation enhancement effect. The fact that all G3NH_2-nPEG1000, irrespective of size and surface charge affect the TEER to the same degree is, to some extent, surprising, as tight junctional proteins are negatively charged and have gaps of the order of 0.8-2 nm depending on cell type.[54] One would have expected, therefore, that the smaller and more positively charged dendrimers would have exerted a greater influence on TEER. Interestingly, it has been shown that tethering of 1 or 2 chains of PEG (MW 750 Da) onto G3.5 and G4.5 dendrimers (hydroxyl terminated dendrimers) decreased the transepithelial permeability of the conjugates across Caco-2 monolayers after 2h incubation, possibly due to relatively lower levels of interaction of PEG modified conjugates with the tight junctions of Caco-2.[21] However, the trend observed here indeed seems to be somewhat universal for positively charged polymers, as PEG modified chitosan, a linear polymer with –NH_2 groups (MW PEG 1900 Da), also reduces the TEER of Calu-3 - down to 40% of the initial value.[52] It was suggested that the reduction in the TEER could be due to the higher equivalent concentrations of chitosan in the conjugates in combination with the unsubstituted amine groups of the PEG modified chitosan backbone.[52]

Another interesting observation was the rapid increase in the transport of G3NH_2-25PEG1000 within the first hour when compared to the other conjugates (ca. 1.4% compared to ca.0.3% in case of G3-NH_2-5 PEG 1000). The presence of PEG on nanocarrier surfaces (in that particular case of solid nanoparticles) has been shown to impart stealth like properties to them thereby facilitating their rapid transport across mucosal barriers.[22, 25] Combining the results discussed above, with the fact that internalization of the carriers within Calu-3 cells decreases upon PEGylation (discussed below), one could argue that a fast transport across the mucosal layer, and decreased interaction with and internalization within Calu-3 cells may provide an opportunity for the more densely PEGylated nanocarriers to achieve enhanced transport across the monolayer. Of course this assumes a dominant paracellular transport, which seems plausible given the information, but has not been determined in this work. These studies are ongoing in our laboratory.

4.4.5 Cellular Uptake and Flow Cytometry.

The effect of PEGylation on the extent of cellular uptake of the G3NH_2-nPEG1000 conjugates onto polarized Calu-3 monolayers was also determined. Cellular internalization was evaluated by cell lysate and flow cytometry. The cell lysate results at the end point of transport studies (5 h) are plotted as % uptake in Figure 4.6.

At the end of the transport studies (5h time point), ca. 10% of the G3NH_2-0PEG1000 was internalized into Calu-3. In contrast, PEGylated conjugates had reduced internalization. The total internalized amount (mass basis relative to

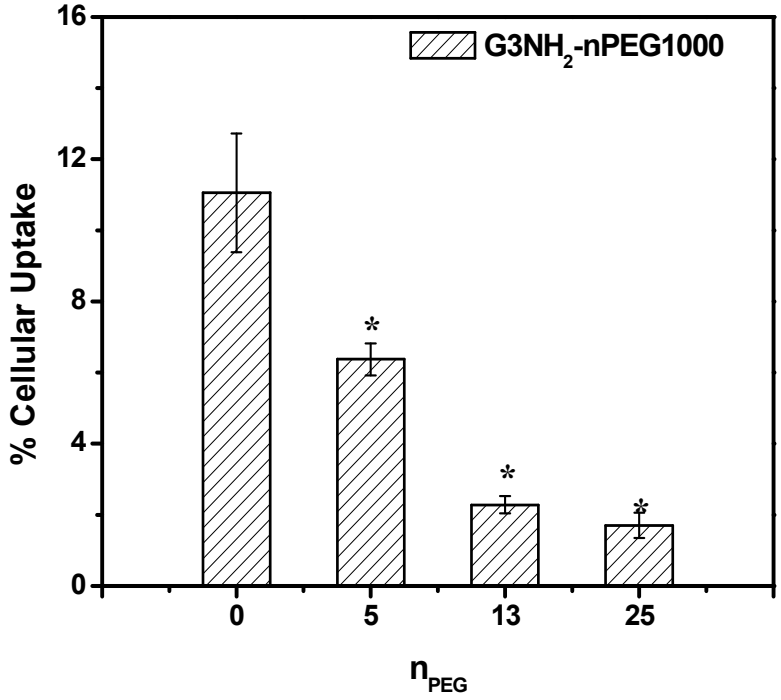

Figure 4.6. Effect of PEGylation density of the $G3NH_2$-nPEG1000 conjugates on the **%** uptake into Calu-3 at t=5h, as measure in the cell lysates. Values represent mean ± s.d (n=4). Statistical significance with respect to control ($p<0.05$) denoted by *.

the amount of dendrimer added in the beginning of the transport study) for $G3NH_2$-5PEG1000, $G3NH_2$-13PEG1000 and $G3NH_2$-25PEG1000 was 6%, 2.2% and 1.7%, respectively. These results, combined with the determination of the amount of dendrimer left in the apical side of the insert at the end of the transport studies, and the cumulative amount collected on the basolateral side also at 5h, allowed us to perform an overall mass balance study. The results yielded a total average recovery of ca. 80% for all conjugates. The ca. 20% not recovered, could be attributed to factors including the presence of conjugates bound to cell surface that remain

adhered to cell debris after lysis, and the adsorption of conjugates to surfaces of the inserts and wells.

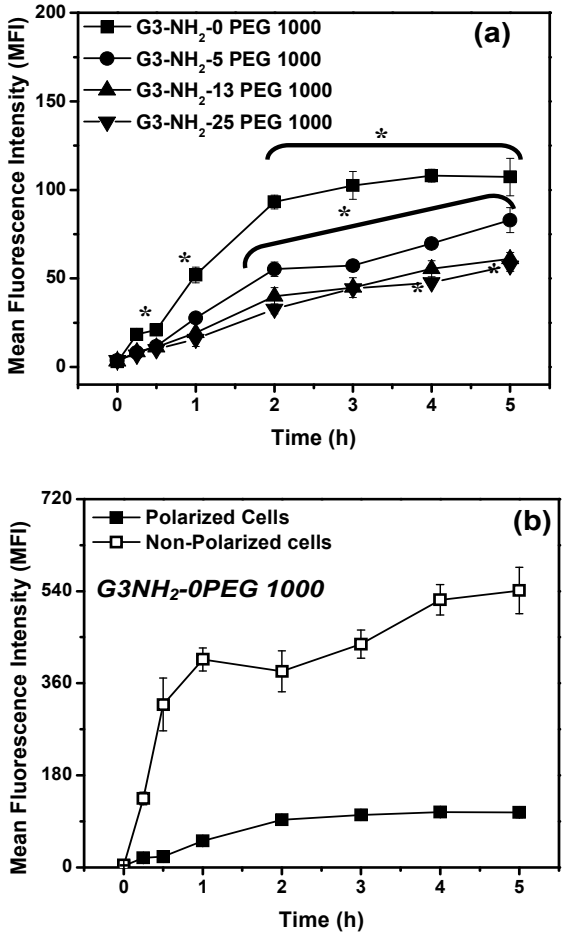

Figure 4.7. (a) Effect of PEGylation density on the cellular uptake of the $G3NH_2$-nPEG1000 conjugates into polarized Calu-3 cell monolayers as a function of time, as determined by flow cytometry. Data represents mean ± s.d (n=6). Statistical significance with respect to control ($p<0.05$) denoted by *. (b) Effect of cell polarization of Calu-3 on the uptake of $G3NH_2$-0PEG 1000

In addition to determining cellular uptake through cell lysis, internalization of the conjugates was monitored as a function of time utilizing flow cytometry. The results of the study are summarized in Figure 4.7(a). The studies were conducted on polarized Calu-3 monolayers as detailed before. Proliferation of Calu-3 till polarization is essential as it facilitates the formation of tight junctions thereby providing a more accurate representation of the true airway morphology.[67] Figure 4.7(a) is a plot of the mean fluorescence intensity (MFI) as a function of time.

From the plot, it is observed that the cellular uptake is reduced as the PEG number on the $G3NH_2$ surface increases, in agreement with what was observed from the cell lysate experiments. However, here we also obtain the kinetics of the process. The maximum cellular uptake was observed for $G3NH_2$-0PEG1000, whose uptake saturates by the 5h time point, as evidenced by the leveling off of the MFI values. This trend in cellular internalization for $G3NH_2$-0PEG1000, can be attributed to the typical trafficking mechanism of cationic dendrimers, that are believed to be taken up by charge mediated endocytosis, facilitated by the presence of negatively charged proteoglycans on cell surface.[32] However, for the PEGylated compounds, the rates of internalization were gradually reduced with the increase in PEG density with $G3NH_2$-25PEG1000 and $G3NH_2$-13PEG1000 having similar (lowest) rates of uptake. Additionally, it is interesting to note that the saturation in uptake observed in the case of the non-PEGylated dendrimer was not seen for the PEGylated carriers, suggesting that PEGylation may be in altering the route of internalization into Calu-3. The surface functionalities of dendrimers has been shown to affect not only the rate and amount of internalization, but also the endocytic mechanism upon which

internalization takes place.[18, 21, 32, 68] PEGylation of the conjugates results in the shielding of charges, which minimizes the interaction of the conjugates with cell surface, resulting in reduced surface adsorption that would subsequently lead to endocytosis.[21] For instance, in an earlier study involving partial PEGylation of $G4NH_2$ conjugates, an increase in surface coverage of PEG 5000 Da resulted in a significant decrease in the cellular uptake in B16F3 cells, as quantified by flow cytometry. It was observed that this reduction had a definite correlation to the zeta potential of the conjugates reiterating the impact of surface charge and surface functionality on cellular uptake.[48] Previous works have also shown that conjugation of PEG 750 Da to the surface of G3.5 PAMAM dendrimers reduced interaction with Caco-2 cell surface. Interestingly, the same study reported that addition of same PEG moiety to G4.5 dendrimers increased cellular uptake, suggesting that an ideal charge density may be required for promotion or reduction of dendrimer trafficking into the cellular milieu.[21]

Uptake experiments reported here were conducted on polarized, well differentiated monolayers of Calu-3. Polarized Calu-3 monolayers form tight junctions and exhibit morphological features native to pulmonary epithelium.[63] The importance of cell polarization in the cellular uptake of the $G3NH_2$ in Calu-3 cells was evaluated, and the results shown in Figure 4.7(b), where the uptake results in polarized cells are contrasted with non-polarized monolayers. Non-polarized cells of Calu-3 were able to internalize $G3NH_2$-0PEG1000 to a much greater extent compared to the polarized cells as evidenced by a five fold increase in the MFI values for the non-polarized cells. Another interesting observation to note from this

figure is the lack of saturation in the uptake of the conjugate exposed to the non-polarized cells when compared to the polarized Calu-3 monolayers. The effect of Calu-3 polarization was also observed in other independent studies where it was reported that well formed, polarized airway epithelial cells were infected to a lesser extent with *Pseudomonas aeruginosa* and *Chlamydia trachomatis* compared to their non-polarized counterparts.[67, 69] These results suggest that it would be prudent to conduct cellular uptake studies of moieties on polarized, well characterized cell monolayers in order to understand the true extent and kinetics of internalization.

Through the collective set of experiments comprising *in vitro* transport and cellular uptake assessed by cell lysis and flow cytometry, transport and TEER, we can gauge the impact of PEGylation on the transport and uptake of $G3NH_2$-nPEG1000 across and into Calu-3 monolayers. The results showcased through these studies, suggest that by suitably tailoring the surface of $G3NH_2$ with PEG1000, once can achieve a great deal of modulation in both transport and cellular uptake of dendrimer nanocarriers across and into such a relevant model of the pulmonary epithelium. The results obtained here also suggest that conjugation to PEG can impart other beneficial characteristics to the $G3NH_2$ nanocarriers, by reducing their toxicity and assisting in overcoming extracellular barriers present in the pulmonary epithelium, such as the mucosal layer.

These results can be utilized to guide the design of polymeric nanocarriers for controlled and targeted local or systemic delivery of therapeutics to (regional delivery) and through (systemic circulation) the lungs. Carriers with reduced transport and enhanced cellular internalization are potential candidates for the regional targeting of

drugs to the lungs, while those that rapidly transport across the pulmonary epithelium, are potential candidates to target the systemic ailments.

While in the previous sections we evaluated the feasibility of using PEGylation to modulate the transport of $G3NH_2$ nanocarriers across the pulmonary epithelium using an *in vitro* model, in the section that follows we evaluate the effect of PEGylation on the transport of $G3NH_2$-nPEG1000 across an *in vivo* model of the lung epithelium, by determining the pharmacokinetic (PK) behavior of selected nanocarriers upon inhalation administration to Balb/c mice.

4.4.6. *In vivo* Pharmacokinetic (PK) Evaluation of $G3NH_2$-nPEG1000.

The plasma concentration-time profile for the $G3NH_2$-nPEG1000 dendrimer conjugates with n = 0, 13 and 25, following administration by pharyngeal aspiration and intravenous route, are shown in Figure 4.8(a) and (b). The PK parameters calculated from plasma concentration versus time profiles from both routes of administration (Figure 4.8(a) and (b)) are shown in Table 4.2:

The results demonstrate that the dendrimers with the highest degree of PEGylation (25PEG) show the highest plasma concentration at all time points. The other two dendrimer systems have significantly lower plasma concentrations as compared to the other $G3NH_2$-nPEG1000 dendrimers. After pharyngeal aspiration of the $G3NH_2$-25PEG1000 conjugate, a peak plasma concentration of ca.4.4 μg was reached at 3h, and stays constant for about 24h after, and then starts to slowly decrease, with dendrimer remaining in plasma at the end of 1 week. In contrast,

$G3NH_2$-0PEG1000 and $G3NH_2$-13PEG1000 had significantly lower peak plasma concentrations at ca.0.2 and 0.4 μg respectively.

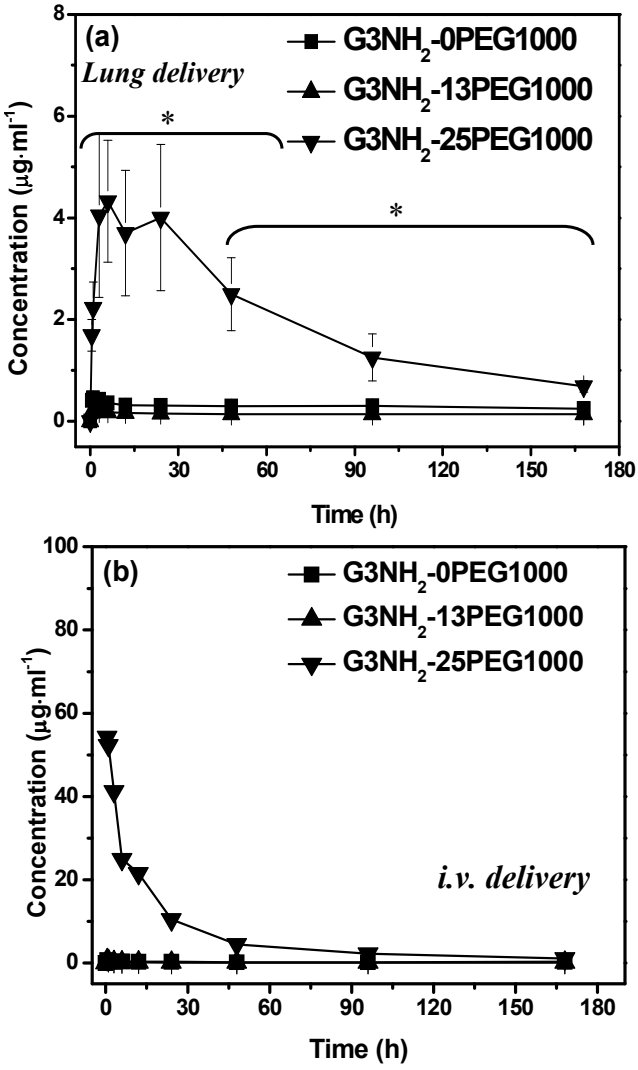

Figure 4.8. Mean plasma concentrations of $G3NH_2$-nPEG1000 conjugates detected by fluorometry after **(a)** pulmonary administration in mice (n=6 for each condition) as a function of time. **(b)** after intravenous (*i.v.)* administration in mice (n=3). In both cases, blood samples were collected from the tail vein using the tail bleeding method. Statistical significance with respect to control ($p<0.05$) denoted by *.

Among the conjugates, $G3NH_2$-25PEG1000 had the highest peak plasma concentration upon *i.v* administration, when compared to both $G3NH_2$-0PEG1000 and $G3NH_2$-13PEG1000. The conjugate $G3NH_2$-0PEG1000 had intermediate clearance. C_{ss} results indicate that among the conjugates, the greatest amount detected in plasma was that for $G3NH_2$-25PEG1000.

Table 4.2. Pharmacokinetic parameters for the $G3NH_2$-nPEG1000 upon administration to the lungs. The clearance (*Cl*) was determined from the data of intravenous administration studies of the same carriers. *Css* = steady state concentration; and *Ro* = rate of absorption.

Dendrimer	***Cl (ml/min)***	***C_{ss} (ng/ml)***	***R_o (ng/min)***
$G3NH_2$-0PEG1000	0.40 ± 0.004	477.09 ± 63.9	193.22 ± 27.93
$G3NH_2$-13PEG1000	7.99 ± 0.1	189.73 ± 11.14	1517.79 ± 112.0
$G3NH_2$-25PEG1000	0.14 ± 0.01	4596.9 ± 1434.8	639.88 ± 232.1

The PK results, to some extent, agreed with the *in vitro* transport studies. For instance, the relatively large rate of absorption seen for $G3NH_2$-25PEG1000 and G3NH2-13PEG1000 *in vivo* (compared to $G3NH_2$-0PEG1000), agreed with the *in vitro* observation pertinent to the apical to basolateral transport of $G3NH_2$-nPEG1000 across Calu-3 monolayers that increased with an increase in PEG density, with the greatest enhancement seen for $G3NH_2$-25PEG1000. However, different from *in vivo* results, the extent of $G3NH_2$-13PEG1000 transport *in vitro* was markedly different.

It is interesting to note that for the $G3NH_2$-13PEG1000 dendrimer, *Ro* is more than 2-fold higher than that for dendrimer with 25 PEG, and more than 7-fold higher than that for non-PEGylated dendrimer. From this observation, $G3NH_2$-13PEG1000 dendrimer would be expected to have higher plasma concentration over the other two systems. However, the dendrimer with $G3NH_2$-25PEG1000 has the highest plasma concentration at all times. This is most likely due to the fact that the clearance for $G3NH_2$-13PEG1000 dendrimer is 57 times higher than that for $G3NH_2$-25PEG1000 dendrimer. Therefore, the 13 PEG dendrimer is very rapidly cleared from the systemic circulation despite its high absorption from the lungs. On the other hand, though the R_o for $G3NH_2$-25PEG1000 dendrimer is less than that for $G3NH_2$-13PEG1000 conjugate, the clearance is drastically lower than that for 13 PEG dendrimer, thus resulting in an extended blood circulation time for 25 PEG dendrimers.

It is well established that PEG acts to increase the circulation time of carriers in the systemic circulation by way of increasing the hydrophilicity of the carrier and reducing opsonization, drastically reducing uptake by the reticuloendothelial system (RES).[16, 31] While there have been several studies delineating the pharmacokinetics of PEGylated dendrimers upon oral and *i.v* administration, to the best of our knowledge, this is the first study evaluating the PK of PEGylated PAMAM conjugates upon pulmonary administration. Pharmacokinetics of PEGylated poly-L-lysine dendrimers administered intravenously to rats, revealed that conjugates with MW>30 KDa exhibited longer circulation times with higher peak plasma concentrations, when compared to the low MW counterparts (<20 KDa), an

observation that was echoed in this study as well.[40] In another study, PEGylated PAMAM dendrimers (G4 and G5, MW ca.160 KDa and 284 KDa respectively) tethered with different MW of PEG (2KDa and 5 KDa), injected to mice were reported to be detected in blood even after 24h, while the acetylated counterparts of the conjugate was largely observed in the kidney.[70]

In the absence of data with respect to translocation of dendrimers from the lung to the systemic circulation upon pulmonary delivery, it would be wise to put these results in perspective with respect to other nanocarriers whose translocation has been evaluated upon lung administration. Less than 0.5% of polystyrene (PS) nanoparticles (NPs) with 20 nm diameter was detected in blood after a week upon pharyngeal aspiration to rat lungs - 70-80% of NPs recovered from the lung after a week.[38] Along similar lines, intratracheal instillation of anionic PS-polyacrylate NPs to rats resulted in over 2% of the conjugate being detected in the lymph nodes within the first hour, while over 40% was detected in the rest of the body.[71] Solid lipid nanoparticles have shown to be rapidly eliminated from rat lungs upon endotracheal administration, and are observed to immediately localize (within minutes) in axillary and inguinal lymph nodes.[72] PEGylated PLGA NPs of ca.200 nm in diameter were shown to remain in C57BL6 mice for as long as 11 days after intranasally administered, as evidenced by live body imaging.[73]

The G3NH_2-25PEG1000 dendrimer conjugate, due to its low clearance, has the highest plasma concentrations, and it remains in systemic circulation for longer than the other two systems. G3NH_2-13PEG1000 dendrimer has a slightly higher plasma concentration as compared to the non-PEGylated dendrimer after pulmonary

administration. It is interesting to note that the non-PEGylated dendrimer has a higher plasma concentration as compared to 13 PEG dendrimer after i.v. administration (Figure 4.8b). This is likely a result of the clearance being signficantly higher for the 13 PEG dendrimer as compared to the non-PEGylated dendrimer. However, the $G3NH_2$-25PEG1000 dendrimer has the highest plasma concentration among the three dendrimer systems, likely a result of extended plasma circulation by RES evasion.[31, 40]

When considering the PK of the dendrimer systems after both pulmonary and intravenous exposure, these results suggest that PEGylation of dendrimer surface has a significant effect on their pulmonary translocation. PEGylation up to a certain degree (13 PEG in this case) enhances the rate of absorption of the dendrimers across the lungs, whereas a higher PEGylation (25 PEG) improves the absorption across the lungs in addition to increasing the circulation time and concentration of the dendrimers in the systemic circulation post absorption from the lungs.

4.5. Conclusions.

In this work we determined the effect of PEGylation onto DNCs, on their interaction with *in vitro* and *in vivo* models of the lung epithelium. The cellular uptake, transport and pharmacokinetics of $G3NH_2$ dendrimers conjugated with PEG 1000 Da at various surface densities (5, 13 and 25 PEGs per $G3NH_2$ molecule) were studied. Cell viability studies conducted on Calu-3 cells revealed that PEGylation improved cell survival rate, with over 90% of the cells viability at concentrations as high as 100 μmol when incubated with $G3NH_2$-25PEG1000 for 24 hours. In contrast, only 30% of

cells incubated with G3NH_2-0PEG1000 survived at the same concentration. *In vitro* transport studies conducted on polarized Calu-3 monolayers revealed an increase in transport of G3NH_2-nPEG1000 with increasing PEG density. As much as 14% (w/w) of G3NH_2-25PEG1000 are transported from the apical to the basolateral side of the monolayer at 5h. On the other hand, only 1% of G3NH_2-0PEG1000 is transported within the same time. PEGylation also resulted in modulation of cellular uptake, as evidenced by flow cytometry and cell lysis studies, where PEGylation of DNCs was seen to decrease cellular uptake. This observation, in conjunction with the observation that the TEER of the monolayers is reduced during the transport studies suggests that the PEGylated conjugates could be traversing paracellularly. Peak plasma concentrations as high as 4.5 μg was detected for G3NH_2-25PEG1000 by 3h, while G3$NH_2$0PEG1000 and G3NH_2-13PEG1000 had very low peak plasma values to the tune of 0.2 and 0.4 μg, respectively corroborating what the *in vitro* transport studies. These results combined suggest that surface modification of G3-NH_2 with appropriate surface densities of PEG can aid in modulation of transport and uptake of the nanocarriers in lung epithelium. These results are promising since the incorporation of versatile drug delivery vehicles like dendrimers can open up new avenues within the realm of pulmonary delivery to target not only local disorders, but also diseases of systemic relevance.

Note – *PK studies was done with the assistance of Dr. Josh Reineke, Asst. Professor, Department of Pharmaceutical Sciences and Mr. Abdul Mohammad*

4.6 References

[1] D.C. Cipolla, I. Gonda, Formulation technology to repurpose drugs for inhalation delivery, Drug Discov Today, 8 (2011) 123-130.

[2] J.S. Patton, P.R. Byron, Inhaling medicines: delivering drugs to the body through lungs, Nat Rev Drug Discov, 6 (2007) 67-74.

[3] R.U. Agu, In vitro and in vivo testing methods for respiratory drug delivery, Expert Opin Drug Deliv, 8 (2011) 57-69.

[4] S.K. Aurora, S.D. Silberstein, S.H. Kori, S.J. Tepper, S.W. Borland, M. Wang, D.W. Dodick, MAP0004, orally inhaled DHE: a randomized, controlled study in the acute treatment of migraine, Headache, 51 (2011) 507-517.

[5] M.B. Dolovich, R. Dhand, Aerosol drug delivery: developments in device design and clinical use, Lancet, 377 (2011) 1032-1045.

[6] O.M. Merkel, T. Kissel, Nonviral Pulmonary Delivery of siRNA, Acc Chem Res, (2011).

[7] S. Azarmi, W.H. Roa, R. Lobenberg, Targeted delivery of nanoparticles for the treatment of lung diseases, Adv Drug Del Rev, 60 (2008) 863-875.

[8] R. Inapagolla, B.R. Guru, Y.E. Kurtoglu, X. Gao, M. Lieh-Lai, D.J. Bassett, R.M. Kannan, In vivo efficacy of dendrimer-methylprednisolone conjugate formulation for the treatment of lung inflammation, Int J Pharm, 399 (2010) 140-147.

[9] A.R. Menjoge, R.M. Kannan, D.A. Tomalia, Dendrimer-based drug and imaging conjugates: design considerations for nanomedical applications, Drug Discov Today, 15 (2010) 171-185.

[10] A. Misra, A.J. Hickey, C. Rossi, G. Borchard, H. Terada, K. Makino, P.B. Fourie, P. Colombo, Inhaled drug therapy for treatment of tuberculosis, Tuberculosis (Edinb), 91 (2011) 71-81.

[11] I. Roy, N. Vij, Nanodelivery in airway diseases: challenges and therapeutic applications, Nanomedicine, 6 (2010) 237-244.

[12] E. Rytting, J. Nguyen, X. Wang, T. Kissel, Biodegradable polymeric nanocarriers for pulmonary drug delivery, Expert Opin Drug Del, 5 (2008) 629-639.

[13] M.E. Davis, Z. Chen, D.M. Shin, Nanoparticle therapeutics: an emerging treatment modality for cancer, Nat Rev Drug Discov, 7 (2008) 771-782.

[14] S.K. Lai, Y.Y. Wang, J. Hanes, Mucus-penetrating nanoparticles for drug and gene delivery to mucosal tissues, Adv Drug Deliv Rev, 61 (2009) 158-171.

[15] U. Pison, T. Welte, M. Giersig, D.A. Groneberg, Nanomedicine for respiratory diseases, Eur J Pharmacol, 533 (2006) 341-350.

[16] S. Svenson, Dendrimers as versatile platform in drug delivery applications, Eur J Pharm Biopharm, 71 (2009) 445-462.

[17] A. D'Emanuele, D. Attwood, Dendrimer-drug interactions, Adv Drug Deliv Rev, 57 (2005) 2147-2162.

[18] S. Sadekar, H. Ghandehari, Transepithelial transport and toxicity of PAMAM dendrimers: Implications for oral drug delivery, Adv Drug Deliv Rev, (2011).

[19] A. Saovapakhiran, A. D'Emanuele, D. Attwood, J. Penny, Surface modification of PAMAM dendrimers modulates the mechanism of cellular internalization, Bioconjug Chem, 20 (2009) 693-701.

[20] Y.E. Kurtoglu, R.S. Navath, B. Wang, S. Kannan, R. Romero, R.M. Kannan, Poly(amidoamine) dendrimer-drug conjugates with disulfide linkages for intracellular drug delivery, Biomaterials, 30 (2009) 2112-2121.

[21] D.M. Sweet, R.B. Kolhatkar, A. Ray, P. Swaan, H. Ghandehari, Transepithelial transport of PEGylated anionic poly(amidoamine) dendrimers: implications for oral drug delivery, J Control Release, 138 (2009) 78-85.

[22] S.K. Lai, D.E. O'Hanlon, S. Harrold, S.T. Man, Y.Y. Wang, R. Cone, J. Hanes, Rapid transport of large polymeric nanoparticles in fresh undiluted human mucus, Proc Natl Acad Sci U S A, 104 (2007) 1482-1487.

[23] S. Dufort, L. Sancey, J.L. Coll, Physico-chemical parameters that govern nanoparticles fate also dictate rules for their molecular evolution, Adv Drug Deliv Rev, (2011).

[24] S. Anabousi, E. Kleemann, U. Bakowsky, T. Kissel, T. Schmehl, T. Gessler, W. Seeger, C.M. Lehr, C. Ehrhardt, Effect of PEGylation on the stability of liposomes during nebulisation and in lung surfactant, J Nanosci Nanotechnol, 6 (2006) 3010-3016.

[25] Y.Y. Wang, S.K. Lai, J.S. Suk, A. Pace, R. Cone, J. Hanes, Addressing the PEG mucoadhesivity paradox to engineer nanoparticles that "slip" through the human mucus barrier, Angew Chem Int Ed Engl, 47 (2008) 9726-9729.

[26] F.M. Veronese, G. Pasut, PEGylation, successful approach to drug delivery, Drug Discov Today, 10 (2005) 1451-1458.

[27] L. Wu, B. Bharatwaj, J. Panyam, S.R.P. da Rocha, Core–shell Particles for the Dispersion of Small Polar Drugs and Biomolecules in Hydrofluoroalkane Propellants, Pharm Res, 25 (2008) 289-301.

[28] G.P. Royer, G.M. Anantharamiah, Peptide Synthesis in Water and the Use of Immobilized Carboxypeptidase Y for Deprotection, J Am Chem Soc, 101 (1979) 3394-3396.

[29] X.Q. Zhang, J. Intra, A.K. Salem, Conjugation of polyamidoamine dendrimers on biodegradable microparticles for nonviral gene delivery, Bioconjug Chem, 18 (2007) 2068-2076.

[30] S.J. Guillaudeu, M.E. Fox, Y.M. Haidar, E.E. Dy, F.C. Szoka, J.M. Frechet, PEGylated dendrimers with core functionality for biological applications, Bioconjug Chem, 19 (2008) 461-469.

[31] N.K. Jain, M. Nahar, PEGylated Nanocarriers for Systemic Delivery, in: Cancer Nanotechnology : Methods in Molecular Biology, Springer, 2009, pp. 221-234.

[32] O.P. Perumal, R. Inapagolla, S. Kannan, R.M. Kannan, The effect of surface functionality on cellular trafficking of dendrimers, Biomaterials, 29 (2008) 3469-3476.

[33] Promega Corp, CellTiter 96® AQueous Non-Radioactive Cell Proliferation Assay, in: Promega Inc. (Ed.), Madison, WI, 2009.

[34] C.I. Grainger, L.L. Greenwell, D.J. Lockley, G.P. Martin, B. Forbes, Culture of Calu-3 cells at the air interface provides a representative model of the airway epithelial barrier, Pharm Res, 23 (2006) 1482-1490.

[35] M. Probes, ZO-1, Mouse Monoclonal Antibody - Alexa Fluor 546, in, Invitrogen, 2010.

[36] I. Buchwalow, V. Samoilova, W. Boecker, M. Tiemann, Non-specific binding of antibodies in immunohistochemistry: Fakes and facts, Nature Preceedings, (2011).

[37] P. Biotechnology, Pierce® BCA Protein Assay, in, Rockford, IL, 2011.

[38] K. Sarlo, K.L. Blackburn, E.D. Clark, J. Grothaus, J. Chaney, S. Neu, J. Flood, D. Abbott, C. Bohne, K. Casey, C. Fryer, M. Kuhn, Tissue distribution of 20 nm, 100 nm and 1000 nm fluorescent polystyrene latex nanospheres following acute systemic or acute and repeat airway exposure in the rat, Toxicology, 263 (2009) 117-126.

[39] A. Gajbhiye, V.P. Kumar, R.K. Tekade, N.K. Jain, Pharmaceutical and Biomedical Potential of PEGylated Dendrimers, Curr Pharm Design, 13 (2007) 415-429.

[40] L.M. Kaminskas, B.J. Boyd, P. Karellas, G.Y. Krippner, R. Lessene, B. Kelly, C.J. Porter, The impact of molecular weight and PEG chain length on the systemic pharmacokinetics of PEGylated poly l-lysine dendrimers, Mol Pharm, 5 (2008) 449-463.

[41] I.J. Majoros, T.P. Thomas, C.B. Mehta, J.R. Baker, Jr., Poly(amidoamine) dendrimer-based multifunctional engineered nanodevice for cancer therapy, J Med Chem., 48 (2005) 5892-5899.

[42] Y. Kim, A.M. Klutz, K.A. Jacobson, Systematic investigation of polyamidoamine dendrimers surface-modified with poly(ethylene glycol) for drug delivery applications: synthesis, characterization, and evaluation of cytotoxicity, Bioconjug Chem, 19 (2008) 1660-1672.

[43] S. Bai, F. Ahsan, Synthesis and evaluation of pegylated dendrimeric nanocarrier for pulmonary delivery of low molecular weight heparin, Pharm Res, 26 (2009) 539-548.

[44] C. Colonna, B. Conti, P. Perugini, F. Pavanetto, T. Modena, R. Dorati, P. Iadarola, I. Genta, Ex vivo evaluation of prolidase loaded chitosan nanoparticles for the enzyme replacement therapy, Eur J Pharm Biopharm, 70 (2008) 58-65.

[45] Y. Kim, B. Hechler, A.M. Klutz, C. Gachet, K.A. Jacobson, Toward multivalent signaling across G protein-coupled receptors from poly(amidoamine) dendrimers, Bioconjug Chem, 19 (2008) 406-411.

[46] R. Jevprasesphant, J. Penny, D. Attwood, N.B. McKeown, A. D'Emanuele, Engineering of dendrimer surfaces to enhance transepithelial transport and reduce cytotoxicity, Pharm Res, 20 (2003) 1543-1550.

[47] A.R. Menjoge, R.S. Navath, A. Asad, S. Kannan, C.J. Kim, R. Romero, R.M. Kannan, Transport and biodistribution of dendrimers across human fetal membranes: implications for intravaginal administration of dendrimer-drug conjugates, Biomaterials, 31 (2010) 5007-5021.

[48] S. Zhu, M. Hong, G. Tang, L. Qian, J. Lin, Y. Jiang, Y. Pei, Partly PEGylated polyamidoamine dendrimer for tumor-selective targeting of doxorubicin: the effects of PEGylation degree and drug conjugation style, Biomaterials, 31 (2010) 1360-1371.

[49] D. Luo, K. Haverstick, N. Belcheva, E. Han, W.M. Saltzman, Poly(ethylene glycol)-Conjugated PAMAM Dendrimer for Biocompatible, High-Efficiency DNA Delivery, Macromolecules, 35 (2004) 3456-3462.

[50] S. Kannan, P. Kolhe, V. Raykova, M. Glibatec, R.M. Kannan, M. Lieh-Lai, D. Bassett, Dynamics of cellular entry and drug delivery by dendritic polymers into human lung epithelial carcinoma cells, J Biomater Sci Polym Ed, 15 (2004) 311-330.

[51] K.M. Kitchens, H. Ghandehari, PAMAM Dendrimers as Nanoscale Oral Drug Delivery Systems, in: M.M. de Villiers, P. AraMWit, G.S. Kwon (Eds.), 2009, pp. 423-459.

[52] L. Casettari, D. Vllasaliu, G. Mantovani, S.M. Howdle, S. Stolnik, L. Illum, Effect of PEGylation on the Toxicity and Permeability Enhancement of Chitosan, Biomacromolecules, (2010).

[53] W. Wang, W. Xiong, J. Wan, H. Xu, X. Yang, The decrease of PAMAM dendrimer-induced cytotoxicity by PEGylation via attenuation of oxidative stress, Nanotechnol, 20 (2009) 105-113.

[54] J.M. Anderson, Molecular Structure of Tight Junctions and Their Role in Epithelial Transport, Physiology, 16 (2001) 126-130.

[55] K.M. Kitchens, R.B. Kolhatkar, P.W. Swaan, N.D. Eddington, H. Ghandehari, Transport of poly(amidoamine) dendrimers across Caco-2 cell monolayers: Influence of size, charge and fluorescent labeling, Pharm Res, 23 (2006) 2818-2826.

[56] D.S. Pisal, V.K. Yellepeddi, A. Kumar, S. Palakurthi, Transport of surface engineered polyamidoamine (PAMAM) dendrimers across IPEC-J2 cell monolayers, Drug Deliv, 15 (2008) 515-522.

[57] N.R. Mathias, J. Timoszyk, P.I. Stetsko, J.R. Megill, R.L. Smith, D.A. Wall, Permeability Characteristics of Calu-3 Human Bronchial Epithelial Cells: In Vitro - In Vivo Correlation to Predict Lung Absorption in Rats, J Drug Target, 10 (2002) 31-40.

[58] J. Linnankoski, J. Makela, J. Palmgren, T. Mauriala, C. Vedin, A.L. Ungell, L. Lazorova, P. Artursson, A. Urtti, M. Yliperttula, Paracellular porosity and pore size of the human intestinal epithelium in tissue and cell culture models, J Pharm Sci, 99 (2010) 2166-2175.

[59] F. Tajarobi, M. El-Sayed, B.D. Rege, J.E. Polli, H. Ghandehari, Transport of poly amidoamine dendrimers across Madin-Darby canine kidney cells, Int J Pharm, 215 (2001) 263-267.

[60] S.T. Buckley, K.-J. Kim, C. Ehrhardt, In Vitro Cell Culture Models for Evaluating Controlled Release Pulmonary Drug Delivery, in: H.D.C. Smyth, A.J. Hickey (Eds.) Controlled Pulmonary Drug Delivery, Springer, New York, 2011, pp. 417-442.

[61] K. Jain, P. Kesharwani, U. Gupta, N.K. Jain, Dendrimer toxicity: Let's meet the challenge, Int J Pharm, 394 (2010) 122-142.

[62] R. Qi, G. Y, Y. Tang, R.-R. He, T.-L. Liu, Y. He, S. Sun, B.-Y. Li, Y.-B. Li, G. Liu, PEG-conjugated PAMAM Dendrimers Mediate Efficient Intramuscular Gene Expression, AAPS J, 11 (2009) 395-405.

[63] B. Forbes, C. Ehrhardt, Human respiratory epithelial cell culture for drug delivery applications, Eur J Pharm Biopharm, 60 (2005) 193-205.

[64] M. Haghi, P.M. Young, D. Traini, R. Jaiswal, J. Gong, M. Bebawy, Time- and passage- dependent characteristics of a Calu-3 respiratory cell model, Drug Dev Ind Pharm, 36 (2010) 1207-1214.

[65] D. Vllasaliu, R. Fowler, M. Garnett, M. Eaton, S. Stolnik, Barrier characteristics of epithelial cultures modelling the airway and intestinal mucosa: a comparison, Biochem Biophys Res Commun, 415 (2011) 579-585.

[66] D.S. Pisal, V.K. Yellepeddi, A. Kumar, R.S. Kaushik, M.B. Hildreth, X. Guan, S. Palakurthi, Permeability of surface-modified polyamidoamine (PAMAM) dendrimers across Caco-2 cell monolayers, Int J Pharm, 350 (2008) 113-121.

[67] I. Bucior, K. Mostov, J.N. Engel, Pseudomonas aeruginosa-mediated damage requires distinct receptors at the apical and basolateral surfaces of the polarized epithelium, Infect Immun, 78 (2010) 939-953.

[68] D.S. Goldberg, H. Ghandehari, P.W. Swaan, Cellular entry of G3.5 poly (amido amine) dendrimers by clathrin- and dynamin-dependent endocytosis promotes tight junctional opening in intestinal epithelia, Pharm Res, 27 (2010) 1547-1557.

[69] M.C. Plotkowski, A.O. Costa, V. Morandi, H.S. Barbosa, H.B. Nader, S. de Bentzmann, E. Puchelle, Role of heparan sulphate proteoglycans as potential receptors for non-piliated Pseudomonas aeruginosa adherence to non-polarised airway epithelial cells, J Med Microbiol, 50 (2001) 183-190.

[70] C. Kojima, C. Regino, Y. Umeda, H. Kobayashi, K. Kono, Influence of dendrimer generation and polyethylene glycol length on the biodistribution of PEGylated dendrimers, Int J Pharm, 383 (2010) 293-296.

[71] H.S. Choi, Y. Ashitate, J.H. Lee, S.H. Kim, A. Matsui, N. Insin, M.G. Bawendi, M. Semmler-Behnke, J.V. Frangioni, A. Tsuda, Rapid translocation of nanoparticles from the lung airspaces to the body, Nat Biotechnol, 28 (2010) 1300-1303.

[72] M.A. Videira, L. Gano, C. Santos, M. Neves, A.J. Almeida, Lymphatic uptake of lipid nanoparticles following endotracheal administration, J Microencapsul, 23 (2006) 855-862.

[73] N. Vij, T. Min, R. Marasigan, C.N. Belcher, S. Mazur, H. Ding, K.T. Yong, I. Roy, Development of PEGylated PLGA nanoparticle for controlled and sustained drug delivery in cystic fibrosis, J Nanobiotechnology, 8 (2010) 22.

Chapter 5

Pulmonary Inflammatory Response of a Versatile Chitosan-based Co-oligmeric Excipient for Pressurized-Metered Dose Inhalers

5.1. Introduction

Portable oral inhalation (OI) devices, such as such as pressurized metered-dose inhalers (pMDIs) and dry powder inhalers (DPIs), have tremendous relevance in the treatment of pulmonary disorders.[1-6] Such platforms have been also recognized as potential candidates for the delivery of therapeutics intended for systemic circulation, in this case to be delivered non-invasively through the lungs. They both have advantages and disadvantages,[1, 2, 6, 7] and it seems that the ideal scenario would be to offer patients and doctors the option to use either platform, in a way to achieve maximum efficiency based on a series of factors, including disease condition and age of the patient.[2, 8, 9] One major formulation challenge in the case of pMDIs is the fact that the hydrofluoroalkane (HFA) propellants utilized in those devices are somewhat hydrophobic and lipophobic at the same time,[5, 10, 11] and as a result, are not good solvents for most therapeutics of interest.[5, 11-14] One then often needs to resort to dispersion-based formulations in pMDIs,[5, 13, 15, 16] but the design of dispersants is also no easy task.[3, 17, 18]

We have developed a versatile biodegradable excipient that is capable of forming stable dispersions of a variety of therapeutics and drug delivery systems in pMDIs, and consequently, formulations that give rise to aerosols that are inductive to enhanced deep lung deposition.[13, 15, 19, 20] One of the strategies consists in

forming polymeric nanoparticles of this excipient – co-oligomer of oligo(lactic acid) (OLA) grafted onto chitosan (CS; OLA-g-CS), which can act as a steric barrier to the flocculation of micron-sized colloidal drug particles (crystals or amorphous) due to its high stability in the propellant,[13] due to the presence of the ester groups in the co-oligomer, that interact well with the propellant.[15, 17] Another pMDI platform that may find application in the delivery of therapeutics to and through the lung, is the formation of core-shell micron particles containing polymeric nanoparticles (NPs; the drug carriers) in the interior (core) of the micron-particles, which are 'coated' with the co-oligomeric shell. We have shown that the shell is capable of enhancing the aerosol characteristics of such formulations, so as to achieve high fine particle fractions (deep lung deposition) of the NPs. This is an important platform, as polymeric NPs have great versatility, and may be used for the controlled and targeted delivery to the lung tissue. These can be designed to have enhanced extra-cellular transport and improved cellular uptake,[19, 20] thus opening up new opportunities for the delivery of a range of therapeutics to and through the lungs.[1, 21, 22]

Is this work we have evaluated the *in vivo* residence time and inflammatory response of this OLA-g-CS co-oligomer upon lung delivery, in conditions representative of the study where NP of this co-oligomer were capable of stabilize drug dispersions in HFAs.[15] We also studied the *in vivo* interaction of the OLA-g-CS co-oligomer in the presence of poly(lactic glycolic) (PLGA) NPs, in a composition similar to that used in the formation of the core-shell particle formulations in pMDIs.[19] We determined the impact of this versatile excipient on the inflammatory status of the lungs by evaluating the changes in inflammatory cell population by

bronchoalveolar lavage (BAL) and collagenase tissue dispersion of the tissue upon transnasal administration. Experiments were conducted to assess the impact of the OLA-g-CS accumulation in the lungs upon repeated administration, and the lung's ability to deal with an allergen induced immune response was also studied. The inflammatory response of co-oligomer administered with the PLGA NPs nanoparticles was also assessed.

5.2. Materials

Chitosan (CS, medium molecular weight) was obtained from Aldrich Chemicals. Toluene, hydrochloric acid, hydrogen peroxide and sodium hydroxide were sourced from Fisher. Deionized water (NANOpure DIamond UV ultrapure water system, Barnstead International, DI water) was used in all experiments. D,L-lactide, poly(vinyl alcohol) (PVA, 87-90 KDa, cold water soluble), fluorescein isothiocyanate (FITC), fluoresceinamine (FA), dicyclohexylcarbodiimide (DCC), N-hydroxysuccinimide (NHS), and stannous octoate were purchased from Sigma. Ester and carboxylate terminated poly(lactic-co-glycolic) acid (PLGA, 50:50, 31.3-45 KDa) was purchased from Birmingham Polymers. Anhydrous dimethylformamide (DMF) was procured from Acros Organics. All other chemicals were purchased from Fisher and used as received, unless otherwise specified.

Pathogen free female Balb/c mice, 8-10 weeks old, weighing between 17 and 23 g (Hilltop farms, Scottsdale, PA) were housed in polycarbonate cages upon arrival, and kept under high efficiency particulate filtered air (HEPA). The mice were quarantined for a week prior to experiment. They received food and water ad

libitum. The protocols used in this study were approved by Wayne State University's Institutional Animal Care and Use Committee (IACUC), consistent with guidelines prescribed by the US government. Sodium pentobarbital was obtained from Meds for Vets and was diluted to 50 $mg \cdot Kg^{-1}$ in PBS. Protein microassay was purchased from BioRad Labs. Isoflurane was purchased from VetOne Pharmaceuticals. Collagenase (100 $IU \cdot ml^{-1}$) was obtained from Worthington Biochemical. Fetal Bovine Serum (FBS) was procured from Gibco. Tissue strainer was purchased from BD Falcon. Cytospin slides and cytology funnels were purchased from Fisher Scientific. Ethylenediaminetetraacetic acid (EDTA), RPMI medium (without phenol red), isotonic saline, DNase (50 $U \cdot ml^{-1}$), Ovalbumin (OVA, grade V), and phosphate buffered saline (PBS) (1X, pH 7.4) were procured from Sigma. Zap-O-Globin Lytic reagent was purchased from Beckman Coulter. Wright's Giemsa stain (Diff Quik) was obtained from Fisher chemicals.

5.3. Methods.

5.3.1 Synthesis and characterization of OLA-g-CS cooligomer.

OLA-g-CS was prepared and characterized as detailed in our previous work.[13, 15] Commercial CS was depolymerized using hydrogen peroxide. The resulting degraded CS was characterized using size exclusion chromatography (SEC) using a Shimadzu LC-10ADVP liquid chromatograph equipped with a seven angle static light scattering detector (BIMWA) and a differential refractometer (Brookhaven Instruments). The CS was degraded down to 1350 Da as determined by SEC, which corresponds to ca. 8 repeat units of CS. Oligo-lactic acid (OLA) was

grafted onto the degraded CS backbone by ring opening polymerization. A known amount of CS NPs was charged into a round bottom flask containing D, L Lactide and stannous octoate in toluene. The mixture was stirred at 373K in an atmosphere of nitrogen for 24h. The water soluble product was washed multiple times with acetone, dried and characterized by ^{1}H-NMR and FTIR. For ^{1}H-NMR (Varian Mercury 400) ca.10 mg of OLA-g-CS was dissolved in 0.8 mL DMSO-d_6 for analysis. For FT-IR, 5 mg of OLA-g-CS was ground with potassium bromide, pressed into a pellet and subjected to FT-IR spectroscopy (Bruker Tensor 27). The molar grafting ratio of CS to OLA was determined from ^{1}H-NMR to be 2.4, resulting in a highly water soluble co-oligomer of 1730 Da, as estimated from ^{1}H-NMR. From the FT-IR spectra, the presence of a sharp peak at 1750 cm^{-1} can be attributed to the carbonyl bond arising from the LA graft.[15] The length of LA units tethered onto CS chain was estimated to be ca.3. The molar ratio of CS to LA in the co-oligomer was determined from ^{1}H-NMR to be 2.4.

5.3.2 Synthesis of FITC-labeled OLA-g-CS and FA-labeled PLGA.

FITC labeled Polylactic acid -Chitosan (PLA-g-CS) oligomer was synthesized according to an earlier method described in the literature.[22] Briefly, known amounts of OLA-g-CS (4 mg•ml-1) and FITC (1.5 mg•ml-1) were dissolved in deionized water and anhydrous methanol respectively. Both solutions were added into a round bottom flask containing 10 ml of anhydrous methanol. The contents were stirred in dark at ambient temperature for 5 hours after which, they were precipitated in excess of acetone. The precipitate was centrifuged and washed further with

copious amounts of acetone to remove unreacted FITC. After each wash a sample of the supernatant was analyzed spectrophotometrically for the presence of FITC. The washing was continued until no FITC was detected in the supernatant. The FITC labeled OLA-g-CS was solubilized in DI water and lyophilized in order to obtain the final product. The resulting product was characterized by 1H-NMR (Varian 400) and UV-spectroscopy (Cary50) to obtain the final product.

FA conjugated PLGA NPs were prepared according to procedure detailed in the literature with minor modifications.[23] The fluorophore was conjugated to PLGA through a simple coupling reaction wherein the carboxylic acid end of the polymer is coupled to the primary amine group of FA via an amide linkage. Briefly, 500 mg of PLGA was dissolved along with equimolar amounts of DCC (1 mmol) and NHS (1 mmol) in anhydrous DMF. The contents were stirred under room temperature for 4h in order to activate the carboxylic end groups located on PLGA. To the activated polymer solution, 25mg (0.07 mmol) of fluoresceinamine solubilized in 2 ml DMF was added and the reaction was continued overnight. The insoluble dicyclohexylurea (DCU) formed as a byproduct of the reaction was removed by filtration. The polymer was isolated by precipitating the filtrate into cold anhydrous diethyl ether followed by purifying the contents in methylene chloride and precipitating the resulting solution back into anhydrous diethyl ether. The precipitate was then subjected to repeated washings in 5 mM HCl to remove any remnants of unconjugated fluoresceinamine and was lyophilized and stored at -20°C until further use. The polymer was characterized using 1H-NMR (Varian 400 MHz) in d-DMSO in order to confirm the chemical structure.

5.3.3 Preparation and characterization of FA-PLGA nanoparticles.

FA-PLGA NPs were prepared by emulsification solvent evaporation as described earlier.[24] Briefly, 100mg of FA-PLGA was dissolved in 3 ml of a mixture containing 4 parts dichloromethane (DCM) and 1 part acetone. The organic mixture containing PLGA was emulsified over an ince bath with 5 ml of 2% PVA using a sonicating probe (OMNIruptor 250) set a 50W power for 3 minutes. The resulting primary emulsion was immediately added to a solution containing 150ml of 0.5% PVA maintained under stirring. The diluted emulsion was stirred overnight to evaporate the organic solvent. The NPs were collected by centrifugation (Thermo Fisher) at 12000 RPM, and washed thrice with DI water to remove the residual PVA. The NPs thus obtained were snap frozen in liquid N_2 and lyophilized to obtain the final product. The particles were then physically characterized for size and shape using scanning electron microscopy (SEM, Hitachi S2400) and dynamic light scattering (DLS, 90Plus Brookhaven Instruments).

5.3.4 Administration of OLA-g-CS and OLA-g-CS laden PLGA NPs to mice.

Transnasal administration was employed to deliver the OLA-g-CS co-oligomer, and the combination of co-oligomer and PLGA NPs to mice. OLA-g-CS solutions were freshly prepared on the day of the experiment by dissolving a known amount of the co-oligomer in sterile isotonic saline and filtered using a 0.22μM syringe filter (VWR).[25-27]. The mice were weighed and anesthetized under isoflurane in an oxygen atmosphere for 30s, with the help of an integrated multi-patient anesthesia center (IMPAC, Pfizer). Mice were held under vertical position, and 15μL of OLA-g-

CS or co-oligomer and PLGA NPs was administered transnasally, followed by 15μL of isotonic saline as chaser. The material thus administered is rapidly taken into the lungs, and mice recovered within a couple of minutes. Mice were allowed to recover after instillation, before returning them back to their cages.

Acute dose experiments were conducted with three co-oligomer dosages: 10, 100 and 500μg per 15μl of saline, and a control - 15μl of saline only. For each condition, a cohort of six mice was used. The estimated dose of material reaching the lungs using this delivery strategy was evaluated with the help of a tracer. Transnasal administration of Evans' Blue dye (0.5% w/v in isotonic saline) and chaser followed by immediate excision of the lungs and quantification of the amount recovered, showed that that 39±4% of the dye reached the peripheral parenchymal regions of the lungs. This result compares well with the previous literature, thus confirming the reproducibility of the approach.[25]

For ***repeated administration*** experiments, mice were initially placed in nose-only exposure chambers and allowed to inhale sterile, aerosolized saline for 60 minutes. Prior to aerosol exposure, on day 1, mice were instilled with saline solutions of OLA-g-CS via transnasal administration of 10 or 100μg ·per 15μl solution, followed by chaser. The inhalation of saline aerosols is not expected to adversely affect the inflammatory state of the lung and was done here, in order to compare the results obtained in this study to that of data obtained from the allergen induced response experiment (where mice are exposed to aerosols containing an allergen, as discussed below). The aerosols were generated by a collision nebulizer (CH Systems, New York) that supplies a relatively mono-dispersed aerosol with a mean

aerodynamic diameter of 0.25 μm. On day 2, mice were exposed to saline aerosols for an hour, followed by administration of the co-oligomer (3h after saline exposure). This aerosol exposure was repeated four more times, resulting in a total of 5 consecutive days of aerosol exposures and six consecutive excipient administrations. 24h after the last exposure to saline (day 7), the animals were subjected to brochoalveolar lavage (BAL), and collagenase digestion of the lung tissue to assess the inflammatory cell population. These steps are detailed in sections that follow. Mice exposed to saline aerosols and administered with only 15μl saline and the chaser, also for a total of six times, were used as controls

For studying the ***allergen induced immune response***, animals were sensitized with intraperitoneal (IP) injection of with 0.2 ml of sterile isotonic saline containing 10 μg ovalbumin (OVA) and 2 mg of aluminum hydroxide.[28] Sensitization procedure was undertaken on day 1 and day 14, and daily aerosolized OVA (1% ovalbumin in sterile saline) exposures were conducted 21 days after the first sensitization. The procedure for aerosol exposure was similar to that described above. Cohorts of OVA-sensitized mice were treated (transnasal administration) with saline carrier containing 0 (just saline), 10, or 100μg OLA-g-CS per 15μl, 24h prior to first OVA exposure. On day 2, cohorts were exposed to OVA aerosols for 60 minutes, followed by the second administration of OLA-g-CS. This procedure was repeated, as mentioned before, 4 more times for 4 consecutive days amounting to a total of 5 OVA exposures and 6 transnasal administrations of OLA-g-CS at stipulated dosages.. Generation of OVA aerosols was done using a nebulizer as described before and the airflow was adjusted to ensure a constant concentration of 25 mg

$OVA \cdot m^{-3}$ is supplied to the animals as described in previous studies.[25, 28] The animals were then subjected to BAL, and collagenase digestion of the lungs to estimate the inflammatory cell populations 24h after the final OVA exposure.

Administration of Combination of OLA-g-CS and PLGA NPs. Known concentrations of the NPs (10 and 30μg per 15 μl) were dispersed in a saline solution of OLA-g-CS using gentle sonication for 30s. The resulting solution was administered to mice transnasally, as explained earlier. The animals were then subjected to BAL, to estimate the inflammatory cell population, 24h after dosing. Mice were also administered with two different dosages of bare PLGA NPs – no co-oligomer (10 and 30μg NP per 15μl isotonic saline solution) in order to assess the impact of NPs on the inflammatory state of the lung. A total of 4 mice were used for each condition.

5.3.5 Estimation of inflammatory cell infiltration into lungs.

The infiltration of inflammatory cells in mice receiving the OLA-g-CS and NPs was estimated using BAL and collagenase tissue dispersion of perfused lung as described earlier.[26, 29] For BAL, the treated animals were sacrificed with a lethal injection of sodium pentobarbital, their chest opened, and the mice were exsanguinated by incising the heart to release the blood pressure from the lung. The lungs were perfused with warm isotonic saline via the pulmonary artery, lavaged with 1ml warm (37 °C) PBS (pH 7.4), which was collected in centrifuge tubes and stored at -80ºC for protein analysis. This was followed by serial lavages with PBS-EDTA (3 mM EDTA, 1 mL) of the lung 5 times to ensure maximum recovery of inflammatory

cells. The recovered BAL fluid (BALF) was centrifuged at 300×g (Sorvall) at 4 °C, for 12min to obtain the inflammatory cell population as a pellet. The washed cells were resuspended in a 0.3 ml of PBS-EDTA, diluted in Isotone® II Diluent (Beckman Coulter), treated with two drops of Zap-O-Globin Lytic reagent (to mask the red blood cell population) and counted using a Coulter Counter (Coulter Electronics, Hialeah, FL) calibrated against a haemocytometer to obtain the total cell count. The cells were then cytospun and stained with Wright's Giemsa Stain to estimate the individual inflammatory cell populations viz. macrophages (MAC), lymphocytes (LYM), neutrophils (PMN), and eosinophils (EOS). A total of at least a 100 cells was counted per slide.

Tissue dispersion studies to estimate the total cell count was performed according to procedure detailed in the literature.[28] Lungs subjected to BAL, were excised from mice, washed in saline and sliced into tiny pieces. They were subjected to collagenase digestion for 90min in a shaker maintained at 37°C. The digestive agent was freshly prepared on the day of the experiment and it comprised of a 60ml RPMI solution supplemented with DNase and 100 Units per ml collagenase and 5% FBS. The digested tissue components were filtered using a cell strainer (BD Falcon) to separate the undigested components, and the filtrate was centrifuged at 1250 RPM for 12min to recover the cell pellet. The supernatant obtained was discarded, and the recovered cells were resuspended in RPMI medium supplemented with FBS. They were subjected to another round of centrifugation at same conditions (described above) after which they were washed and redispersed in PBS-EDTA. Total cell count in the dispersion was estimated using Coulter counter as described earlier.

Finally, the dispersed cell pellet was cytospun and the slides were stained as detailed before using Wright's Giemsa stain. In addition to the Wright Stain, cells were also subject to a nonspecific esterase stain for the identification of monocytes and MAC.[26]

5.3.6 Recovery and estimation of FITC-labeled OLA-g-CS from lungs.

Mice were exposed to the FITC-labeled OLA-g-CS using transnasal instillation as detailed before. In this study, a concentration of 500μg per 15 μl of the FITC labeled OLA-g-CS was utilized. This concentration was chosen in order to ensure detection of the co-oligomer spectrophotometrically at various time points. Here, an untreated mouse and a mice lung spiked with the FITC-labeled copolymer in saline were used as controls. A single cohort for this experiment comprised of the controls (n=3 for each condition) and the mice treated with the labeled co-oligomer (n=4). The exposed mice were exsanguinated at different time points in order to track the presence of the labeled co-oligomer within the tissue. Mice were euthanized, their lungs were excised, homogenized in saline and extracted with 1.5ml of 3N Sodium Hydroxide for 72h. The extract was then subject to ultracentrifugation (Sorvall) at 12000×g for 20 min. The supernatant was carefully removed without disturbing the tissue layer and was subjected to spectroscopic analysis (DU70, Beckman) at 495 nm. The values were corrected for tissue absorbance and compared against a previously prepared calibration curve of OLA-g-CS labeled FITC to estimate the concentration of the excipient in the lung at different times. The results were plotted as percent retained in the lung as a function of time. The data obtained at time t=0

was deemed as 100%, and the values obtained at later times were normalized with respect to this value. In order to unambiguously ensure that the approach utilized in detecting the co-oligomer was accurate, mice lungs were excised, spiked with a known amount of FITC labeled OLA-g-CS (500μg per 15μl), and extracted as described above. The absorbance values obtained from this study were tissue corrected and compared against the calibration curve. This approach yielded a recovery of 88±4% (n=3) of the spiked co-oligomer.

A similar methodology was employed to study the clearance of FA-PLGA NPs from the airspace. In this case, 10μg per 15μl of NPs dispersed in a saline solution of OLA-g-CS (100μg) was administered to the mice via transnasal administration. The extraction procedure was performed in a 2 ml solution of 0.5% sodium sulfate in acetone for 72h in darkness.

5.3.7 Serum protein determination.

Determination of serum protein in BALF was accomplished using a Bio-Rad Micro Assay procedure (Bio-Rad labs). Frozen BALF was thawed and diluted in the ratio 1:100 with DI water. The diluted samples were then treated with 250μl of filtered BioRad protein assay, mixed thoroughly and analyzed using a UV-spectrophotometer (DU-70, Beckman Instruments) at 595 nm . The absorbance of each sample was compared against a previously prepared calibration curve of to determine the protein content in the BALF.

5.3.8 Statistical analysis.

Data from these studies were analyzed for statistical significance using one-way analysis of variance (ANOVA). Comparisons of means were conducted using Dunnett's or Student-Newman-Keul's multiple range tests. Data with $p<0.05$ was deemed significant.

5.4. Results and Discussion.

5.4.1 Retention of FITC-labeled OLA-g-CS in the lungs after transnasal administration.

Conjugation of FITC to the water soluble OLA-g-CS co-oligomer with a 2.4 CS:LA molar ratio) was accomplished by linking the isothiocyanate group of FITC to the amine groups on the CS backbone through the thiourea bond.[23] The presence of FITC on the backbone was ascertained based on the aromatic proton (4H) peak between 6.42 and 6.7 ppm observed in the ^{1}H-NMR spectra. UV spectroscopy of the co-oligomer revealed a distinct peak at 495 nm, which can be attributed to the UV absorbance of FITC.

The lung retention of FITC-labeled OLA-g-CS after transnasal administration was assessed by quantifying the amount of co-oligomer in the lung homogenates as a function of time after instillation. The retention results are shown in Figure 5.1. Unexposed lung homogenates were used as baseline - to remove contributions from auto-fluorescence of the tissue.

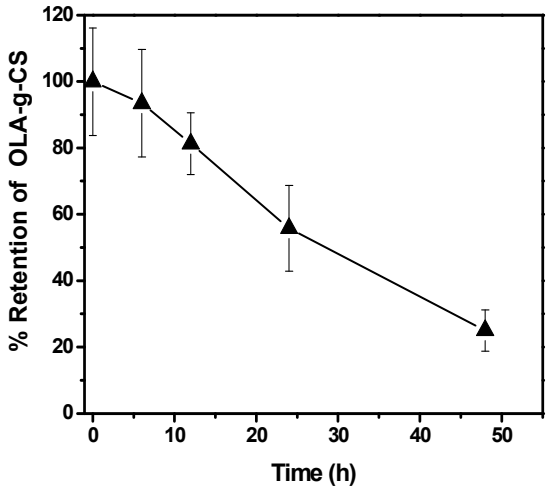

Figure 5.1. Retention of FITC-tagged OLA-g-CS in the lungs as a function of time after transnasal administration. OLA-g-CS was administered at 500 μg in 15 μl of saline. Unexposed lung homogenates were used as baseline. Results represent mean ± s.d, with n=4 mice per time point.

The results are shown relative to the amount delivered at zero time, which was determined to be 42.2% of the total dosage, a number consistent with that determined for Evan's blue in this study, and also consistent with results obtained for dendrimer-FITC conjugates delivered using the same methodology,[25] indicating the reliability of the approach chosen for this study.

From the results, as much as 42% of the OLA-g-CS co-oligomer that reaches the lungs is cleared by 24h, and only 22% is left by 48h. Assuming a linear trend in Figure 1, the results suggest a half-life for the co-oligomer in the lungs of 31.6h, and total clearance after 62h. A study conducted with generation 4 (G4) poly(amido amine) dendrimers with 18 times the MW of the co-oligomer investigated in this study

revealed that the clearance of those compounds from the peripheral regions of the lung to be as high as 14 days. In contrast, bare FITC, with MW of 390Da, is eliminated from the lungs within a few hours, with as little as 12% of the compound recovered from the peripheral part of the lung by 2h.[25]

Previous studies have shown that CS alone may reside in the airspace for extended time periods of time, in some cases for several days, owing to its mucoadhesiveness,[30, 31] which can be traced back to its cationic nature that help interact with hydrophilic biomacromolecules present in the lung tissue.[32] However, most of the experiments conducted *in vivo* on rodent models employed CS with MW greater than 30 KDa,[31, 33] whose aqueous solubility is very low in aqueous environments (at physiological pH). The relatively rapid clearance of the CS-g-LA co-oligomer from the airspace can be, therefore, attributed to a combination of low molar mass and enhanced aqueous solubility.

A size dependent clearance of intratracheally instilled hydrophilic molecules such as proteins has been reported in the literature, with larger protein molecules being cleared at a slower rates (days) compared to their smaller MW counterparts (peptides), which are cleared from the lung within a matter of hours.[3, 34, 35] For instance, albumin, a 66 KDa protein, is cleared from the lungs of various animal models at a rate of ca.1-2% per hour.[34] Along similar lines, rapid disappearance of hydrophilic molecules of ca.1000 Da has also been well documented in literature.[36] For instance, FITC-labeled calcein, a hydrophilic molecule with a MW of 623 Da, when administered intratracheally, cleared from the airspace of rat lungs within 3 hours.[35] Interestingly, OLA-g-CS, based on size alone, would be expected to be

cleared out from the very rapidly. However, we expect the co-oligomer to interact with compounds in the lung tissue to a larger extent than biomacromolecules (proteins and peptides), and thus possess longer residence times in the lungs.[3] Additionally, since not all the administered OLA-g-CS reaches the lung upon transnasal administration, there is a possibility that the co-oligomer trapped in the nasal cavity and the upper airways could translocate to the airspace during the course of the study, thereby contributing towards the detection of the excipient during the latter part of the study.

5.4.2 Estimation of Inflammatory Status of the Lungs upon Transnasal Administration of the OLA-g-CS Co-oligomer.

Single Acute Dose. The inflammatory status of the lungs was evaluated after single and repeated dose administration of OLA-g-CS using BAL and collagenase tissue dispersion analysis. The dosages of OLA-g-CS administered were 10μg (0.5mg/Kg body weight), 100μg (5.0mg/Kg body weight) and 500μg (25mg/Kg body weight) - the dosages were estimated based on average weight of the animals at ca.20g. BAL was used to investigate the cell population present in the airways and the lower respiratory tracts. This was done by sampling both the cellular and acellular components recovered from the bronchi and alveolar regions of the lungs.[37] Analysis of BALF was done for total and differential cell counts. Additionally, specific cell types (MAC, PMN, EOS, and LYM) that populate the airspace were identified by appropriate staining procedures, and counting of the cells was achieved using an optical microscope.[26] A summary of the percentage of cell

population recovered from BALF after transnasal administration is shown in Figure 5.2.

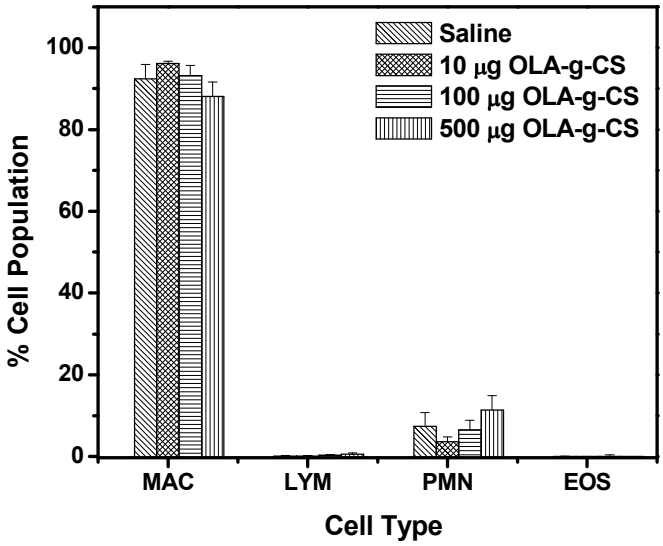

Figure 5.2. Percentage of individual cell population recovered from bronchoalveolar lavage fluid (BALF) of healthy mice 24h after transnasal administration of single acute doses of OLA-g-CS at different concentrations. Animals treated with sterile isotonic saline were used as control. Data shown as average ± s.d (n=6), for each condition. MAC = macrophages; LYM = lymphocytes; PMN= neutrophils; EOS = eosinophils.

The total cell count recovered from mice exposed to OLA-g-CS and control using BAL averaged $2.8\pm0.7\times10^5$ per lung, which are values similar to what has been reported in the literature upon administered of various excipients to the lungs of mice.[25, 29, 38] As much as 95% of the cells recovered were MAC, at 0.5 and 5.0mg per Kg dosages. These figures are within the stipulations prescribed by the

American Thoracic Society (ATS), which suggests that a lavage of a typical healthy lung is expected to comprise primarily of alveolar macrophages (95-99%).[39, 40]

A dose dependent increase in the PMN content was observed, as mice were exposed to 10, 100 and 500 μg of the co-oligomer. The cohort exposed to 500 μg of OLA-g-CS showed a neutrophil count of $0.42\pm0.17\times10^5$ cells, which corresponded to ca. 11.5±4.9% of the total cells recovered. This represents a percentage that is higher than what is recommended for a typical healthy lung. Interestingly, the data was not significant with respect to control, as mice exposed to saline had ca.7±3.2% of cells recovered as PMN. While this dosage elicited a slight increase in the PMN content, it was within the statistical purview when compared to control, and all other cell types were well within the recommendations of the ATS.

Mice exposed to a single dose of 10 and 100μg of the co-oligomer did not exert any noticeable increase in granulocyte counts, suggesting that the co-oligomer was benign within those dosages. Interestingly, BALF recovered from mice exposed to isotonic saline also contained neutrophils, however they were around the stipulated 3% recommendation.[37] These results indicate that the excipient, upon a single acute dose administration, induces no noticeable inflammatory response above and beyond that of the carrier up to a dosage of 100μg per 15μl carrier, or 5mg/Kg body weight of mice. To put these results in perspective we can extrapolate the dosages administered to mice in this study to that of a typical MDI formulation administered to humans. The concentration of OLA-g-CS required to stabilize aerosols of drug particles in typical concentrations found in commercial pMDI formulations is 2 mg OLA-g-CS per mL of the propellant. Upon actuation,

through a 50 μl metering valve, about 100 μg of the OLA-g-CS will be released out through the aerosol plume. Based on the assumption that the aerosol plume is orally inhaled by a healthy human of 75 Kg, the single puff dose delivered to the lungs would be 1.3μg per Kg body weight. Along similar lines, a 500μg dose of the excipient delivered to 20g mice (taking into account 40% dose delivery to the lung) would correspond to 30 mg/kg human, which corresponds to 3000 doses (administered simultaneously) to a healthy individual, thus further indicating the fact that the co-oligomer is highly benign at doses expected in typical formulations.

Repeated Administration. In order to understand the effect of excipient accumulation in the lung on the infiltration of inflammatory cell population, repeated administration of OLA-g-CS to mice was undertaken. A total of 6 administrations for each condition (saline, 10 and 100μg) were conducted, after which mice were sacrificed and subjected to lavage. Percentages of cells recovered from this study are shown in Figure 5.3(a). The 500μg dose was not implemented here owing to the fact that it represents an exceedingly high concentration when compared to typical formulations as detailed above, and it was shown to cause an inflammatory response at a single dose.

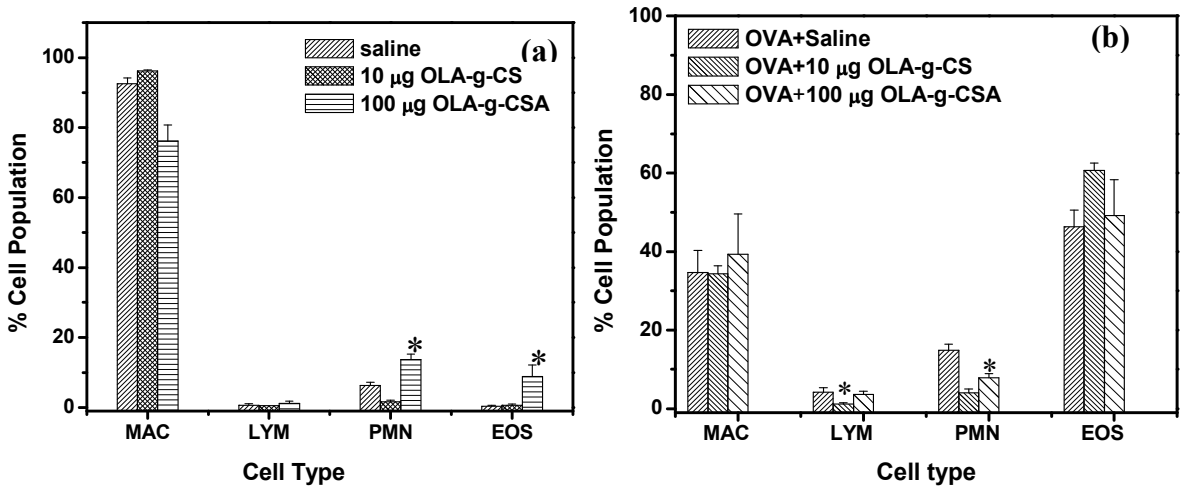

Figure 5.3. Percentage cell population of the total recovered from bronchoalveolar lavage fluid (BALF) of mice initially exposed to **(a)** saline aerosols, and **(b)** ovalbumin (OVA) aerosols, and subsequent intranasal administrations of six repeated doses of OLA-g-CS in sterile isotonic saline. Dosages administered of OLA-g-CS were 10μg and 100μg. Animals treated with sterile isotonic saline were used as controls. Data shown as average ± s.d (n=6), for each condition. MAC = macrophages; LYM = lymphocytes; PMN = neutrophils; EOS = eosinophils. * denotes statistically significant data compared to control ($p<0.05$).

The data from Figure 5.3(a) suggests an increase in inflammatory cell infiltration into the lung milieu with an increase in OLA-g-CS concentration. Total cells recovered from mice in this study were slightly higher than the single dose studies, with average cell counts estimated to be ca.$4.0\pm0.2\times10^5$ cells, with macrophages contributing to the majority of the cell count (>92%) for both saline and 10 μg OLA-g-CS. However, a reduction in the percentage of macrophages to

ca.76% was observed for the cohort administered repeatedly with 100μg per μL. At this dosage dosage, a significant increase in the presence of inflammatory cell population was detected with counts of both PMN and EOS being statistically significant ($p<0.05$) over and above the effect of the carrier, amounting to 14% and 9% of the total cell population. The enhanced recovery of the granulocytes at dosages beyond 10μg of the co-oligomer is indicative of the biological effect caused due to the accumulation of the excipient in the peripheral part of the lung at these elevated dosages. Such responses are expected as this represents a total accumulation of 1.65 g per Kg body weight.

It is instructive to compare and contrast the results obtained here with those reported in the literature with other polymers that have been tested for drug delivery applications to the lungs. CS in the form of particles has been tested extensively for pulmonary toxicity after intratracheal administration in rodents.[41-44] Inflammatory responses to CS have been shown to be size and charge dependency.[44] Medium MW CS microspheres when insufflated to rats at concentrations of 4 and 10mg per Kg were shown to induce severe inflammation in the animals as evidenced by protein analysis and BAL (high PMN recruitment).[41] The toxicity in this case, was attributed to the MW of CS and the high surface charge of the particles (+45 mV), which could lead to their binding with lung tissue enabling them to persist in the airspace for an extended times – note such a MW of CS is not soluble in water at physiological pH.[41] A similar observation was reported in another study involving high MW CS (100-500 KDa) administered to rats, where acute structural damage and high PMN infiltration was reported as evidenced by histopathological evaluation.[33]

The effect of the cationic character of biocompatible polymers on pulmonary inflammation has been documented in an another study, where repeated administration of 0.15mg of PLA-polyethylene glycol (PLA-PEG) NPs modified with stearylamine (a cationic compound) to mice endotracheally resulted in severe pulmonary toxicity, as evidenced by BAL experiments, with high recruitment of eosinophils and lymphocytes.[45] Interestingly, the same study reported that unmodified PLA-PEG NPs (no cationic grafts) had no effect on lung status after 5 days of exposure. While medium and high MW CS have been shown to induce pulmonary inflammation, studies conducted using short chained chitosan oligomer (10-18 monomer units) did not induce any noticeable inflammatory response in mice upon intratracheal instillation as evidenced by BAL and histology studies.[46] Those studies were conducted at dosages of 0.6μg per μg DNA delivered.

5.4.3 Effect of OLA-g-CS on allergen induced lung inflammation.

Sensitization and aerosol challenge of mice with OVA results in airway eosinophilia and pulmonary damage analogous to those observed in asthma, causing a heavy recruitment of inflammatory cells (EOS in particular) within the airspace.[47] The rationale behind this portion of our study was to determine whether the co-oligomer interferes with the ability of the lung to deal with an allergen induced immune response in either a positive or negative way. This information was necessary for later studies with the co-oligomer and a therapeutic molecule, where such effects should not be confounded. Figure 5.3(b) is a summary of the percent of individual cell populations extracted from the BALF of animals exposed to OVA, and

treated repeatedly with the co-oligomers at dosages of 10 and 100μg per 15 μL, as detailed in *Methods*.

While the average cell numbers recovered from mice exposed to saline aerosols was quantified to be $3.0\pm0.2\times10^5$ (mean ± s.d) for all conditions tested, the total cell recovery from OVA exposed mice increased to $11\pm2.5\times10^5$. Cell recovery for the studies with OVA+10μg co-oligomer was $9\pm0.9\times10^5$, and that for OVA+100μg co-oligomer $12.1\pm2\times10^5$. In addition to a change in cell recovery, significant changes in the individual inflammatory cell count were also observed upon OVA administration, as expected. While the cell counts of MAC increased, their presence in the total cells recovered diminished to as low as ca.34% (under all conditions tested) for cohorts exposed to OVA, representing a dramatic reduction when compared to mice exposed to saline only. This also greatly contrasts with a much higher MAC recovery observed after repeated administration of the the co-oligomer alone, where the lowest MAC recovery in that case (for 100μg OLA-g-CS) was still at 76%. These results are similar to what has been previously reported in the literature for OVA exposed mice.[26, 28]

The average percent of EOS in the BALF of OVA-exposed mice was 52±7%, which is also in agreement to literature values.[28] It was observed, however, that the EOS count does not change significantly among the cohorts treated with OVA alone and those with OVA along with various doses of OLA-g-CS, indicating that the administration of the co-oligomer did not interfere with the EOS infiltration into airspace arising from OVA exposures, which is a very important observation, as it may suggest that this excipient could be potentially used to deliver asthma related

therapeutics. Mice exposed to OVA and treated with CS nanoparticles for 24 days, were also shown to have an increase in EOS count as evidenced by BAL analysis.[42] In this study, the MAC count upon OVA exposure remained fairly similar in all the conditions tested. Interestingly, while the BAL data indicated that infiltration of EOS into the airspace was not affected for all excipient dosages investigated, a statistically significant reduction in the PMN was observed for cohorts treated with OLA-g-CS when compared to that of those treated with saline only after OVA exposure. The reduction in these numbers indicates that the excipient could be suppressing MAC associated recruitment of PMN, but not EOS. However, categorical establishment of this hypothesis would require further, more elaborate studies. Another interesting observation from this study is the reduction in the LYM numbers for cohorts administered with 10μg OLA-g-CS when compared to contents recovered from control mice. However, this observation was not extended to the cohorts receiving 100μg OLA-g-CS; the percentage of LYM recovered in that case was similar to what was observed for control mice.

In addition to BAL, inflammatory cell populations isolated from collagenase tissue dispersions of mice lungs exposed to OVA (allergen induced / inflamed lungs) and administered with repeated doses of OLA-g-CS were counted and compared to those from animals exposed to saline aerosols and the co-oligomers. These results are complementary to the BALF studies, and provide a more detailed picture of the inflammatory status of the lungs, and any changes in inflammatory status upon further exposure to the co-oligomer (beyond that induced by OVA) .[26, 28, 48] This approach is important as it helps us correlate the time course of inflammatory events

with airway reactivity, and other relevant provocative occurrences in the lung.[28, 48] For instance, studying inflammatory cells recovered from BALF combned with cell contents from marginated tissue and interstitial compartments can provide a platform for the correlation with airway responses to methacholine challenge. This data could provide us with a better perspective on the inflammatory status of the lung.[26, 28, 48]

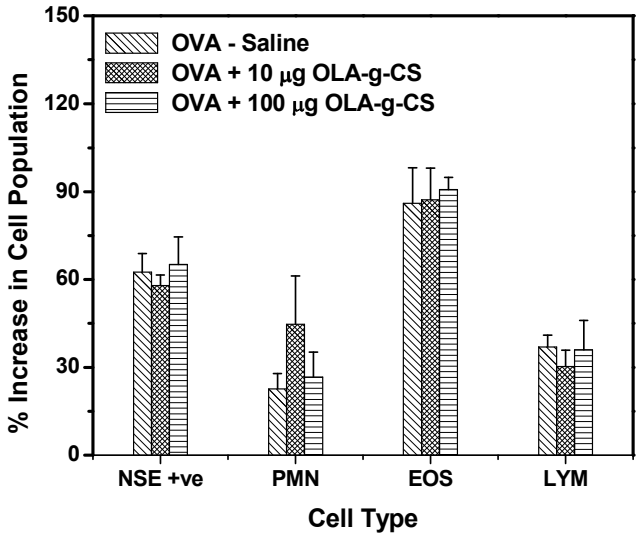

Figure 5.4. Percent increase in cell population recovered from collagenase tissue dispersion of lungs administered with repeated doses of OLA-g-CS at 10 and 100μg following exposures to OVA aerosol. Data was obtained by comparing the individual cell counts to those of cohorts exposed to saline aerosol followed by repeated dosing of OLA-g-CS. Data shown as average ± s.d (n=6), for each condition. NSE +ve = non-specific esterase positive; LYM = lymphocytes; PMN = neutrophils; EOS = eosinophils.

Consistent with previous trends, cell populations isolated from tissue dispersion after mice exposed to OVA aerosols were significantly higher compared to those isolated from mice exposed to saline aerosols.[25, 26, 28] Among the individual cell populations, the greatest increase was in the EOS count, which amounted to a 90% increase when compared to that of mice exposed to saline aerosols only. This dramatic increase in the eosinophils from OVA-exposed mice agrees well with previous report in the literature.[28, 48] The impact of OVA exposure can also be attributed to the increase in NSE +ve cells whose increase was 60% greater than that of NSE +ve cells recovered from saline exposed aerosols. It is also worth noting that, for the mice exposed to OVA, the extent of increase in cell counts, particularly for EOS and LYM, were similar for all conditions tested viz., saline, 10 and 100μg per μL, reaffirming the fact that the presence of co-oligomer in the lungs does not seem to interfere with the allergen induced response.

Overall, from our set of experiments comprisied of BALF and tissue dispersion analyses we conclude that the inflammatory potential of OLA-g-CS on mice lung is dose dependent, with dosages as high as 100μg (5mg per Kg body weight) being tolerable to mice upon single acute exposure. Repeated exposures of OLA-g-CS resulted in increasing lung inflammation for mice administered (after 6 exposures) over with 100μg OLA-g-CS, while10 μg (0.5mg per Kg body weight) was found not to cause any inflammatory response above and beyond that of the saline control. It can be also concluded that, within the dosage ranges studied, the excipient did not interfere with the allergen-induced immune responses in OVA exposed mice.

5.4.4 Integrity of Pulmonary Epithelium.

The membrane integrity of the pulmonary epithelium is the most important barrier to the systemic circulation. It controls and regulates the transport of different species across the air-blood barrier, and thus the permeability of the epithelium.[49] Infections in the lower respiratory tract can lead to an influx of protein rich fluids into the airspace due to increased epithelial cell permeability.[50] This influx of proteins can also be accompanied by an enhanced recruitment of PMN into the airspace.[51] This protein increase was quantitatively assessed from the BALF using a protein assay procedure as detailed in the methods section. The results are summarized in Figure 5.5.

In Figure 5.5(a) we report the total protein content of the BALF after single acute intranasal exposure of the co-oligomer. The results indicate no significant exudation of serum protein into the airspaces compared to saline controls after a single acute exposure of the co-oligomer. In Figure 5.5(b) we report the protein concentration following repeated doses of the co-oligomer. We can observe that while mice exposed to repeated doses of OLA-g-CS at 10μg did not develop any significant damage to the epithelium when compared to saline control cohorts repeatedly exposed to 100 μg of OLA-g-CS had an increase in flux of protein into the airspaces. These results corroborate our earlier observations that show that mice repeatedly exposed to 100μg of OLA-g-CS, developed an increased recruitment of PMN - Figure 5.5(a). These results, in conjunction with BAL and tissue dispersion analyses further confirm the dose dependent inflammatory effect exerted by OLA-g-CS in the airspace.

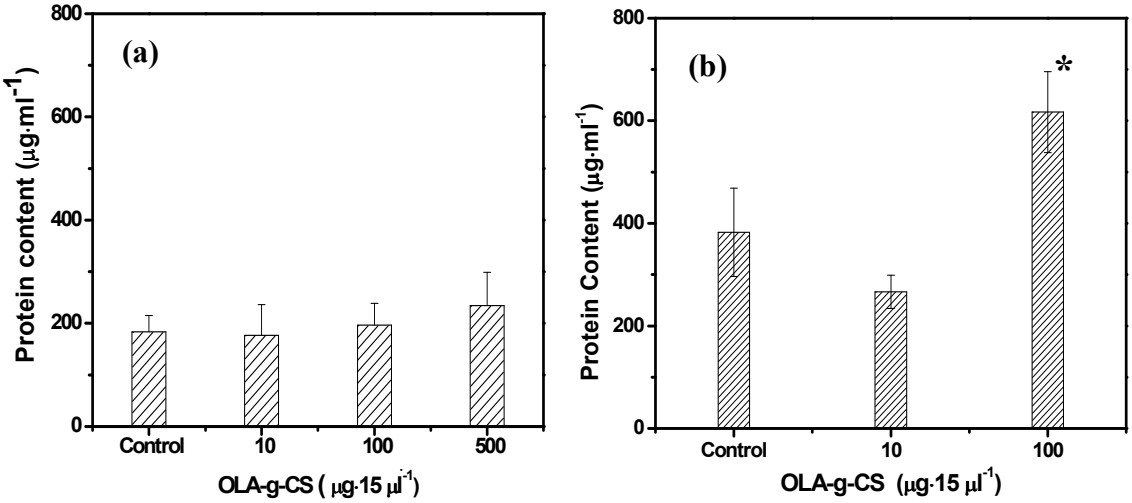

Figure 5.5. Total protein content recovered from BALF of mice exposed to a **(a)** single acute dose of OLA-g-CS; **(b)** repeated administration of OLA-g-CS. Protein content is plotted as a function of OLA-g-CS concentration. Data shown as mean ± s.d n=6, for each condition. * denotes statistical significance ($p<0.05$)

While, mice exposed to repeated doses of OLA-g-CS at 10 μg concentrations did not develop any significant damage to the epithelium compared to saline controls, cohorts repeatedly exposed to 100 μg of OLA-g-CS had an extensive in flux of protein into the airspace as shown in the plot. Furthermore, BAL studies conducted on mice exposed to 100 μg of OLA-g-CS resulted in an increased recruitment of neutrophils to lungs as evidenced by cell recovery plots shown in Figure 5.4 corroborating earlier observation.[48] These results, in conjunction with BAL and tissue dispersion analyses, further confirm the dose dependent inflammatory effect exerted by OLA-g-CS in the airspace.

5.4.5 Retention of PLGA NPs in the lungs after transnasal administration with the co-oligomer.

Retention of the FA-labeled PLGA NPs in the lungs as a function of time after transnasal administration is shown in Figure 5.6. Conjugation of FA to the carboxyl end of PLGA was determined by the presence of the aromatic proton peak between 6.5 and 7 ppm in the ^{1}H-NMR spectrum.[24] NPs with the FA-PLGA were formed by emulsification solvent evaporation, and had an average diameter of 260nm, and a polydispersity of 0.2, as determined by DLS (90Plus, Brookhaven Instruments). The ζ potential of the NPs was determined to be -12.3±1.2 mV. The particles were smooth spheres as evidenced by the SEM micrograph shown as inset in Figure 6. The sizes from were also estimated from SEM suing ImageJ (v1.4, NIH), and the values were in good agreement with the DLS (240nm).

The NPs were administered at a concentration of 10μg in 15 μl of saline, with 100μg of the OLA-g-CS co-oligomer. This concentration was selected as it represents the mass ratio of the NP formulation in the propellant-based inhalers that we have recently reported,[19] where we have shown that the formulation possesses aerosol characteristics conducive to deep lung deposition of the NPs.

It can be observed that a large percentage (ca. 60%) of the NPs was flushed out from the airspace within the first two hours. This was followed by a period where the removal of NPs from the lung was relatively slow, with only about 5% of the NPs eliminated within the next 10 hours. By 24h, almost 90% of administered NPs were eliminated from the airspace, and by 48h, as little as 5% of the administered NPs remained in the lung. To put these results in perspective, a comparison of

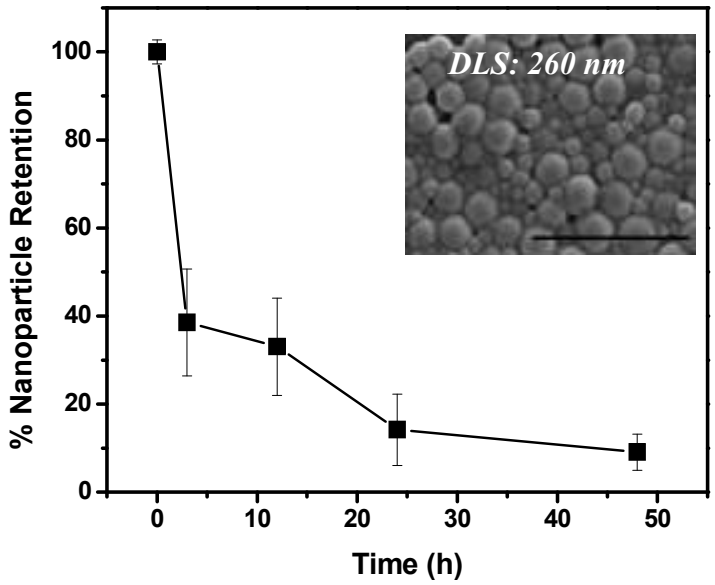

Figure 5.6. Retention of FA-labeled PLGA NPs in the lungs as a function of time after transnasal administration. NPs administered at 100μg in 15 μl of saline, with 100μg of the OLA-g-CS co-oligomer. Unexposed lung homogenates were used as baseline. Results represent average ± s.d, with n=4 mice per time point. *Inset:* electron micrograph of the FA-PLGA NPs prepared with the emulsion solvent evaporation technique. Bar denotes 1 μm.

elimination rates of various polymeric NPs from the lungs was made. The rapid elimination of PLGA NPs upon pulmonary administration has been also reported in earlier studies by others.[31, 52] The majority of the PLGA NPs administered intratracheally to guinea pigs was shown to be eliminated within the first hour of administration. In the latter study, over 75% of the administered dose was cleared from the lungs by 2h and corroborate the observations made in our study.[31] However, in the same study, authors reported that CS coated PLGA NPs persisted

longer within the lung owing to the mucoadhesive nature of CS coating the NPs. It is worth mentioning that the profile observed in our study (and those in the literature as well), may potentially include NPs that are initially trapped in the upper region of the airways and the nasal cavity following administration, and that may later descend to the airspace.

The residence time of NPs in the airways has also been shown to be a strong function of the particle chemistry. In general, polystyrene (PS) NPs have been shown to persist in the airspace for extended durations, owing to their non-biodegradable, and hydrophobic nature.[53] PS NPs (100 nm in size) pharyngeally aspirated to rats, were reported to linger in the lungs for extended periods of time, having half-lives as high as 44 days.[54] In another independent study, PS NPs of size 220 nm modified with polyacrylate were administered intratracheally to rats. Elimination of these NPs from the lungs was found to be very sluggish, with <0.02% of NPs observed in lymph nodes 1h after administration.[55]

5.4.6. Inflammatory response of the lungs upon transnasal administration of PLGA NPs combined with the OLA-g-CS co-oligomer.

We have demonstrated that we can successfully encapsulate PLGA NP within a shell of OLA-g-CS, and shown that such structures can be stably dispersed in pMDIs and produce aerosols that enhance the deposition of NPs in the deep lungs.[19] *In vitro* toxicity studies indicated that these core-shell structures were non-toxic to pulmonary epithelial cell lines (A549 and Calu-3) within the concentration ranges tested. Here, we extend the study to evaluate the inflammatory status of the

lungs upon *in vivo* administration of PLGA NP mixed with the OLA-g-CS co-oligomer that form the shell discussed in the study above.

PLGA NPs formed as described above were gently dispersed in a 100 μg OLA-g-CS solution at concentrations of 10μg and 30 per 15μl, and administered transnasally to mice. The dosages were chosen in order to mimic the typical composition of a core-shell formulation administered using a pMDI. As a comparison, bare NP (without OLA-g-CS in sterile saline) dispersions of the same dosages were prepared and their response in mice were evaluated as well. The data reported here are the analysis inflammatory response from mice subjected to BALF 24h after instillation of the core-shell formulation – PLGA NP and co-oligomer. Individual cell counts recovered from mice are given in Table 5.1, and the results are recast in Figure 7 as percentages to better highlight the composition of each cell type after administration of individual formulations.

Total cell population recovered from mice instilled with various formulations varied greatly with respect to the formulation. While mice instilled with OLA-g-CS had an average recovery of ca.4×10^5 cells from BALF (n=4), cells isolated from mice treated with NPs only and those instilled with the NPs and the co-oligomer averaged ca.2.5×10^5 cells, with mice administered with 30μg NPs having the fewest cells recovered. Data obtained here are similar to an earlier study by others, where lavage of mice administered with PLGA NPs at concentrations of 1 and 2.5μg per μl carrier resulted in cell recoveries of ca.2.5×10^5 cells per cohort.[38] Except for the formulation comprising of 30μg PLGA NPs in combination with OLA-g-CS, MAC count recovered from all other systems exceeded 90%. For the formulation

comprising of 10μg NP in combination with the co-oligomer, no appreciable inflammatory response was detected. This is important as this concentration range is the typical composition of the core-shell particles describe earlier; the loading deduced from our previous studies confirm 10% loading of NPs within the OLA-g-CS shell.[19]

Table 5.1. Individual count of inflammatory cells population recovered from the bronchoalveolar lavage of mice after intranasal administration of nanoparticles and/or the OLA-g-CS co-oligomer. Results represent mean ± s.d, with n=4 for each condition.

Dosage ($\mu g \cdot 15\ \mu l^{-1}$)	Macrophages ($\times 10^3$)	Lymphocytes ($\times 10^3$)	Neutrophils ($\times 10^3$)	Eosinophils ($\times 10^3$)
0 (Saline)	279.6±49.6	30.2±16.4	6.1±2.4	0
100 OLA-g-CS	410.7±54.1	31.6±12.5	27.5±11	0.6±0.02
10 PLGA NPs	341.4±80.5	34.1±1.4	14.9±1.3	0
30 PLGA NPs	181.1±17	25.1±1.13	15±3.3	0.7±0.1
100 OLA-g-CS + 10 PLGA NPs	251.3±78.9	21±10.2	16.8±4.6	1.23±0.12
100 OLA-g-CS + 30 PLGA NPs	243.2±52.4	0	132.7±58*	14.1±4.7*

Data represents mean±s.d. (n=4)

Cells were recovered from treated mice by bronchoalveolar lavage. Data shown here represents average cell population recovered from lungs of 4 animals per condition.

* represents statistically significant data compared to control (saline)

Interestingly, the results obtained for the bare NPs and the NPs along with the co-oligomer compare well with other biodegradable polymeric NPs that have been

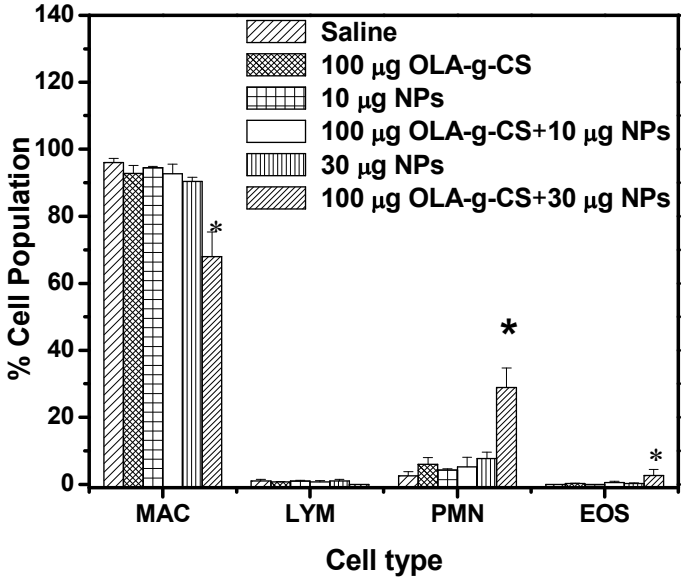

Figure 5.7. Percentage of individual cell population recovered from bronchoalveolar lavage fluid (BALF) of healthy mice treated with single acute doses of the NP and co-oligomer. OLA-g-CS concentration was maintained at 100 μg of per 15 μl, while the NP concentration was set to either 10 or 30 μg per 15 μl of carrier. Data shown as mean ± s.d (n=4), for each condition. MAC = macrophages; LYM = lymphocytes; PMN = neutrophils; EOS = eosinophils. *- indicates statistically significant data when compared to carrier.

tested for potential inflammation in lungs. For instance, PLGA NPs (ca.100 nm) and another variant of PLGA, DEAPA-PVAL-g-PLGA NPs (ca. 200 nm) administered to mice at a concentration of 1μg and 2.5μg per μl carrier did not induce any pronounced adverse effect in the lungs 24h after intratracheal instillation.[38] Within the same observation times as this study, in another study, polystyrene NPs of

220nm in size had a substantial toxic effect on the lungs, with PMN recruitment as high as 80%. In another study, anionic PLA-PEG NPs administered to Balb/c mice at dosages of 0.15mg per 25μl carrier via endotracheal instillation, did not induce any appreciable inflammation compared to their cationic counterparts.[45] Along similar lines, repeated administration of solid lipid NPs (100 nm, -15 mV) for 16 days did not induce any notable inflammation as evidenced by absence of PMN and lack of increase in protein content in the BALF.[29]

The formulation of 30μg PLGA NPs in the presence of 100μg OLA-g-CS caused a reduced percentage of MAC (68%), and infiltration of inflammatory cell populations evidenced by increased PMN content to as high as 29%. The percentage of EOS recovered from mice receiving this formulation was as high as 3%. However, NPs administered at the same dosages in the absence of OLA-g-CS, did not induce an inflammatory response, and their cell counts were similar to saline control. It is interesting to observe that only at the highest dose of NPs in combination with the excipient was a statistically significant spurt in the PMN and EOS ($p<0.05$) is observed. One potential explanation to this effect may be a lower physical stability of the NPs in a physiological environment when at higher concentrations, when aggregates would behave differently compared to free/unaggregated NPs. It is worth mentioning, however, that DLS results show that aggregation does not happen *in vitro* (buffer with NPs).

5.5. Conclusions.

In this work we evaluated the lung inflammatory potential of a versatile, water-soluble, biodegradable co-oligomeric excipient for pMDIs, namely OLA-g-CS through an extensive set of *in vivo* experiments encompassing BAL, collagenase tissue dispersion analysis and serum protein evaluation. Retention studies of the co-oligomer revealed that ca. 80% of the OLA-g-CS co-oligomer was removed from the lungs within 48h. Results from the inflammatory response suggest a dose dependent increase in the response upon intranasal administration of a single acute dose of OLA-g-CS, with the co-oligomer eliciting an inflammatory response only at very high dosages - greater than 5 mg/Kg body weight. However, repeated administration of OLA-g-CS to mice resulted in adverse infiltration of granulocytes into the lung milieu at lower dosages (>0.5 mg/Kg body weight) possibly due to the enhanced accumulation of the excipient in the peripheral part of the lung. This concentration is still exceedingly high compared to typical dosages from pMDI formulations – this would be equivalent of 1400 puffs per day, for a total of 6400 puffs within 6 days. BAL and collagenase tissue dispersion analysis conducted on mice exposed to OVA demonstrated that the co-oligomer does not interfere with the ability of the lung to deal with an allergen as showcased by the increase in eosinophil content in the lungs of mice upon exposure to OVA. PLGA NPs administered along with the OLA-g-CS co-oligomer at concentrations similar to that utilized in the preparation of core-shell formulations for pMDIs did not elicit a significant immune response as indicated by BAL results. It is also observed that the NPs are rapidly flushed from the airways - > 90% within the first 24h. These results taken together suggest that the co-oligomeric

excipient has great potential to be employed safely not only in the treatment of acute conditions of the lungs, but also for patients with chronic lung diseases, and for the controlled and targeted delivery to and through the lungs, potentially with the help of biodegradable polymeric NPs formulations.

Note – *This work was done with the assistance of Dr. David J P Bassett, Professor of Occupational and Environmental Health and Mr. Xiufeng Gao.*

5.6 References.

[1] M.M. Bailey, C.J. Berkland, Nanoparticle formulations in pulmonary drug delivery, Med Res Rev, 29 (2009) 196-212.

[2] W. Berger, Aerosol devices and asthma therapy, Curr Drug Deliv, 6 (2009) 38-49.

[3] J.S. Patton, P.R. Byron, Inhaling medicines: delivering drugs to the body through lungs, Nat Rev Drug Discov, 6 (2007) 67-74.

[4] G. Pilcer, K. Amighi, Formulation strategy and use of excipients in pulmonary drug delivery, Int J Pharm, 392 (2010) 1-19.

[5] P. Rogueda, Novel hydrofluoroalkane suspension formulations for respiratory drug delivery, Expert Opinion in Drug Delivery, 2 (2005) 625-638.

[6] N. Islam, E. Gladki, Dry powder inhalers (DPIs)--a review of device reliability and innovation, Int J Pharm, 360 (2008) 1-11.

[7] R.U. Agu, In vitro and in vivo testing methods for respiratory drug delivery, Expert Opin Drug Deliv, 8 (2011) 57-69.

[8] B. Laube, The Expanding Role of Aerosols in Systemic Drug Delivery, Gene Therapy, and Vaccination, Respir Care, 50 (2005) 1161-1176.

[9] H. Chrystyn, D. Price, Not all asthma inhalers are the same: factors to consider when prescribing an inhaler, Prim Care Respir J, 18 (2009) 243-249.

[10] D.S. Conti, J. Grashik, L. Yang, L. Wu, S.R.P. da Rocha, Solvation in hydrofluoroalkanes: how can ethanol help?, J Pharm Pharmacol, (2012).

[11] H.D.C. Smyth, Propellant-driven metered-dose inhalers for pulmonary drug delivery, Expert Opinion in Drug Delivery, 2 (2005) 53-74.

[12] J. Bell, S. Newman, The rejuvenated pressurized metered dose inhaler, Expert Opin Drug Deliv, 4 (2007) 215-234.

[13] L. Wu, S.R.P. da Rocha, Nanoparticle-Stabilized Colloids in Compressible Hydrofluoroalkanes, Langmuir, 27 (2011) 10501–10506.

[14] D. Lechuga-Ballesteros, B. Noga, R. Vehring, R.H. Cummings, S.K. Dwivedi, Novel cosuspension metered-dose inhalers for the combination therapy of chronic obstructive pulmonary disease and asthma, Future Med Chem, 3 (2011) 1703-1718.

[15] L. Wu, B. Bharatwaj, J. Panyam, S.R.P. da Rocha, Core–shell Particles for the Dispersion of Small Polar Drugs and Biomolecules in Hydrofluoroalkane Propellants, Pharm Res, 25 (2008) 289-301.

[16] L.A. Dellamary, T.E. Tarara, D.J. Smith, C.H. Woelk, A. Adractas, M.L. Costello, H. Gill, J.G. Weers, Hollow porous particles in metered dose inhalers, Pharm Res, 17 (2000) 168-174.

[17] R.P.S. Peguin, L. Wu, S.R.P. da Rocha, The ester group: How Hydrofluoroalkane-philic is it?, Langmuir, 23 (2007) 8291-8294.

[18] L. Wu, S.R.P. da Rocha, Applications of Atomic Force Microscope in the Development of Propellant-based Inhalation Formulations, KONA Powder and Particle Journal, 26 (2008) 106-128.

[19] B. Bharatwaj, L. Wu, J.A. Whittum-Hudson, S.R. da Rocha, The potential for the noninvasive delivery of polymeric nanocarriers using propellant-based inhalers in the treatment of Chlamydial respiratory infections, Biomaterials, 31 (2010) 7376-7385.

[20] D.S. Conti, B. Bharatwaj, D. Brewer, S.R. da Rocha, Propellant-based inhalers for the non-invasive delivery of genes via oral inhalation, J Control Release, 157 (2012) 406-417.

[21] S. Azarmi, W.H. Roa, R. Lobenberg, Targeted delivery of nanoparticles for the treatment of lung diseases, Adv Drug Deliv Rev, 60 (2008) 863-875.

[22] M. Smola, T. Vandamme, A. Sokolowski, Nanocarriers as pulmonary drug delivery systems to treat and to diagnose respiratory and non respiratory diseases, Int J Nanomedicine, 3 (2008) 1-19.

[23] M. Huang, E. Khor, L.Y. Lim, Uptake and cytotoxicity of chitosan molecules and nanoparticles: effects of molecular weight and degree of deacetylation, Pharm Res, 21 (2004) 344-353.

[24] P. Xu, E. Gullotti, L. Tong, C.B. Highley, D.R. Errabelli, T. Hasan, J.X. Cheng, D.S. Kohane, Y. Yeo, Intracellular drug delivery by poly(lactic-co-glycolic acid) nanoparticles, revisited, Mol Pharm, 6 (2009) 190-201.

[25] R. Inapagolla, B.R. Guru, Y.E. Kurtoglu, X. Gao, M. Lieh-Lai, D.J. Bassett, R.M. Kannan, In vivo efficacy of dendrimer-methylprednisolone conjugate formulation for the treatment of lung inflammation, Int J Pharm, 399 (2010) 140-147.

[26] M.P. DeLorme, H. Yang, C. Elbon-Copp, X. Gao, H. Barraclough-Mitchell, D.J.P. Bassett, Hyperresponsive airways correlate with lung tissue inflammatory cell changes in ozone-exposed rats, J. Toxicol. Environ. Health. A, 65 (2002) 1453-1470.

[27] A.H. Schultheis, D.J. Bassett, A.D. Fryer, Ozone-induced airway hyperresponsiveness and loss of neuronal M2 muscarinic receptor function, Journal of Applied Physiology, 76 (1994) 1088-1097.

[28] D. Bassett, F. Hirata, X. Gao, R. Kannan, J. Kerr, N. Doyon-Reale, S. Wilson, M. Lieh-Lai, Reversal of methylprednisolone effects in allergen-exposed female BALB/c mice, J Toxicol Environ Health A, 73 (2010) 711-724.

[29] M. Nassimi, C. Schleh, H.D. Lauenstein, R. Hussein, H.G. Hoymann, W. Koch, G. Pohlmann, N. Krug, K. Sewald, S. Rittinghausen, A. Braun, C. Muller-Goymann, A toxicological evaluation of inhaled solid lipid nanoparticles used as a potential drug delivery system for the lung, Eur J Pharm Biopharm, 75 (2010) 107-116.

[30] J.C. Sung, B.L. Pulliam, D.A. Edwards, Nanoparticles for drug delivery to the lungs, Trends Biotechnol, 25 (2007) 563-570.

[31] H. Yamamoto, Y. Kuno, S. Sugimoto, H. Takeuchi, Y. Kawashima, Surface-modified PLGA nanosphere with chitosan improved pulmonary delivery of calcitonin by mucoadhesion and opening of the intercellular tight junctions, J Control Release, 102 (2005) 373-381.

[32] M. Amidi, E. Mastrobattista, W. Jiskoot, W.E. Hennink, Chitosan-based delivery systems for protein therapeutics and antigens, Adv Drug Deliv Rev, 62 (2010) 59-82.

[33] B.I. Florea, M. Thanou, H.E. Junginger, G. Borchard, Enhancement of bronchial octreotide absorption by chitosan and N-trimethyl chitosan shows linear in vitro/in vivo correlation, J Control Release, 110 (2006) 353-361.

[34] K.J. Kim, A.B. Malik, Protein transport across the lung epithelial barrier, Am J Physiol Lung Cell Mol Physiol, 284 (2003) L247-259.

[35] C. Lombry, C. Bosquillon, V. Preat, R. Vanbever, Confocal imaging of rat lungs following intratracheal delivery of dry powders or solutions of fluorescent probes, J Control Release, 83 (2002) 331-341.

[36] M. Sakagami, In vivo, in vitro and ex vivo models to assess pulmonary absorption and disposition of inhaled therapeutics for systemic delivery, Adv Drug Deliv Rev, 58 (2006) 1030-1060.

[37] R.A. Goldstein, P.K. Rohatgi, E.H. Bergofsky, E.R. Block, R.P. Daniele, D.R. Dantzker, G.S. Davis, G.W. Hunninghake, T.E. King, Jr., W.J. Metzger, et al., Clinical role of bronchoalveolar lavage in adults with pulmonary disease, Am Rev Respir Dis, 142 (1990) 481-486.

[38] L.A. Dailey, N. Jekel, L. Fink, T. Gessler, T. Schmehl, M. Wittmar, T. Kissel, W. Seeger, Investigation of the proinflammatory potential of biodegradable nanoparticle drug delivery systems in the lung, Toxicol Appl Pharmacol, 215 (2006) 100-108.

[39] H. Klech, W. Pohl, Technical recommendations and guidelines for bronchoalveolar lavage (BAL): report of the European Society of Pneumology Task Group on BAL., Eur Resp. J, 2 (1989) 561-585.

[40] O. Kowal-Bielecka, K. Kowal, K.B. Highland, R.M. Silver, Bronchoalveolar Lavage Fluid in Scleroderma Interstitial Lung Disease: Technical Aspects and Clinical Correlations: Review of the Literature, Semin Arthritis Rheum, (2009).

[41] Y.C. Huang, A. Vieira, K.L. Huang, M.K. Yeh, C.H. Chiang, Pulmonary inflammation caused by chitosan microparticles, J Biomed Mater Res A, 75 (2005) 283-287.

[42] M. Kumar, X. Kong, A.K. Behera, G.R. Hellermann, R.F. Lockey, S.S. Mohapatra, Chitosan IFN-gamma-pDNA Nanoparticle (CIN) Therapy for Allergic Asthma, Genet Vaccines Ther, 1 (2003) 3.

[43] A. Grenha, S. Al-Qadi, B. Seijo, C. Remunan-Lopez, The potential of chitosan for pulmonary drug delivery, J Drug Deliv Sci Tec, 20 (2010) 33-43.

[44] B. Sarmento, J. das Neves, A.S. Halim, L.C. Keong, I. Zainol, A.H.A. Rashid, Biocompatibility and Biodegradation of Chitosan and Derivatives, in: B. Sarmento, J. das Neves (Eds.) Chitosan-Based Systems for Biopharmaceuticals: Delivery, Targeting and Polymer Therapeutics, John Wiley & Sons, Chichester, UK, 2012.

[45] O. Harush-Frenkel, M. Bivas-Benita, T. Nassar, C. Springer, Y. Sherman, A. Avital, Y. Altschuler, J. Borlak, S. Benita, A safety and tolerability study of differently-charged nanoparticles for local pulmonary drug delivery, Toxicol Appl Pharmacol, 246 (2010) 83-90.

[46] M. Koping-Hoggard, K.M. Varum, M. Issa, S. Danielsen, B.E. Christensen, B.T. Stokke, P. Artursson, Improved chitosan-mediated gene delivery based on easily dissociated chitosan polyplexes of highly defined chitosan oligomers, Gene Ther, 11 (2004) 1441-1452.

[47] G.R. Zosky, A.N. Larcombe, O.J. White, J.T. Burchell, T.Z. Janosi, Z. Hantos, P.G. Holt, P.D. Sly, D.J. Turner, Ovalbumin-sensitized mice are good models for airway hyperresponsiveness but not acute physiological responses to allergen inhalation, Clin Exp Allergy, 38 (2008) 829-838.

[48] M.A. Birrell, C.H. Battram, P. Woodman, K. McCluskie, M.G. Belvisi, Dissociation by steroids of eosinophilic inflammation from airway hyperresponsiveness in murine airways, Respir Res, 4 (2003) 3.

[49] R. Lucas, A.D. Verin, S.M. Black, J.D. Catravas, Regulators of endothelial and epithelial barrier integrity and function in acute lung injury, Biochem Pharmacol, 77 (2009) 1763-1772.

[50] J.P. Mizgerd, Acute lower respiratory tract infection, N Engl J Med, 358 (2008) 716-727.

[51] S.P. Kantrow, Z. Shen, T. Jagneaux, P. Zhang, S. Nelson, Neutrophil-mediated lung permeability and host defense proteins, Am J Physiol Lung Cell Mol Physiol, 297 (2009) L738-745.

[52] F. Alexis, E. Pridgen, L.K. Molnar, O.C. Farokhzad, Factors affecting the clearance and biodistribution of polymeric nanoparticles, Mol Pharm, 5 (2008) 505-515.

[53] J. Todoroff, R. Vanbever, Fate of nanomedicines in lungs, Curr Opin Coll Int Sci, 16 (2011) 246-254.

[54] K. Sarlo, K.L. Blackburn, E.D. Clark, J. Grothaus, J. Chaney, S. Neu, J. Flood, D. Abbott, C. Bohne, K. Casey, C. Fryer, M. Kuhn, Tissue distribution of 20 nm, 100 nm and 1000 nm fluorescent polystyrene latex nanospheres following acute systemic or acute and repeat airway exposure in the rat, Toxicology, 263 (2009) 117-126.

[55] H.S. Choi, Y. Ashitate, J.H. Lee, S.H. Kim, A. Matsui, N. Insin, M.G. Bawendi, M. Semmler-Behnke, J.V. Frangioni, A. Tsuda, Rapid translocation of nanoparticles from the lung airspaces to the body, Nat Biotechnol, 28 (2010) 1300-1303.

CHAPTER 6

Conclusions and Future Directions

Although universally recognized as one of the fastest modes for non-invasively administering therapeutics to the bloodstream, the lungs have been highly underutilized in the targeting systemic ailments. More surprising is the fact that no commercial formulation is used for the treatment or to support the treatment of serious pulmonary disorders such as cancer and tuberculosis. Lack of delivery vehicles to overcome cellular barriers and effective therapeutic modulation to ensure efficient delivery of the drug to either the regional milieu or the bloodstream are some of the impediments that need to be addressed in order to develop new opportunities in the oral inhalation (OI) market. Another important issue to be addressed is the poor (at best) understanding of the interaction of biomaterials that can serve as deliver vehicles and the lung tissue. More research in this area will be necessary to improve on the design of safe chemistries that have the appropriate functionality to achieve the tasks expected from the drug delivery carriers.

Polymeric nanocarriers (PNCs) are excellent delivery vehicles as they have several advantageous traits that can be harnessed to address some of these issues. The synergy of PNCs with compact OI devices such as pressurized metered-dose inhalers (pMDIs) is expected to greatly expand the spectrum of diseases that can be targeted utilizing such inexpensive devices. However, the size range of PNCs falls well outside the stipulated aerosol size range required for effectively targeting the

alveolar region of the lungs, which is in the micron range. Within this context, we have put forth in this work, approaches to formulate PNCs in pMDIs, the least expensive portable inhalers in the market, and efficiently deliver them to deep lungs. Furthermore, the interaction of PNC candidates with *in vitro* and *in vivo* models of pulmonary epithelium was evaluated, in an effort to understand their ability to modulate transport and uptake into and across well characterized monolayers, and to gain a better understanding of the toxic profile of those biomaterials.

Some of the main conclusions drawn from this work are:

(i) *We were the first group to develop a propellant-based inhaler formulation for the delivery of PNCs to the lungs.* Poly(lactic-glycolic acid) PLGA NPs were successfully encapsulated as core-shell structures within a HFA-philic, biodegradable co-oligomeric shell. The structures formed were characterized to have an aerosol size range between 1 and 5 μm, effective for deep lung deposition and the NP loading within the shell was determined to be ca.10%. Dispersion formulations thus formed were stable in HFA over extended time periods and exhibited respirable fractions as high as 60%, as evidenced by cascade impaction studies.

While NPs were successfully encapsulated within the co-oligomeric shell, the loading obtained through this strategy was relatively poor, especially in settings where the quantity of payload required is high. Therefore, suggested future work in this area would be to devise strategies to enhance and optimize the loading of NPs within the shell, which in turn could improve the payload of the therapeutic to be administered via this approach. Furthermore, another relevant study for the future

would be preparation of these structures through spray drying (in an effort to improve loading of the encapsulants) and formulating them as powders in DPIs, another class of compact OI devices that are highly used commercially – in spite of being more expensive, they are somewhat more straight forward in terms of formulations.

(ii) *We have devised several strategies for the modulation of transport of therapeutics across the pulmonary epithelium, and to also modulate their cellular internalization.* Many of these studies represent innovative concepts and systems in the pulmonary drug delivery field. The interaction of PNCs with *in vitro* models of airway epithelium was investigated in this work.

a. Fluorescence microscopy studies involving PLGA NPs loaded with a coumarin-6 (fluorescent dye) released from the core-shell formulation indicated that the NPs were internalized into Calu-3 cells, a model airway epithelium. In order to guage the applicability of the core-shell NP system, we tested its trafficking on cells infected with a respiratory pathogen, *Chlamydia pneumoniae*. Fluorescence and confocal microscopies conducted suggested that the NPs were not only taken up by Calu-3 cells (as observed before), but were also trafficked into the inclusions housing the bacterium. While these results are promising, the applicability of this approach can be greatly expanded and validated if these experiments can be transitioned to incorporate therapeutics instead of surrogate moieties. Preparing and characterizing PLGA NPs loaded with antibiotics, optimizing their size and loading and studying their internalization and their efficacy in eradicating the infection after administering

them as core-shell formulation could be a potential study that can be undertaken in the future. *In vivo* studies would also be of great relevance.

b. The internalization and transport of DNCs and DNCs loaded into NPs were also investigated in this study. DNC loaded NPs were prepared and characterized by emulsification solvent evaporation technique. The results from this study indicated that bare DNCs administered onto the apical side of the insert were able to traverse across confluent Calu-3 monolayers, while the DNC from those loaded into NPs did not. Uptake experiments performed on polarized Calu-3 cells using flow cytometry and cell lysis revealed that the kinetics of uptake for both systems were markedly different. While the uptake of free dendrimers saturated by 5h, DNCs formulated into PLGA NPs did not attain levels of saturation within the same time frame and took much longer, suggesting that this approach can be used as a potential strategy to enhance the rate and total amount of dendrimer uptake, and can thus be utilized to modulate not only transport across the monolayer, but also cellular internalization. Additionally, we demonstrate that the rate of uptake of DNCs was markedly reduced in polarized Calu-3 cells when compared to their non-polarized counterparts, which serves to emphasize the need to use polarized models. This represents the first study where the transport of dendrimers was investigated in a polarized *in vitro* model of the lung epithelium, and that such nanoblends has been proposed to modulate drug carrier compounds.

c. We also evaluated the effect of PEG density on the surface of DNC on the uptake and transport into and across confluent Calu-3 monolayers. DNCs with varying PEG densities (5, 13 and 25 PEG per DNC) were synthesized and

characterized. The synthesized conjugates showed no reduction in the viability of Calu-3 within the concentration range that would be employed for transport and uptake experiments. Our results indicate that PEGylation greatly enhances the transport of DNCs across Calu-3, with a tenfold increase in transport observed for the DNC with 25 PEG when compared to DNC with no PEG on the surface. The PEGylation can also be used to modulate cellular internalization. Within the same duration, the uptake of DNCs increases as the degree of PEGylation decreases, as evidenced by flow cytometry analysis. These results indicate that tailoring DNCs with appropriate surface density of PEG can greatly assist in the modulation of therapeutics across Calu-3. These represent the first study where the functionalization of dendrimers has been studied as an attempt to modulate transport across a model pulmonary epithelium. Preliminary PK evaluation of DNCs delivered to Balb/c mice via pharyngeal aspiration revealed that DNCs with greatest PEG surface density translocated much faster from the airspace into systemic circulation and persisted in the bloodstream for a longer duration compared to DNCs possessing 5 and 13 PEG. The bioavailability reported for DNC with 25 PEG was ca.20%. While this data is preliminary, it gives us great insight into the applicability of PEG DNCs within the context of being utilized as nanocarriers to modulate therapeutic transport across lung epithelia. Prospective studies of relevance for this part of the study include studying the biodistribution of PEG DNC after pharyngeal aspiration to understand the trafficking of the conjugate from the lung milieu, and the *in vivo* targeting with relevant therapeutics.

In this study, as a model molecule, we employed FITC in order to detail the proof of concept study. Future studies in this area includes conjugating therapeutics (to target either local or systemic circulation), and relevant biomolecules to the DNC surface and evaluating the transport and uptake of the resultant conjugate across and into Calu-3 monolayers. Another avenue that would benefit from future experiments is to enhance and optimize the poor loading of DNCs in the PLGA NPs. While all of our studies regarding transport were conducted in Calu-3, a model airway epithelial cell line, a lot of our pMDI formulation is delivered to the deep lung, populated by the alveolar epithelial cells who cellular properties are different from that of Calu-3. Evaluating the transport and uptake of DNCs, PEGylated DNCs and DNC loaded PLGA NPs, can be performed on alveolar epithelial cells by mimicking the actual dosage that is effectively delivered to the deep lung. The effect of dendrimer generation and PEG MW on the transport and uptake of PEGylated DNCs across Calu-3 can be evaluated.

While our results showed that DNCs were able to effectively traffic into Calu-3 or transport across Calu-3 monolayers, the exact mechanism for either study was only hypothesized and not studied in detail. Hence, future studies in this case should narrow down the exact mechanism and transport of the DNCs across Calu-3 monolayers. Prospective experiments here include labeling cell organelles with specific antibodies, to track the intracellular fate of the DNCs internalized into cells (where the DNCs are being trafficked into within the cell cytosol) using confocal microscopy. Furthermore, cellular uptake in the presence of inhibitors of specific internalization mechanisms like colchicines, cytochalisins, chlorpromazine, and

phorbol-12-myristrate-13-acetate could be conducted in order to deduce the mechanism with DNCs are taken up by Calu-3.

(iii) The interaction of a versatile co-oligomer that can be used to formulate PNCs and DNCs in pMDIs, and also as NP to stabilize drug particles (crystal/amorphous/hydrophobic/lipophobic) in pMDI formulations and the lung tissue was investigated. Retention studies and the inflammatory potential of the co-oligomer and the co-oligomer with PLGA PNPs system that mimics the core-shell formulation described in this dissertation were investigated *in vivo*. Our results indicate that the compound exerted little or no toxicity for dosages up to 5 mg/Kg (100 $\mu g \cdot 15\ \mu l^{-1}$) bodyweight upon a single acute dose, and up to 0.5 mg/Kg (10 $\mu g \cdot 15\ \mu l^{-1}$) bodyweight upon repeated administration of the co-oligomer as evidenced by analyzing the inflammatory cell populations isolated from BAL and tissue dispersion studies. Furthermore, the combination of OLA-g-CS and PLGA NPs (to mimic the NP laden core-shell formulation) did not induce any pronounced inflammation within the dosages that would mimic the actual core-shell formulation. The excipient had a half-life of 31h in the airspace, while ca. 90% of PLGA NPs administered as core-shell formulation were flushed out from the airways within 24h.

It must be mentioned that, for this study, OLA-g-CS was delivered intranasally to anaesthetized mice and hence we expect only about 40% of the formulation administered to reach the lung lobes. Although this is acceptable, a better approach would be to study the inflammatory response after administering the dose utilizing another technique that can better control the total deposition – such as instillation or pharyngeal aspiration – techniques that would ensure maximal deposition of the

formulation in the deep lung. A potential future study could be to administer the formulation through an alternative strategy as mentioned above and then evaluate the inflammatory response in the lung using BAL and tissue dispersion analysis. Future work here could include the histological evaluation of mice lung administered with OLA-g-CS, and to encapsulate a therapeutic molecule into the proposed PNPs. Additionally, biodistribution studies can be conducted to determine the fate of the PLGA NPs administered as core-shell particles to the lungs, and to evaluate the PK of therapeutics relevant to both local and systemic delivery.

APPENDIX A

CHARACTERIZATION OF G3-NH_2-nPEG1000

A1. Characterization of carboxy-methyl poly ethylene glycol (cmPEG).

cmPEG (MW 1000 Da)was synthesized according to method detailed in the literature and the procedure has been explained in the manuscript. The compound sourced was purified and characterized using ^{1}H-NMR, MALDI-TOF and FT-IR spectroscopies. The results of the characterization is given in Figure a1. The formation of cmPEG can be corroborated by the absence of peak at 4.6 ppm attributed to the –OH peak of mPEG. The unique stretching band at 1735 cm^{-1} (distinct to carbonyl moiety of cmPEG) in the FT-IR peak (Figure a1(b)) also confirms the conversion. MALDI-TOF analysis, shows an increase in MW of the mPEG from 1035 Da to 1201 Da with a distinct change the MW distribution also attributed to the formation of cmPEG (Figure a1(c)).

A2. Characterization of PEGylated G3-NH_2

cmPEG was tethered to the G3-NH_2 surface using a widely accepted EDC-NHS chemistry. The characterization of the final product was done using ^{1}H-NMR and MALDI-TOF. The conjugation of FITC to G3-NH_2 was accomplished through the formation of the thiourea bond.[3] Reaction between cmPEG, FITC and G3-NH_2 was done as a one pot reaction. Figures a2 to a5 are the MALDI and NMR spectras of the prepared G3-NH_2-nPEG 1000 conjugates starting with 0 (a2), 5(a3), 13(a4) and 25(a5) PEGs on G3-NH_2 surface.

All NMR spectras are shown In Figures a2(a) – 0 PEG, a3(a) – 5 PEG, a4(a) – 13 PEG and a5 (a) – 25 PEG. The presence of multiplets between 6 and 7 ppm can be attributed to the presence of aromatic protons of FITC. Singlet at 2.2 ppm is due to the presence of methylene protons of G3-NH_2 and they were set as an internal standard at 120 in order to estimate the extent of PEG conjugation. Broad peaks arising between 3.2 and 3.6 ppm can be traced to the CH_2CH_2O repeat unit of PEG.[5] The singlet at 3.23, due to the presence of $–CH_3$ group of PEG was used to determine the number of tethered PEG molecules on the G3-NH_2 backbone.

The increase in MW of the prepared G3-NH_2-nPEG 1000 compounds was documented using MALDI TOF and the resulting spectras are given in the figures a2(b) – 0 PEG, a3(b) – 5 PEG, a4(b) – 13 PEG and a5 (b) – 25 PEG. A gradual rise in MW with increase in PEG density is evident along with the change in the MW distribution when compared to bare G3-NH_2 (Figure a2(b) –Inset). The combination of NMR, MALDI and DLS results (discussed in the manuscript) confirm the presence of PEG on the dendrimer surface.

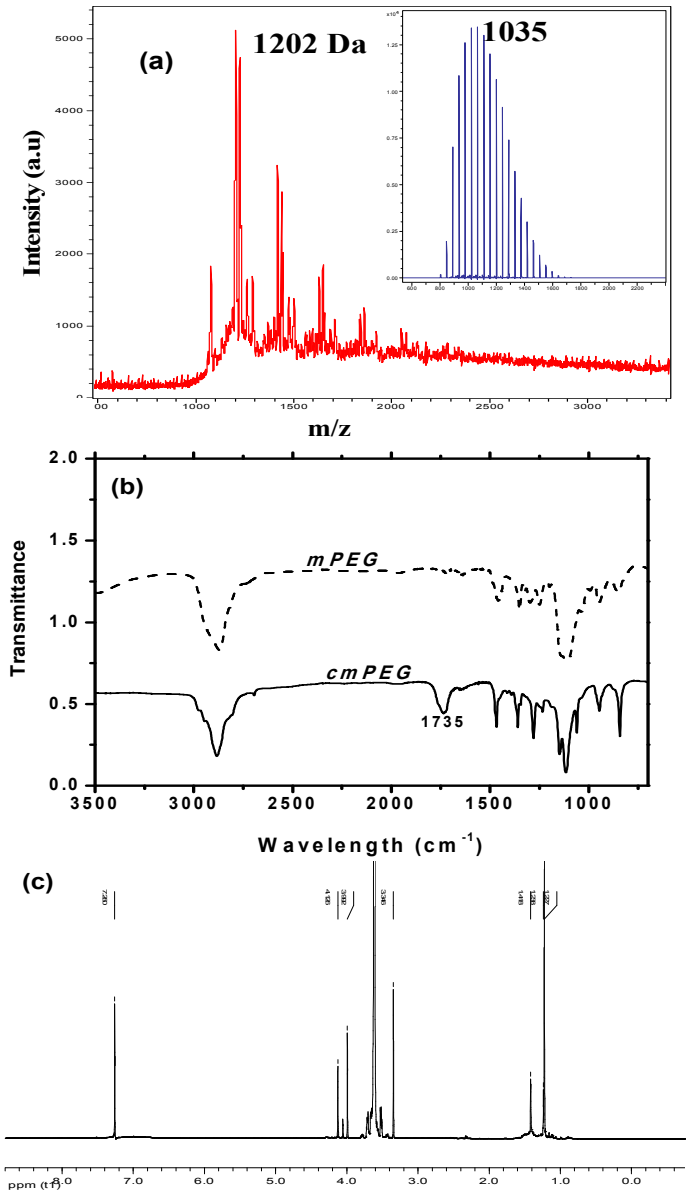

Figure a1. (a) MALDI-TOF spectra of cmPEG obtained using DHB as a matrix. *(inset)* MALDI-TOF spectra of mPEG. (b) FT-IR spectra of mPEG and cmPEG obtained using a KBr crystal. The distinct stretching at 1735 cm^{-1} is assigned to the *C*=*O* bond formed in the cmPEG. (c) ^{1}H-NMR spectra of cmPEG - $CdCl_3$ as the solvent. The absence of an -OH peak at ca. 4.6 ppm indicates the conversion of mPEG to cmPEG.

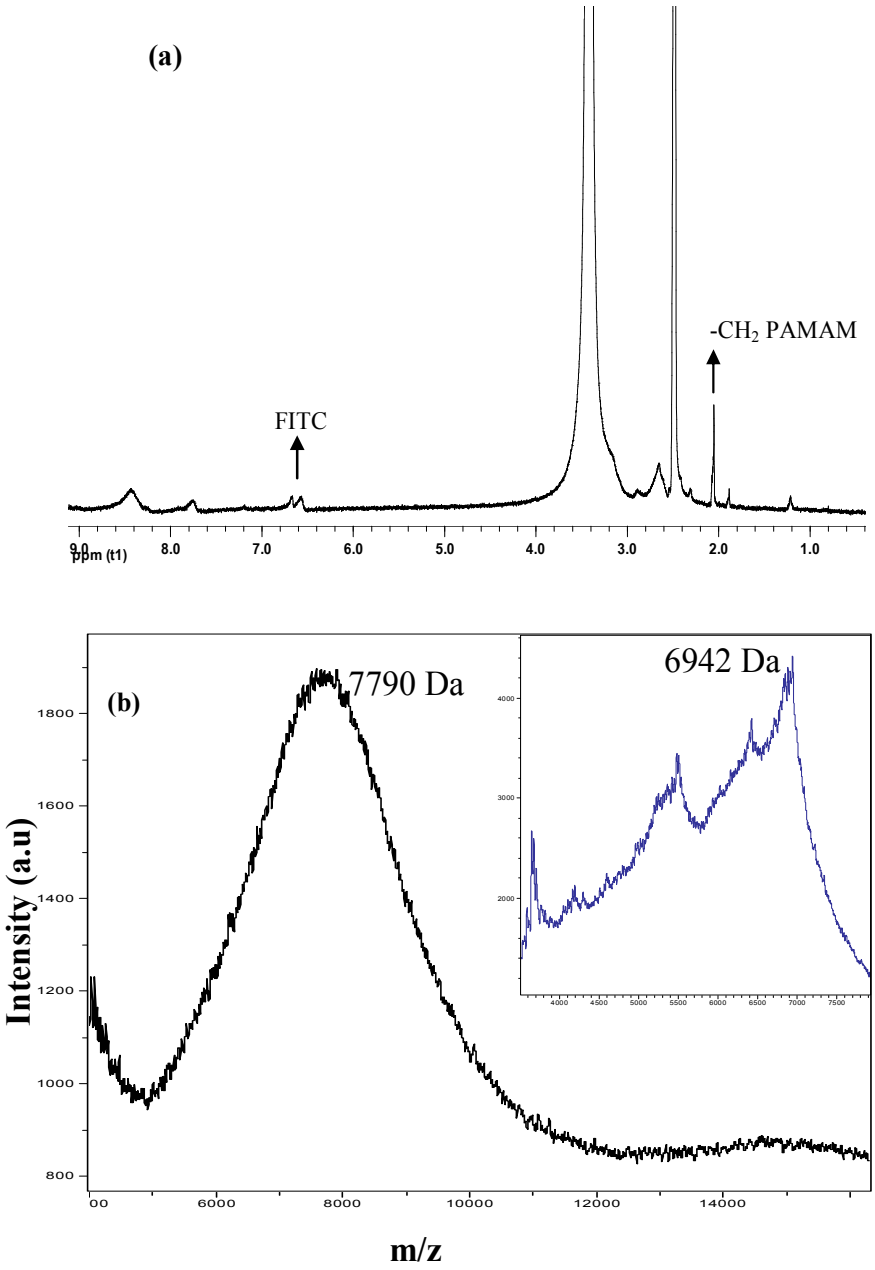

Figure a2. (a) ^{1}H-NMR spectra of G3-NH_2-0PEG1000 (b) M ALDI-TOF spectra of G3-NH_2-0PEG1000 determined using DHB as a matrix. The average number of FITC molecules conjugated here were 2. (*(inset)* MALDI-TOF spectra of pure G3-PAMAM dendrimer.

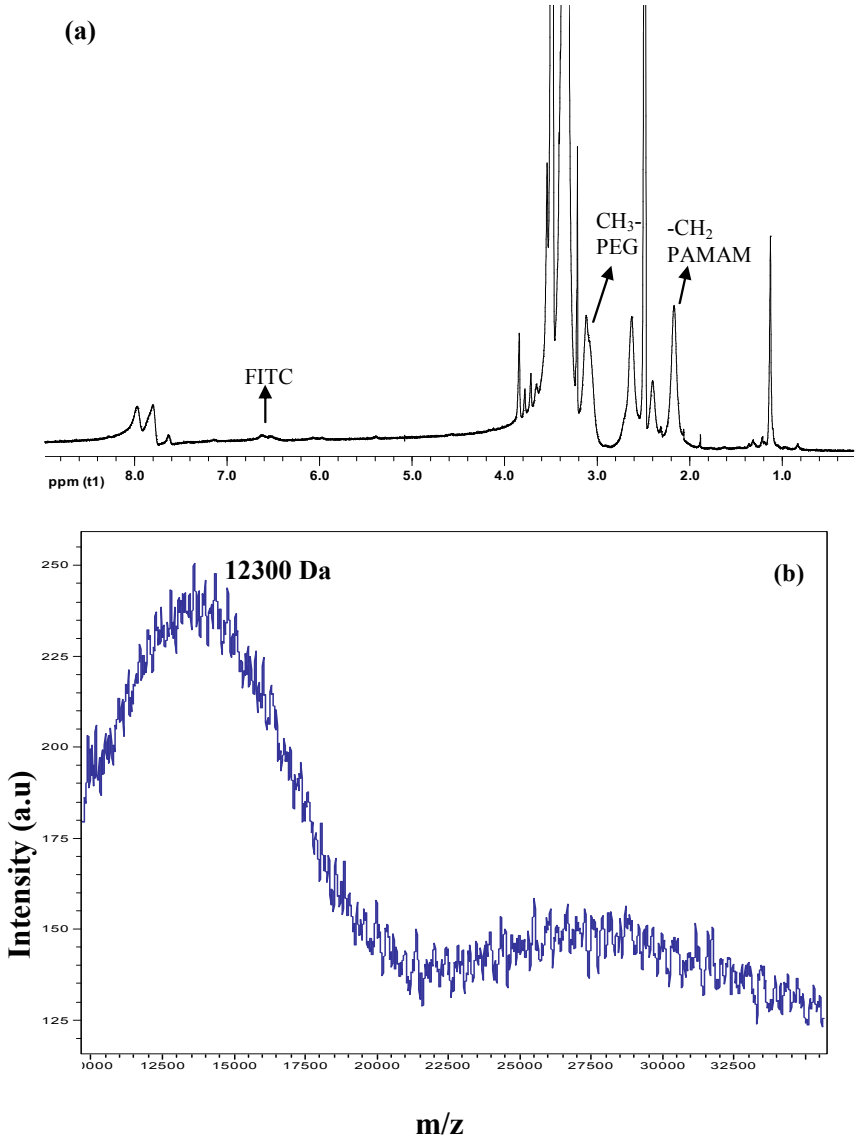

Figure a3. (a) ^{1}H-NMR spectra of G3-NH_2-5PEG1000 (b) MALDI-TOF spectra of G3-NH_2-5PEG1000 determined using DHB as a matrix. The average number of FITC molecules conjugated here were 1.5.

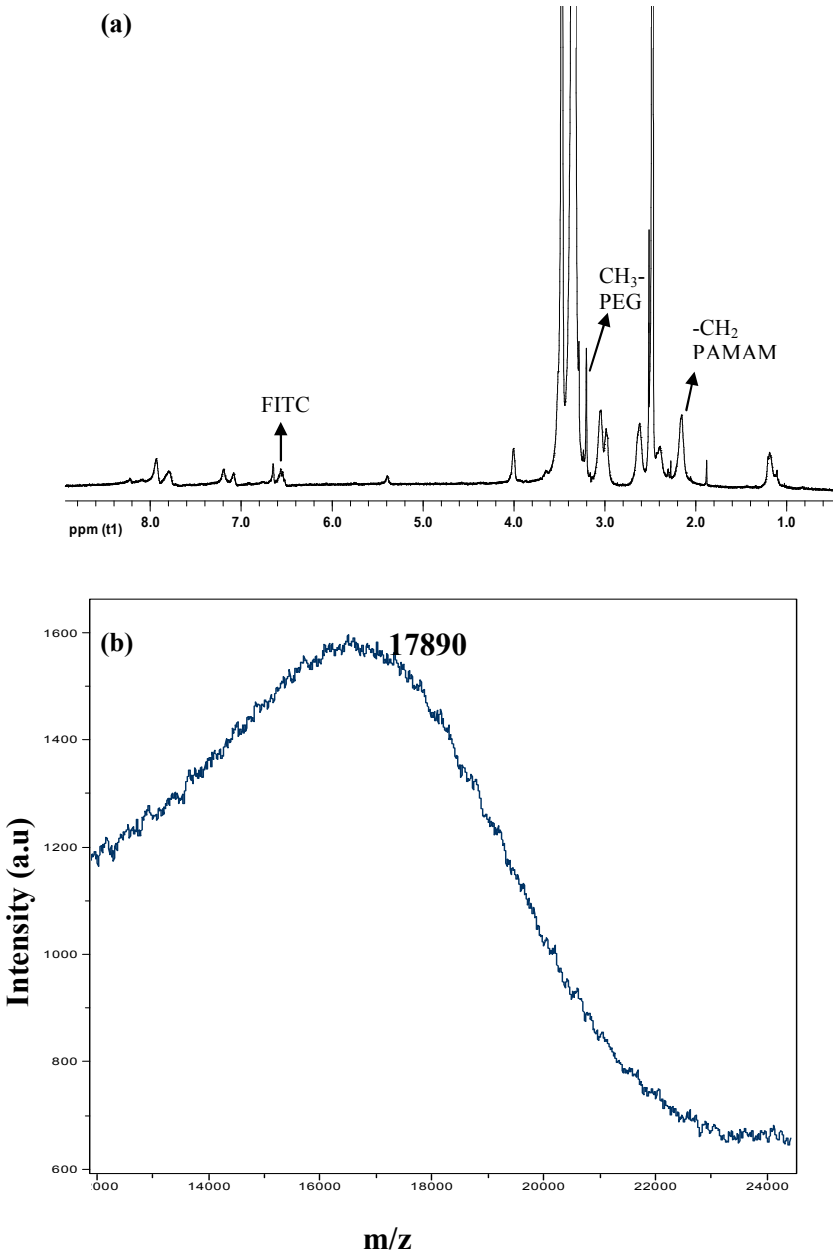

Figure a4. (a) ^{1}H-NMR spectra of G3-NH_2-13PEG1000 (b) MALDI-TOF spectra of G3-NH_2-13PEG1000 determined using DHB as a matrix. The average number of FITC molecules conjugated here were 1.7.

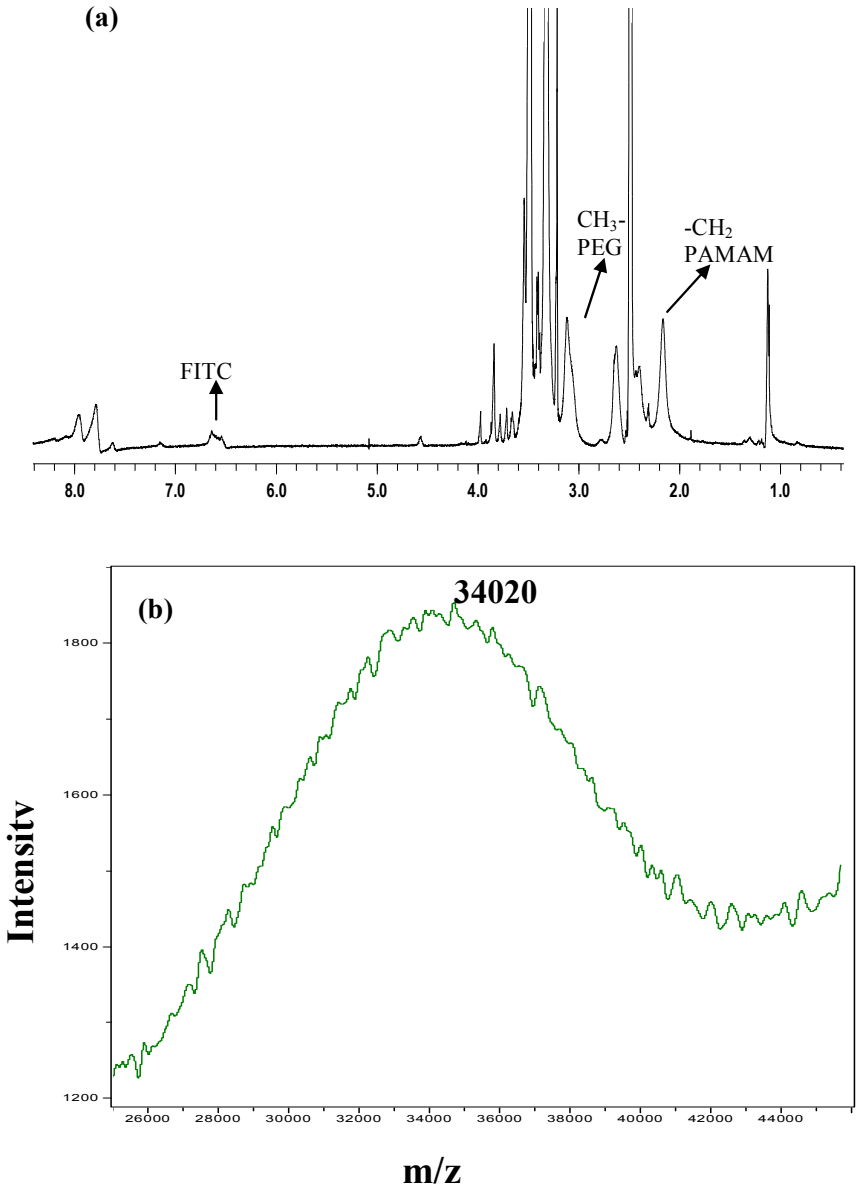

Figure a5. (a) ^{1}H-NMR spectra of G3-NH_2-13PEG1000 (b) MALDI-TOF spectra of G3-NH_2-25PEG1000 determined using DHB as a matrix. The average number of FITC molecules conjugated here were 2.

APPENDIX B

PUBLICATION 1

Brazilian Journal of Chemical Engineering

ISSN 0104-6632
Printed in Brazil
www.abeq.org.br/bjche

Vol. 23, No. 02, pp. 183 - 190, April - June, 2006

INTERFACIAL PHENOMENA AT THE COMPRESSED CO_2-WATER INTERFACE

B. Bharatwaj and S. R. P. Rocha*

Chemical Engineering and Materials Science,
Wayne State University, Detroit, MI 48202, USA.
E-mail: sdr@eng.wayne.edu

(Received: October 20, 2004 ; Accepted: December 19, 2005)

Abstract - Compressed CO_2 is considered to be a viable alternative to toxic volatile organic solvents with potential applications in areas including separation reactions, and materials formation processes. Thus an interest in CO_2 stems from the fact that it is very inexpensive, has low toxicity, and is not a regulated. However, compressed CO_2 has a zero dipole moment and weak van der Waals forces and thus is a poor solvent for both polar and most high molecular weight solutes, characteristics that severely restrict its applicability. In order to overcome this inherent inability, surfactant-stabilized organic and aqueous dispersions in CO_2 have been proposed. This work will discuss fundamentals and recent advances in the design of amphiphiles for the novel CO_2-water interface.

Keywords: High pressure; Interfacial tension; Surfactants; Water-in-CO_2 microemulsions.

INTRODUCTION

Development of energy-efficient and "green" alternatives to conventional separation and materials formation processes are keys to economical development in times of uncertainties in the world petroleum market and of tighter environmental regulations. CO_2 is cheap, is not regulated by either the FDA or EPA, has tunable solvent strength, and that are capable of efficiently stabilizing water-dispersed domains in CO_2, and yet are environmentally friendly and inexpensive (Eastoe, *et al.*, 2003). Current limitations are the small number (mostly fluorinated) of molecules with significant interfacial activity at the CO_2-water (C|W) interface and the generally high pressures required to stabilize formulations involving water and compressed CO_2. The properties of the C|W interface are strikingly

APPENDIX C

PUBLICATION 2

Langmuir 2007, *23*, 12071−12078

Biocompatible, Lactide-Based Surfactants for the CO_2−Water Interface: High-Pressure Contact Angle Goniometry, Tensiometry, and Emulsion Formation

Balaji Bharatwaj, Libo Wu, and Sandro R. P. da Rocha*

Department of Chemical Engineering and Materials Science, Wayne State University, 5050 Anthony Wayne Dr., Detroit, Michigan 48202

Received June 20, 2007. In Final Form: August 29, 2007

The unique properties of compressed CO_2, including its low cost, nontoxicity, easily tunable solvent strength, and favorable transport properties, make it an environmentally attractive alternative to volatile organic solvents. Suitable surface-active species can be utilized to realize the full potential of clean, CO_2-based technologies, by helping to overcome the low solubility typically associated with many solutes of interest in CO_2. In this work we synthesize and investigate the interfacial activity of a series of nonionic amphiphiles with a biocompatible and biodegradable CO_2-phile at both the CO_2−water (C|W) and CO_2−water−solid (C|W|S) interfaces. We developed a high-pressure pendant drop tensiometer and contact angle goniometer that allows us to measure both tension and contact angle in tandem. The tension of the C|W interface was measured in the presence of the lactide (LA)-based surface active agents with varying molecular weight and hydrophilic-to-CO_2-philic ratios. Emulsion studies with an optimum balanced surfactant were performed. The contact angle of water droplets against a silane-modified (hydrophobic) substrate under CO_2 atmosphere was also measured in presence of a selected LA-based amphiphile. The results demonstrate that the nonionic copolymers with the biodegradable and biocompatible LA-based group can significantly reduce the tension of the C|W interface. The LA-based surface active species are also capable of forming stable emulsions of water and CO_2 and reducing the angle of the three-phase C|W|S contact line.

Introduction

Supercritical or near-critical fluids are environmentally benign candidates for the replacement of volatile organic solvents.[1] They possess solvent strength that can be tuned with not only temperature but also pressure.[2] The ability to achieve wide variations in density with small changes in pressure has tremendous practical relevance, as for example by facilitating downstream separation processes.[3] CO_2 is a particularly attractive compressible solvent because of its low cost, nontoxicity, mild critical point, and nonflammability.[4,5] CO_2-based systems have shown promise in a range of chemical, separation, and materials processing technologies including extraction,[6,7] polymerization,[8−10] organic reactions,[11] biocatalysis,[12,13] nanoparticle synthesis and separations,[14−16] and cleaning in the microelectronic industry.[17,18]

In spite of all the recognized advantages of CO_2-based technologies, their applicability is often limited by the fact that CO_2 is a poor solvent to many solutes of interest.[19] Suitable amphiphiles can be used to overcome some of the limitations associated with processing species that are weakly solvated by CO_2. Within that context, both the CO_2−liquid (C|L)and the CO_2−liquid−solid (C|L|S) interfaces are of relevance.[1,20] Polymeric[3,21] and small molecular weight amphiphiles[22,23] can be used in the formation and stabilization of CO_2-based dispersions.[6] Copolymer surfactants have been successfully employed in stabilizing growing polymer nuclei in dispersion polymerizations in CO_2.[24] Large molecular weight amphiphiles have been also used to stabilize the CO_2−water interface.[25−27] Dispersions of water and CO_2 have found several potential uses, including media for inorganic reactions,[28] template for the

* To whom correspondence should be addressed. Tel.: +1-313-577-4669. Fax: +1-313-577-3810. E-mail: sdr@eng.wayne.edu.

(1) Dickson, J. L.; Gupta, G.; Horozov, T. S.; Binks, B. P.; Johnston, K. P. *Langmuir* **2006**, *22*, 2161−2170.
(2) Bharatwaj, B.; da Rocha, S. R. P. *Braz. J. Chem. Eng.* **2006**, *23*, 183−190.
(16) Sane, A.; Thies, M. C. *J. Supercrit. Fluids* **2007**, *40*, 134−143.
(17) Denison, G. M.; Jones, C., III; DeYoung, J.; Gross, S.; McClain, J.; Zannoni, L.; Hicks, E.; Wood, C.; Bruggiano, M. K.; Visintin, P.; Beuel, C.; Schauer, C.; DeSimone, J. M. *PMSE Prepr.* **2004**, *90*, 152−153.
(18) King, J. W.; Williams, L. L. *Curr. Opin. Solid State Mater. Sci.* **2003**,

APPENDIX D

PUBLICATION 3

Pharmaceutical Research, Vol. 25, No. 2, February 2008 (© 2007)
DOI: 10.1007/s11095-007-9466-2

Research Paper

Core–shell Particles for the Dispersion of Small Polar Drugs and Biomolecules in Hydrofluoroalkane Propellants

Libo Wu,[1] Balaji Bharatwaj,[1] Jayanth Panyam,[2] and Sandro R. P. da Rocha[1,3]

Received July 13, 2007; accepted October 1, 2007; published online October 17, 2007

Purpose. Demonstrate the applicability of a novel particle-based technology for the development of suspensions of small polar drugs and biomolecules in hydrofluoroalkane (HFA) propellants for pressurized metered-dose inhalers (pMDIs).

Materials and Methods. Emulsification diffusion was used to prepare core–shell particles. The shell consisted of oligo(lactide) grafts attached onto a short chitosan backbone. The active drug was arrested within the particle core. Colloidal Probe Microscopy (CPM) was used to determine the cohesive forces between particles in a model HFA propellant. The aerosol characteristics of the formulations were determined using an Anderson Cascade Impactor (ACI). Cytotoxicity studies were performed on lung epithelial and alveolar type II cells.

Results. CPM results indicate that particle cohesive forces in liquid HFA are significantly screened in the presence of the polymeric shell and correlate well with the physical stability of suspensions in propellant HFA. The proposed formulation showed little or no cytotoxic effects on both Calu-3 and A549 cells.

Conclusions. Core–shell particles with a shell containing the lactide moiety as the HFA-phile showed excellent dispersion stability and aerosol characteristics in HFA-based pMDIs. This is a general strategy that can be used for developing novel suspension pMDIs of both small polar drugs and large therapeutic molecules.

KEY WORDS: biomolecules; colloidal probe microscopy; pressurized metered-dose inhaler; pulmonary drug delivery; salbutamol sulfate.

INTRODUCTION

In spite of the recognized potential advantages in delivering large therapeutic molecules such as peptides, DNA and proteins through the pulmonary route (1–9), Exubera® is the only inhalation formulation approved by the FDA for the delivery of a systemically acting biomolecule (insulin) (10). Studies have indicated that biomolecular ar- site for the delivery of large therapeutic molecules can be attributed, to a large extent, to challenges in the development of appropriate inhalation formulations (3,5,10,13–15).

Pressurized metered dose inhalers (pMDIs) are the least expensive and most widely used devices for the delivery of drugs to the lungs (8,14,16–18). pMDIs are, therefore, potential candidate devices for the development of formulations containing large therapeutic molecules. However, both small and

APPENDIX E

PUBLICATION 4

Biomaterials 31 (2010) 7376–7385

Contents lists available at ScienceDirect

Biomaterials

journal homepage: www.elsevier.com/locate/biomaterials

The potential for the noninvasive delivery of polymeric nanocarriers using propellant-based inhalers in the treatment of Chlamydial respiratory infections

Balaji Bharatwaj [a], Libo Wu [a,1], Judith A. Whittum-Hudson [a,b], Sandro R.P. da Rocha [a,*]

[a] Chemical Engineering and Materials Science, College of Engineering, Detroit, USA
[b] Immunology and Microbiology, School of Medicine, Wayne State University, Detroit, MI 48202, USA

ARTICLE INFO

Article history:
Received 25 March 2010
Accepted 1 June 2010
Available online 7 July 2010

Keywords:
Pulmonary drug delivery
Pressurized-metered-dose inhalers
Polymeric
Nanocarriers
Nanomedicine
Chlamydia pneumoniae

ABSTRACT

A novel strategy for pulmonary delivery of polymeric nanocarriers (NCs) pressurized-metered dose inhalers (pMDIs) is reported in this work. Core–shell particles consisting of a water soluble, hydrofluoroalkane(HFA)-philic biodegradable copolymer of chitosan and poly(lactic acid), and a core of poly(D, L-lactide-co-glycolide) (PLGA) NCs were prepared by a modified emulsification–diffusion methodology. Dispersions of the core–shell particles in HFA propellant revealed enhanced physical stability compared to polymeric NCs alone, and more importantly, excellent aerosol characteristics as determined by inertial impaction studies. Confocal microscopy revealed that the polymeric NCs from such core–shell particles are capable not only to be taken up by Calu-3 (airway epithelial) cells that have been infected with *Chlamydia pneumoniae*, an intracellular pathogen, but are also internalized within chlamydial inclusions. Our results suggest that the proposed methodology can be used as a general platform for the delivery of polymeric NCs to the respiratory tract using the inexpensive pMDIs, and that such an approach may be used to target and deliver drugs to treat chlamydial-related infections.

1. Introduction

Besides its non-invasive nature, pulmonary drug delivery has many other advantages compared to alternative drug delivery strategies, including a large surface area for solute transport, fast drug uptake, and improved drug bioavailability [1,2]. It is, therefore, not surprising that oral inhalation therapy is considered not only as the preferred mode of administration of drugs to the lungs (regional drug delivery), but also as a potential pathway to the blood stream [1]. However, many challenges in formulation development [3], and little understanding of the interactions between the therapeutic molecules and the respiratory surfaces has significantly constrained advances in pulmonary drug delivery strategies [4,5]. In this work we integrate aspects of both formulation development and therapeutic–tissue interaction. We propose a strategy to deliver polymeric nanocarriers (NCs) to the lungs using propellant-based formulations, and investigate the ability of such carriers to gain access to inclusions of an intracellular pathogen (*Chlamydia pneumoniae*), which is associated with a host of chronic and acute lung diseases [6,7].

One natural (but as will be discussed, non-trivial) step towards the development of the next generation of formulations that may help achieve the full potential of oral inhalation formulations is to take advantage of the high functionality that may be embedded into polymeric nanocarriers (NCs) [8,9]. However, there are several issues associated with the delivery of polymeric NCs to the lungs. Biocompatibility and clearance are two very important considerations [8,10]. A stringent aerosol particle size requirement represents another important challenge [11,12]. The delivery efficiency of many traditional aerosol formulations is low due to the fact that a large fraction of the particles have aerosol sizes that are too large ($>\sim 5$ μm), and are thus retained in the mouth and throat to reach in the digestive tract rather than lungs. In contrast, aerosol particles that are too small (<0.4 μm, which is within the range of typical polymeric NCs described in the literature) are also expected to have very low deposition efficiency [11].

Several approaches have been suggested in order to address the issues related to the aerosol size of polymeric NCs for oral inhalation formulations. However, most studies have focused on dry powder inhalers (DPIs) and nebulizers [10,13,14]. While the formulation of nanoscale active pharmaceutical ingredients in pressurized-metered-dose inhalers (pMDIs) has been documented in the literature [10,15], to the best of our knowledge, there has been no previous study on the formulation of polymeric NCs in propellant-based inhalation devices [16,17].

* Corresponding author. Tel.: +1 313 577 4669; fax: +1 313 578 5820.
E-mail address: sdr@eng.wayne.edu (S.R.P. da Rocha).
[1] Present address: MAP Pharmaceuticals, Mountain View, CA 94043, USA.

APPENDIX F

PUBLICATION 5

GENE DELIVERY

Journal of Controlled Release 157 (2012) 406–417

Contents lists available at SciVerse ScienceDirect

Journal of Controlled Release

journal homepage: www.elsevier.com/locate/jconrel

Propellant-based inhalers for the non-invasive delivery of genes via oral inhalation

Denise S. Conti, Balaji Bharatwaj, Daniel Brewer, Sandro R.P. da Rocha *

Department of Chemical Engineering and Materials Science, College of Engineering, Wayne State University, Detroit, MI, 48202, USA

ARTICLE INFO

Article history:
Received 16 March 2011
Accepted 23 September 2011
Available online 1 October 2011

Keywords:
Pulmonary gene delivery
Pressurized-metered dose inhalers
Alveolar epithelium
CS–DNA polyplexes
Core–shell particles

ABSTRACT

In this work we describe the development of a propellant-based, portable oral inhalation platform for the pulmonary delivery of genes. A core–shell strategy is utilized to efficiently disperse cationic-polymer-DNA nanoparticles in hydrofluoroalkane propellants, and to generate aerosols from the corresponding pressurized metered-dose inhaler formulations (pMDIs) that have excellent aerosol characteristics, suitable for deep lung deposition. The engineered polyplexes and core–shell structures were fully characterized, and their ability to transfect model lung alveolar epithelium cells in vitro was demonstrated. We also show that the propellant does not affect the biological activity of the plasmid DNA, and that the core–shell formulations have no in vitro cytotoxicity. The relevance of this work stems from the fact that pMDIs are the least expensive and most widely used portable oral inhalation devices, and are thus promising platforms for targeting genes to the lungs for the treatment of medically relevant diseases including asthma, cystic fibrosis, chronic obstructive pulmonary disease, and lung cancer.

1. Introduction

There is tremendous potential in targeting genes to the lungs [1–3]. Asthma, cystic fibrosis, chronic obstructive pulmonary disease (COPD), emphysema, and lung cancer are just some of the many examples of pulmonary diseases that can be potentially treated by gene therapy [1,2,4–6]. However, there are several challenges associated with the formulation and regional delivery of genes via oral inhalation (OI) [1], the preferred mode of administration of therapeutics to the lungs.

The mucus layer in the airways and the lung surfactant in the alveolar region represent important extracellular barriers to the delivery of genes to the respiratory tract [7,8]. As transfection with free DNA is not efficient, the choice of the gene carrier system is also of great relevance [9]. For polymeric carriers, the polymer chemistry, and the physical properties of the polymer-DNA complexes (polyplexes), including their size, surface charge, and DNA loading greatly affect the transfection efficiency [10,11]. In addition, those parameters also influence the uptake and trafficking of the gene carriers and the release of DNA in the cellular environment, which are examples of intracellular barriers that need to be overcome [12]. The choice of the aerosolization technique is also expected to influence the transfection efficiency as the dose and location where the polyplexes will be delivered depend on device characteristics and particle engineering [5,13,14].

The ideal scenario in terms of gene delivery to the lungs would be for both patients and health care providers to be able to choose from a host of different delivery devices, as patient compliance and device suitability depends on the patient and disease state/condition. Nucleic acids can be potentially delivered to the lungs via nebulizers, dry powder inhalers (DPIs) or pressurized metered dose inhalers (pMDIs) [15]. Nebulization has many advantages [5,13,15,16], but it is less efficient and less convenient than portable devices [5]. Therapeutically active molecules can also be delivered to the lungs by DPIs. The delivery of such molecules using DPIs have several advantages, including the fact that DPIs are propellant-free, portable, simple use, have good shelf-life, and reduced time of administration [17]. Some studies have demonstrated the potential of liposomal gene powders [17], and also of gene powders prepared by supercritical CO_2 using chitosan (CS) as non-viral carriers for use in DPIs [18,19]. However, there are also some disadvantages associated with the delivery of genes with DPIs, as for example potential problems in dose uniformity, dependency on patient's inspiratory flow rate, and less protection from environmental effects [20].

Genes can also be delivered to the lungs using pMDIs. However, pMDIs have received considerably less attention than DPIs and nebulizers. The only work discussing gene delivery in hydrofluoroalkane (HFA)-based pMDIs consists in using surfactant-coated DNA particles prepared by reverse microemulsion [13]. However, liposomes were needed during transfection to improve the in vitro transfection efficiency of the particles used in the formulation. In spite of the limited amount of work on pMDIs, such devices offer a potentially more efficacious and convenient alternative than DPIs and nebulizers, especially for repeat administration [13], and serve as a complementary

* Corresponding author at: Wayne State University, College of Engineering, Chemical

APPENDIX G

PUBLICATION 6

International Journal of Pharmaceutics 422 (2012) 428–435

Contents lists available at SciVerse ScienceDirect

International Journal of Pharmaceutics

journal homepage: www.elsevier.com/locate/ijpharm

Pharmaceutical nanotechnology

Reverse aqueous microemulsions in hydrofluoroalkane propellants and their aerosol characteristics

Parthiban Selvam[a,1], Balaji Bharatwaj[a], Lionel Porcar[b,2], Sandro R.P. da Rocha[a,*]

[a] Department of Chemical Engineering and Materials Science, Wayne State University, 5050 Anthony Wayne Dr., Detroit, MI 48202, United States
[b] Institut Laue-Langevin, 6 rue Jules Horowitz, B.P. 156, F-38042 Grenoble, Cedex 9, France

ARTICLE INFO

Article history:
Received 22 July 2011
Received in revised form 6 October 2011
Accepted 18 October 2011
Available online 21 October 2011

Keywords:
Microemulsions
Metered dose inhalers
Interfacial tension
SANS
Anderson cascade impactor
Cell toxicity

ABSTRACT

In this work we describe the structure and environment of reverse aqueous microemulsions formed in 1,1,1,2-tetrafluoroethane (HFA134a) propellant in the presence of a non-ionic ethoxylated copolymer, and the aerosol characteristics of the corresponding pressurized metered dose inhaler (pMDI) formulations. The activity of selected polypropylene oxide–polyethylene oxide–polypropylene oxide ($PO_mEO_nPO_m$) amphiphiles at the HFA134a–water interface was studied using *in situ* high-pressure tensiometry, and those results were used as a guide in the selection of the most appropriate candidate surfactant for the formation of microemulsions in the compressed HFA134a. The environment and structure of the aggregates formed with the selected surfactant candidate, $PO_{22}EO_{14}PO_{22}$, was probed via UV–vis spectroscopy (molecular probe), and small angle neutron scattering (SANS), respectively. High water loading capacity in the core of the nanoaggregates was achieved in the presence of ethanol. At a water-to-surfactant molar ratio of 21 and 10% ethanol, cylindrical aggregates with a radius of 18 Å, and length of 254 Å were confirmed with SANS. Anderson Cascade Impactor (ACI) results reveal that the concentration of the excipients (C_{exp}, including surfactant, water and ethanol) has a strong effect on the aerosol characteristics of the formulations, including the respirable fraction, and the mass mean aerodynamic diameter (MMAD), and that the trend in MMAD can be predicted as a function of the C_{exp} following similar correlations to those proposed to common non-volatile excipients, indicating that the nanodroplets of water dispersed in the propellant behave similarly to molecularly solubilized compounds. Cytotoxicity studies of $PO_{22}EO_{14}PO_{22}$ were performed in A549 cells, an alveolar type II epithelial cell line, and indicate that, within the concentration range of interest, the surfactant in question decreases cell viability only lightly. The relevance of this work stems from the fact that aqueous-based HFA-pMDIs are expected to be versatile formulations, with the ability to carry a range of medically relevant hydrophilic compounds within the nanocontainers, including high potency drugs, drug combinations and biomacromolecules.

1. Introduction

Aqueous reverse microemulsions in propellant-based inhalers have been suggested as a possible vehicle for the delivery of polar drugs, including biomolecules, to and through the lungs (Patton and Byron, 2007; Rogueda, 2005; Courrier et al., 2002; Williams and Liu, 1999; Blondino, 1995; Selvam et al., 2008; Bharatwaj et al., 2010; Wu et al., 2008). Encapsulation and delivery of polar drugs in reverse aqueous microemulsions seems to be not only viable, but also very attractive, given the advantages of portable inhalers such as pMDIs (Selvam et al., 2008; Meakin et al., 2006; Steytler et al., 2003; Patel et al., 2003a,b; Peguin et al., 2006; Chokshi et al., 2009). The strategy is very simple, and consists in solubilizing the therapeutic of interest within the core of the nano-sized aqueous reverse aggregates stabilized by surfactant molecules, which are homogeneously dispersed in the propellant (Selvam et al., 2008; Wu et al., 2008; Meakin et al., 2006; Chokshi et al., 2009; Butz et al., 2002). This approach may also have some potential advantages over traditional dispersion-based (micronized drugs) pMDI formulations. For example in the case of high potency therapeutics, where drug losses due to interactions between the crystals and the canister walls may compromise the reliability of the dosage, as the total drug surface area may approach that of the walls of the container (Traini et al., 2005, 2006). This problem is expected to be mitigated by formulating the drug within the microemulsion core. Microemulsions could also be amenable to the formulation of combination therapies.

However, very few studies have reported the formulation of

* Corresponding author. Tel.: +1 313 577 4660; fax: +1 313 578 3820.
E-mail address: sdr@eng.wayne.edu (S.R.P. da Rocha).
[1] Currently at Savara Pharma, Lawrence, KS.

ABSTRACT

POLYMERIC NANOCARRIERS FOR THE REGIONAL AND SYSTEMIC DELIVERY OF THERAPEUTICS TO AND THROUGH THE LUNGS

by

BALAJI BHARATWAJ

May 2012

Advisor: Dr. Sandro R P da Rocha

Major: Chemical Engineering

Degree: Doctor of Philosophy

The lungs are considered as one of the fastest portals of entry to the bloodstream and oral inhalation (OI) has long been accepted as the preferred mode of administration of therapeutics to the respiratory tract. However, despite its advantages, the lungs have been largely underutilized to target ailments not only of systemic relevance but also several other grave conditions including lung cancer and tuberculosis. Polymeric nanocarriers (PNCs) have several advantages over other drug delivery vehicles including sustained release of moieties, ease of cellular internalization and improved targeting, and hence hold the promise to greatly augment the potential of OI therapies. The surface chemistry, architecture, and size of PNCs may be potentially altered in order to modulate their interaction with the extra and intracellular barriers present in the lung epithelia, and thus their transport, overcoming challenges observed when delivering free drug molecules. They can be utilized to enhance the residence time of drugs required to exert prolonged

therapeutic effect in the airspace (regional therapy), and conversely speed up the transport of drug molecules that would traverse sluggishly to the bloodstream (systemic therapy). In this work, we report the preparation, characterization of a series of PNCs ranging from polymeric nanoparticles (PNPs) to surface modified dendrimer nanocarriers (DNCs) and we studied their interaction with *in vitro* and *in vivo* models of the lung epithelium. We observed that transport and cellular uptake can be efficiently modulated as the surface characteristics of the PNCs is varied, suggesting that OI strategies incorporating such nanoscopic entities may potentially be employed for targeting regional diseases and also the systemic circulation. Finally, we also discuss the formulation, dispersion stability and aerosol characteristics of the aforementioned PNCs in portable, inexpensive pressurized metered dose inhalers (pMDIs).

AUTOBIOGRAPHICAL STATEMENT

Balaji Bharatwaj

Balaji Bharatwaj received his B.E (Bachelor of Engineering) in Chemical Engineering from Visweswariah Technological University in 2004. He joined Wayne State University, MI, US in Fall 2004 to pursue a Masters degree in Chemical Engineering and continued on to pursue his doctorate. His research, under the guidance of Prof. Sandro da Rocha is focused on strategies to develop and formulate polymeric nanocarriers for the regional and systemic delivery of therapeutics to and through the respiratory tract. He has authored or coauthored 6 peer reviewed publications and book chapters. He will be submitting 4 more publications with contributions as a first author.